



HAL
open science

Study of complex formulations based on vitrimer matrices: application to flame retardants

Louis Meunier

► **To cite this version:**

Louis Meunier. Study of complex formulations based on vitrimer matrices: application to flame retardants. Material chemistry. Université de Lille, 2023. English. NNT: 2023ULILR079. tel-04566495

HAL Id: tel-04566495

<https://theses.hal.science/tel-04566495>

Submitted on 2 May 2024

HAL is a multi-disciplinary open access archive for the deposit and dissemination of scientific research documents, whether they are published or not. The documents may come from teaching and research institutions in France or abroad, or from public or private research centers.

L'archive ouverte pluridisciplinaire **HAL**, est destinée au dépôt et à la diffusion de documents scientifiques de niveau recherche, publiés ou non, émanant des établissements d'enseignement et de recherche français ou étrangers, des laboratoires publics ou privés.



Université
de Lille

UMET
Unité Matériaux Et Transformations



PhD MANUSCRIPT

Study of complex formulations based on vitrimer matrices – Application to flame retardants

Etude de formulations complexes à matrice vitrimère – Application aux retardateurs de flamme

Thesis prepared and publicly defended at

University of Lille

Doctoral School of Material Science, Radiation and Environment, ED 104
Materials and Transformation Unit, UMR CNRS 8207

For the degree of

DOCTOR OF PHILOSOPHY

Specialty: Material chemistry

By

Louis MEUNIER

Thesis supervised by

**Pr. Sophie DUQUESNE, Pr. Valérie GAUCHER, Dr. Fabienne SAMYN and Dr. David
FOURNIER**

Thesis defended on September, 27th 2023 before an Examination Committee comprised of:

DR. Véronique BOUNOR- LEGARE	University of Lyon 1, IMP	Chair of the jury
Pr. Laurent FERRY	Mines d'Alès, CM2A	Reviewer
Dr. HDR Sandrine HOPPE	University of Lorraine, LRGP	Reviewer
Dr. Damien MONTARNAL	University of Lyon 1, CP2M	Examiner
Pr. Sophie DUQUESNE	Centrale Lille Institut, UMET	Thesis director
Pr. Valerie GAUCHER	University of Lille, UMET	Thesis co-director
Dr. Fabienne SAMYN	Centrale Lille Institut, UMET	Thesis supervisor
Dr. David FOURNIER	University of Lille, UMET	Thesis co-supervisor



MANUSCRIT DE THESE

Etude de formulations complexes à matrice vitrimère – Application aux retardateurs de flamme

Study of complex formulations based on vitrimer matrices – Application to flame retardants

Thèse préparée et défendue publiquement à

L'Université de Lille

Ecole doctorale de la Science de la Matière, du Rayonnement et de
l'Environnement, ED 104

Unité Matériaux et Transformation, UMR CNRS 8207

Pour le diplôme de

DOCTEUR

Specialité : Chimie des matériaux

Par

Louis MEUNIER

Thèse supervisée par

**Pr. Sophie DUQUESNE, Pr. Valérie GAUCHER, Dr. Fabienne SAMYN et Dr. David
FOURNIER**

Thèse défendue le 27 septembre 2023, devant un jury composé de :

DR. Véronique BOUNOR- LEGARE	Université de Lyon 1, IMP	Présidente du Jury
Pr. Laurent FERRY	Mines d'Alès, CM2A	Rapporteur
Dr. HDR Sandrine HOPPE	Université de Lorraine, LRGP	Rapporteur
Dr. Damien MONTARNAL	Université de Lyon 1, CP2M	Examineur
Pr. Sophie DUQUESNE	Centrale Lille Institut, UMET	Directrice de thèse
Pr. Valerie GAUCHER	Université de Lille, UMET	Co-directrice de thèse
Dr. Fabienne SAMYN	Centrale Lille Institut, UMET	Encadrant
Dr. David FOURNIER	Université de Lille, UMET	Co-encadrant

« L'avenir de Monsieur est devant lui, et il l'aura dans le dos chaque fois qu'il fera demi-tour. »

Pierre Dac

Acknowledgments

The work presented in this manuscript was carried out in the UMET laboratory (CNRS UMR 8207), led by Prof. Patrice WOISEL. More precisely, most of the experiments and discussions were conducted within the PREF (Procédés de Recyclage et de Fonctionnalisation) team led by Sophie Duquesne and Ulrich Maschke.

First and foremost, I would like to express my sincere gratitude to my supervisors, Prof. Sophie Duquesne, Prof. Valerie Gaucher, Dr. David Fournier, and in particular Dr. Fabienne Samyn, whose invaluable guidance and support have been instrumental in establishing the foundations of this thesis project and bringing it into fulfillment. Without their unwavering dedication and expertise, this work would not have come to fruition.

Of course, what will be a lab without the technical expertise of its engineers, starting with Johan Sarazin, without whom most of the DSC and TGA would be out of order. I really enjoyed our long discussions, technical or not, as well as your availability and the effort you made to help us out of certain predicaments with certain machines. It turns out that I will be defending my thesis first after all! Of course, how could we forget Pierre, whose kindness and joyfulness bring a smile even to the most stubborn of sourpusses. I certainly do not forget Anais for her calmness and interpersonal skills. I would also like to mention Benjamin Dewailly, who as a former lab technician deserves his place in this paragraph. Thank you for the numerous discussions we had during these 3 long years, and our shared passion for aquascaping.

I would like to express my gratitude to Prof. Laurent Ferry and Dr. Sandrine Hoppe for generously dedicating their time and sharing their expertise as examiners to evaluate this thesis. I am also thankful to DR. Veronique Bounor-Legare for accepting the role of jury chair. I would also like to extend my warm appreciation to Dr. Montarnal, who has accepted to be a member of the jury as an examiner, for his valuable expertise in the field of vitrimers, although I regret not having had the opportunity to engage with him earlier in the thesis. His insights and contributions have been highly valuable to the development of this research.

We also extend my sincere gratitude to the rest of the permanent staff of the laboratory: Severine, Maude, Charaffedine, Mathilde, Fanny, Ulrich, Frederic, Serge, Gaele, Nicolas...

Of course, what would a lab be without its interns, fellow doctoral students, postdocs, research engineers, and so on who spice up the daily life of the lab, without whom research would inevitably be duller. It is challenging to do justice to each and every one of them in these limited lines, but I would like to express my deep appreciation for their contributions and remember them fondly. To mention indiscriminately: Melvin, Eric, Guillaume, Jihane, Kevin, Matthieu, Bernard, Nathan, Marco, Paola,

Mingwei, Qi, Xavier, Yue, Lotfi, Julie, Marie-Odile, Manon, Laura, Fei, Alexandre, Aditya... Special thanks to my internship students: Cloé, Ryan and Dalila.

It is impossible for me not to thank my long-time friends, for whom a thesis holds a mystical aspect: Vianney, Hugo, Djaffar, Charles, Julie, Marie, Kenza...

What would a complete being be without their other half, which is why I would like to thank my girlfriend Rebeca, who has been by my side for a good part of these 3 (and a half) years of my PhD journey. Also, my brother, for giving me a glimpse of what a thesis is like and encouraging me to pursue one.

I would also like to extend my heartfelt thanks to my parents, whose unwavering support has been a source of strength and encouragement throughout my life. This thesis manuscript is dedicated to them.

Table of content

General introduction.....	1
Chapter 1 - Towards flame-retarded vitrimer – A bibliographic study.....	5
1.1 Vitrimer: a promising new class of polymeric materials	6
1.1.1 Thermoplastics and thermosets	6
1.1.2 Covalent adaptive networks (CANs).....	7
1.1.3 Vitrimers.....	9
1.1.4 Conclusion.....	13
1.2 Vitrimers based on transesterification reaction	14
1.2.1 Reaction mechanism.....	14
1.2.2 Transesterification catalysis	14
1.2.3 PBT-vitrimers based on transesterification chemistry.....	18
1.2.4 Epoxy-based vitrimers	23
1.2.5 Conclusion.....	26
1.3 Flame retardancy of materials	27
1.3.1 Approaches to flame retard polymer materials.....	27
1.3.2 Major families of flame retardant systems	27
1.3.3 Flame-retardancy of vitrimers	29
1.3.4 Conclusion on flame retardancy of vitrimers	36
1.4 Effect of additives and fillers on the dynamic of reaction in vitrimers	37
1.4.1 Nanoparticles.....	37
1.4.2 Conclusion.....	40
1.5 Additives used to flame retard PBT.....	41
1.5.1 Phosphate esters	41
1.5.2 Phosphonates	42
1.5.3 Phosphinates salts.....	42
1.5.4 Phosphine oxides	43
1.5.5 Red phosphorus	44
1.5.6 Phosphorus- and Nitrogen-based additives	44
1.5.7 Conclusion.....	44
1.6 FR additives used to flame retard epoxy	45

1.6.1	Metal hydroxides	45
1.6.2	Nitrogen-based FR.....	46
1.6.3	Phosphorus-based FR	46
1.6.4	Phosphorus-nitrogen FR.....	46
1.6.5	Intumescent formulations	46
1.6.6	Hyperbranched FR.....	47
1.6.7	DOPO	47
1.6.8	Conclusion.....	48
1.7	Ph.D. objectives.....	48
Chapter 2 - Impact assessment of flame retardant additives on PBT		
vitriimer synthesis and properties		
		51
2.1	Introduction	52
2.2	Experimental.....	52
2.2.1	Material description.....	52
2.2.2	Material processing	54
2.2.3	Characterization.....	56
2.3	Influence of FRs on the formation of a PBT vitriimer	59
2.3.1	Reference system without FR.....	59
2.3.2	Systems with AlPi	65
2.3.3	Systems with ZnPi.....	70
2.3.4	System with HM1100.....	74
2.4	Characterization of the relaxation behavior of the cross-linked systems.....	87
2.4.1	Relaxation of cross-linked vs thermoplastic systems	87
2.4.2	First method: the Maxwell model	88
2.4.1	Stress-relaxation behavior of partially cross-linked systems	91
2.4.2	Second method: the Kohlrausch-Williams-Watts (KWW) model	92
2.4.3	Conclusion on stress-relaxation	96
2.5	Thermal and crystalline characterization of the materials.....	96
2.5.1	Pristine PBT vitriimer system.....	96
2.5.2	20 wt.-% AlPi filled formulations	99
2.5.3	PBT+ZnPi system.....	102
2.5.4	PBT+HM1100 system.....	106
2.5.5	Conclusion.....	108
2.6	Conclusion	109

Chapter 3 - Evaluating the performance of aluminum phosphinate as flame-retardant and transesterification catalyst.....	111
3.1. Introduction	112
3.2. Experimental.....	112
3.2.1. Material description.....	112
3.2.2. Material processing	113
3.2.3. Characterization methods	113
3.2.4. Ageing scenarios	117
3.3. Synthesis of materials without the Zn—transesterification catalyst	117
3.3.1. Reactive extrusion.....	118
3.3.2. Thermal characterization of the materials	121
3.3.3. Rheological behavior	122
3.3.4. Impact of the vitrimer network on the FR dispersion and structure	125
3.4. Evaluation of the performances of the AlPi-based vitrimer	128
3.4.1. Resistance to creep	128
3.4.2. Mechanical characterization.....	131
3.4.3. Flame-retardancy of AlPi-filled vitrimer.....	134
3.4.4. Behavior upon ageing	138
3.4.5. Upscaling PEA ₂₀ vitrimer through continuous reactive extrusion.....	147
3.5. Conclusion	149
Chapter 4: Addition of flame-retardant additives to epoxy-based vitrimer	151
4.1 Introduction	152
4.2 Experimental.....	152
4.2.1 Material description.....	152
4.2.2 Synthesis of flame-retarded epoxy vitrimer	154
4.2.3 Characterization.....	155
4.3 Flame-retarded vitrimer coatings	157
4.3.1 Material aspect and recyclability.....	157
4.3.2 Performance of the flame-retarded vitrimer coatings.....	158
4.3.3 Conclusion.....	161
4.4 Comparing DOPO in reactive or additive way	161
4.4.1 Characterization of the DOPO-based vitrimers.....	162
4.4.2 Impact of recyclability of the DOPO-based vitrimer	165
4.4.3 Rheological and mechanical behavior of DOPO-based vitrimers.....	167

4.4.4	Flame-retardancy of DOPO-based vitrimers.....	169
4.4.5	Conclusion.....	171
4.5	Conclusion	172
	General conclusion	173
	References	177
	Appendix 1 : Generalities on PBT	197
	Appendix 2 : Relaxation curves fitting data	199

General introduction

In recent years, the consumption of plastic materials has been steadily increasing, with polymer-based materials finding applications in various sectors ranging from packaging and construction to automotive and electronics. However, this surge in plastic consumption has also resulted in a significant rise in plastic waste generation, posing challenges for waste management and environmental sustainability. In the *Global Plastics Outlook: Policy Scenarios to 2060*, OECD reports that under current policies, by 2060, the use of plastics (and, consequently, the production of plastics wastes) could almost triple globally, driven by economic and population growth¹. To bend the plastic consumption curve, recycling plastic materials has become a critical aspect of mitigating these challenges and moving towards a circular economy.

Among the various types of plastics, thermoset polymers, which are mainly used for high-end applications^{2,3}, have posed challenges for recycling due to their cross-linked nature, which limits their reprocessability. However, the development of vitrimer materials has emerged as a promising alternative for addressing the recycling issues associated with such type of polymers. Vitrimer materials exhibit unique properties that allow dynamic bonds exchanges and reprocessing, enabling their reshaping and remolding, similarly to thermoplastics. This peculiar characteristic has raised substantial interest and attention within the scientific community since their discovery in 2011⁴, up to reaching few hundreds of publications each year (Figure 1).

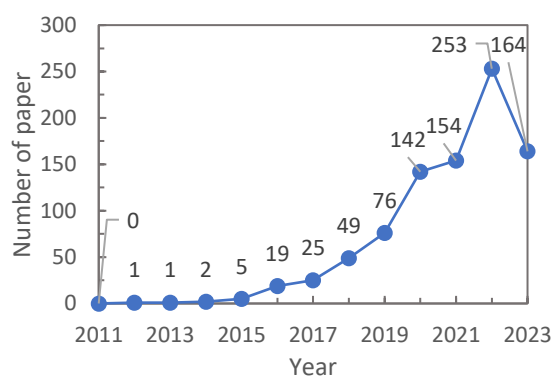


Figure 1 : Number of papers including the term “vitrimer” in their title and abstract, by year since 2011. Those results were obtained using the dimensions.ai database (10.06.2023).

However, even if the chemistry of vitrimers was particularly investigated, the functionalization of such materials is still at its early stages whereas it is crucial to enter the market. Among the various properties required by materials to be used in building, transportation..., flame retardancy has to be considered. In such cases, materials have to comply with stringent safety standards. The regulations or standards ensure that materials or products reach the necessary safety thresholds, encompassing factors such as ignitability, fire behavior, and the emission of toxic gases. To achieve these requirements, flame-retardants moieties are commonly added into the polymer matrix either as additives or through reactive methods (in this latter case the FR moiety is covalently bound to the polymer matrix), before or after polymerization. Flame-retardants is a generic term that refers to a range of divers organic and inorganic compounds, including halogens, nitrogen, phosphorus, sulfur, or metallic salts that will contribute to

prevent or reduce fire growth or spread. In this context, the next step toward industrially relevant vitrimer materials would be to increase their flame-retardancy to ensure compliance with safety regulations and standards, mitigating the risk of fire-related incidents and their potential consequences and this is the main objectives of this PhD thesis.

Interestingly, while much research has been dedicated to the development of vitrimers and their potential applications, there has been relatively little exploration of flame-retardant properties in vitrimer materials. Indeed, only around 20 papers reporting solutions on that topic have been identified (Figure 2) and those papers focus on a reactive approach.

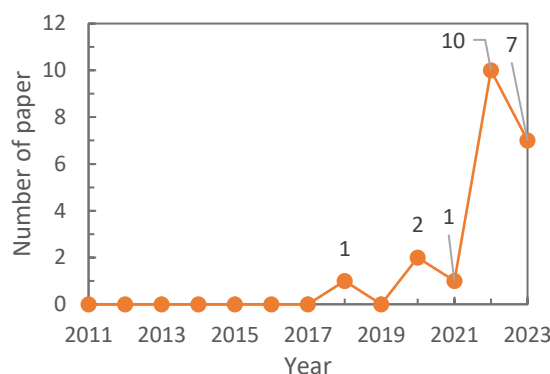


Figure 2 : Number of papers including the term “vitrimer” AND “flame” in their title and abstract, by year since 2011. Those results were obtained using the dimensions.ai database (10.06.2023)

The perceived lack of academic research interest in this field served as the primary motivation for the development of this thesis topic. The combination of flame-retardant properties with the dynamic and recyclable nature of vitrimers presents significant potential in addressing fire safety concerns while facilitating the recycling and reprocessing of polymer materials. Further exploration and understanding of flame-retardant vitrimer systems are necessary to fully harness their advantages and potential applications. Moreover, for flame-retardancy promoted through the “additive approach” (flame retardant additives are added in the formulation but are not linked to the polymer chain), numerous effects have to be taken into consideration. It will be fully considered in this work.

The addition of flame-retardant additives has been investigated in two distinct vitrimer systems, each relying on transesterification as dynamic covalent bond exchange reaction. The first system consists in a poly(butylene terephthalate) matrix cross-linked by dynamic bonds using epoxy. This cross-linked polyester could be used to replace thermosets in its application in E&E on the condition to be flame retarded. Indeed, the cross-linking of PBT can result in improved mechanical performance and enhanced flow resistance. This makes it suitable for applications that require higher performance levels and superior properties. The other system is an epoxy-based vitrimer. Epoxy is widely used in lots of applications as binder for paints, as matrix in composites... Its replacement by a vitrimer equivalent would be particularly interesting in terms of recycling. It is however important to ensure that the flame retardant properties are maintained in the vitrimer material.

The manuscript has been divided into four chapters.

Chapter 1 introduces the concept of vitrimers, highlighting their main characteristics and unique features. The focus then shifts to the transesterification chemistry employed in the vitrimer systems considered in this study. A brief overview is provided of previously developed flame-retarded systems for vitrimer materials, highlighting the limited research conducted on flame-retardant additives in this area. The subsequent discussion explores the influence of certain additives on modifying the vitrimer properties of materials. Additionally, a concise review is presented of commonly used flame-retardant additives for PBT (Polybutylene Terephthalate) and epoxy-based thermosets.

Chapter 2 deals with the impact of adding various FRs to a PBT vitrimer matrix synthesized by reactive extrusion⁵. Two phosphinate salts and one phosphonate thermoplastic were chosen. The impact of those flame-retardants was firstly assessed by quantifying the amount of insoluble fraction left after reactive extrusion compared to reference PBT formulation. Complementary studies were conducted to understand the various side-effect induced by those flame-retardants on the network structure. Then, their influence on the viscosity and, consequently, bond-exchange dynamics was assessed. Finally, the thermal characteristic and crystalline morphology of each material was studied.

In Chapter 3, a deeper investigation was conducted on the most promising flame-retarded vitrimer system, the one comprising aluminum phosphinate as a flame-retardant additive. This part focused on assessing the material's performance. The mechanical behavior was studied through tensile tests. The effectiveness of flame-retarded PBT vitrimer compared to thermoplastic equivalents for commercial applications at different loading ratios and after ageing was also assessed. The advantageous impact of AlPi on the viscosity of the final material will also be studied by proposing the synthesis of novel vitrimers through continuous reactive extrusion.

Chapter 4 finally focuses on the synthesis of flame-retarded epoxy vitrimer through the addition of commercially available flame-retardants. Firstly, a recyclable intumescent epoxy resin coating was synthesized. Then, a study was conducted comparing the effect of adding a well-known flame-retardant to a Phenol-Novolac-epoxy/fatty acid system using either a reactive or an additive approach. The impact of these two approaches on cross-linking reactions and bond-exchange kinetics was analyzed, and the suitability of those solutions was assessed by analyzing their mechanical and flame-retardancy performances.

Chapter 1 - Towards flame-retarded vitrimer – A bibliographic study

1.1 Vitrimer: a promising new class of polymeric materials

1.1.1 Thermoplastics and thermosets

Most of the commodity plastics used in our everyday life are thermoplastics. They are inherently reshapable above a certain temperature enabling their recycling. They are composed of macromolecular chains whose interchain cohesion is ensured by secondary bonds (Van der Waals interaction and eventually Hydrogen bonds) and physical entanglements (if molar mass is high enough). In the equilibrium state, chains are entangled random coils. While at low temperature, the entangled random coils are “frozen”, they can slide relative to each other at high temperature inducing the polymer to flow. In the case of amorphous materials, the macromolecular chains can flow at temperature above the glass transition temperature (T_g), as the thermal energy provided to the molecules allow them to overcome the intermolecular forces and move more easily. In the case of semi-crystalline polymers which contains crystalline arrangements, flow occurs at temperature above the crystal melting. The flowing behavior of thermoplastics allows their great malleability and their numerous processing possibilities. Thermoplastics can be dissolved in an appropriate solvent, as long as the temperature is high enough to shift the equilibrium toward a solution state. One of the weak points of thermoplastics is their limited creep resistance, particularly at high temperatures, due to the weakness of the intermolecular bonds. Also, for demanding applications, industries turn to another category of polymers: thermosets. Thermosets' chains are chemically bonded together by cross-links (Figure 3). They are typically composed of a mixture of monomers (or prepolymers) and hardeners that are cured or cross-linked to form a rigid and durable material with superior properties compared to thermoplastics. Thermosets usually show higher Young's modulus than their thermoplastic counterpart, and their operating temperature can go above 300°C while most of thermoplastics are melted in this temperature range. As such, the behavior of the material, in particular its thermomechanical stability and its resistance to solvents, is greatly improved at the expense of recyclability.

Thermoplastic and thermosets are easily distinguishable regarding their processing methods. Thermosets are usually manufactured from a liquid or semi-solid resin solution containing monomers and hardeners. They then have to undergo a chemical reaction, usually triggered by temperature, called curing or cross-linking that irreversibly transforms them into a rigid and durable state. Thermoplastics need to be raised to temperatures higher than their T_g or T_m , in order to reach a sufficient fluidity to be shaped. They are mainly processed by injection, extrusion, thermoforming, and its derivatives: extrusion-blowing, extrusion-inflation, over-injection... Those techniques usually involve very expensive tooling, but are profitable for large scale production thanks to short cycle times, low quantity of workforce needed, and ease of automation. Thus, while thermoplastics are widely used in packaging, consumer goods, automotive, and construction industries due to their versatility, lightweight, and ease

of processing, thermosets are commonly used in high-performance applications such as aerospace, automotive, and electronics.

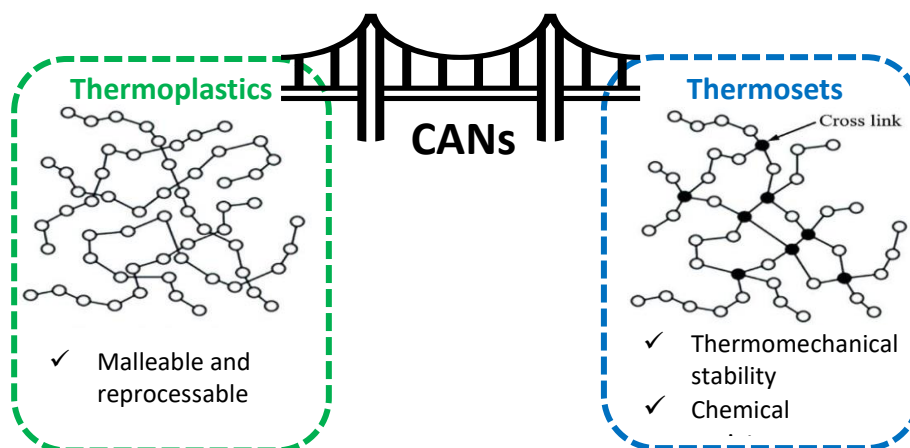


Figure 3: Macromolecular structure and main characteristics of thermoplastic and thermosetting resins. Inspired from ref⁶

The main issue of thermosets comes from their irreversibly cross-linked network, which makes recycling extremely difficult, with only mechanical downcycling (grinding), thermal or chemical recycling being seriously considered⁷. Both are considered for the recovery of the fillers of the composites but recycling of the thermoset resin by itself is poorly reported. The mechanical recycling consists of decreasing the size of the sample to scrap pieces which can be segregated into thermoset-rich powder or fibrous-rich powder, but it represents low-value applications because it does not recover individual fibers, with fiber length greatly diminished. The thermal or chemical recycling implies either the pyrolysis⁸ or chemical processes^{9,10} to break down the thermoset matrix. Since the realization of the impact of human activity on the environment in the early 2000s and the pollution that waste causes on the environment, intensive research to find a solution to obtain thermoset-like materials which could flow at high temperature, ideally above their operating temperatures, rendering them recyclable, has been investigated by the academic and industrial communities. The different solutions that have been reported in the literature are described and discussed below.

1.1.2 Covalent adaptive networks (CANs)

The synthesis of Covalent Adaptive Networks has also been demonstrated as an efficient way to obtain recyclable cross-linked networks. They are a type of polymer network, composed of reversible covalent bonds that can undergo exchange reactions in response to external stimuli such as heat, light, or chemical reagents (solvent, humidity). While inherently cross-linked, CANs are usually categorized as a third class of polymer materials, a bridge between thermosets and thermoplastics (Figure 3). Two different types of dynamic covalent adaptive networks exist¹¹. They differ by the type of mechanism involved: dissociative or associative networks (Figure 4).

Reversible covalent networks, also called dissociative CANs^{12,13}, are based on fully reversible exchange reactions. Under stimuli, the network dissociates into monomers. This leads to a decrease in network density, allowing the matrix to flow or even depolymerize. The flowing behavior of such matrices is consequently directly linked with the equilibrium conversion toward the gel point¹⁴. The shifting of the thermodynamic equilibrium, inducing the formation or the rupture of chemical bonds, depends on the application of a stimulus, which can be light, temperature or acidity. This type of CANs becomes soluble in solvents if network density decreases too much.

Associative CANs, on the other hand, keep the same cross-linking density at any temperature through dynamic exchange¹¹. These bond-exchange reactions enable the exchange of fragments that connect individual polymer chains while keeping the number of chemical bonds in the system constant, thereby preserving the chemical composition of the network. Usually, this includes the formation of short-lived intermediates which will spontaneously fragment, returning to the same functionality while rendering a different connectivity¹⁵. As a result, they facilitate the reorganization of the network's topology without depolymerization. Vitrimers are commonly considered as part of the associative CANs category, whose bond-exchange reactions are triggered by thermal stimuli.

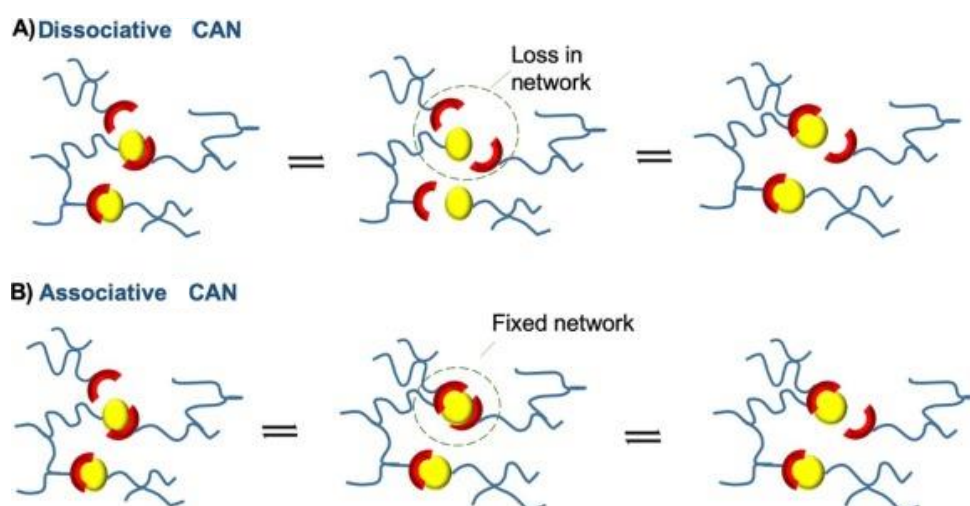


Figure 4: Schematic representation of dissociative and associative CAN Main Covalent Exchange Reactions That Enable Malleability in CANs. Taken from reference¹⁶

The difference between the two types of exchange mechanisms is however not as evident as it appears, particularly for dissociative CAN presenting a short lifetime of the dissociated intermediate state. This was highlighted in the review of Elling and Dichtel¹⁵ on most dissociative exchange reactions. Indeed, in this paper, CAN systems based on typical dissociative bond-exchange reactions such as transalkylation¹⁷ or disulfide exchange¹⁸ displayed a temperature-dependency of their viscosity following an Arrhenius law, characteristic of the vitrimer behavior. These materials are generally referred to in other publications as vitrimer-like materials (Figure 5). In the present manuscript, the term vitrimer will be used for both vitrimer and vitrimer-like materials.

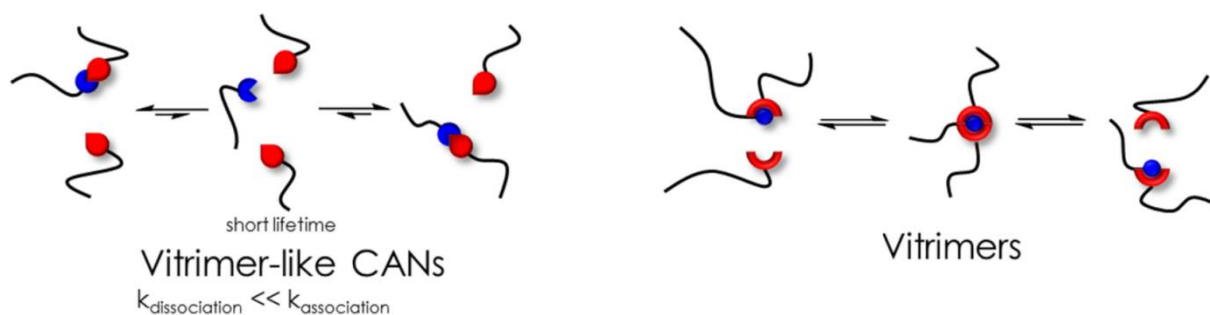


Figure 5: Differences between vitrimer-like CANs (short lifetime of the dissociative intermediate), and vitrimer. Adapted from reference¹⁹

1.1.3 Vitrimers

Vitrimers were introduced in 2011 by the team of Pr. Ludwig Leibler⁴ as a promising material to solve the problem of recyclability found on thermosets, while keeping their advantages over thermoplastics. Consequently, it allows a thermally driven rearrangement of the topology of the network without depolymerization. This gives this class of materials very peculiar properties due to their unique flowing behavior.

1.1.3.1 Vitrimer transition temperature (T_v)

Similarly to the glass transition defining the transition from a hard and brittle state to a soft and rubbery state in amorphous polymers, vitrimers behave as traditional cross-linked thermosets below a temperature called either topology freezing transition temperature²⁰ or vitrimer transition temperature²¹, T_v .

Leibler et al. defined T_v as the temperature at which the viscosity of the material reaches 10^{12} Pa*s, conventionally chosen at the solid-to-liquid transition, and as a point beyond which the occurrence of bond-exchange reactions occurs too slowly to be considered significant⁴. While a correlation could be made between vitrification and the glass transition, they are radically different as most vitrimers exhibit two distinctive T_g and T_v : while T_g is based on the chemical structure of the polymer chain (T_g is the thermal onset of long-range cooperative chain motion between repeating units), T_v is directly linked to the chemical nature and density of bond-exchange reactions. Capelot et al.²² compared different known transesterification catalysts, concluding that the T_v of the vitrimer directly depended on the nature of the catalyst, while T_g remained unmodified. In the case of vitrimer seemingly displaying the same value for T_g and T_v (Figure 6-b), the actual T_v might be lower than T_g , but with the exchange reactions hardly diffusing in the limited chain mobility and lack of free volume of a glassy state, a lower T_v is not visible by usual rheological testing^{6,23}. It follows that T_g is the limiting factor for viscoelastic fluidity. It has also been demonstrated that T_v could be controlled by changing the type and concentration of catalyst used in the systems, effectively tuning the vitrimer to dictate the occurrence of viscous behavior. T_v is usually assessed or extrapolated by stress-relaxation²⁴⁻²⁶, creep-recovery, dilatometry^{4,20,27}, or aggregation-induced-emission (AEI) luminogens²⁸. Moreover, it has been reported that the measure of

T_v can vary between the type of analysis, linked with its strong dependence on the applied stress and heating rate²⁰.

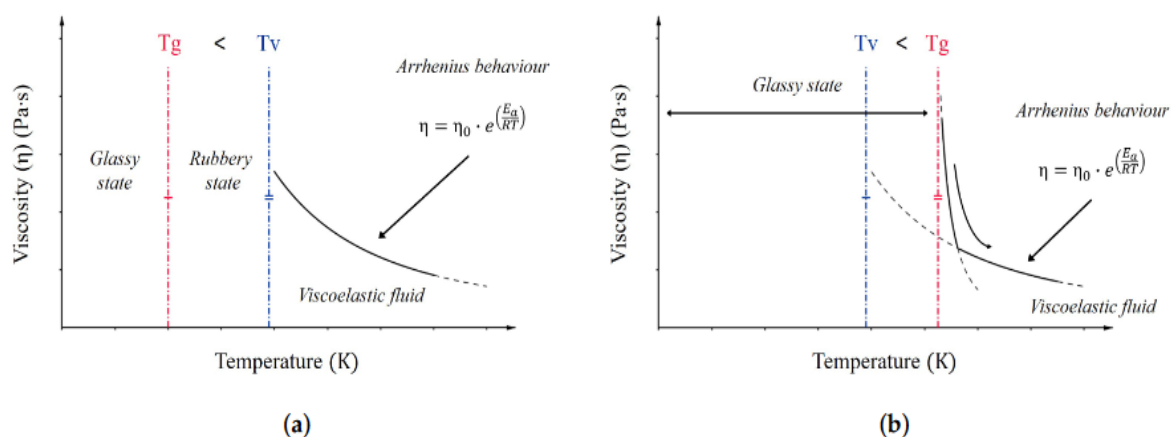


Figure 6 : (a) If $T_g < T_v$, the glassy state can be distinguished from the rubbery state. (b) If $T_v < T_g$, the material starts to flow only above T_g , with significant bond-exchange reactions eventually occurring at higher temperature. Adapted from Alabiso et Schögl⁶ and Denissen et al²³

1.1.3.2 Unique flowing behavior

Vitrimers, like polymers, display mechanical properties that are influenced by both time and temperature due to their cross-linking mechanism based on temperature-dependent reactions. Their viscosity shows an Arrhenius-type dependence on temperature and rheological measurements can be used to determine the chemical activation energy of these materials. The common way to characterize a vitrimer is by analyzing its relaxation to a sinusoidal deformation applied at different frequencies and/or temperature with dynamical mechanical analysis (DMA)^{18,29}, or molten-state rheology^{4,5,30,31}.

Usual amorphous thermoplastics share the same stress-relaxation behavior between T_g and T_g+100 , as their viscosity evolves following the Williams-Landel-Ferry (WLF) theory^{15,32}, due to the macromolecular chains sliding relative to each other in the amorphous phase of the polymer. Besides, they exhibit fast relaxation behavior, under 0.1s, while thermosets depict a limited relaxation linked with their cross-linking density. Some thermosets with lower cross-linking density can relax faster, but never as fast as being able to repair themselves or being reprocessed.

On the other hand, vitrimers are considered as viscoelastic liquid and, as such, are assumed to follow a Maxwell model for relaxation. They exhibit a characteristic relaxation time (τ) to stress with τ usually defined as being equal to $1/e$ (~37%) of the initial deformation value³³. When developing their first vitrimer, Leibler et al. characterized their material as a dynamic cross-linked system that can flow above their T_v , followed by a predictable Arrhenius-dependency toward temperature, similar to silica-based glasses⁴. As, interactions inside the materials are driven by bond-dynamic exchange reactions, its activation energy (E_a), is usually obtained through the Arrhenius equation:

Equation 1

$$\tau = \tau_0 \exp\left(\frac{-E_a}{RT}\right)$$

with τ_0 , T, E_a , and R respectively being the pre-exponential factor (s), the temperature (K), the exchange reaction activation energy (J.mol⁻¹), and the universal gas constant (J.mol⁻¹.K⁻¹).

From this equation, it is possible to obtain the value of the activation energy of a system. Vitrimer usually depicts an activation energy between 30 and 180kJ/mol. This value is very sensitive for vitrimer, as for the same system, it can be modified depending on the used catalyst, the cross-linking density³⁴, the presence of fillers³⁵, or other internal interactions (Van-Der-Walls, oxygen bonds...). Despite the drawbacks that this may provoke, such sensitivity can also be beneficial, as controlling the activation energy to adapt the system to a wide range of flowing gives vitrimer compounds the ability to be specially adapted to demanding applications.

1.1.3.3 Numerous chemistries

The catalog of bond-exchange reactions that enable the formation of vitrimer is rich of a variety of mechanisms. The most common chemistries taking part in vitrimer synthesis are reported in Figure 7 : The transesterification^{4,36,37} and transalkylation^{17,26,38} chemistries involve the exchange of ester or alkyl groups between cross-linkers, while transcarbamoylation^{39,40} utilizes carbamate reacting with a primary or secondary amine to promote bonds exchanges. Disulfide exchange^{41,42} and thiol-ene reactions⁴³ are based on the exchange of sulfur-sulfur or carbon-carbon bonds, respectively. Transamination of vinylogous acyls^{23,30,44,45} involves the exchange of a nitrogen-containing group between a carbonyl compound and an amine. Imine bond exchange chemistry may encompass either transimination, where an amine group is exchanged from one imine group to another, or imine metathesis, where carbon-nitrogen double bonds are exchanged between imine compounds⁴⁶⁻⁴⁸. Other reactions, such as siloxane exchange⁴⁹⁻⁵¹, silyl ether exchange^{52,53}, dioxaborolane metathesis⁵⁴⁻⁵⁶ or olefin metathesis^{57,58} have also been implemented to create vitrimer and vitrimer-like systems. Each of these chemistries has its own set of advantages and disadvantages in terms of reaction rate, temperature dependence, and product properties. This diversity of bond-exchange chemistries provides a versatile platform for the development of vitrimer materials with tailored properties for a wide range of applications.

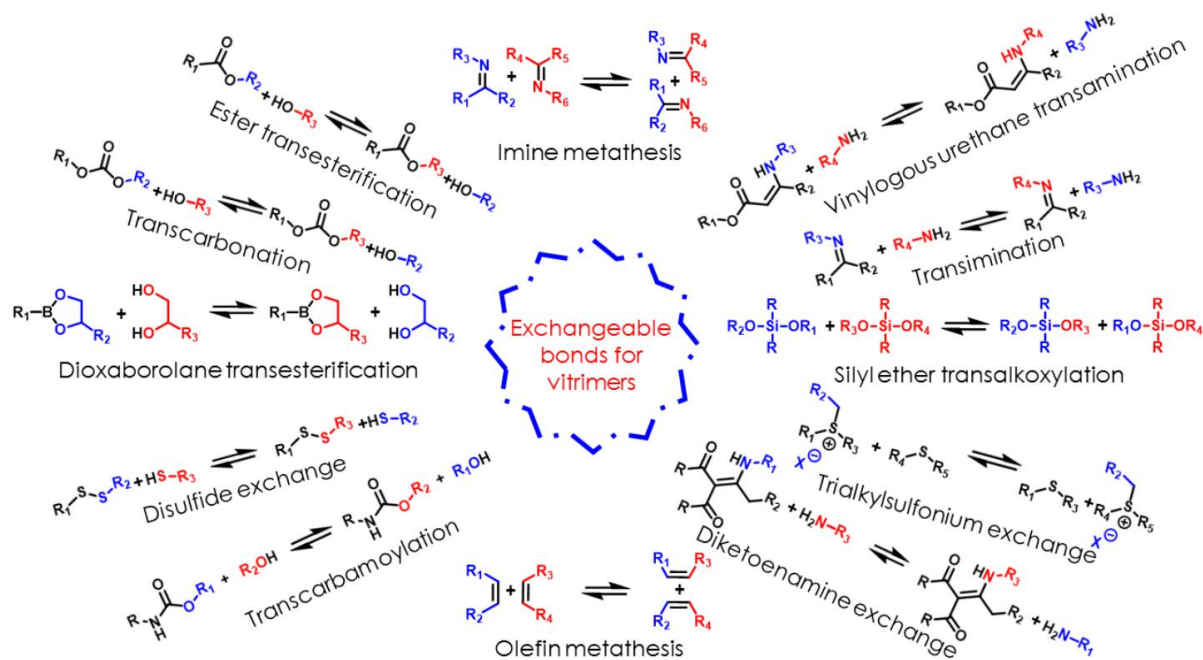


Figure 7 : Main Covalent Exchange Reactions in Vitrimers. Taken from reference¹⁹

1.1.3.4 Synthesis of vitrimers

Two approaches can be used to obtain vitrimer, one involving a mixture of monomers and the other involving the use of polymer chains (Figure 8). When using monomers with functionality greater than two, the resulting vitrimer can display numerous reversible reactions where almost all molecules are covalently linked with at least one other molecule at any given temperature and time, resulting in a high cross-linking percentage of typically 95 to 100% of the material weight. Following the second approach, vitrimer may be considered the cross-linking of commodity polymers. Vitrimer made from polymer chains has a lower cross-linking density as it is limited by the number of pendant reactive functions per chain. The objective of such approaches is to improve the properties of the polymer (thermoplastics can be made stiffer and more durable) while keeping its recyclability. A pioneering series of vitrimer studies was carried out for polyesters by incorporating the trans-esterification bond exchange mechanism^{5,59,60}. Polyester-based vitrimers have shown promise in applications such as coatings, adhesives, and biomedical materials, where the combination of thermoplastic behavior and reversible cross-linking provides unique properties and processing advantages. Overall, tuning thermoplastics into vitrimers is an effective way to offset some inherent flaws of those materials, like low mechanical behavior, low viscosity^{5,61}, or solubility^{5,62}. Especially, the crystallinity of some thermoplastics may lead to unique behavior like triple-shape memory effect^{62,63}.

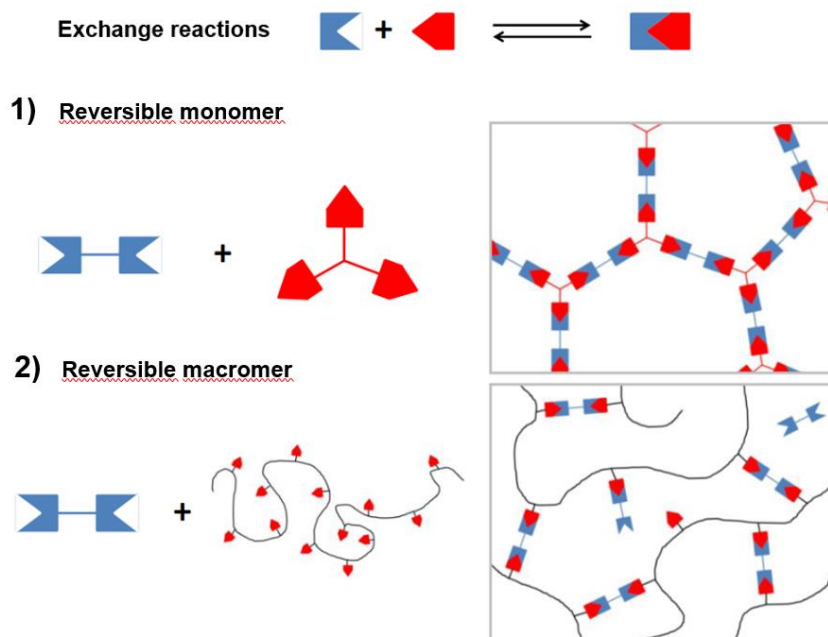


Figure 8 : Formation of a vitrimer obtained through (1) the reaction between two monomers; 2) the cross-linking of a polymer chain with previously grafted functional groups. Scheme adapted from reference⁶⁴

1.1.4 Conclusion

Vitrimers represent a new class of materials presenting good mechanical properties^{65,66} while maintaining its reprocessability. In the field of thermoset materials, the development of such material represents a significant advancement. These materials offer a unique combination of desirable properties such as high strength, chemical resistance, and thermal stability, while also providing the crucial advantage of recyclability. The concept was also applied to commodity polymers including thermoplastics to improve their mechanical properties such material becoming competitive with high performance materials including thermoset. Among the different vitrimers chemistry, transesterification offers a promising way for developing dynamic materials with unique properties. Dynamic transesterification reactions (DTER) have been firstly reported and is largely studied in the literature, becoming the most widespread vitrimer chemistry. In addition to being the reaction governing the network dynamics of the first synthesized vitrimer⁴, the transesterification mechanism could be easily applied to a large variety of thermosetting polymer matrices, including epoxy resins, or vitrimerized thermoplastic resins, including poly(butylene terephthalate)⁵, poly(lactic acid)⁶⁰ or poly(ethylene)⁶⁷. Moreover, transesterification can benefit from a high reaction temperature, usually over 120°C, paving the way for the development of new recyclable rigid polymers with high service temperatures. In the following part, we will thus be focusing on the category of vitrimers whose network dynamics are driven by transesterification.

1.2 Vitrimers based on transesterification reaction

1.2.1 Reaction mechanism

Transesterification consists of the reaction between the sp^2 carbon atom of an acyl group undergoing a nucleophilic attack by an alkoxide group (Figure 9). A tetrahedral intermediate is formed, which can either revert to the starting configuration or to a transesterified product. Three types of transesterification are known^{68,19}: ester-alcohol (alcoholysis), ester-acid (acidolysis) and ester-ester type (genuine transesterification). In the case of vitrimer, DTER was first applied to thermoset-like networks, synthesized in bulk. Originally, two different types of matrices have been synthesized: a hard matrix comparable in chemistry to usual vitreous epoxy thermoset materials, and a soft matrix whose behavior was close to elastomeric compounds⁴. Both matrices rely on the condensation of an acyl group (acid for the elastomeric-like matrix and anhydride for the hard-type matrix), with hydroxyl groups (usually originating from epoxy resins).

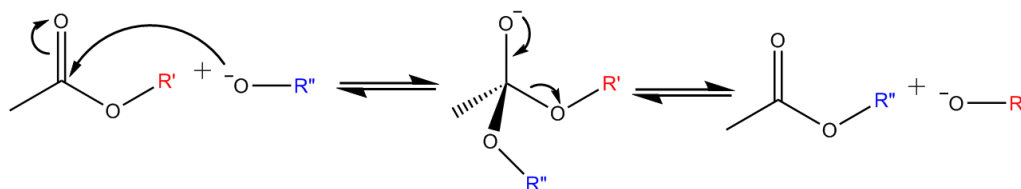


Figure 9: Mechanism of transesterification

As thermally dependent reactions, the kinetics of the bond-exchange reactions relies on high temperatures to be effective within reasonable time frames. However, side reactions, like nucleophilic substitution, elimination, or oxidation are also thermo-dependent and can decrease the dynamic properties of the network. Exchange reactions must therefore be accelerated to reduce the heating time required to repair or shape a part, and thus preserve the integrity of the material. The most general approach to obtain and drive dynamic exchange kinetics is to use catalysis, that can manipulate exchange rates or mechanisms.

1.2.2 Transesterification catalysis

Since the 40s, transesterification has been intensely used for biodiesel fuel production and the synthesis of polyesters among others. Thus, numerous transesterification catalysts have been already developed before the conceptualization of vitrimer. Different categories of catalysts are found for vitrimer synthesis, external, internal catalyst and neighboring group catalysts (Figure 10). The main catalyst used for the synthesis of vitrimers are reported below.

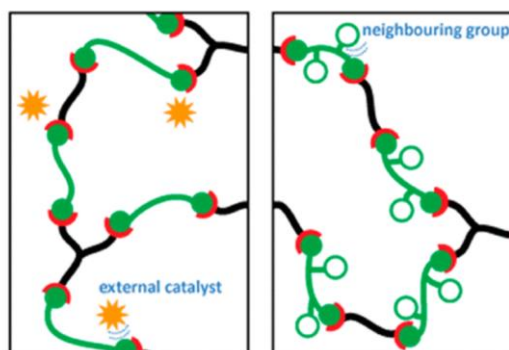


Figure 10 : Mode of action of an external catalyst compared with neighboring group catalyst⁶⁹

1.2.2.1 Internal catalysts

Internal catalysts involve the action of the functional group within the reacting molecule itself to facilitate the reaction. The functional group acts as a catalyst by participating directly in the reaction, promoting bond formation or breaking. For vitrimer, it revolves around adding one of the reactants in large excess so that the cross-link is constantly surrounded by reactive moieties to trigger bond-exchange without the addition of any catalytic elements.

Altuna et al. were the first to report a vitrimer back in 2013 without the addition of any extrinsic catalyst. Epoxidized soybean oil (ESO) was reacted with citric acid (SA) as hardener⁷⁰, obtaining a cross-linked network with β -hydroxyester groups and vicinal diols groups. However, the relaxation rate of the network was slow, 5.5h to reach 1/e of initial modulus at 160°C compared to 1h for Leibler et al.⁴.

Zhang and coworkers reported a vitrimer with DTER provided by internal catalysis thanks to multifunctional hyperbranched reactants providing a large number of accessible hydroxyl groups. They first synthesized a hyperbranched epoxy (HBE) containing abundant free hydroxyl groups by reacting bisphenol A epoxy resin with trimethylolpropane⁷¹. Free hydroxyl groups could then react with succinic anhydride (SA), forming an efficient DTER network without the need for catalysts. The material displayed a high T_g (96°C after curing for 48h) and could relax at lower temperatures (120°C) than previously reported epoxy/anhydride vitrimer. The main drawback of HBE was its high viscosity of 8400 Pa.s at 60°C, rendering it unadapted for low-viscosity demanding applications like coatings. In their following work⁷², they added extra DGEBA during the curing step, increasing cross-linking density and effectively considering HBE as a modifier rather than the main reactant of the bulk matrix (Figure 11). After curing, a 1:1 DER/HBE/SA mixture could relax in 67 min compared to 775 min for their previous HBE/SA, thanks to the higher number of ester bonds. The material exhibited promising performances as coating agent. They also worked on the synthesis of another epoxy-anhydride with graphed glycerol as curing agent and promoter of hydroxyl group⁷³. The material exhibited fast transesterification and good reparability at high glycerol loading (1/e reached in 85.6 min at 180°C for a 1/0.5 epoxy/glycerol network), but at the expense of a lower cross-linking density and T_g .

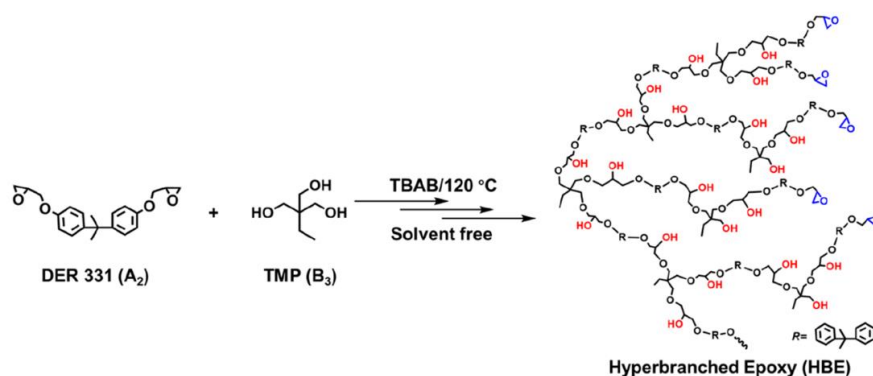


Figure 11 : Synthesis of a hyperbranched epoxy. The epoxy-rich environment obtained allows for internally catalyzed transesterification⁷²

1.2.2.2 Neighboring group participation (NGP)

Neighboring group participation, involving the presence of a catalytically active group in the backbone of the network chains enhancing the reactivity of the reaction site, can promote DTER. This approach eliminates the need to address issues related to poor compatibility, inadequate dispersion, and chemical instability. Several activating groups have already been studied to promote DTER (Figure 12).

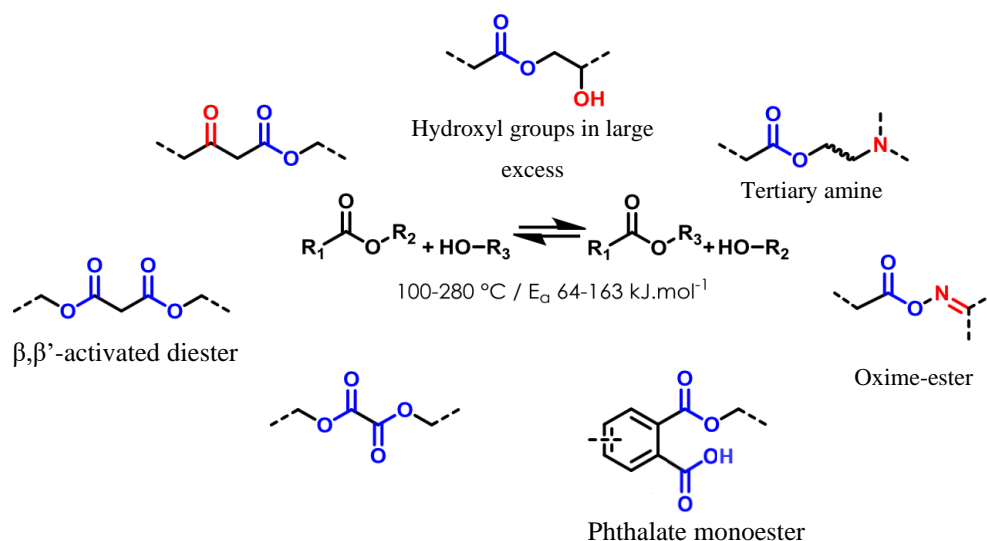


Figure 12 : Examples of activating groups that promote DTER. The temperature range used for stress-relaxation experiments, as well as the range of activation energies calculated for exchange reactions in vitrimer is provided. Adapted from reference

Russell et al. developed a poly(oxime-ester) (POE) vitrimer through photoinitiated thiol-ene click chemistry⁷⁴. The lower pK_a of oxime chemistry compared to aliphatic alcohol could carry out transesterification in a POE vitrimer without the need of external catalysts. Several POE networks were synthesized through photo polymerization with different ratios of monomer. They exhibited roughly the same activation energy as the model molecules (~65 kJ.mol⁻¹), with relaxation times ranging from ~ 5100 to 2725 s at 100°C with free oxime hydroxyl groups content increasing from 0% to 5%. Besides, they were insoluble in organic solvents above T_v while being reprocessable without loss of mechanical properties.

Altuna et al reported a vitrimer obtained by in-situ formation of tertiary amines issued from the reaction of bisphenol-A epoxy with either secondary or primary amines, cross-linked once again with a mixture of citric and sebacic acid⁷⁵. The material depicted eight times faster relaxation times with secondary amine (dibutylamine) than with primary amine, attributed to lower cross-link density and higher mobility of single-bonded tertiary amine.

Another team cross-linked amorphous polyesters bearing numerous carboxyl group side groups with tetra epoxy compounds bearing tertiary amines⁷⁶. The catalyst effect of the tertiary amines was evidenced in comparison with similar cross-linked systems, which could not relax with classic epoxy compounds. The cross-linking density played a major role in bond exchange rates compared with amino group concentration. Later, they synthesized a polyester precursor bearing both tertiary amino groups and carboxyl groups⁷⁷. Once cured with diepoxy cross-linker, the material could relax stress 20 times faster than their previous material.

Delahaye et al. combined the NGP effect of both tertiary amines and phthalate monoester to obtain very fast relaxations (relaxation reached in 1 second for their fastest network)⁷⁸. They even succeeded in processing the material through a mini-extruder. However, they showed that phthalate monoesters were relatively sensible to hydrolysis, as the material breaks down into small flakes in hot water (80°C).

1.2.2.3 External catalysts

External catalysts, unlike the two previous categories, are effective catalytic compounds that are not linked with covalent bonds to the matrix. Their main purpose is either to discriminate one potential reaction or to lower the barrier for the rate-determining reaction step in the uncatalyzed pathway. Those interactions between the matrix and an external catalyst alter the kinetics of an exchange reaction and permit the conception of a strong temperature-dependent network. The chemical nature of external catalysts may vary from Brønsted/Lewis acid and bases^{79,80} to metallic salts^{60,81}.

Most reported catalysts include tin(II) 2-ethylhexanoate ($\text{Sn}(\text{Oct})_2$)⁸², zinc(II)(acetylacetonate) ($\text{Zn}(\text{acac})_2$)⁵, as well as organic bases such as triphenylphosphine (TPP)²² and 1,5,7-triazabicyclo[4.4.0]dec-5-ene (TBD)⁸³. Zn (II) catalysts are commonly used thanks to their high thermal resistance as well as their solubility in fatty acids. Demongeot et al.⁸¹ studied the coordination and catalysis of Zn^{2+} in an epoxy/acid vitrimer and showed that Zn^{2+} can exert catalytic action toward transesterification even at a low concentration by stabilizing alkoxide groups, activating ester carbonyl groups, and bringing reactive groups closer to each other. Many research groups are currently developing and optimizing new catalysts for vitrimer chemistry. For example, Niu et al. reported the synthesis of a poly(acrylonitrile-co-zinc methacrylate) (Zn-PAM) synthesized by random copolymerization of zinc methacrylate and acrylonitrile with promising results⁸⁴. Under the same loading content, its catalytic effect, used on a DGEBA/sebacic acid network, proved to be more efficient than TBD and $\text{Zn}(\text{ac})_2$, efficiently catalyzing transesterification even at low loading (~ 0.75 mol%). Most epoxy vitrimers require a high catalyst concentration (from 5 mol% on epoxy/acid to 10 mol% on epoxy/anhydride).

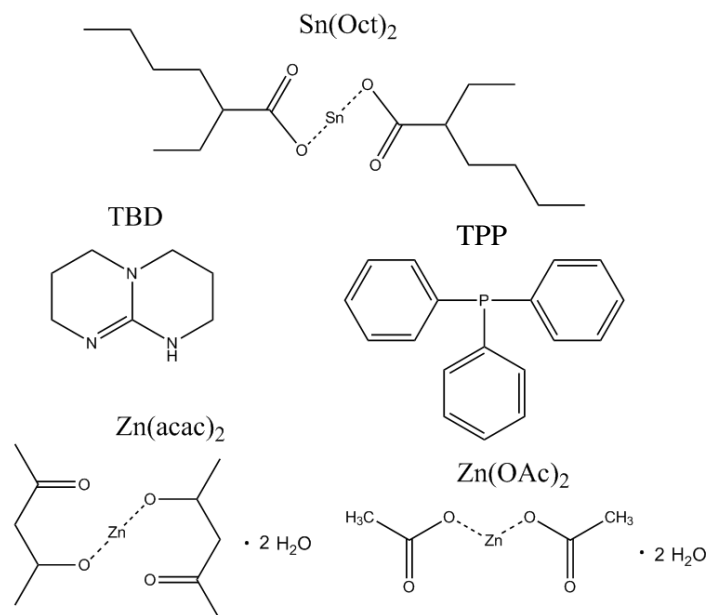


Figure 13: Common catalysts used to monitor transesterification in vitrimer. From top to bottom and left to right: Tin(II) 2-ethylhexanoate ($\text{Sn}(\text{Oct})_2$), 1,5,7-triazabicyclo[4.4.0]dec-5-ene (TBD), triphenylphosphine (TPP or PPh_3), zinc acetylacetonate dihydrate ($\text{Zn}(\text{acac})_2$), zinc acetate dihydrate ($\text{Zn}(\text{OAc})_2$)

1.2.2.4 Conclusion

Various catalytic systems were used to synthesize vitrimers considering transesterification as an exchange reaction. Even if the approach consisting in the use of neighboring group catalysts has been developed to answer the problems of long term stability of external catalyst, knowledge on this topic remains scarce and the systems developed following this approach are complex. Moreover, by using an external catalyst, it is easy to play with its quantity to change the kinetics of bond exchange. This approach will thus be followed in the present work. The next sections of this report describe the different approaches and chemistries that have been developed for the synthesis of Poly(Butylene Terephthalate) (PBT)- and epoxy-based vitrimers considering transesterification chemistry.

1.2.3 PBT-vitrimers based on transesterification chemistry

Poly(Butylene Terephthalate) is a semi-crystalline thermoplastic in which chains are naturally weakly entangled due to its low molar mass (see Appendix 1 for further details). This renders the material weak to extensional deformation and its viscosity becomes too low to withstand high strain. This behavior prevents the material from being used in processing techniques requiring elongation flows, like blow molding, foaming, film, or sheet extrusion. Several methods have been implemented to improve the melt strength of PBT without impacting its recyclability. During polymerization, further solid-state polycondensation steps allow to reach very high molecular weight, and polydispersity to improve melt strength. Supplementary chain extension steps can be conducted by reactive extrusion with bifunctional chain extenders, like diepoxide⁸⁵. However, increasing the molecular weight of PBT above its critical

molecular weight M_c , proved to be difficult. Dynamic cross-links were also considered in PBT matrix to increase the melt strength, while maintaining processability. This is further described in the following part.

1.2.3.1 PBT vitrimer synthesised by solid-state polymerization (SSP)

Zhou et al developed a semi-crystalline vitrimer based on PBT and glycerol, a ring-opened analogue of epoxy groups³⁴. The reaction is reported in Figure 14. It occurs in a two-step (co)polymerization by solid-state polymerization (SSP) at 180°C, i.e. below the melting temperature of PBT (~ 225°C). In presence of $Zn(acac)_2$, they obtained a high degree of incorporation of the glycerol within the polymeric system, obtaining a highly cross-linked material. As the SSP occurs below the melting temperature of PBT, cross-linking only occurs inside the amorphous phase, thus the crystallinity is conserved. Interestingly, melt temperature increases up to 23°C with increasing reaction time, which was attributed to a thickening of crystalline lamellae induced by the thermal annealing during the cross-linking process.

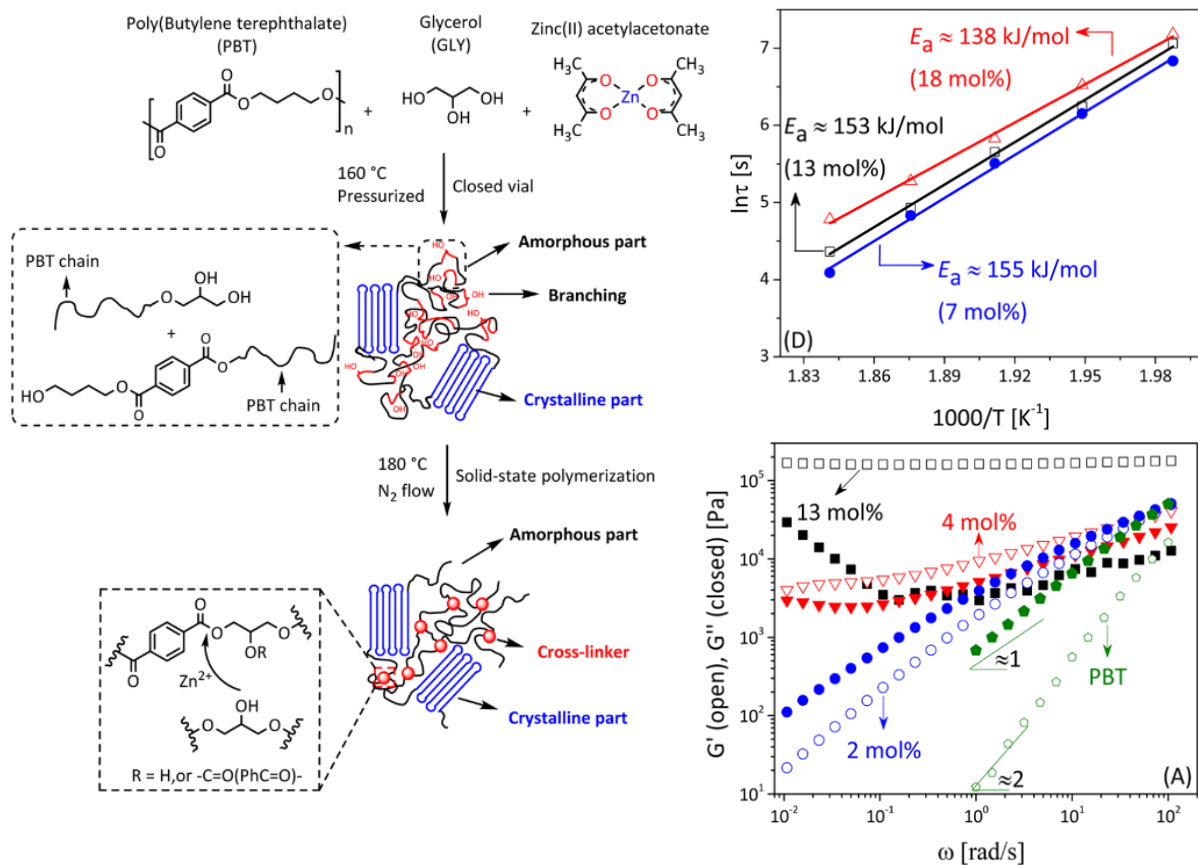


Figure 14 : Left: Synthesis route of a PBT/glycerol vitrimer by a two-step SSP process. Firstly, esterification of carboxyl end groups occurs, with possible elimination of 1,4-butanediol. Then, cross-linking and recombination occurs by transesterification. Right: Arrhenius plots of the stress-relaxation times and frequency dependence of G' (open symbols) and G'' (filled symbols) at 240°C, in function of glycerol loading ratios. Adapted from reference³⁴

Compared to neat PBT, the storage modulus E' of all vitrimers exhibit a second plateau above their T_m , due to the cross-linked network. Besides, the value of the plateau was clearly dependent on the cross-

linking ratio and thus on the quantity of glycerol added. Cross-linking density also increases T_g . Oscillatory frequency tests showed interesting results, with a notable difference in storage moduli between low and highly cross-linked networks. When glycerol content is higher than 7 mol%, G' depicts a constant plateau, characteristic of a fully cross-linked material⁸⁶. They observed a direct correlation between cross-linking density and relaxation times, with 37% relaxation obtained at 57s with 7 mol% glycerol, and 120s with 18 mol% glycerol. Those values are much lower than usual relaxation times found elsewhere in the literature for epoxy/acid networks thanks to the flexibility of the thermoplastic backbone and lower cross-linking density. Wide-angle X-ray diffraction showed that the PBT/glycerol-based vitrimer exhibited the same triclinic α -crystal structure of neat PBT. They also found that catalyst concentration does affect the relaxation behavior of the matrix, with higher Zn(II) catalyst content leading to lower relaxation times⁸⁷. Besides, activation energy was conserved between each catalyst concentration at 150–170 kJ mol⁻¹, except the lowly catalyzed formulation that reached 200 kJ mol⁻¹. Keeping the same catalyst-to-cross-linker constant, increasing the overall cross-linking density of the network increases relaxation time without affecting activation energy. Panagiotopoulos et al⁸⁸ aimed at optimizing the PBT/glycerol-based protocol developed by Zhou et al. They found the optimal solid-state temperature to be 180°C, obtaining a material with the highest cross-linking content and melt strength. At this temperature, the higher amount of cross-linker and catalyst could be added to the system without initiating thermal decomposition of the polymer and catalyst, thus obtaining better properties. They also conserved the same semi-crystallinity as their reference PBT (34%) since the cross-links were segregated in the amorphous phase of the polymer during SSP, while T_g drastically increased from 35°C to 97°C. However, if temperature rises above T_m , glycerol moieties in the cross-linked structure have a nucleation effect, which tends to lower the energy barrier for crystallization (T_c) and reduces both crystallinity and crystallization rate.

In another work⁸⁹, Zhou and coworkers tried to cope with the high viscosity of PBT vitrimer (up to 10⁷ Pa.s at 250°C) by controlling the network formation with the help of protection–deprotection chemistry. They used benzaldehyde protection chemistry to convert pentaerythritol into 5,5-bis(hydroxymethyl)-2-phenyl-1,3-dioxane (BPO) before introducing it into the PBT backbone by SSP. Then, they either removed the benzal group by treatment with trifluoroacetic acid (TFA), obtaining pendant-free hydroxyl groups on the polymer chain eager to promote cross-linking and transesterification thanks to the Zn(II) catalyst (Figure 15). Interestingly, they found out that cross-linking could be obtained without the TFA treatment thanks to the presence of OH-bearing terminal carboxylic acid groups in the material. Gel point was reached faster with TFA-deprotected PBT/BPO samples (17min vs 65min for 1.0 mol% BPO). After curing, both materials exhibited the same gel fraction of around 76% and solid-like behavior (i.e., $G' > G''$). Increasing BPO content leads to a higher cross-linked network depicting longer relaxation times³⁴, with TFA-deprotected samples relaxing faster. Vitrimer obtained by both deprotection approach have an energy activation of 230-250 kJ mol⁻¹ with 3.5 mol% of BPO, which is much higher than their previous work on PBT/glycerol vitrimer, as well as

reported values in the literature for epoxy/acid networks^{4,5,90}. Two other protection groups were studied, exhibiting various gelation times. Those results open the way for tunable process-induced deprotection chemistry to control the cross-linking density of the vitrimer network and the duration of the pregel period, promising for fast processing using current extrusion or injection molding equipment of PBT vitrimer.

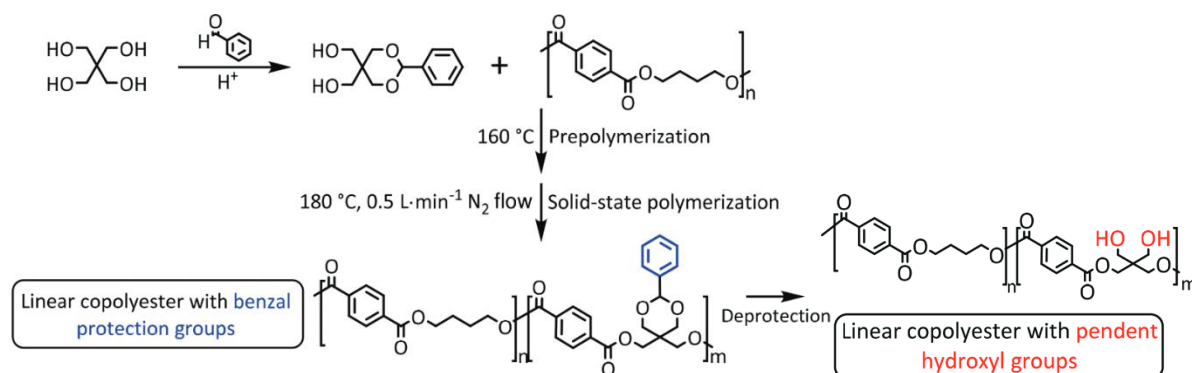


Figure 15 : Benzaldehyde protection–deprotection chemistry used to synthesize PBT/pentaerythritol-based vitrimer via solid-state (co)polymerization (SSP). Adapted from reference⁸⁹

1.2.3.2 PBT vitrimer by reactive extrusion

To develop an industrially viable process to chemically transform thermoplastics into vitrimer, Kar et al, in their paper “Scalable upcycling of thermoplastic polyolefin into vitrimer through transesterification”⁶², have listed several challenges which have to be overcome. One of the key factors is to find an easily upscalable process able to cope with the high demands of the thermoplastic industry. This process should be used for the synthesis of high performance vitrimer through both pristine and recycled polymers. Nowadays, reactive extrusion is seen as the most promising process that could overcome this challenge.

Demongeot et al were the first to develop a cross-linking method based on reactive mixing and extrusion⁵. They based their synthesis on the addition of DGEBA to a commercial PBT, with either zinc(II) acetylacetonate (Zn(acac)₂) or 2-methylimidazole (2-MI), a known catalyst for the epoxy–acyl addition reaction. Epoxy resin was preferred over the highly volatile glycerol as epoxy allows chain extension and branching without releasing small molecules (Figure 16) which would not be extracted during the reaction. While 2-MI could better promote chain extension by grafting DGEBA to PBT than Zn(acac)₂, it did not catalyze transesterification as no cross-linking occurred. On the other hand, Zn(II) catalyst effectively catalyzed transesterification, with a reaction occurring under 10 minutes in the extruder. Various cross-linking densities could be obtained by tuning the amount of DGEBA and Zn(II) catalyst. Besides, PBT with lower molar mass leads to faster reaction, higher cross-linking density, and higher G' plateau for fully cured samples.

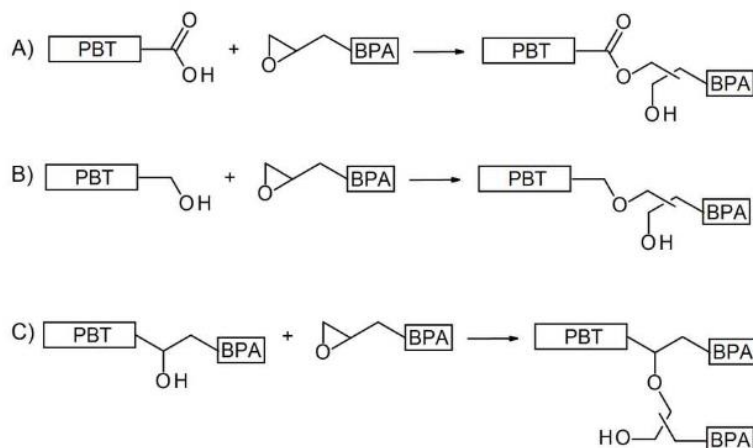


Figure 16 : Possible addition reactions between reactive mixing of PBT/epoxide: Esterification of carboxyl end group (A) and etherification of hydroxyl end groups (B); Branching from the secondary hydroxyl groups produced from reaction (A) and (B). Adapted from reference⁵

During synthesis, two concurring effects impacted crystallinity: cross-linking, which is detrimental to crystallization, and as developed by Panagiotopoulos et al⁸⁸, epoxy moieties have a nucleation effect. Compared to vitrimer synthesized by SSP^{34,88}, reactive extrusion is conducted at temperatures above T_m , thus the impact of cross-linking on crystal formation is significant. At low loadings of epoxy, cross-linking and nucleation compensate each other, resulting in a crystallinity roughly equivalent to neat PBT. However, at high loading of epoxy, the nucleation effect does not increase while cross-linking density still increases. Thus, the PBT vitrimer with a gel ratio of 74% exhibited a lower crystallinity compare to neat PBT. This material could withstand 30 minutes in the oven at 250°C without flowing, while precursor PBT flowed within a minute. This shows that the relatively slow transesterification reaction radically improves dimensional stability above T_m . Thus, the authors showed multiple possibilities to control the relative kinetics of chain extension, chain branching, and cross-linking by choosing the right catalyst, the molecular weight of the precursor PBT chains and the suitable diepoxide content.

Most of the studies conducted on semi-crystalline thermoplastics were focused on the characterization of the material above T_m ^{5,53,60}. Farge et al aimed at assessing if the improvement of vitrimer mechanical behavior remained visible in the solid-state, between T_g and T_m ^{91,92}. They synthesized PBT vitrimer using the same method developed by Demongeot et al.⁵. Monotonic tests, applied at different temperatures, shows that vitrimer could deform plastically with a uniform strain over the entire sample during the whole duration of the tests, while PBT precursor showed a characteristic necking due to chain elongation. Furthermore, the phase during which strain localization occurs decreases with increasing cross-linking density. This absence of necking was associated with a strain-hardening increase due to two complementary effects: decrease of chain length between bond-exchange reaction centers, and the pre-orientation of the network induced by injection molding of the highly viscous polymer. The authors also proposed a synthesis route allowing for the production of any vitrimer

based on thermoplastic precursors on a larger scale by a two-step process¹³⁰. A first step consists of the production of pre-vitrimer by continuous reactive extrusion by limiting the reaction time inside the extruder, preventing the risk of a steep rise in viscosity, which could stop the extruder. This step was followed by curing the pre-vitrimer above T_m inside a rheometer. While it is a promising solution to cope with the high melt viscosity of vitrimer materials, the curing step has yet to be applied to a batch of pre-vitrimer materials.

1.2.4 Epoxy-based vitrimers

Epoxy-based thermosets offer several advantages that make them widely used in various applications, like their excellent mechanical properties, chemical resistance, adhesive properties, thermal stability and electrical insulation. Thanks to these advantages, a wide range of formulations is now available on the market. However, most epoxy-based vitrimers exhibit high modulus and a brittle behavior, which limits their use in applications requiring high flexibility or impact resistance. Besides, once cured, those thermosets are rarely repairable, and cannot be reshaped or remolded, which implies that both the matrix and potential fillers are very hard to recycle and reuse.

Considering these challenges, epoxy-based resins were the first category of thermosets considered for the development of vitrimers⁴.

1.2.4.1 Epoxy-acid

Leibler and al. synthesized the first DTER vitrimer by curing in bulk a diacid and triacid mixture (Pripol 1040) with bisphenol-A epoxy resin (DGEBA), combined with 5 mol% zinc acetate ($Zn(OAc)_2$) as catalyst. Several side reactions can occur during the curing step, rendering the epoxy-acid reaction hard to monitor^{93,94}. Thus, catalysts are usually added to prioritize the ring opening of the epoxy. The three-membered ring of epoxy presents a high degree of tension and is thus active and easy to be opened. They chose a 1:1 acid:epoxy stoichiometry, obtaining a material rich in repeating units containing both β -hydroxyl ester and hydroxyl functions (Figure 17) whose bond-exchange reactions are triggered at high temperatures. They obtained an elastomer-like network ($T_g=20^\circ C$) that could rearrange its topology in the presence of exterior mechanical stress thanks to ester exchange reactions. This rearrangement was highlighted by the ability of the material to be reshaped at high temperatures by compression molding, injection molding, or even deformed to obtain complex shapes.

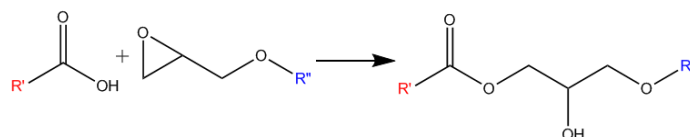


Figure 17: Mechanism of the reaction between an epoxide and carboxylic acid

The main drawback of the newly-found material was the kinetics of relaxation. Its very high viscosity, even at high temperatures, prevented it from being processed by usual thermoplastic means, mainly

extrusion, and gives a hard time for injection molding. Indeed, with a 10mol% of $\text{Zn}(\text{OAc})_2$, the polymer needed several hours to relax its stress at 150°C , with an activation energy of $80 \text{ kJ}\cdot\text{mol}^{-1}$ and a T_v of 53°C . Capelot, Montarnal et al. conducted several studies on the effect of the nature of the catalyst and their impact on the healing and assembling of epoxy vitrimer^{22,36}. Besides, through their use of hydroxyl ester and diester model-molecules, they highlighted the key role of hydroxyl groups on the kinetics of transesterification³⁶. At 150°C , full transesterification with hydroxyl ester groups occurred within two hours. Only 50% of exchanges were obtained after 30h between hydroxyl ester and diester. No exchange occurred between two diester after 24h. The presence of numerous hydroxyl groups is thus mandatory to achieve fast transesterification. Then, they compared different known transesterification catalysts, $\text{Zn}(\text{OAc})_2$, TBD and TPP to the epoxy-acid vitrimer, obtaining three vitrimers with distinct T_v and activation energy (Figure 18). Other studies followed, conducting extensive studies on similar formulations, especially the influence of reprocessability⁹⁵, welding^{96,97}, and stoichiometry⁹⁸. For example, Yu et al.⁹⁸ published on the effect of stoichiometry on the glass transition temperature of the material, and established a correlation between the rise of T_g and the higher thermal energy needed to obtain similar stress-relaxation times.

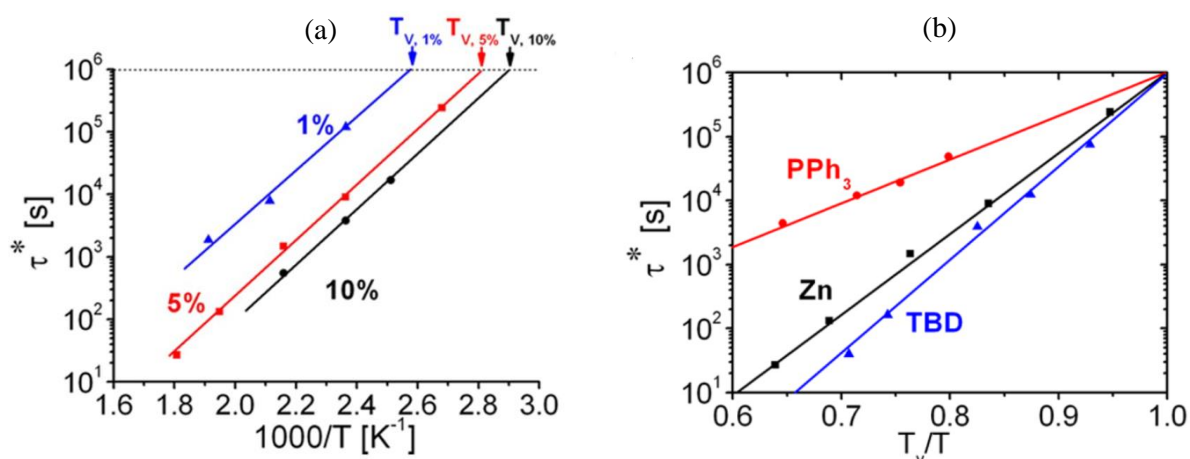


Figure 18: (a) Arrhenius plot of the measured relaxation times for 1, 5, and 10 mol% of $\text{Zn}(\text{Ac})_2$. (b) Angell fragility plot normalized at T_v obtained by Capelot et al. for an epoxy-acid vitrimer system with three transesterification catalysts

Chen et al.⁹⁰ aimed at tailoring the mechanical properties of an epoxy-acid vitrimer matrix by adding a 1,4-cyclohexane dicarboxylic acid (CHDA) to a mixture composed of sebacic acid (SA) and bisphenol-A (DGEBA) epoxy using TBD as catalyst. SA/DGEBA matrix behaved like an elastomeric material, with high elongation at break, low tensile strength, and low Young's modulus. Meanwhile, adding CHDA to the mixture radically changed its physical properties. For a vitrimer prepared using a 80/20 ratio between SA and CHDA, the glass transition increased from 31 to 40°C , while over a 70/30 ratio, the vitrimer mechanical behavior effectively turned into a hard and brittle plastic-like behavior, including a longer relaxation time due to the increased stiffness of the vitrimer backbone. Those results show that epoxy vitrimer can be tunable by incorporating different varieties of hardener without losing the recyclability.

1.2.4.2 Epoxy-anhydride

Leibler and al. also worked on the synthesis of a second epoxy DTER vitrimer, called “hard network”, based on an epoxy-anhydride system⁴. They added to the bisphenol-A epoxy used for their precedent material a cyclic anhydride, catalyzed with Zn(acac)₂. Compared to industrial applications, where the epoxy:anhydride ratio ranges from 1:0.8 to 1:1, they used a ratio of 1:0.5. Indeed, transesterification needs the presence of hydroxyl groups, and the addition-esterification reaction between epoxy and anhydride does not promote the formation of new hydroxyl groups. Thus, effective vitrimer with an epoxy-anhydride network can only be obtained when an excess of epoxy is present³⁶. The reaction can be divided into three steps (Figure 19). Firstly, nucleophile groups, mainly present within the enol function of the acetylacetonate or water from the catalyst, will open the oxirane functions of the epoxides (a). Then, the presence of the newly formed hydroxyl groups will provoke the opening of the anhydrides, forming carboxylic acids (b). Finally, this newly formed acidic compound will open an epoxy ring to form a diester and a new hydroxyl group (c). At the end of the alternated ring-opening polymerization of anhydrides and epoxy rings, the excess of epoxide groups introduced on purpose will homopolymerization, forming a material rich in both ester and hydroxyl groups (d).

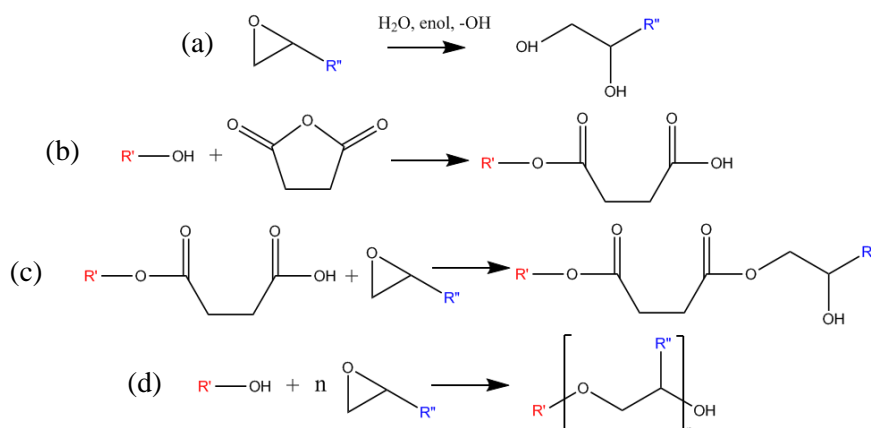


Figure 19: Reaction mechanisms between epoxides and anhydrides. Step (c) will be able to react to other anhydrides and propagate the reaction until total consumption of the reactants. Then, homopolymerization of excess epoxy will propagate hydroxyl groups by ring opening.

Liu et al⁹⁹ synthesized an epoxy-anhydride vitrimer based on eugenol-derived biobased epoxy. While their 1:0.5 epoxy/anhydride epoxy ratio mixture exhibited fast stress-relaxation, shape-changing, and crack-healing, they could not obtain a reprocessable material with stoichiometric ratios of 1:1 and 1:0.7 as their transesterification rates were too slow due to a lack of hydroxyl groups⁴⁶. A major drawback that came with vitrimer and other self-healing materials is their low T_g¹⁰⁰. Usual epoxy-based thermosets depict T_g higher than 100°C, while DTER vitrimer networks studied so far had a T_g lower than 60°C, glutaric anhydride-BPA epoxy systems being the exception¹⁰¹. This can be explained by two reasons. The first one is, as explained previously, that having a high curing agent/epoxy ratio does not leave enough reactive hydroxyl groups to enable transesterification. The second one is the higher network rigidity brought by the use of rigid chains like anhydride and higher cross-linking density, limiting the

mobility of polymer chains and leading to higher relaxation times⁹⁰. The aforementioned team thus developed a biobased triepoxy (TEP) by grafting vanillin and guaiacol to form a triphenol which was then epoxidized (Figure 20)¹⁰². The obtained TEP had a viscosity equivalent to bisphenol A epoxies at 90°C, allowing it to be used as a reagent in usual epoxy processes when heated. By curing this TEP with an anhydride on a 1:1 epoxy/anhydride equivalent ratio, they obtained a material with very high T_g of 187°C, 30°C higher than BPA epoxy thermosets. The material was able to repair a crack within 10 min with 10 mol% Zn catalyst, thanks to sufficient number of hydroxyl groups present to ensure transesterification, and the non-coplanar structure of the TEP epoxy which provided free volume, allowing a greater mobility of the polymer chains at healing temperature. In a more recent study, a high T_g of 140°C was obtained by curing tri- and tetra-functional amino glycidyl epoxy monomers with glutaric anhydride¹⁰¹.

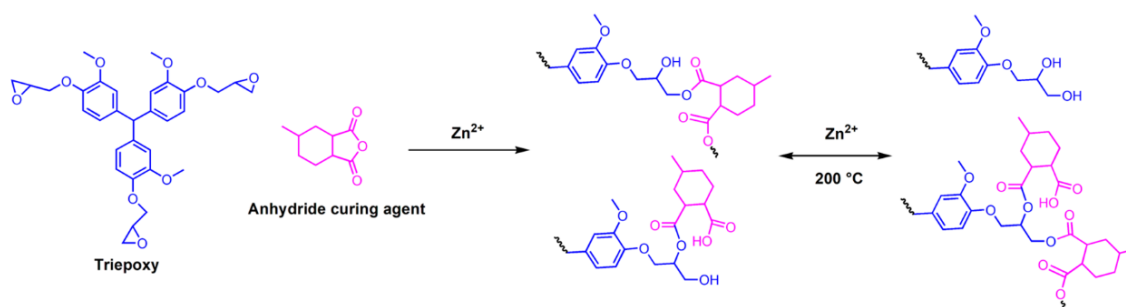


Figure 20: Curing reaction of TEP and anhydride, followed by transesterification reactions. Taken from reference¹⁰²

1.2.5 Conclusion

Various vitrimer systems based on DTER have been documented in the literature. In the case of PBT, it enhances thermal stability, resistance to creep, while the flexible thermoplastic structure facilitates bond-exchange reactions, thereby maintaining its reprocessability and recyclability. Additionally, the material can be synthesized using reactive extrusion, a potentially scalable process that paves the way for industrial manufacturing. Epoxy-based vitrimers were widely considered in the literature, answering the issue of reprocessability of thermoset material. However, while those studies reported the synthesis and mechanical as well as rheological properties of vitrimers, only few of them considered their functional properties such as the flame retardant properties that are needed for such materials to enter the market. The following section of this manuscript will thus review the papers dealing with flame-retarded vitrimer after a brief presentation of the different families of flame retardant existing on the market and the different existing approaches.

1.3 Flame retardancy of materials

1.3.1 Approaches to flame retard polymer materials

It is first important to note that flame retardancy of materials and in particular of polymer may be achieved following two different approaches, similarly to what was reported in the case of catalysis. Additive flame-retardants can be chemically bonded to the polymer, resulting in improved compatibility and durability of the flame-retardant effect. On the other hand, flame-retardancy can be achieved through the addition of specific chemical compounds which are blended or mixed with the polymer resin, either in liquid or solid form. This second method is more suitable for industrial applications as it is relatively easy to adapt according to the materials and processing methods. Furthermore, it is possible to adjust the desired performances based on the regulatory requirements of different sectors by varying the amount of additives (yield ratios from 5 to 60 wt.-%). However, for these flame retardants added in an additive manner, considerations of aging, homogeneity, and interfacial compatibility must also be taken into account. An example of additive and reactive pathways for phosphorus-containing flame-retardants is illustrated in Figure 21.

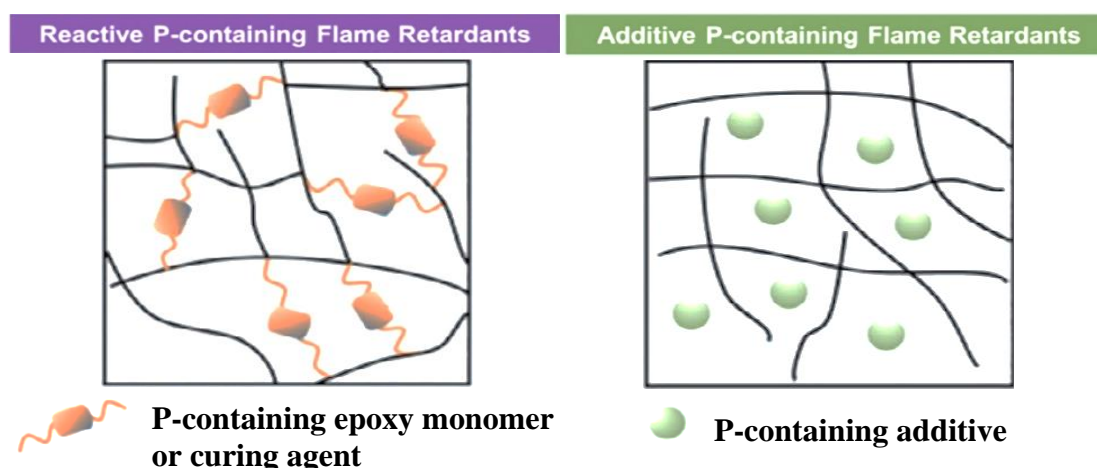


Figure 21 : Examples of application pathways for phosphorus-containing flame-retardants. Adapted from ref⁴⁰³

1.3.2 Major families of flame retardant systems

The following paragraph provides an overview of the major families of flame-retardants, including halogenated flame-retardants, phosphorus-based compounds, metal hydroxides and intumescent systems.

1.3.2.1 Halogenated FR

Halogenated based flame retardants contain elements such as bromine or chlorine. They exhibit excellent flame-retardant properties by scavenging free radicals and interfering with the chain reaction necessary to interrupt a fire propagation. Their cost-effectiveness, availability and good compatibility with many polymer matrices results in its use in highly demanding sectors like electrical and electronic

fields until the middle of the 2000s¹⁰⁴, with excellent flame retardant capabilities at around 10 wt.-% loadings, sometimes combined with other flame-retardants like antimony oxide^{105,106}. However, their hazardous effect on human life and on the environment¹⁰⁷ leads them to be progressively withdrawn from the market, encouraged by the Registration, Evaluation, Authorization and restriction of CHemicals (REACH) regulation.

1.3.2.2 Phosphorus-based FR

Phosphorus-based flame retardant materials belong to an extensive family, such as phosphates, phosphonates, phosphinates, phosphine oxides and phosphorus-nitrogen compounds. Those compounds are containing various levels of phosphorous oxidation^{108,109}, with their structure defining their activation in the gas phase or the solid/condensed phase by the formation of active scavenger radicals in the gas phase and enhancing the char formation in solid phase.

1.3.2.3 Metal hydroxides

Metal hydroxides are cost-effective, readily available, non-toxic, and environmentally friendly. Metal hydroxides exhibit a condensed phase mechanism, where they decompose into metal oxides and water upon exposure to heat¹¹⁰. This highly endothermic decomposition process absorbs energy from the ignition source, as the released water evaporates cooling the surface of the polymer while diluting the decomposition gases. The remaining metal oxides create a protective layer on the surface of the polymer, acting as a barrier that hinders further decomposition. This barrier reduces the heat release rate and limits the release of toxic gases.

1.3.2.4 Nitrogen-based FR

Nitrogen-based flame-retardants can act as flame retardants by releasing inert gases that dilute the flammable gases and reduce the combustion temperature. They are usually added in combination with other flame-retardants^{111,112} or by combining several nitrogen-containing FRs.

1.3.2.5 Intumescent formulations

Intumescent systems are unique flame retardant formulations that expand when exposed to heat or flames. A scheme of the intumescent char layer formation is presented in Figure 22. These systems typically consist of a combination of a carbon source, an acid source, and a blowing agent. Upon heating, the carbon source undergoes a chemical reaction, releasing gases that cause the formation of a protective and insulating char layer. The carbonaceous char layer acts as a protective shield, impeding the transfer of heat from the fire source to the substrate and effectively preventing additional degradation of the underlying material¹¹³.

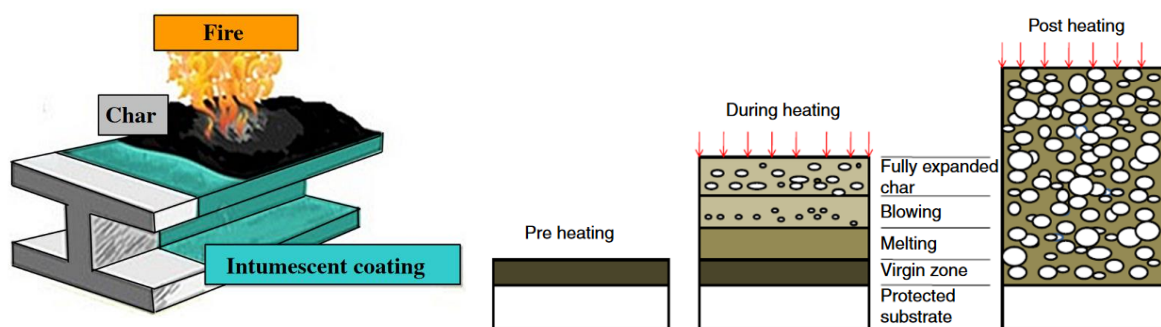


Figure 22 : Schematic representation of the intumescence process¹¹⁴

1.3.3 Flame-retardancy of vitrimers

Even if the flame retardancy of polymers is widely investigated on the literature, only few papers are interesting in applying the approaches and chemistry related before to improve the flame retardant properties of vitrimer. Acrylate, imine, urethane, epoxy and very recently PBT have been considered. The studies dealing with those systems are described in the following section.

1.3.3.1 Flame retardancy of acrylate vitrimers

Feng et Li have succeeded in developing a UV-curable, recyclable, and flame-retarded vitrimer via catalyst-free mixed transesterification of a UV-curable phosphate diester-based acrylate cross-linker¹¹⁵. They used a commercially available dimethacrylate monomer containing a phosphate diester structure, bis[2-methacryloyloxy]ethyl] phosphate (BPA) (Figure 23). Compared with a conventional 1,6-hexanediol dimethacrylate (HDA) cross-linker, the BPA shows higher tensile strength and toughness than its HDA counterpart thanks to a high number of hydrogen bonds combined with a high cross-linking density leading to a mechanically robust thermoset network. Besides the good recyclability of such CANs, the BPA vitrimer showed a fast extinguishment of the flame and the presence of an intumescent residue, which did not appear with the flame retardancy test with HDA. The BPA sample started burning after 12 seconds ignition and extinguished after 15s while the HDA sample burned out completely, and thermogravimetric analysis showed the presence of a 39 wt.-% residual char at 485°C compared to 9.4 wt.-% for HDA.



Figure 23. Performance comparison between the conventional cross-linker (HDA) and the dynamic phosphate diester-based cross-linker (PBA)¹¹⁵

1.3.3.2 Flame retardancy of polyimine and polyimide vitrimer

Zhang and coworkers reported the use of a cyclophosphazene, bearing aldehyde groups, for an application in the flame-retardancy of polyimine vitrimer⁴⁶. They aimed at synthesizing a moderately functionalized cyclotriphosphazene in order to avoid a brittle-like behavior of fully functionalized cyclotriphosphazene caused by high density of cross-links^{48,116}, limiting also its reprocessability and avoiding side reactions induced by using multifunctional groups cross-linker^{117,118}. The cyclophosphazene was prepared by a two-step substitution reaction, firstly with sodium phenolate, and then by a sodium salt containing aldehyde groups to limit the number of aldehyde to an average of three per cyclophosphazene. The obtained cyclophosphazene (Figure 24) was then reacted with two types of aromatic diamines at different loadings to form a recyclable cross-linked vitrimer by imine exchange bonds ($E_a = 59-77 \text{ kJ.mol}^{-1}$). The material still exhibited a relatively brittle behavior (elongation at break, $\epsilon_b=8-16\%$, tensile strength $\sigma_m=44-56 \text{ MPa}$), especially with higher loading of diamines, due to both increase of rigid imide and higher cross-linking density⁴⁷. The presence of phosphazene in the vitrimer allowed for remarkable flame retardancy properties, with easily passed V-0 UL94¹ classification and LOI values $>34 \text{ vol.-%}^2$, reaching above 40 vol.-% with the highest loading of phosphazene. The authors classed their vitrimer in the family of intumescent materials, thanks to the formation of a phosphate-rich protective barrier, like other studies on cyclophosphazene suggest^{48,116,119,120}. They also described a flame-retardant mechanism in the condensed and gaseous phase, with non-combustible gas diluting the oxygen concentration around the material. The same approach to flame-retard vitrimer was developed by Yang's team, using bio-based reactive. A hexasubstituted cyclotriphosphazene (HVP) was synthesized from lignin-derived monomer vanillin and hexachlorocyclotriphosphazene¹²⁰. They reacted their FR with several types of alkyl- and alkoxy-containing diamines, obtaining a cross-linked network composed of reversible imine bonds formed from Schiff-based reactions¹²¹. The material had similar mechanical behavior as the one synthesized by Zhang et al.⁴⁶ despite the use of a high-functionalized cyclotriphosphazene ($\epsilon_b=6-16\%$; $\sigma_m=35-57 \text{ MPa}$), thanks to the linear chain structure of the diamines limiting its brittleness. Overall, the fire performances of the polymer networks mainly depended on the nature of the diamines, with alkyl-containing diamines exhibiting excellent flame retardancy (28 vol.-%LOI, V-0 UL-94), while alkoxy-containing diamines were flammable networks. This was attributed to the oxygen present in the backbone of alkoxy diamines, which upon combusting, produced more gases and limited the formation of a thick carbon layer, insufficient to extinguish a flame after removing the burner.

¹ The UL-94 test is a standardized test method used to assess the flammability of plastic materials. From worst to best classification: N/C, V-2, V-1 and V-0.

² The LOI (Limiting Oxygen Index) test is a measure of the minimum concentration of oxygen required to sustain combustion of a material.

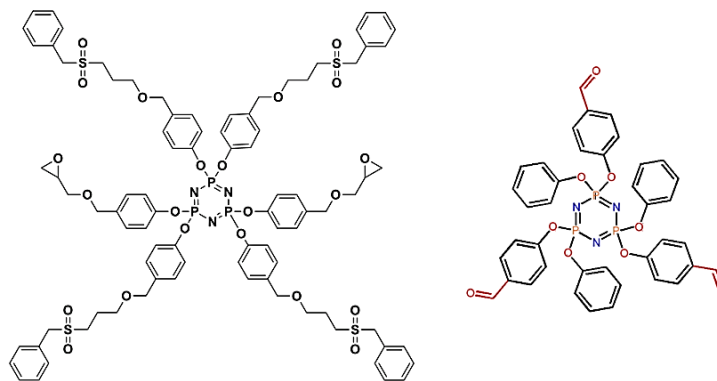


Figure 24: Cyclotriphosphazene synthesized by Zhou et al.¹¹⁶ and Zhang et al.⁴⁶

A recent patent reports the addition of a wide range of additives on a imine-based oligomer cured with various epoxides¹²². The samples formulated with flame-retardants additives obtained various UL-94 classifications results depending on the nature of the filler and the loading (from 10 to 60 wt.-%), but reprocessability was maintained for all samples after curing. To our knowledge, no additional investigation was carried out regarding the rate of cross-linking and bond-exchange reactions in presence of FR additives.

1.3.3.3 Flame retardancy of polyurethane vitrimers

Markwart and coworkers have developed a phosphonate-based flame retardant vitrimer through vinylogous polyurethane chemistry¹²³. Compared with an analog phosphorus-free vitrimer, they had a higher residual char of 8 wt.-% at 700°C and a V-2 UL-94 rating. The cone calorimeter³ test showed a reduction of the total heat released (THR) by 27% and peak heat release rate (pHRR) by 33% between the phosphonate-containing vitrimer and the reference vitrimer. Besides, the phosphate-containing matrix was used for the preparation of glass-fiber reinforced composites and showed encouraging results, reaching similar bending strength and modulus than fiber-reinforced permanently cross-linked epoxy resins¹²⁴ and a good load transfer from the polymer to the fibers.

³ The cone calorimeter test is a method used to evaluate the flammability and fire behavior of materials by measuring heat release, smoke production, and other fire-related parameters under controlled conditions. Parameters typically measured include heat release rate (HRR), total heat release (THR), peak heat release rate (PHRR), time to ignition (TTI), mass loss rate (MLR) and smoke production rate (SPR).

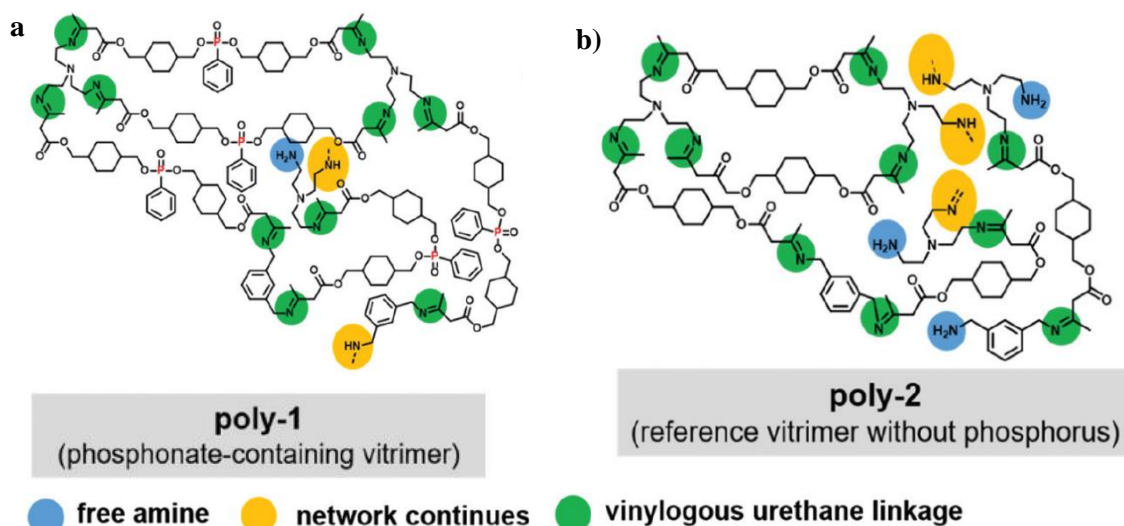


Figure 25 : (a) Phosphonate-based flame retardant vitrimer issued from the formation of the vinylogous polyurethane network by polycondensation with amines. (b) Reference vinylogous urethane without phosphonate. Taken from reference⁶.

1.3.3.4 Flame retardancy of epoxy vitrimers

Epoxy vitrimers was the first system for which flame retardant performance was reported and optimized. Zhou and coworkers¹¹⁶ synthesized a cyclolinear cyclotriphosphazene-linked bifunctional epoxy resin and combined it with an aromatic diamine hardener, which was previously reported associated with DGEBA in obtaining an epoxy vitrimer¹⁸. The synthesized vitrimer based on reversible exchange of aromatic disulfides using cyclotriphosphazene-linked bifunctional epoxy showed promising flame retardancy behavior with UL94 V0 rating, LOI of 30.5 vol.-% and 43.3 wt.-% residue at 800°C. Comparatively, the DGEBA resin with exchangeable disulfide cross-links did not reach any UL94 rating, had a LOI of 24.1 vol.-%, and only 15.3 wt.-% of residue at 800°C.

Among other papers dealing with the flame retardancy of epoxy vitrimers, Liu et al. achieved flame-retardancy of a catalyst-free itaconic acid-based epoxy vitrimer by using phytic acid, a biobased, phosphorus-rich (28 wt.-%P) component issued from distilled plant tissues¹²⁵. They compared their results with a control vitrimer composed of DER 331 epoxy resin and phytic acid cross-linked by phosphate without carboxylate. For all their formulations, they obtained a brittle material (strain < 3.5%), with no evident loss in mechanical properties after recycling. Compared to previously studied carboxylate reactions without catalysts, the phosphate reaction dynamic exhibited faster relaxation rate and lower activation energy, which the authors attributed to the presence of P-OH bonds catalyzing the transesterification. UL94 V-0 classification was easily obtained even for the lower phosphorus-content formulations (4.17 wt.-%P) with fast self-extinguishing behavior, as well as high LOI values (>30 vol.-%). DER based resin would generate toxic black smoke due to benzene rings, which were absent when burning itaconic acid-based epoxy resin.

In another work, Feng et al. developed a β -hydroxy phosphate ester based vitrimer¹²⁶ that has good mechanical behavior, malleability and recyclability (Figure 26). The high content of phosphate provided

by the phosphate monoester makes it significantly safe to fire. The material auto-extinguished itself after 12 seconds under a flame, and could not be re-ignited thanks to the formation of a compact char layer of phosphoric acid composed of P-O-C and P-O-P groups. During the first ignition, the flame disappeared after 12s without switching off the burner. Based on previous studies¹²⁷, phosphoric acid char has a naturally condensed nature, which can prevent the combustible gas from diffusion while cutting the oxygen supply. Zhou and coworkers have then used this vitrimer as a fire- and corrosion-proof coating for steel. The covered steel plate's temperature reached only 250°C with a gas burner while a bare plate's temperature could go up to 750°C. The char forming ability of the vitrimer rapidly lead to a low thermal conductive cellular char layer on the steel plate surface, thus protecting the steel from high-temperature flame.

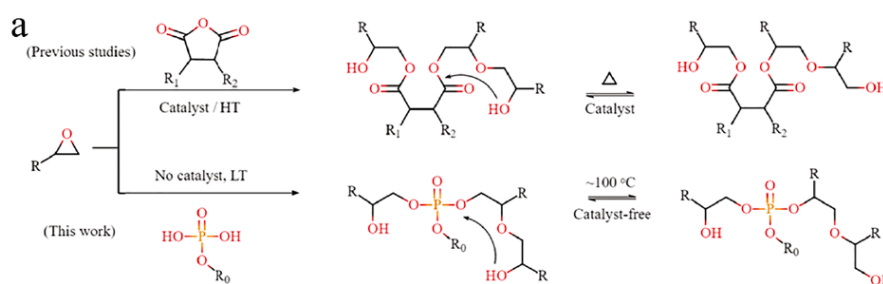


Figure 26: Comparison between curing conditions and exchange reactions of carboxylate esters and phosphate esters¹²⁶

Very recently, Gaan et al. reported a phosphonated thermoset network whose internal transesterification could occur through the presence of dynamic phosphonate ester (P–O) bonds¹²⁸. The network was composed of DGEBA pre-reacted with a phosphonate-containing reagent (bis spiro H-phosphonate (TDPSD)) and cured with an aliphatic amine. Providing a sufficient amount of phosphonate ester was present, reparability, self-healing and recycling could be triggered. At 6 wt.-% phosphorus loading, the material could be fully recycled within only 5min at 160°C in a hydraulic press. Flame retardancy is also greatly enhanced compared to DGEBA-aliphatic amine thermosets, with 75% pHRR and ~31% THR reduction, as well as V-0 classification reached with only 2.5 wt.-%P loading. The material also exhibited promising flame-retardant performances as coating on medium-density fiberboard (MDF).

Ren and coworkers also very recently addresses the issues of flammability and waste disposal in carbon-fiber composites by incorporating a diol containing phosphinate, tertiary amine, and primary hydroxyl structures into a conventional DGEBA-anhydride curing system¹²⁹ (Figure 27). Higher loading of diols significantly increased relaxation thanks to the additional primary hydroxyl and tertiary amines. The covalently bonded phosphinate group significantly improved flame-retardancy, with the material achieving a UL-94 V-0 rating as well as a LOI value of ~33 vol.-% for 0.30 mol% diol. Compared to pristine DGEBA-anhydride, THR decreased by 44% and pHRR by 44%.

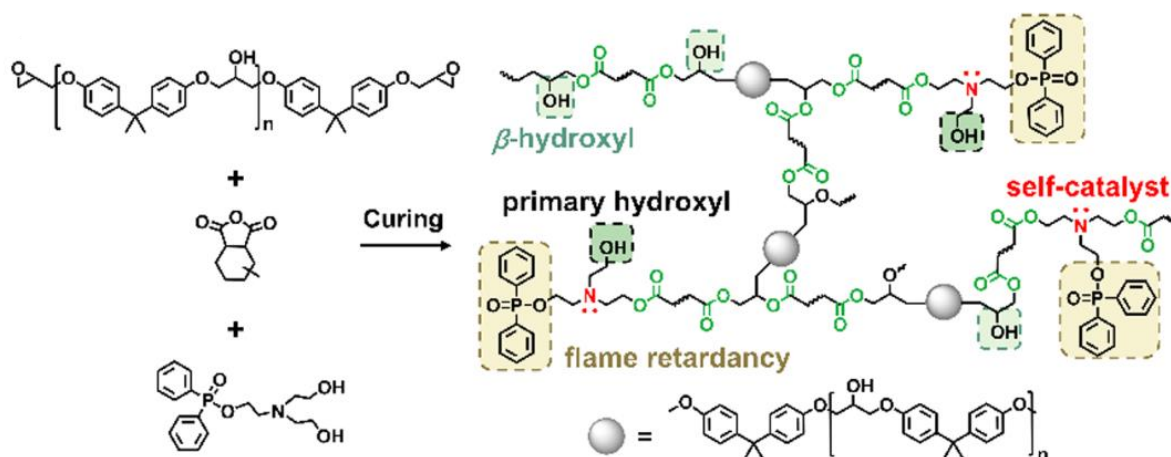


Figure 27 : Curing reaction of an epoxy-anhydride network containing phosphinate groups. Primary hydroxyl and tertiary amines trigger transesterification by neighboring group participation (NGP). Taken from ref²⁹

DOPO (9,10-dihydro-9-oxa-10-phosphaphenanthrene-10-oxide) is a versatile flame-retardant, known for, among other things, improving the flame retardancy of epoxy-based materials. Due to the high reactivity of the O=P-H bond, DOPO can undergo reactions with a variety of chemicals^{130–132}. This allows for the preparation of various DOPO derivatives using straightforward synthetic approaches. Li et al. synthesized a recyclable epoxy composite based on disulfide metathesis bond-exchange reactions whose flame-retardancy was assured by grafting DOPO on the DGEBA before curing with 4-Aminophenyl disulfide⁴². The consumption of a fraction of the oxirane groups during the reaction (Figure 28) leads to a lower amount of available epoxides, leading to a diminution of the cross-linking density, decreasing the final T_g of the material. They conducted fire tests on recyclable epoxy resin (REP) with a 1 wt.-% to 4 wt.-% DOPO loading. REP-DOPO presented higher LOI and UL94 compared to its pristine counterpart. With 4 wt.-% DOPO, LOI rises from 21.7 vol.-% to 29.5 vol.-%. UL94 presented a V-2 rating with 2 wt.-% DOPO and a V-0 rating for 3 wt.-% and more. Those good results are explained by the DOPO's ability to scavenge the free radical, leading to the suppression of the flame combustion process^{133,134}. Cone calorimeter also shows the flame-retardancy ability promoted by the presence of DOPO, leading to a pHRR decrease of up to 43.5% with 4 wt.-% DOPO thanks to a charring effect. In the condensed phase, the phosphorus improves dehydration and char formation, creating a protective layer limiting the release of heat and oxygen from the material. In the gas phase, PO^\bullet and HPO^\bullet will scavenge H^\bullet and OH^\bullet radicals originating from the combustion. The material exhibited good recyclability ability thanks to exchangeable disulfide cross-links, with similar mechanical properties between DOPO and non-DOPO filled REP.

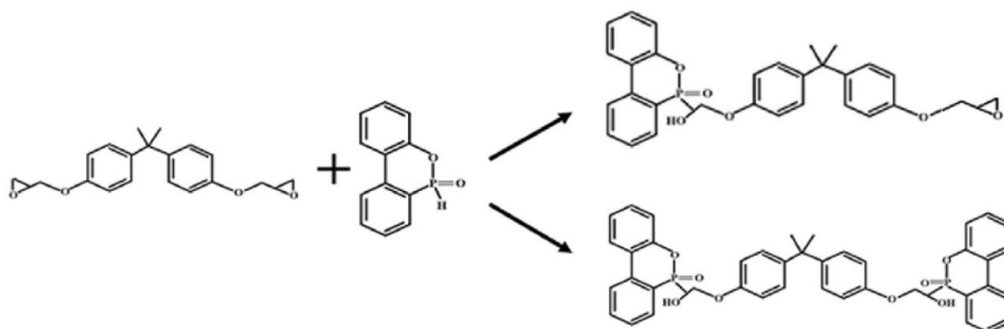


Figure 28 : Reaction between a bisphenol-A epoxy resin and DOPO

In another work⁶³, a DOPO-based diacid (DDP) was selected as co-curing agent of a bisphenol-A epoxy/adipic acid system. With 30 wt.-% DDP, T_g increased by 50°C and significantly improved the Young's modulus of the epoxy network system due to enhanced rigidity. In addition, UL94 V-0 rating, 6.5 vol.-% increase in LOI rating compared to pristine matrix and 63% lower pHRR and 32% THR due to DOPO mainly operating in the condensed phase was obtained. Despite those good fire results, tensile strength evolution and relaxation rate decreased significantly with high DDP ratios due to increased rigidity of the network, while at lower ratios (10 wt.-%), a V0 UL94 could not be achieved. Despite this, the material was capable of reconfigurable/multi-shape memory behavior thanks to its dynamic transesterification network. Feng et al. grafted DOPO to maleic anhydride before curing with epoxy. Higher T_g (133°C) could be obtained in comparison to the author's previous work³⁷ due to steric effect induced by the incorporation of the large DOPO unit. In addition to the good flame-retardancy behavior, with flames extinguishing in a mere two seconds after the removal of the lighter, the material depicted unique flame-triggered shape recovery. The material could withstand a cycle of flame-triggered recovery in addition to the classic thermal-shape recovery, despite the formation of a thin char layer. Despite those promising behavior toward flaming impact, the material exhibited a brittle mechanical behavior when recycled.

1.3.3.5 Flame retardancy of PBT vitrimers

Very recently (03/05/23, after the end of the PhD project) a patent was submitted by SHPP Global Technologies dealing with encapsulation of flame retardant agents for improved flame retardant formulations¹³⁵. The main objective of this patent is not to develop flame retardant vitrimer but rather to develop FR additives exhibiting hydrolytic stability and better dispersion/compatibility in polymeric matrixes. However, the described compositions contain a polycondensation polymer; and an encapsulated flame retardant agent, wherein the encapsulated flame retardant agent comprises a coating and a catalytic flame retardant core and potentially a coupler component. The patent, even if mentioning vitrimer based-formulation (call in the patent dynamically cross-linked polymer system) do not detailed any fire performance. They discovered, without further details, that aluminum diethyl-phosphinate (Exolit 1230 and Exolit 1240) could play the role of transesterification catalyst and promote cross-linking. Silica (SiO_2) and alumina (Al_2O_3) were deposited on the surface of the phosphinate salt by atomic

layer deposition process (ALD) through the use of a precursor, like tetraethoxysilane for the silica coating, or trimethyl aluminium for alumina coating. The coated phosphinates were then blended with a PBT and an epoxy cross-linker through reactive extrusion. The alumina coating only slowed reaction speed by several seconds. However, the silica coating (1nm to 100nm thickness, with phosphorus to silica ratio comprised between 5:1 and 100:1) effectiveness was assessed as it could effectively pacify the phosphinate catalyst action by delaying the cross-linking reaction by hundreds of seconds. In addition, layer thickness was an effective parameter to control the duration of the passivity.

1.3.4 Conclusion on flame retardancy of vitrimers

Flame-retardancy of vitrimer materials is poorly reported in the literature. Among the different studies, a reactive approach is mainly considered, where flame-retardant compounds are chemically incorporated into the polymer matrix during its synthesis. Most of the paper revolves around improving flame-retardancy of epoxy-based vitrimer whereas only one recent patent mentioned dynamically cross-linked PBT¹³⁵. Flame-retardancy is mainly obtained through grafting reactive phosphorus-rich compounds, including phosphonate, phosphinate, DOPO or hyperbranched polymers like cyclophosphazene. The presence of multi-functional compounds tends to increase the rigidity network, leading to higher glass transition temperature, high Young's modulus and brittle behavior with low tensile strength. Those behaviors render those flame-retarded vitrimer matrixes hard to upscale for an industrial application. Additionally, the limited availability and higher cost of reactive flame retardants may pose challenges for large-scale commercial applications. That is the reason why, in the field of flame retardancy, the additive approach is usually preferred since materials can be easily formulated and processed. However, the presence of additives in vitrimers requires careful consideration of the reaction kinetics and compatibility with the polymer matrix that are for the moment poorly investigated and this is thus one of the main objective of this work. Before presenting the flame retardant additives that can be used in PBT and epoxy, the next section of the manuscript will describe the scarce literature reporting the effect of additives and fillers on the dynamic of the reaction in vitrimers without considering FR additives since no paper exist on that topic.

1.4 Effect of additives and fillers on the dynamic of reaction in vitrimers

1.4.1 Nanoparticles

The heat-driven dynamic of vitrimer provides unique opportunities to develop smart materials through the incorporation of specific nanoparticles (NPs)¹³⁶ capable of converting IR or visible light radiation into heat (photothermal effect), or magnetic NPs to produce heating by exposure to a magnetic field (magnetic hyperthermia). Combined with the shape-memory effect of vitrimer material, this enables the activation of bond-exchange reactions, leading to a change of shape. Thanks to the confined thermal expansion of the irradiated area, photo-thermal heating allows the healing of fracture surfaces in close contact without the need for external pressure. Carbon nanotubes, (CNTs), metallic NPs or graphene present the unique particularity to absorb light at specific wavelengths, generating a large amount of heat.

1.4.1.1 Carbon nanotubes (CNTs)

Yang et al¹³⁷ showed in 2014 that the photo-thermal effect of multi-walled carbon nanotubes was strong enough to activate transesterification, obtaining a cross-linked epoxy network that could be welded using light. Vitrimer containing only 1 wt.-% of CNTs reached a temperature of about 180 °C when infrared light was applied for 20 s with a power of 0.84 W/cm², and lap-shear tests proved that 30 s of irradiation provided a better bonding than 10 min of direct heating in an oven at 180°C. They also succeeded to weld their vitrimer with common epoxy thermoset or even thermoplastics (polyethylene) (Figure 29), which open the way for photo-modulating welding without glues and molds or in situ joining and repairing of epoxy networks. Pei and al welded together three epoxy vitrimer networks with different T_g, and used CNTs to locally heat the sample by IR irradiation¹³⁸. They obtained a vitrimer with distinct shape memory structures thanks to different shape recovery temperatures, while the original permanent shape could be recovered at higher temperatures.

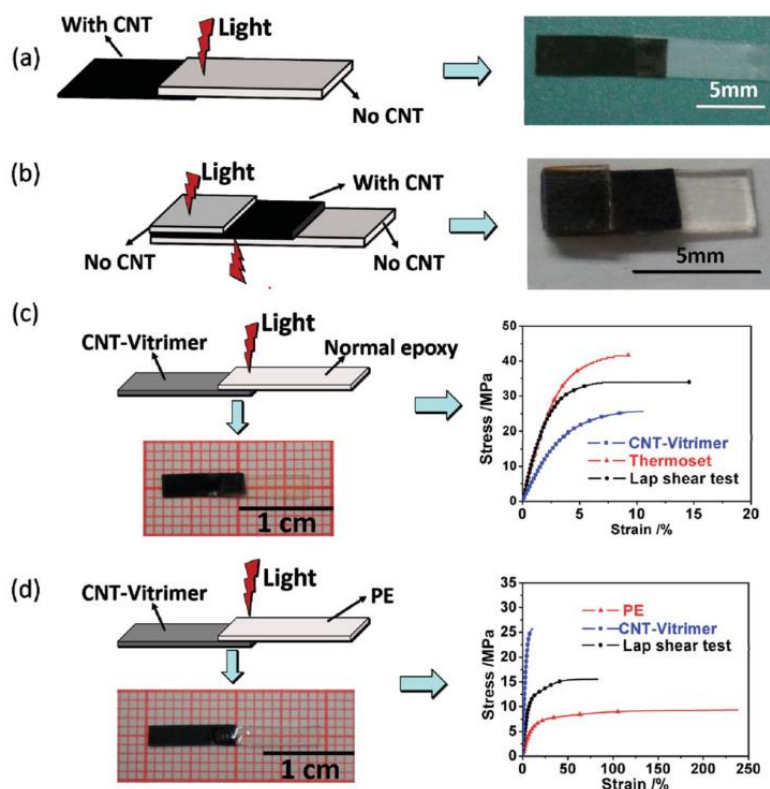


Figure 29 : Transmission welding (a) joining non-CNT vitrimer with CNT-vitrimer. (b) Joining two pieces of non-CNT vitrimer using CNT-vitrimer as an “adhesive”. (c) Joining normal epoxy with CNT-vitrimer. (d) Joining thermoplastic PE with CNT-vitrimer. Taken from reference ¹³⁷

1.4.1.2 Graphene

Like CNTs, graphene is often used as photo-thermal transformation material to convert light energy to thermal energy due to its fast and efficient photo-thermal transformation performance. By adding graphene to an epoxy-acid network, another team¹³⁹ obtained a graphene-vitrimer with both thermal and near-infrared triggered recovery and shape reconfiguration, as well as enhanced toughness with a classical ductile fracture. From 0 wt.-% to 1 wt.-% graphene, yield strength and strain at break increased from 12.0 MPa and 6% to 22.9 MPa and 44%, respectively. In another study, Poutrel and coworkers¹⁴⁰ compared the effect of the incorporation of 4 types of graphene (graphene nanoplatelets (GNP), graphene oxide (GO), reduced graphene oxide (rGO) and silane bearing functionalized graphene nanoplatelets (GPTS-GO)) in an epoxy vitrimer matrix at low loading (0.1 to 1 wt.-%). In all cases, the network could totally relax stress at high temperatures. Low functionality particles (GNP and rGO) only decrease τ' (τ/E) due to their tendency to transfer heat in a system with a thermally driven relaxation dynamic. On the other hand, functionalized nanofillers (GO and GPTS-GO) hinder chain motion which ultimately increases τ' at higher particle loadings. Nonetheless, activation energy remains overall similar to neat vitrimer in all cases, ranging from 111 kJ.mol⁻¹ to 128 kJ.mol⁻¹ at best. Mechanical properties also improved for vitrimer with graphene presenting active functional groups (GO and GPTS-GO).

1.4.1.3 Metallic nanoparticles

Altuna et al studied the incorporation of metallic nanoparticles as another route for the light triggering of the self-healing of epoxy vitrimer. Polyvinylpyrrolidone (PVP)-capped gold NPs were added to their previously reported epoxidized soybean oil (ESO) with citric acid (CA) vitrimer system⁷⁰. The main advantage of over CNTs and graphene is the very low amounts of gold lead needed to obtain significant temperature increases, with temperatures 80°C and 130°C reached in 3-4 minutes with respectively 0.02 and 0.08 wt.-% of gold, thus the material remains with a high degree of transparency in wide regions of the visible spectrum. Bigger polydopamine-modified Au microspheres (around 1300nm compared to usual 10-20 nanometer-sized NPs) have also been added to a DGEBA, sebacic acid and TBD vitrimer matrix, obtaining similar results¹⁴¹. Remote heating can also be obtained by introducing magnetic NPs to the matrix but has only so far been applied to shape-memory epoxy thermosets^{142,143}.

1.4.1.4 Silica

Legrand and Soulié-Ziakovic³⁵ compared the physical behavior of a non-functionalized and functionalized silica in a silica-epoxy vitrimer nanocomposite. The interfacial adhesion between the fillers and the matrix is a crucial issue to ensure good mechanical properties of nanocomposite-filled materials, as the mechanical properties of the material are bound to the effectiveness of transfer stress between the matrix and the filler. It is mainly dependent on the dispersion of the particles within the polymer and the chemical nature of the interface between fillers and polymer chains. In this context, the silica was functionalized by a solvent-free hydrolysis and condensation step using tetraethyl orthosilicate, followed by condensation of (3-Glycidyoxypropyl)trimethoxysilane (GLYMO), an organosilicate possessing pendant epoxide functions (Figure 30). Those functions could form the same β -hydroxy ester bonds with the matrix as the epoxy/acid network, improving interfacial adhesion and improving dispersion. Even though nanoparticles slow down the stress relaxation of the vitrimer network (10 times slower relaxation with 40 wt.-% bare silica loading), they obtained a 3 times faster relaxation for functionalized nanocomposites thanks to surface exchangeable bonds compared to nonfunctionalized nanocomposites. Besides, an increase in loading leads to higher modulus materials in both glassy and rubbery regions, and better tensile strength at 25°C was found for functionalized silica vitrimer nanocomposites compared to bare silica ones.

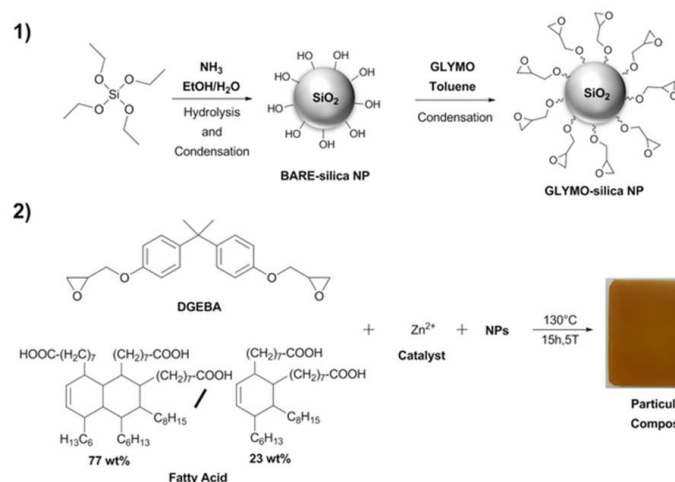


Figure 1. Synthetic procedures. (a) Synthesis and functionalization of monodisperse silica NPs. (b) Composites composition and formulation.

Figure 30: (1) Functionalization of silica with pendant epoxy functions; (2) Silica-composite composition and formulation³⁵

Another study relates the use of an epoxy group-functionalized silica as both cross-linker and reinforcing agent. Silica was prepared by a one-step silanization process using (3-glycidyloxypropyl)trimethoxysilane¹⁴⁴. Then, they incorporated pendant acid functions using mercaptopropanoic acid onto SBR chains through thiol-ene click reaction. When silica and modified SBR with 1,2-dimethyl-imidazole (DMI) and 1,5,7-triazabicyclo[4.4.0]dec-5-ene (TBD) as cocatalysts are compounded together, the exchangeable β -hydroxyl ester bonds could be formed at the rubber–filler interface. The resulting composite material exhibited a stress-relaxation behavior similar to other values reported in the literature^{4,22}, with an activation energy of 83.2 kJ/mol. Higher modified silica content leads to longer relaxation times (2000s for a 10 wt.-% silica vs 7000s for a 30 wt.-% silica vitrimer at 140°C), attributed to both the increasing number of exchange reactions required to achieve network topological rearrangement, as well as silica restricting rubber chain mobility and retard exchange reaction. Moreover, the material exhibited excellent recycling capabilities, with the samples recovering most of the mechanical properties after multiple generations of recycling.

1.4.2 Conclusion

Most of the paper dealing with the incorporation of filler or additives in vitrimers considered either reinforced fibers (in the case of composite) or nanoparticles. In the case of fibers, it is reported that it does not sharply affect the dynamic of the system even if compatibilization issue were stated. The question appears more complex for nanoparticle and depends on their chemistry. Usually, pristine nanoparticles tend to increase relaxation time³⁵. Except the very recent patent dealing with surface modification of FR additives mentioning dynamically cross-linked polymer, no paper studies the effect of FR additives on the dynamic of the reaction of vitrimers. This is the main objective of this research. The last section of this chapter thus detailed the FR additives that are usually used to flame retard PBT and epoxy that are the two polymers considered in this study.

1.5 Additives used to flame retard PBT

Flame-retardant additives requirements for PBT are high, mainly due to high processing temperatures and sensibility to degradation caused by reactive chemical species. Besides, long-term dimensional stability is mandatory to cope with the long-term applications of this engineering polymer. Metal hydroxides and hydrocarbonates, while considered environmentally friendly, have either low thermal stability¹⁴⁵, with the need for specific surface treatment, or require high loading content (45-50 wt.-%)¹⁰⁶. This renders this category of FR inadequate for industrial use. At the opposite, phosphate-based additives have shown high efficiency and will be considered in this study.

1.5.1 Phosphate esters

Self-charring cyclic phosphates (Figure 31) were mainly used in PBT, especially combined with other charring additives like melamine compounds. Alone, 10 wt.-% of bisphenol A bis(diphenyl phosphate) (BDP) provides self-extinguishing in the UL94 tests, but is not sufficient to pass above V-2 ratings^{106,146,147}. Bisphenol F bis (diphenyl phosphate) and derivatives only moderately improves the flame-retardancy of such matrixes^{106,148}. Nevertheless, the addition of melamine derivatives to aryl phosphates significantly improves the flame-retardancy of PBT. Indeed, adding 20 wt.-% resorcinol bis(diphenyl phosphate) (RDP) or triphenylphosphate added with 15 wt.-% melamine cyanurate (MCA) to a PBT-GF matrix allows to reach a UL94 V-0 rating^{106,149}. RDP and BDP have been reported by Levchik and coworkers to develop synergy well with high charring agents like phenolic resins (Novolac). V-0 rating was reached with PBT filled with 10 wt.-% Novolac and 15 wt.-% of either RDP or BDP¹⁴⁷. Adding triphenyl phosphate (TPP), a volatile compound acting on the gas phase, to RDP or BDP allowed to reach V-0 for PBT-GF with higher loadings of 10 wt.-% BDP, 5 wt.-% TPP and 10 wt.-% Novolac. The necessary addition of a gas-phase action to obtain the same results compared with neat PBT is attributed to glass fibers preventing the swelling of a char layer and reducing the formation of a protective barrier.

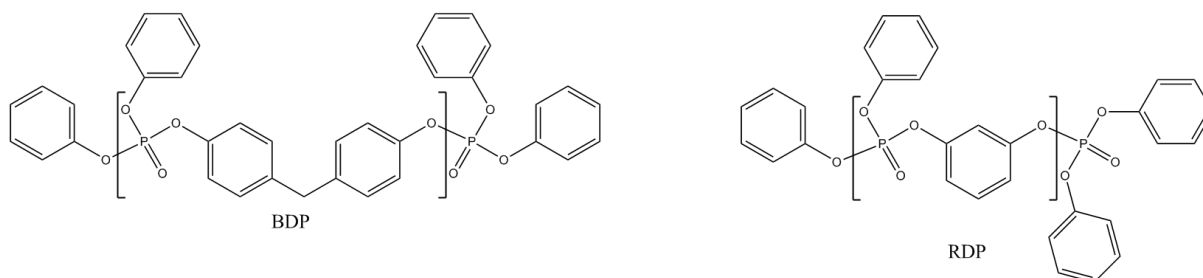


Figure 31: Chemical structure of aromatic phosphates bisphenol A bis(diphenyl phosphate) (BDP) and of resorcinol bis(diphenyl phosphate) (RDP).

1.5.2 Phosphonates

Cyclic phosphonates (Antiblaze 1045 from Rhodia) have been added in Glass Fiber-filled PBT. For example, V-0 ratings have been reported for combinations of 10 wt.-% Antiblaze and either 10 wt.-% talc (MgOH_2) in PBT-25 wt.-%GF¹⁵⁰, or 15 wt.-% melamine cyanurate in PBT-30 wt.-%GF¹⁵¹. Balabanovich et al. found the optimum ratio between cyclic diphosphonate ester and melamine to be 2:3 and a minimum load of 20 wt.-% to obtain a V-0 rating and 30.4 vol.-% as LOI index¹⁵². Antiblaze 1045 combined with melamine to form a phosphorus-nitrogen solid layer which acts as a protective barrier for PBT¹⁰⁶. Various other dimethyl methylphosphonate combined with various metallic salts and methyl methyphosphonic acid did not produce ratings higher than V-2^{106,153}.

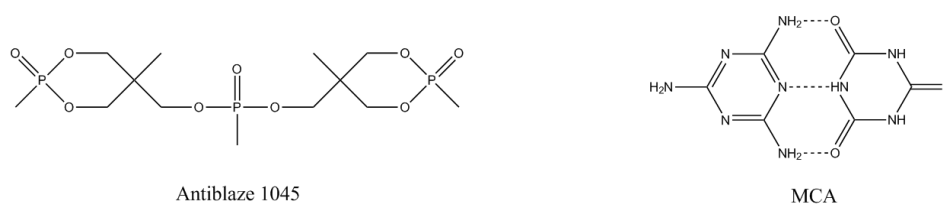


Figure 32: Chemical structure of cyclic diphosphonate ester (Antiblaze 1045) and melamine cyanurate (MCA)

1.5.3 Phosphinates salts

Aluminum- and zinc-coordinated phosphinate (AlPi and ZnPi) salts have been extensively studied in polyesters and polyamides in the 80s and 90s, with various patents. Nowadays, aluminum phosphinate is recognized as an effective flame-retardant for PBT applications. 20 wt.-% of aluminum dialkylphosphinate is enough to obtain a V-0 rating on PBT-30 wt.-%GF^{154–156}, with some studies going as low as 15 wt.-% for pristine PBT matrixes¹⁵⁵. Reported LOI values for a PBT-30 wt.-%GF with 20 wt.-% aluminum dialkylphosphinate are comprised of between 42 vol.-%¹⁵⁷ and even 50 vol.-% with an aluminum methylpropylphosphonic acid¹⁵⁵. Zinc phosphinate, on the other hand, is less efficient to flame-retard PBT-30 wt.-%GF, with no classification obtained in UL94 using 20 wt.-% content¹⁵⁸, and reaching V-2 with 10 wt.-% ZnPi when combined with 10 wt.-% melamine phosphate (LOI of 27 vol.-%)¹⁵⁶. The mode of action of aluminum diethylphosphinate has been investigated by Braun and coworkers^{157,158} and is presented in Figure 33. They propose that dialkylphosphinate acts in the gas and condensed phase, with a stronger effect in the gas phase.

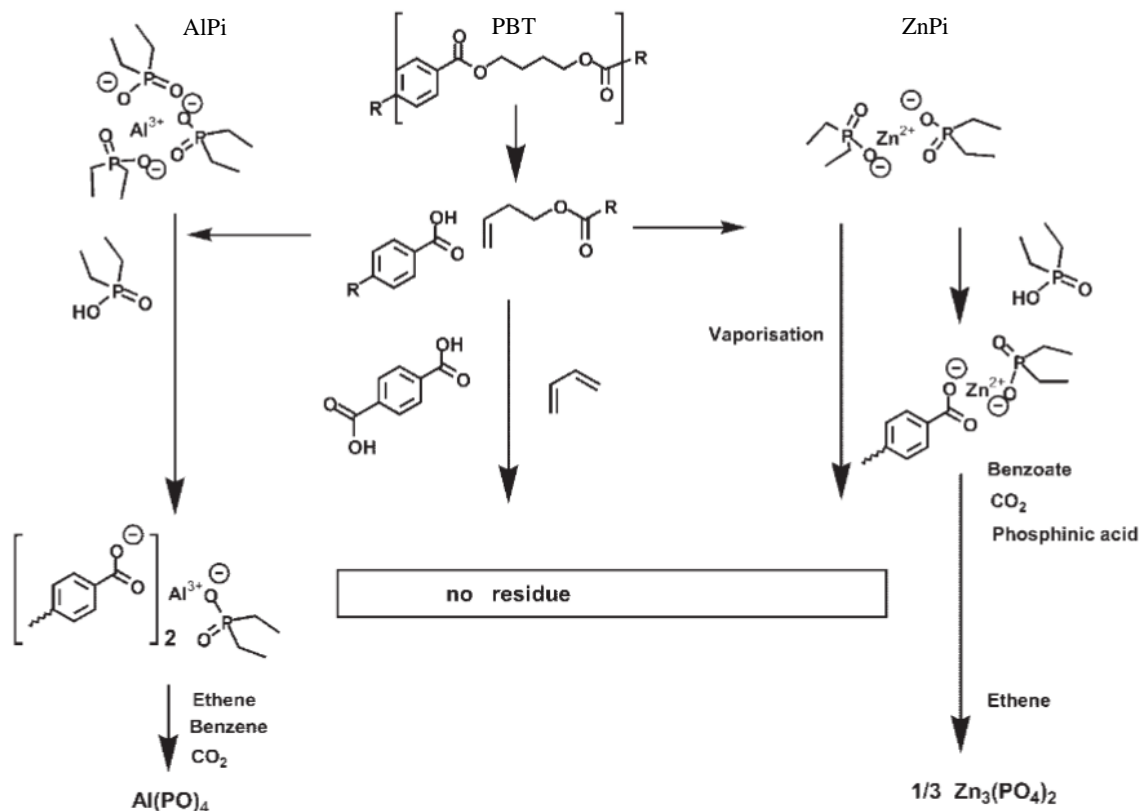


Figure 33 : Main decomposition pathway of PBT and interaction with phosphinate additive (aluminum- or zinc-diethylphosphinate (AlPi or ZnPi))¹⁵⁸. Diethylphosphinic acids are released in the gas phase to act as inhibitors of the combustion reaction, while aluminum phosphinate-terephthalate complexes are formed in the condensed phase. Then, at higher temperature (above the usual decomposition temperature for PBT), the aluminum phosphinate-terephthalate decomposes to form aluminium phosphate. For zinc phosphinate, part of the salt vaporizes in addition to the formation of zinc phosphinate-terephthalate.

Synergists acting on the solid phase (charring effect) have been studied with AlPi to increase the condensed phase action of metal phosphinate. Braun and coworkers combined AlPi with melamine salts, specifically melamine cyanurate (MCA)¹⁵⁷ and melamine polyphosphate (MPP)¹⁵⁸ to flame retard PBT-30 wt.-%GF. They observed a synergistic effect between AlPi and melamine salts by keeping the total FR loading ratio at 20 wt.-% (~13 wt.-% AlPi, ~7 wt.-% MC) and obtained a V-0 rating with slightly higher LOI values (43.5-44 vol%) and slightly better cone calorimeter results. Gallo et al., in their paper, extensively studied the combination of AlPi with different nanometric metal oxides. With only 8 wt.-% AlPi, a V-0 result was obtained by adding 2 wt.-% TiO₂ (LOI 28 vol.-%) and 1 wt.-% Al₂O₃ (LOI 24 vol.-%) whereas 10 wt.-% is needed to obtain a V-1 classification.

Aluminum hypophosphite (APH) has also been combined at 15 wt.-% with 5 wt.-% nanoclays in a PBT-30%GF matrix to obtain a V-0 rating and a LOI value of 29 vol.-%¹⁵⁹.

1.5.4 Phosphine oxides

Phosphine oxides, mainly the most common triphenylphosphine oxide (TPPO) and 1,4-diisobutylene-2,3,5,6-tetrahydroxy-1,4-diphosphine oxide (Cyagard), have not demonstrated efficient

retardancy for PBT. At best, only a borderline V-2/V-0 UL-94 (1.6mm) rating could be obtained with 15 wt.-% Cyagard on pristine PBT¹⁶⁰. On PBT-GF, 20 wt.-% TPPO combined with 15 wt.-% melamine cyanurate could reach V-0 rating¹⁶¹, otherwise, pure TPPO could only obtain V-2 rating.

1.5.5 Red phosphorus

Red phosphorus, an allotropic form of elemental phosphorus, is the most concentrated source of phosphorus among the family of flame-retardants^{104,162}. From a general point of view, less than 10 wt.-% is enough to obtain V-0 ratings for most polyesters due to their thermal oxidation in the presence of oxygen or nitrogen. This oxidation turns red phosphorus into polyphosphoric acids eager to catalyze the dehydration of polymer chain and promote char formation. In PBT, 5-6 wt.-% of coated grade red phosphorus is necessary to provide a V-0 ranking (0.8mm)¹⁶³, while for PBT-GF, the addition of 5.5 wt.-% of high charring Novolac to an equal amount of red phosphorus was used to obtain similar results, as well as high LOI value of 35 vol.-%¹⁶⁴. The high effectiveness of red phosphorus hides undesirable side effects, like its natural red coloring, which is hard to erase even with high loadings of colorant, possible risks of ignition in contact with high temperature or mechanical deformation, as well as release of highly toxic phosphines (PH₃) when in contact with moisture. This last point has been addressed through encapsulating techniques¹⁶⁵.

1.5.6 Phosphorus- and Nitrogen-based additives

The addition of melamine and its salt derivatives to PBT did not exhibit satisfying flame-retardancy^{157,166}, with limited FR efficiency implying high loadings (40 wt.-%¹⁶⁷) required to reach V-0 UL94 registration. However, good synergies may be obtained with melamine in the presence of phosphonates¹⁰⁶.

Despite being nitrogen and phosphorus-rich compounds, cyclophosphazene are not efficient flame-retardants on unreinforced PBT with only reaching V-2 UL-94 classification at 20 wt.-% loading¹⁶⁸. However, a good LOI of 29 vol.-% was reported. Inorganic phosphates, mainly ammonium polyphosphate (APP), are known to improve polymer charring¹⁰⁴, thus are not efficient on low charring polymers like PBT.

1.5.7 Conclusion

The incorporation of phosphorus-based additives in PBT has demonstrated varied results in enhancing its flame-retardancy. Typically, an additive content of 10 to 20 wt.-% is required to achieve satisfactory fire performance. However, when combined with appropriate synergists, lower amounts can yield comparable results. Among the additives tested, aluminum diethyl-phosphinate, cyclic phosphonates, and red phosphorus have shown significant improvements in flame-retardancy, including achieving V-0 UL-94 classifications. It is important to note that red phosphorus poses handling and

processing risks, while cyclic phosphonates and phosphate esters often require synergists to meet regulatory requirements. On the other hand, aluminum phosphinates consistently exhibit superior performance without relying on additional synergists.

1.6 FR additives used to flame retard epoxy

Despite the extensive use of epoxy systems in various applications, one major challenge arises from the fire risks and hazards associated with them. When ignited, epoxy resin polymers can produce highly corrosive and toxic byproducts. To mitigate these fire-related concerns, different approaches can be employed. One approach involves copolymerizing epoxy resins with reactive fire retardants^{46,63,115,123,128,129}, while another approach involves incorporating fire retardant additives into the resin matrix. These strategies aim to enhance the fire retardancy of epoxy systems and reduce the potential risks associated with their ignition. In the following section, we will present some of the main flame-retardant additives commonly found in epoxy resins (Figure 34). In line with the research conducted on PBT, a particular emphasis was placed on phosphorus-based systems.

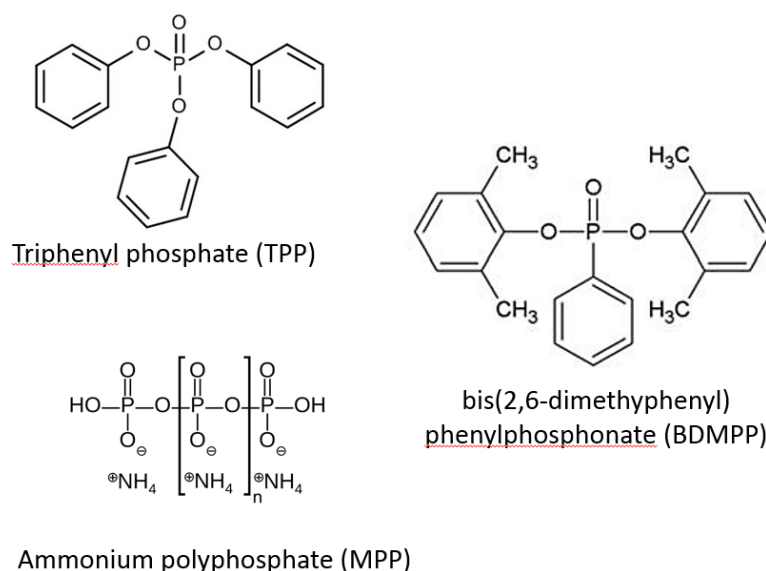


Figure 34 : Example of phosphorus-based flame-retardant additives for epoxy resins

1.6.1 Metal hydroxides

Metal hydroxides commonly used with epoxy resins, such as aluminum (tri-)hydroxide (ATH and $\text{Al}(\text{OH})_3$) and magnesium hydroxide (MDH), are usually added at high loadings to effectively flame-retard epoxy resins, typically around 30-60 wt.-% by weight¹⁶⁹⁻¹⁷¹. While usually considered a cheap alternative to phosphorus or nitrogen-based flame-retardants, such high loadings can negatively impact the properties of the final product¹⁷².

1.6.2 Nitrogen-based FR

Melamine, melamine cyanurate (MC), melamine polyphosphate (MPP) and ammonium polyphosphate (APP) are usually added in combination with other flame-retardants^{111,112} or by combining several nitrogen-containing FRs. For example, good flame-retardancy was reported for a 20 wt.-% APP/MPP glass-reinforced epoxy¹⁷³.

1.6.3 Phosphorus-based FR

Numerous types of phosphorus-containing additives have been studied for epoxy systems, from triphenyl phosphate (TPP)¹⁷³, ammonium polyphosphate (APP)¹⁷³, DOPO derivatives^{174,175}, to phosphonates^{176,177} or aluminum phosphinates¹¹¹. Usually, a filler amount of 10-30 wt.-% is necessary to obtain good performances and classifications. They release phosphorous radicals during flaming, which interfere with the combustion process and reduce the flammability of the epoxy resin. A condensed phase action can also occur leading to a charring phenomenon, this is typically what is called the intumescent effect.

1.6.4 Phosphorus-nitrogen FR

Phosphorus-nitrogen-containing flame retardants have gained in interest in the last decades to flame-retardant epoxy resins as they develop low toxic gases or vapors and are more convenient toward recyclability issues. Derived from phosphazene, cyclotriphosphazene is based on alternating conjugating P and N atoms, combining all the benefits of phosphorus-nitrogen combination including good fire resistance and self-extinguishing ability to the polymer^{119,178}. 9 wt.-% of a bisphenol-S bridged penta(anilino)cyclotriphosphazene (BPS-BPP) was enough to attain a LOI value of 29.7 vol.-%, a PHRR decrease of 46.3% and a total smoke production reduction of 71.6%¹¹⁹.

1.6.5 Intumescent formulations

Primarily developed for coating applications to metallic structures, wood, fabric or indoor thermal insulation, intumescent formulations have gained widespread use due to their advantageous properties like low smoke and toxicity upon combustion. When subjected to thermal degradation, intumescent coating or systems undergo swelling or foaming, leading to the formation of an expanded carbonized layer on the polymer surface. In epoxies, intumescence is usually obtained by adding to the raw material an acid source (ammonium polyphosphate, APP)^{179,180}, often complemented by a carbonizing agent (pentaerythritol, PER)^{181,182} and/or a blowing agent (melamine cyanurate, MCA)^{183,184}. Significant pHRR and HRR reductions are usually obtained with those formulations compared with pristine epoxy, as well as high LOI and UL-94 classifications^{114,176,185}. For example, the addition of 12 wt.-%APP and 3 wt.-%MCA to epoxy resin was enough to pass UL-94 V-0 rating as well as a LOI value of 26.8 vol.-%¹⁸⁴.

1.6.6 Hyperbranched FR

On the other hand, there has been a significant interest in the development of phosphorus-nitrogen-containing hyperbranched polymers for use as multifunctional flame-retardant additives for epoxy resins. Those rich P-N containing polymer high-phosphorus-concentration additives led to the development of hyperbranched phosphorus flame-retardants^{186,175,187}. Very high flame-retardancy with a low amount of additives could be obtained. With only 7 wt.-% of their multifunctional hyperbranched additive, Shi and coworkers¹⁸⁷ obtained an epoxy resin with a LOI of 40 vol.-%, UL-94 V-0 rating as well as a pHRR decrease of ~50%. For example, good flame-retardancy was reported for a 20 wt.-% APP/MPP glass-reinforced epoxy¹⁷³.

1.6.7 DOPO

9,10-dihydro-9-oxa-10-phosphaphenanthrene-10-oxide, or DOPO, is an efficient in flame-retarding epoxy resins due to its unique chemical structure and properties. The presence of a reactive phosphorus atom in DOPO contributes to its high reactivity, while its electron-rich structure enhances its susceptibility to nucleophilic attack. These factors enable DOPO to undergo various chemical reactions, making it a valuable additive for flame-retardant and cross-linking applications. In line with the examples discussed in the section on flame-retarded vitrimers, DOPO is frequently reacted with resins, such as phenolic or epoxy resins, prior to the curing process. Besides, numerous DOPO-derived flame retardant additives for epoxy resins have been reported¹⁸⁸.

For example, DOPO derivatives like tetra-[(acryloyloxy)ethyl] pentaerythritol (DOPP), or heterocyclic tris- [(acryloyloxy)ethyl] isocyanurate (DOPI) were added to a phenol novolac resin¹⁸⁹. The flame-retardant systems, with a P content of 0.6 wt.-%, demonstrated an LOI of 45.3% (DOPI) and 47.7% (DOPP), respectively, and both systems achieved a self-extinguishing capability with a UL-94 V0 rating. Besides, the incorporation of DOPI and DOPP had a significant impact on the peak heat release rate (PHRR) and total heat release (THR) parameters, reducing them by 50% compared to the pristine resin. An other paper reports a phenethyl-bridged DOPO derivative (DiDOPO) to flame-retard DGEBA epoxy resin thermoset¹⁹⁰. When 10 wt.-% DiDOPO is added in an epoxy resin filled with 0.8 wt.-% multi-walled carbon nanotubes (MWNT), LOI rises from 21.8 vol.-% to 38.6 wt.-% and V-0 UL-94 rating is achieved.

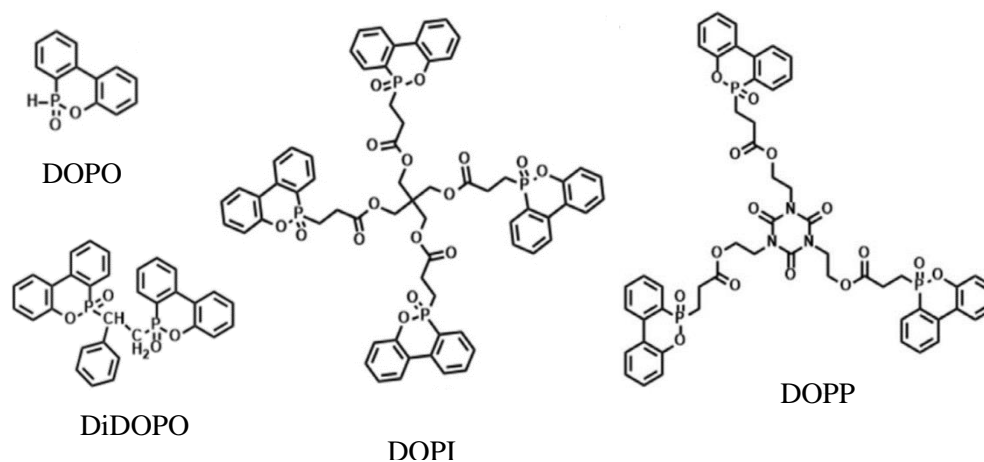


Figure 35 : DOPO and additive derivatives¹⁸⁸

1.6.8 Conclusion

The incorporation of flame-retardant additives, such as DOPO derivatives, phosphorus-based compounds, intumescent formations and metal hydroxides, has shown promising results in improving the fire properties of epoxy resins. These additives act through different mechanisms, including the formation of char layers, release of flame-inhibiting gases, and dilution of heat and flammable gases.

1.7 Ph.D. objectives

Vitrimer materials have emerged as a promising class of materials with unique properties and potential applications. Their dynamic and reversible nature, enabled by thermally-dependent bond-exchange reactions, offers the ability to modify and reshape cross-linked materials. Among those chemistries, dynamic transesterification (DTER) emerges as a robust and easily implementable chemistry for vitrimers that offers excellent mechanical and chemical performance. It provides versatility through the use of a wide range of reactants and could be adapted to existing processes in the near future. The study of transesterification in vitrimers has provided valuable insights into their structure-property relationships and potential applications in fields such as coatings, adhesives, and composites. On the other hand, the field of flame-retardancy solutions for vitrimers is relatively underexplored, yet it holds significant importance in developing commercially viable options to address the limitations of both thermoplastics and thermosets. In addition, for the best of our knowledge, no flame-retardancy of vitrimers has been reported through an additive strategy except the very recent patent mentioning dynamically cross-linked polymer. Besides, there is a lack of understanding on the impact of (micro-sized) additives on DTER vitrimer.

In this context, the goal of this PhD thesis is to apprehend the impact of flame-retardant additives on DTER vitrimer systems on two different systems: one based on PBT and another one based on epoxy.

Chapter 2 of the study will focus on examining the influence of incorporating flame-retardants on the synthesis of a PBT vitrimer. Three distinct types of phosphorus-based flame-retardant additives, comprising two metal salts and one organic molecule, have been carefully chosen for investigation. The study will assess the effects of these additives on the degree of cross-linking and relaxation dynamics within the vitrimer. The most promising material will undergo further analysis in Chapter 3, specifically to gain a deeper understanding of the interactions between the matrix and additive, and to evaluate its fire performance in comparison to thermoplastic counterparts. Chapter 4 will explore the synthesis of flame-retarded epoxy resin. This chapter will begin by addressing the synthesis of intumescent vitrimer coatings. Subsequently, a comparative study will be conducted to assess the performance of flame-retardants added through both additive and reactive approaches in a novel vitrimer system.

Chapter 2 - Impact assessment of flame-retardant additives on PBT vitrimer synthesis and properties

2.1 Introduction

Poly(butylene terephthalate), a semi-crystalline polyester thermoplastic commonly used for electrical and electrotechnical applications¹⁹¹ (E&E), loses rapidly its dimensional stability around the melting temperature due to its barely entangled network^{192–196}. Two factors are responsible for this lack of entanglement: the high critical molecular weight of PBT (M_c about 60 kg.mol⁻¹)¹⁹⁷ and the difficulty to synthesize PBT with very high molar mass^{192–196}. Turning it into a vitrimer is a solution that has been recently proposed in the literature to enlarge its applications and potentially compete with high performance materials such as thermosets. PBT vitrimer can be synthesized by reactive extrusion using a commercially available PBT, an epoxy monomer and a transesterification catalyst. In this case, a crosslink network is formed and transesterification reactions can occur above a certain temperature enabling the flowing of the material. It was demonstrated that, for some PBT vitrimers, it was possible to heat this material above the melting temperature for 30 min without observing any flowing of the material^{5,34}. Thanks to the dynamic network, the material remains additionally recyclable compared to standard cross-link polymers^{198,199}.

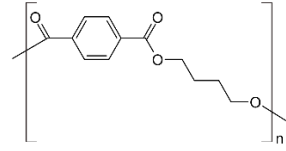
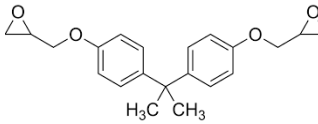
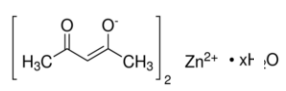
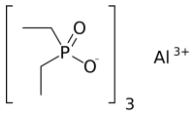
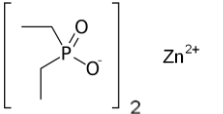
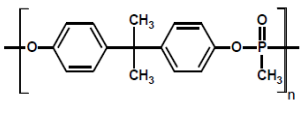
To fulfil the requirements of E&E and develop industrially relevant materials, PBT vitrimer has to demonstrate effective flame-retardancy behavior. Those performances are mostly obtained through the addition of flame-retardants. This chapter aims at understanding if it is possible to flame retard the PBT vitrimer thanks to such additive approach. Three phosphorus based flame-retardant additives recommended for PBT, were selected: aluminum phosphinate (AlPi), zinc phosphinate (ZnPi) and a phosphonate homopolymer (HM1100). Their addition in the PBT together with the epoxy and the transesterification catalyst during the reactive extrusion was tested. The properties of the FR vitrimer are detailed. The chapter is divided into four parts. After describing the materials and methods used in this study in the first part, the second part focused on the synthesis of cross-linked compounds in the presence of each flame-retardant. A systematic study was conducted to explore the interactions between the matrix and the flame-retardant additive, as well as to examine the implications of these interactions on the achieved cross-linking degree. In the second part, the cross-linked formulation dynamics will be characterized by stress-relaxation experiments whereas the last part of this chapter investigates the thermal and structural properties of the cross-linked materials.

2.2 Experimental

2.2.1 Material description

Table 1 presents the different materials used in this study.

Table 1: List of the chemical components used in this study, their function and their main characteristics

Name	Grade (supplier)	Chemical structure	Function	Characteristics
Poly(butylene terephthalate)	Valox 315 (SABIC)		Polymer matrix	[COOH] = 37 mequiv/kg [OH] = 23 mequiv/kg M _n = 47 000 g/mol Density: 1.31 g.cm ⁻³
Bisphenol-A diglycidyl ether	DER 332 (Sigma-Aldrich)		Chain extender and cross-linker	Purity >96% Density: 1.16 g.cm ⁻³
Zn(II) acetylacetonate hydrate	(Sigma-Aldrich)		Transesterification catalyst	Purity >99% Density: 0.5 g.cm ⁻³
Aluminium diethylphosphinate	Exolit OP 1230 (CLARIANT)		Flame retardant	D _{mean} = 20 to 40 μm 23.3 – 24 wt.-% P Density: 1.35 g.cm ⁻³
Zinc diethylphosphinate	Exolit OP 950 (CLARIANT)		Flame retardant	19.5 – 20.5 wt.-% P Density: 1.29 g.cm ⁻³
Phosphorus based homopolymer	HM1100 (NOFIA)		Flame retardant	10.8% wt.-% P Density: 0.73 g.cm ⁻³

2.2.1.1 PBT matrix

The PBT grade used in this part is a Valox[®]315 from Sabic Innovative Plastic. All experiments were conducted on the same batch. The molecular weight of the polymer is 47000 g/mol⁻¹ and the concentration in [OH] and [COOH] end groups are respectively 37 mequiv/kg and 23 mequiv/kg⁵. PBT was dried at 80°C overnight in a oven before any reactive step.

2.2.1.2 Epoxy resin

Bisphenol A diglycidyl ethers (BADGEs or DGEBA) are di-functional epoxy resins usually used in thermosetting applications. DER 332 is a particularly pure grade of BADGE produced by Dow Chemical and commercialized by Sigma Aldrich. Its high purity comes from a very low homopolymerization degree (<0.03), allowing for a maximum epoxide equivalent weight of 178g/eq.

2.2.1.3 *Transesterification catalyst*

The transesterification catalyst was chosen according to the literature. Metallic salts are known to effectively catalyze transesterification in epoxy-acid vitrimer systems. Mainly, zinc catalysts are proven efficient to catalyze transesterification in PBT vitrimer systems. Thus, we chose zinc acetylacetonate ($\text{Zn}(\text{acac})_2$) as transesterification catalyst. It is a hydrated metal-organic complex composed of a tetra coordinated Zinc bonding each oxygen atom to form a chelate ring.

2.2.1.4 *Flame retardants*

As highlighted in chapter 1, phosphorus-based flame-retardants are the most commonly used FR in a PBT matrix. Usually, high loadings (>20wt %) are required to pass the demanding restrictions of E&E applications. Three different FRs were chosen. Following are the characteristics of the three of them.

Aluminum diethylphosphinate (AlPi) was chosen because of its excellent flame-retardant properties in PBT. It has a high phosphorus content of around 24wt %. Commercialized by Clariant under trademark Exolit[®], OP 1230 and OP 1240 are both suited and commercially used for PBT grades, with OP 1240 leading to a little lower reduction of viscosity when incorporated in a compounding step. In our case, having a lower viscosity is an asset during the synthesis of PBT vitrimer, thus we chose OP 1230. It is a fine-grained white powder with an average particle size between 20 to 40 μm , thermally stable up to 300°C.

Zinc diethylphosphinate (ZnPi) is another phosphinate-based salt flame retardant, considered less efficient than its aluminum counterpart. Commercialized by Clariant under the trademark Exolit[®] OP 950, it has a phosphorus content of around 20 wt.-%. It was chosen to evaluate the impact of the metallic cation on the potential interaction with the dynamic system. It is an irregular-sized white-powdered fusible additive. It decomposes at temperatures superior to 350°C.

The last flame-retardant is an oligomeric methylphosphonate commercialized by FRX Polymers under the name Nofia[®] HM1100. It is an amorphous high-flowing polymer (MVR of 5-9 $\text{cm}^3/10$ min at 210°C) effective as flame-retardant additive for PC, PET and PBT applications^{200,201}. It is used in several patented compounds²⁰²⁻²⁰⁴. It has a phosphorus concentration of 10.8 wt.% and decomposes above 440°C.

2.2.2 *Material processing*

The synthesis of PBT vitrimers was carried out by adapting the protocol developed by Demongeot et al⁵. It consists in adding a diepoxy (DGEBA) and a transesterification catalyst ($\text{Zn}(\text{acac})_2$) during an extrusion step. Formulations from Table 2 were prepared using a twin-screw extruder (15 cm^3 DSM micro-explorer) under nitrogen flux to prevent oxidation. PBT and the three FRs were previously dried at 80°C overnight before processing to prevent hydrolysis from occurring during the compounding step. All the components were premixed before being inserted in the micro-extruder and then processed at 270°C at a screw speed of 60 rpm. The stoichiometric ratios used in this study were fixed at 2:1

[epoxy]/([OH]+[COOH]) and 0.11:1 [catalyst]/([OH]+[COOH]). Those ratios were chosen to obtain a material with significant gel content while still being processable without damaging the extruder (force kept under 6000 N). The total volume of reactants was fixed at 10 cm³ to keep the torque under the 8000 N limit of the machine. Preliminary analysis showed that the high viscosity of some of the materials did not allow an extraction through the die of the extruder. To ensure consistent thermal history across all formulations, the extruder was stopped after 8 minutes and the material was extracted by opening the extruder. Specimens for rheology tests were prepared using a DSM Xplore 12 cm³ Laboratory Injection-Molding Machine. The injection temperature was set to 270°C and the mold temperature to 100°C.

In the mixtures, the materials will be defined accordingly to the following abbreviations (Table 2): P for PBT, E for epoxy, Z written as subscript for the transesterification catalyst, A for AlPi, Z for ZnPi and H for HM1100. As an example, the material referred to as PE_ZZ₂₄ was formulated with PBT, the epoxy resin, the transesterification catalyst and 24 wt.-% ZnPi.

Table 2: Abbreviation and quantities of reactants for all formulations of this chapter

Abb.	Mass of components (g), (percentage, wt.-%)					
	PBT	DGEBA	Zn(acac) ₂	AlPi	ZnPi	HM1100
PBT	12 (100)					
PE _Z	11.7 (98)	0.23 (1.9)	0.021 (0.18)			
PA ₂₀	9.5 (80)			2.41 (20)		
PE _Z A ₂₀	9.5 (78)	0.19 (1.6)	0.017 (0.14)	2.41 (20)		
PZ ₂₄	8.9 (76)				2.86 (24)	
PE _Z Z ₂₄	8.9 (75)	0.18 (1.5)	0.016 (0.13)		2.86 (24)	
PE _Z Z ₁₀	10.6 (88)	0.21 (1.8)	0.019 (0.16)		1.15 (10)	
PE _Z H ₄₄	4.8 (54)	0.097 (1.1)	0.0087 (0.10)			3.95 (44)
PH ₂₀	8.1 (80)					2.03 (20)
PE _Z H ₂₀	8.1 (78)	0.16 (1.6)	0.015 (0.15)			2.03 (20)
PE _{5Z} H ₂₀	8.1 (78)	0.16 (1.5)	0.075 (0.72)			2.03 (20)
P5E _Z H ₂₀	8.1 (74)	0.80 (7.3)	0.015 (0.14)			2.03 (18)
P5E _{5Z} H ₂₀	8.1 (74)	0.80 (7.3)	0.075 (0.68)			2.03 (18)

2.2.3 Characterization

Torque versus residence time. This parameter, which is proportional to the viscosity of the material processed, was recorded as a function of the residence time during each test. Figure 36 shows a typical curve observed during the preparation of a PBT vitrimer. It has been demonstrated that the addition of epoxy on the carboxylic chain ends of PBT leads to chain extension without torque increase whereas as soon as the crosslinking occurs because of transesterification reactions, a sharp increase of this parameter is observed^{5,91}. Repeatability was conducted at least 4 times between each tests.

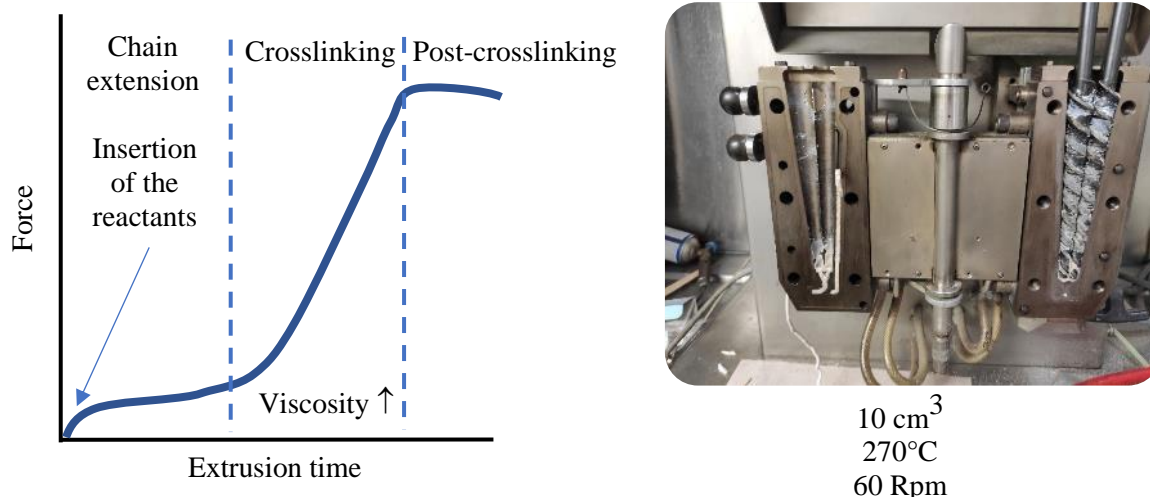


Figure 36 : Left: Model curve of the evolution of the viscosity during the synthesis of a PBT vitrimer; Right: Picture of the micro-extruder with barrel opened

Elemental analysis. These analyses have been performed to quantify the amount of Zn from the catalyst and Al, Zn and P from the additives. They have been performed externally by the laboratory Crealins from 6NAPSE group by ICP-AES (iCAP 6500 Duo from Thermo Scientific) after mineralization of the sample in acidic media. From the phosphorus quantifications, the fraction of additive in the materials has been calculated as presented in Equation 2, where FR_m is the fraction of FR in the material (m), $\%P_m$ is the weight percentage of phosphorus in the material, and $\%P_{FR}$ is the weight percentage of phosphorus in the FR (calculated from the molar masse of the FR).

$$\text{Equation 2} \quad FR_m = 100 \times \left(\frac{\%P_m}{\%P_{FR}} \right)$$

Gel and soluble fraction separation. 200 mg of each formulation (m_0) were immersed in 20 mL of 1,1,1,3,3,3-hexafluoro-isopropanol (HFIP) (purity >99%, supplied by Fluorochem), a well-known solvent for Poly(butylene terephthalate)^{87,88} for 4 days under stirring at room temperature and filtered using a Büchner funnel. The results for each samples are based on a minimum of five tests to ensure results with pertinent uncertainty values.

The insoluble gel fraction collected on the filter was dried for 4 days at room temperature and then weighed (m_{gel}). The gel ratio was calculated using Equation 3, with m_0 and FR_m respectively the

initial mass of formulation used and the FR fraction contained in the formulation, and m_{gel} and FR_{gel} respectively the weight of gel and the FR fraction contained in the gel.

$$\text{Equation 3} \quad \%gel = 100 \times \frac{m_{gel} (1 - FR_{gel})}{m_0 \times (1 - FR_m)}$$

In parallel, the filtrate was evaporated to weigh the solubilized fraction. For vitrimer materials, characterizations of the solubilized and the gel fractions will be performed and referred to as explained hereafter. The authors will refer to the solubilized part or gel fraction using the name of the sample with “sol” and “gel” as subscripts (PE_{Zsol} for instance or PE_{Zgel} for instance).

The FR percentage contained in the gel (FR_{gel}) and soluble fraction (FR_{sol}) of the materials were obtained from Equation 4 and

Equation 5, with $\%P_{gel}$ and $\%P_{sol}$ their respective weight percentage of phosphorus.

$$\text{Equation 4} \quad FR_{gel} = 100 \times \left(\frac{\%P_{gel}}{\%P_{FR}} \right)$$

$$FR_{sol} = 100 \times \left(\frac{\%P_{sol}}{\%P_{FR}} \right), \text{ with}$$

Equation 5

$$\%P_{sol} = \frac{\%P_{polymer} - \%P_{gel} \times \%Gel}{1 - \%Gel}$$

FTIR spectroscopy. Fourier Transform Infrared Spectroscopy (FTIR) was conducted to investigate the chemical composition of the samples by using a Nicolet iS50 FTIR Spectrometer. Spectra were acquired by scanning the samples in the infrared region ($4000-400 \text{ cm}^{-1}$) over a specified wavelength range. 32 scans were collected to improve the signal-to-noise ratio and ensure reliable data.

Solid state NMR analysis. Solid state NMR has been used to follow the environment changes of the phosphorus and aluminium nuclei in the formulations. The analyses were conducted using a Bruker Avance II 400 on cryoground samples. Analysis was conducted on at least two samples for each formulation.

^{31}P NMR measurements were performed at 40.5 MHz using a 4 mm probe, with dipolar decoupling (DD) and magic angle spinning (MAS) at a speed of 20 kHz. The delay time between two impulsions was fixed at 120 s (because of the relaxation time of the phosphorous nucleus). The spectra were acquired after 16 or 32 scans in order to get a correct signal to noise ratio. The reference used was 85 % H_3PO_4 in aqueous solution. The results were compared to already-known NMR chemical shift ranges of phosphorus²⁰⁵.

^{27}Al NMR measurements were performed at 104 MHz using a 4 mm probe, with MAS at a speed of 20 kHz. The delay time between two impulsions was fixed at 1s (quick relaxation time of quadrupolar nuclei). 512 to 2048 scans have been acquired to increase the signal/noise ratio. The reference used is a 1 M solution of aluminium nitrate.

^{13}C NMR measurements have been performed at 100.4 MHz using 7 mm probes, with CP 1H-13C, dipolar decoupling (DD) and magic angle spinning (MAS) at a speed of 10 kHz. For all samples, a delay time between two impulsions of 5 s and a contact time of 1 ms were used. Tetramethylsilane (TMS) is used as reference for the chemical shift.

SEM microscopy and EPMA. The morphology of the materials was characterized by scanning electron microscopy (SEM) using a Jeol JSM-IC 848 SEM with an acceleration voltage of 15 kV. A Cameca SX100 electron probe microanalyzer (EPMA) was used to perform elemental analysis. X-ray mappings were carried out at 15 kV, 40 nA. A TAP crystal is used to detect the Al $K\alpha$ X-ray and a PET crystal to detect the P $K\alpha$ X-ray. The samples were embedded into epoxy resin, polished with SiC polishing sheets from grade 80 up to grade 4000 and carbon coated with a Bal-Tec SCD005 sputter coater.

Thermal analysis. Differential scanning calorimetry (DSC) analyses were performed using a Discovery DSC from TA Instrument under nitrogen ($50 \text{ mL}\cdot\text{min}^{-1}$) on at least three samples per formulation. Temperature and heat flow were calibrated with a high-purity indium sample using standard procedures. Aluminum pans and lids were used but the crucible was not hermetically sealed. The sample (5 mg) was heated from -40 to 270 °C at 20 °C/min, held at 270 °C for 2 min, then cooled to -40 °C at 20 °C/min, held at -40 °C for 2 min, and finally heated to 270 °C at 20 °C/min. The glass transition temperature (T_g , °C), the melting temperature (T_m , °C), as well as the melting enthalpy (ΔH_f , $\text{J}\cdot\text{g}^{-1}$) were measured from the second DSC heating cycle. The crystallization temperature (T_c , °C), as well as the crystallization enthalpy (ΔH_c , $\text{J}\cdot\text{g}^{-1}$) were measured from the first DSC cooling cycle. The crystallinity ratio (χ_c) was obtained using Equation 6 with $\Delta H_{m100\%}$ the enthalpy of melting for a 100% crystalline PBT (140 J/g)²⁰⁶, ΔH_m the experimentally measured melting enthalpy and F_{FR} the fraction of flame-retardant additives left in the matrix.

Equation 6

$$\chi_c = \frac{100 \times \Delta H_m}{\Delta H_{m100\%} (1 - F_{FR})}$$

Thermogravimetric analyses (TGA) were realized in alumina pans with a gold foil (to prevent reaction between the sample and the crucible) using a Discovery apparatus from TA Instrument under nitrogen flow ($20 \text{ mL}/\text{min}$). A purge of 60 min at 40 °C was carried out before heating the sample (around 10 mg, powder) from 40 to 800 °C at a heating rate of 20 °C/min.

Stress relaxation experiments. Stress-relaxation experiments were conducted to record the time and temperature-dependent stress relaxation properties of the different semi-crystalline PBT vitrimer formulations using an Anton Paar MCR 301 Rheometer equipped with a 25mm diameter plate geometry. The deformation was applied at 1% strain, well into the linear viscoelastic regime of the material. The gap was maintained at 1.5mm during the whole experiment. Analyses were conducted with a temperature range between 235 and 265°C depending on the material, and the relaxation modulus was recorded as a function of time. Values of zero-shear viscosity (η) and relaxation time (τ) were evaluated from the relaxation modulus, $G(t)$ through Equation 7. At least two samples per formulation were tested to validate the veracity of the relaxation profiles obtained.

Equation 7

$$\eta = \int G(t)dt ; \tau = \frac{1}{\eta} \int tG(t)dt$$

Wide angle X-ray diffraction. WAXD experiments were carried out at room temperature on a Xeuss 2.0 (Xenocs) operating under vacuum, with a GeniX3D microsource ($\lambda = 1.54 \text{ \AA}$) at 0.6 mA and 50 kV and a 2D Pilatus 3 R 200 K detector. Analyses were performed for 300s acquisition time in transmission mode, with a sample-to-sample distance of 150 mm. WAXS scattered intensities were integrated and plotted against the scattering angle 2θ and the scattering vector, $q = (4\pi/\lambda)\sin\theta$.

2.3 Influence of FRs on the formation of a PBT vitrimer

In this part of the study, the effect of the flame-retardant presence on the formation of the vitrimer material through reactive extrusion was studied. The evolution of the torque and quantification of the gel ratios of FR materials were first used as marker of the formation of vitrimers. The reference material without FR was prepared and its behavior explained thanks to the literature and our experiments. Then materials were prepared in the same processing conditions in presence of AlPi, ZnPi and finally HM1100. The interaction between the constituent of the formulations were analysed and explained.

2.3.1 Reference system without FR

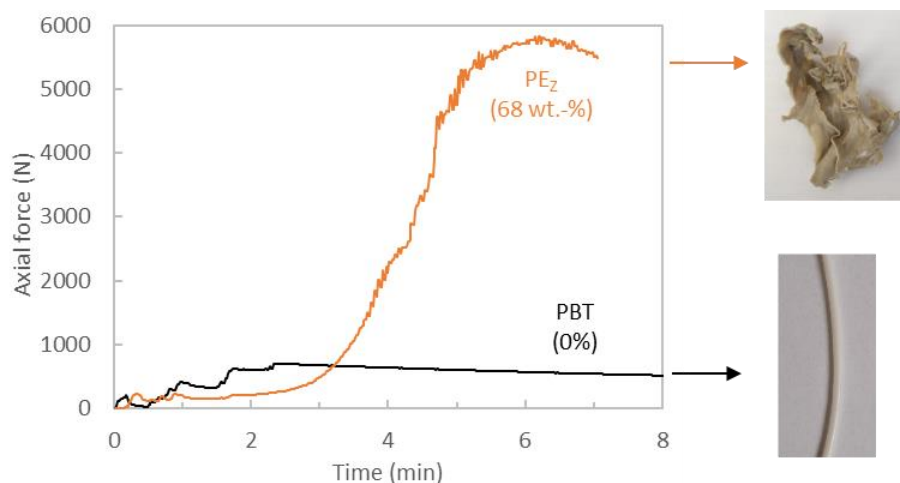


Figure 37 : Evolution of the axial force as a function of the residence time in the extruder without flame retardant (270 °C, 60 rpm, N₂ flow), picture of the samples and gel ratio indicated in bracket)

For the reference PBT, the curve is quite stable with a low axial force of around 500 N after a first rise corresponding to the introduction of the raw materials in the first minutes of processing (Figure 37). This indicates that after the melting of the polymer, only mixing of the formulation is performed and no cross-linking occurs.

In the case of PE_Z, on the contrary, a steep rise in axial force occurs after a residence time of 3 minutes and reaches a maximum of approximately 6000 N after 6-7 minutes. This rise in axial force is correlated with the increase of the viscosity, as cross-linking occurs thanks to the presence of the Zn(II) transesterification catalyst⁸¹. The obtained material presents a slightly grey/yellowish color (Figure 37).

This behavior was already explained by Demongeot et al⁵ as an evolution of the viscosity due to two reactions happening during the process. During a first step, chain extension occurs. One of the oxirane rings of the diepoxy opens and reacts with either the –COOH or –OH end groups of PBT. In both cases, a pendent hydroxyl function is formed (Figure 38). No evolution in the recorded force is visible, as chain extension does not significantly impact the overall viscosity of the material. This step can occur between –COOH and epoxy groups without the use of any catalysts^{207,208}, but reaction times are counted more in hours through reactive extrusion. The addition reaction of terminal hydroxyl functions with epoxy has to be taken into account. The resulting ether function is non-exchangeable, but may not be of significant concern as per the presence of numerous ester groups in the backbone of PBT. The addition of a catalyst is necessary to increase reaction rates. Demongeot et al. studied the reaction kinetics of epoxy with –COOH/–OH model molecules catalyzed with Zn(acac)₂⁵. He showed that in the presence of Zn(acac)₂, total consumption of –COOH groups occurred within 6 minutes, while 50% total consumption of –OH groups was obtained in over 20 minutes. Thus, most of the hydroxyl end chains may not react with epoxy in our reaction time scale (<10min)⁵.

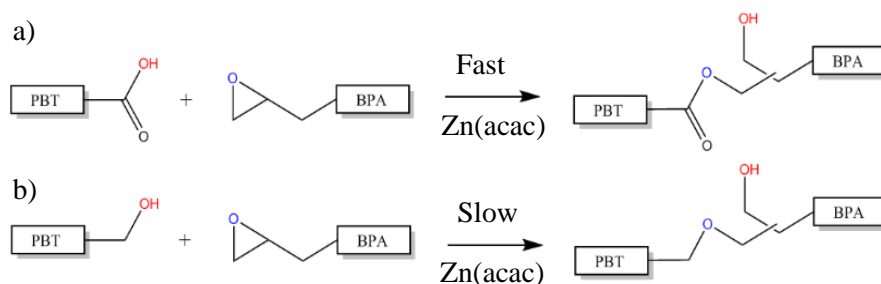
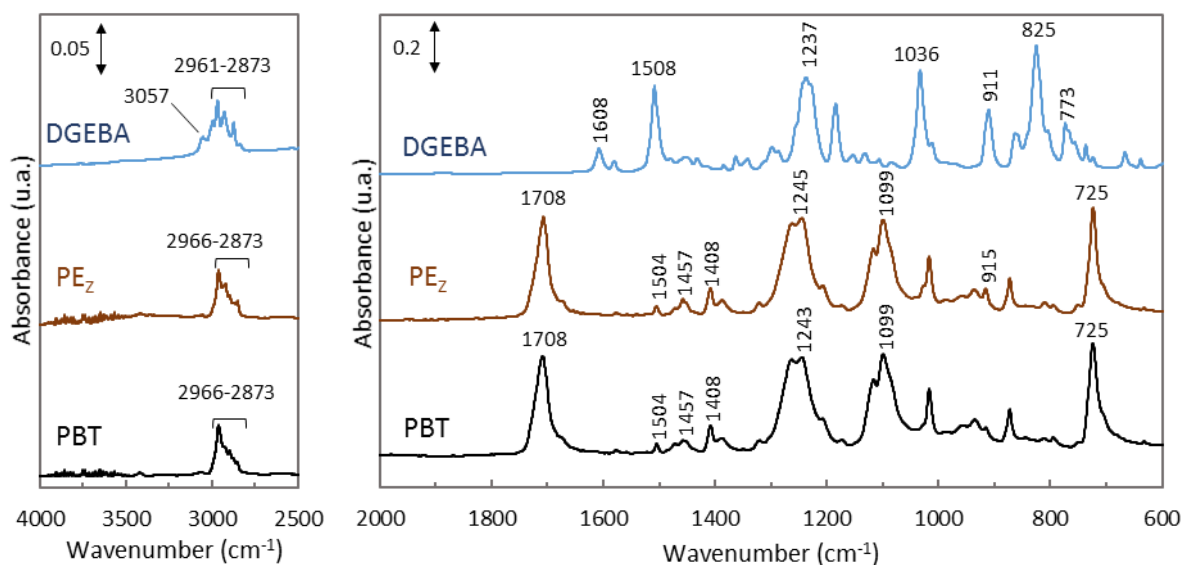


Figure 38 : Possible reactions involved during chain extension step (a) Reaction between carboxylic acid and epoxy to form an ester; (b) Reaction between hydroxyl and epoxy. Both reactions lead to the formation of a pendent alcohol, which can in turn react with other epoxy (slow) or participate in transesterification reactions

The second step involves the cross-linking of the polymer through transesterification reactions between β -hydroxyl ester and pendent hydroxyl functions formed during the chain extension step. The presence of a proper catalyst is necessary to speed up the reaction^{5,36}. Cross-linking is known for radically increasing the viscosity of the material, which is translated into a rise in force recorded by the micro-extruder (Figure 36).

To verify the molecular structure of the synthesized vitrimer, sets of ATR-FTIR and ^{13}C NMR investigations were performed. Figure 39 shows the FTIR spectra of PBT, PE_Z, and DGEBA, with main vibration bands for PBT and DGEBA described in Table 3. For DGEBA, the bands at 3057cm^{-1} , 911cm^{-1} and 825cm^{-1} respectively corresponds to the $-\text{CH}$, $\text{C}-\text{O}$ and $\text{C}-\text{O}-\text{C}$ stretching of the oxirane group. In PE_Z, only the stretching vibration of the $\text{C}-\text{O}$ bonds is visible and slightly shifts at 915cm^{-1} . This result is on par with the 2:1 [epoxy]/([OH]+[COOH]) ratio. No significant O-H stretching band is visible at around 3500cm^{-1} for all materials. In the case of DGEBA, this result is easily explained by the very low homopolymerization degree of the DER 332 grade. In the case of PE_Z, while the opening of the oxirane should promote the formation of O-H bonds, quantification is difficult because of the low amount of reactant and the particularly large absorption band. At the same time, chain extension reactions also lead to the formation of esters in detriment to end chain carboxylic acids. However, those reactions do not affect the intensity of the absorption band of esters at 1715cm^{-1} due to the already high concentration of ester groups present in the PBT backbone.

Figure 39: IR spectra of PBT, DGEBA and PE_ZTable 3 : Characteristic IR-absorption bands of DGEBA and PBT in IR^{209,210}

Formulation	Band (cm ⁻¹)	Assignment
DGEBA	3057	Stretching of C-H of the oxirane ring
	2966-2873	Stretching C-H of CH ₂ and CH in aromatic and aliphatic groups
	1608	Stretching C=C of aromatic rings
	1508	Stretching C-C of aromatic rings
	1036	Stretching C-O-C of ether
	911	Stretching C-O of oxirane group
	825	Stretching C-O-C of oxirane group
	773	Rocking CH ₂
PBT	2966-2873	Stretching C-H of CH ₂ and CH aromatic and aliphatic
	1708	Stretching C=O of ester group
	1504	Stretching C-C of aromatic rings
	1457	Bending vibration of C-H bonds
	1408	Bending vibration of C-H bonds
	1245	Stretching of C-O bonds
	1099	Stretching of C-O-C bonds
	725	Stretching of aromatic ring C-H out-of-plane deformation

¹³C ss NMR spectra of PBT and cross-linked DGEBA, along with their respective peak assignments, are shown in Figure 40. Figure 41 presents the spectra of PBT, DGEBA, and PE_Z. In PE_Z, the characteristic chemical displacement peaks of PBT are observed at 164.7, 132.8, 129.3, 128.19, 64.15 and 25.4 ppm²¹¹. However, no peaks relating to the epoxy are observed.

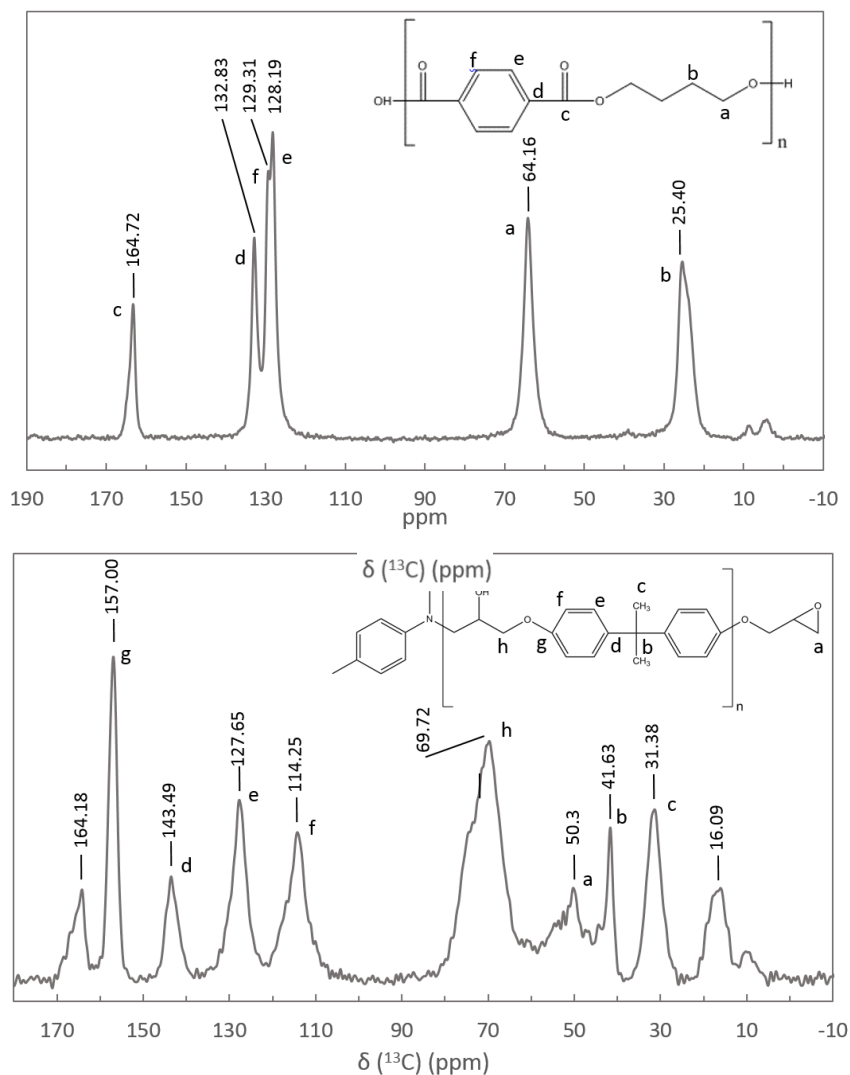


Figure 40 : Top: ^{13}C ss NMR spectrum of PBT. Bottom: ^{13}C ss NMR spectrum of a DGEBA cross-linked with an amine-based hardener. Only the referenced peaks have to be taken into consideration²¹²

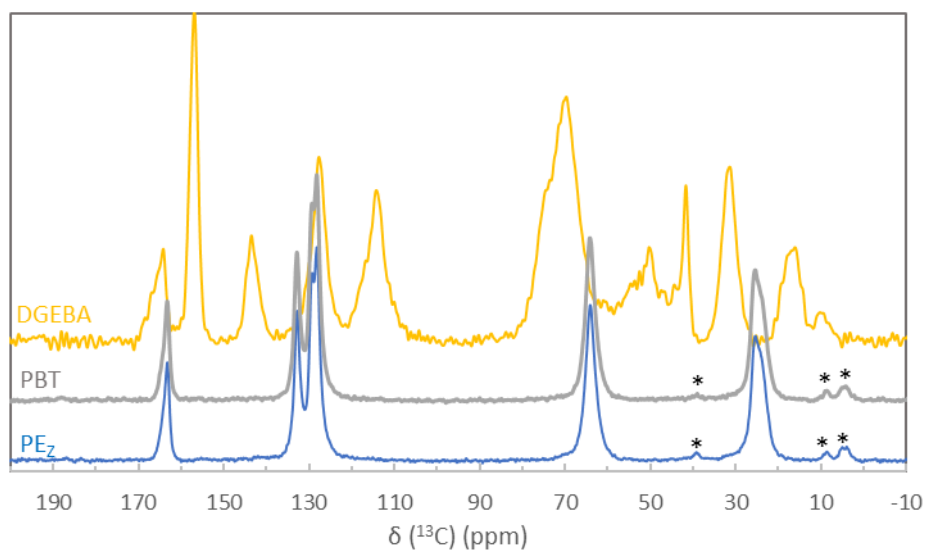


Figure 41 : Comparison between the ^{13}C ss NMR spectra of the different formulations. (* rotation bands)

To summarize, both FTIR and ^{13}C NMR analyses were carried out on the PE_Z sample, revealing no significant differences that would suggest the occurrence of cross-linking. The evaluation of the reaction between the diepoxide and the chain ends of PBT could not be performed due to the limited quantity of epoxy introduced into the system.

To confirm the formation of the network and quantify its cross-linked fraction, the gel content of PE_Z was determined by immersing both samples in 1,1,1,3,3,3-hexafluoroisopropanol at room temperature under gentle stirring for 4 days. PBT expectedly dissolves totally and presents no significant gel fraction. However, PE_Z is only partially soluble and exhibits a gel fraction of around 68 wt.-%. This demonstrates the presence of a cross-linked network, highlighted by the rise in viscosity previously seen in the micro-extruder. Demongeot et al. obtained an insoluble fraction of 43 wt.-% and 75 wt.-% with an [epoxy]/([OH]+[COOH]) ratio of respectively 1.7 and 3.4⁵. Several differences between the two studies can explain the apparent discrepancy between the gel ratio values. The first one concerns the quantification of the gel ratio. Two different protocols have been used. Demongeot et al. proceed in two steps by first immersing the material in 1,1,2,2-tetrachloroethane for 16 h at 120 °C then washing it in chloroform for 24 h. In the present study, a different solvent was used and no washing step was performed after the dissolution of the thermoplastic part, what could lead to the obtention of higher gel value. Then, a slightly higher [epoxy]/([OH]+[COOH]) ratio of 2.0 was used in our study that is also partly responsible for the higher gel value. Eventually, they also used an antioxidant during processing that could prevent some degradation of the PBT during the processing. In our case, no antioxidants was added in the formulations in order to avoid undesired reactivity in presence of flame-retardants. It is known that during extrusion of PBT, hydroxybutyl end groups could degrade through homolytic cleavage with the PBT chain, leading to the formation of volatile THF species while increasing the fraction of carboxylic end-group in the material and decreasing the fraction of hydroxyl end groups²¹³⁻²¹⁵ (Figure 42). This leads to a higher amount of carboxylic acids that can react quickly with epoxy, leading to a higher concentration of pendent hydroxyl groups, increasing the quantity of cross-linking bonds formed in the polymer. However, no significant differences in the intensity of the carbon ester peak was observed by ^{13}C NMR at 164.72 ppm. This result can be attributed to the relatively small quantity of newly formed esters in comparison to the existing esters present in the PBT backbone, making it challenging to monitor this evolution accurately.

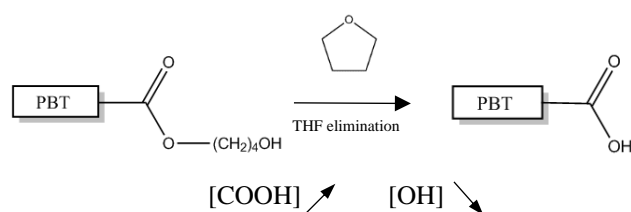


Figure 42 : Main degradation pathway of hydroxybutyl end groups in PBT, leading to a higher concentration of carboxylic end groups

In conclusion, a cross-linked PBT material was successfully synthesized through reactive extrusion, resulting in a gel fraction of approximately 70 wt.-%. The assessment of the reaction between the diepoxide and the end chains of PBT using NMR or FTIR was limited due to the low level of epoxy that effectively reacted with the PBT end chains for cross-linking. This cross-linked PBT material, referred to as PE_Z, will serve as the reference material for subsequent investigations in the following sections.

2.3.2 Systems with AlPi

AlPi is an effective flame-retardant for PBT systems. As reported in Chapter 1, studies have been conducted on its effectiveness as flame retardant additives, with 20 wt.-% AlPi-filled PBT exhibiting excellent flame-retardant properties²¹⁶. Thus, 20 wt.-% of AlPi was added during the synthesis of PBT vitrimer by reactive extrusion.

No significant rise in force is visible for compound PA₂₀ (Figure 43). However, in the case of PE_ZA₂₀, the axial force rises after 1 minute, with a maximum peak reached after 5 min of extrusion. This maximum is reached significantly sooner than for PE_Z (6-7 minutes). For PA₂₀, which is composed of AlPi particles dispersed in PBT, both soluble in HFIP, no insoluble fraction could be measured. PE_ZA₂₀, however, exhibits a gross 63 wt.-% gel ratio. This value includes both the cross-linked polymer matrix and the remaining flame-retardant which was not washed away with the solvent.

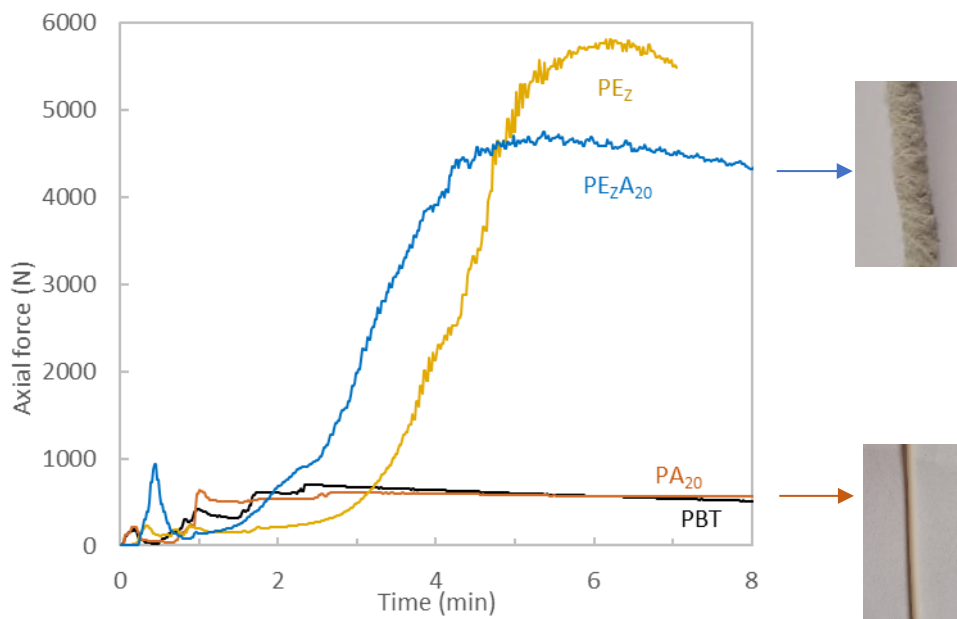


Figure 43 : Evolution of the axial force as a function of the residence time in the extruder in presence of AlPi (270 °C, 60 rpm, N₂ flow)

Table 4 : Gel ratio and weight percentage of aluminum, phosphorus and zinc remaining in each cross-linked formulation based on elemental analysis. The calculated amount of FR in the formulation was obtained from the amount of phosphorus measured. *Results obtained from Equation 5.

Sample	Gel ratio (wt.-%)	Elemental composition (wt.-%)			FR _{calculated} (wt.-%)	FR _{expected} (wt.-%)
		Al	Zn	P		
PE _Z	68 ±4	/	/	/	/	/
PE _Z A ₂₀	69 ±3	1.20 ±0.04	0.0340 ±0.0006	4.35 ±0.02	18.3	20
PE _Z A _{20gel}	100	0.78 ±0.01	0.0200 ±0.0004	2.70 ±0.04	11.3	
PE _Z A _{20sol} *	0	2.13 ±0.10	0.0652 ±0.0024	8.02 ±0.10	33.7	

To better quantify the gel fraction of the polymer matrix, it is first necessary to determine the amount of FR additives remaining in the gel. Since aluminum phosphinate is soluble in HFIP, elemental analyses were performed on the polymer obtained directly after the extrusion as well as on its insoluble part, PE_ZA_{20gel}. Table 4 presents the quantities of phosphorus, aluminum and zinc in both samples. 4.35 wt.-% phosphorus is present in PE_ZA₂₀ after extrusion, which is 0.45 wt.-% lower than the calculated amount of Phosphorus added to the extruder (4.8 wt.-%). This implies that some of the AlPi was lost during the reactive extrusion, certainly during the integration of the reactant inside the extruder under N₂ flux, as AlPi powder is very volatile. In PE_ZA_{20gel}, 2.70 wt.-% phosphorus is present. As Phosphorus informs on the presence of heavier phosphinate groups bearing the majority of the weight of the AlPi compound, we considered only the amount of phosphorus to calculate the real concentration of FR inside the matrices. Through Equation 2, Equation 4 and Equation 5, it is possible to calculate both the amount of FR in the polymer and the gel fraction. The calculated concentration of FR in PE_ZA₂₀ is 18.3 wt.-%, while only 11.3 wt.-% remains in PE_ZA_{20gel}.

The calculation of the gel ratio of the flame-retarded materials was then done according to the equation given in the experimental part (Equation 3). The values obtained with and without FR are reported in Table 4. It appears that an equivalent gel ratio of 69 wt.-% is obtained for PE_ZA compared with the reference PE_Z. Consequently, AlPi does not hinder cross-linking.

First, the distribution of the flame retardant (FR) in both PE_ZA₂₀ and PE_ZA_{20gel} was analyzed using an EPMA (Figure 44). The non-fusible AlPi remains present in the vitrimer matrix in the form of agglomerates. However, when the gel alone is analyzed no agglomerate is seen anymore. This indicates that AlPi in the gel has been solubilized and interact with the matrix. To confirm this conclusion solid-state analyses have been performed.

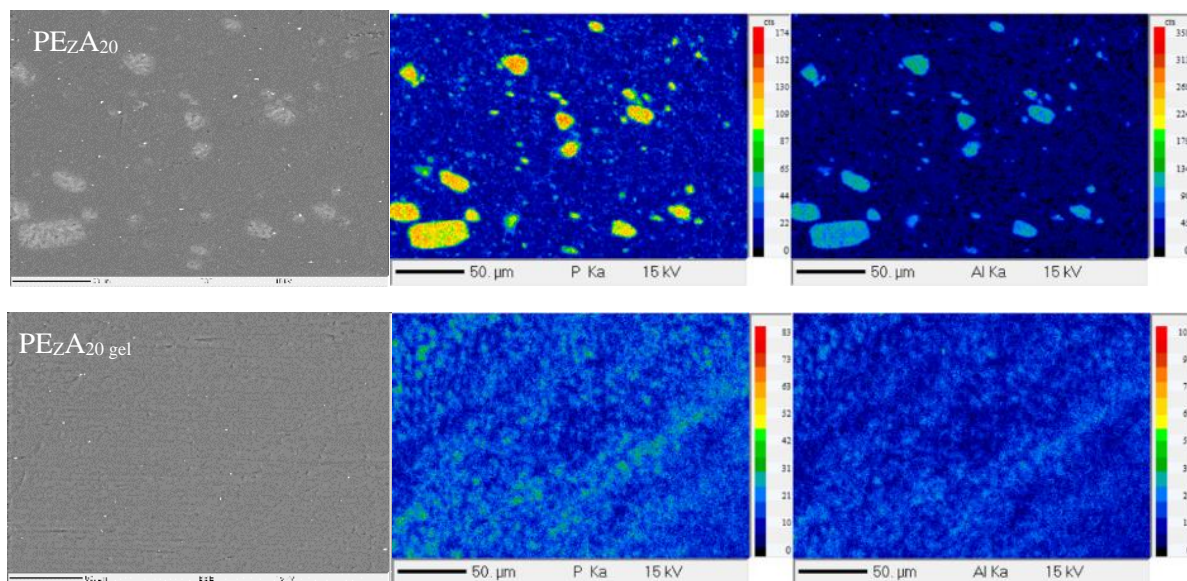


Figure 44 : EPMA analysis of PE_ZA₂₀ and PE_ZA_{20gel}

³¹P and ²⁷Al solid-state (ss) NMR analyses were performed on the vitrimer and isolated gel part to detect modification of the chemical environment around the aluminum and phosphorus atoms. The obtained spectra are presented in Figure 45. The ²⁷Al ss NMR spectrum of AlPi exhibits a single peak at -12 ppm due to the octahedral geometry of Al³⁺ cations, coordinated to phosphorus in their second coordination sphere.²¹⁷ On the other hand, ³¹P ss NMR spectrum presents two peaks between 38 and 45 ppm, characteristic of phosphinate sites²¹⁸. Those peaks on ²⁷Al and ³¹P spectra are present in PE_ZA₂₀ and PE_ZA_{20gel}. In addition, the analysis of the gel fraction highlights the presence of new, low-intensity signals at around 47 ppm for ²⁷Al analyses, indicating either a pentacoordinated or hexacoordinated aluminum, and at 52-58 ppm for ³¹P analyses. This peak could be attributed to diethylhypophosphorus acid also named diethylphosphinic acid that is observed around 53 ppm²¹⁹. The presence of these peaks in the gel fraction could be related to the ligand exchange of Al³⁺.

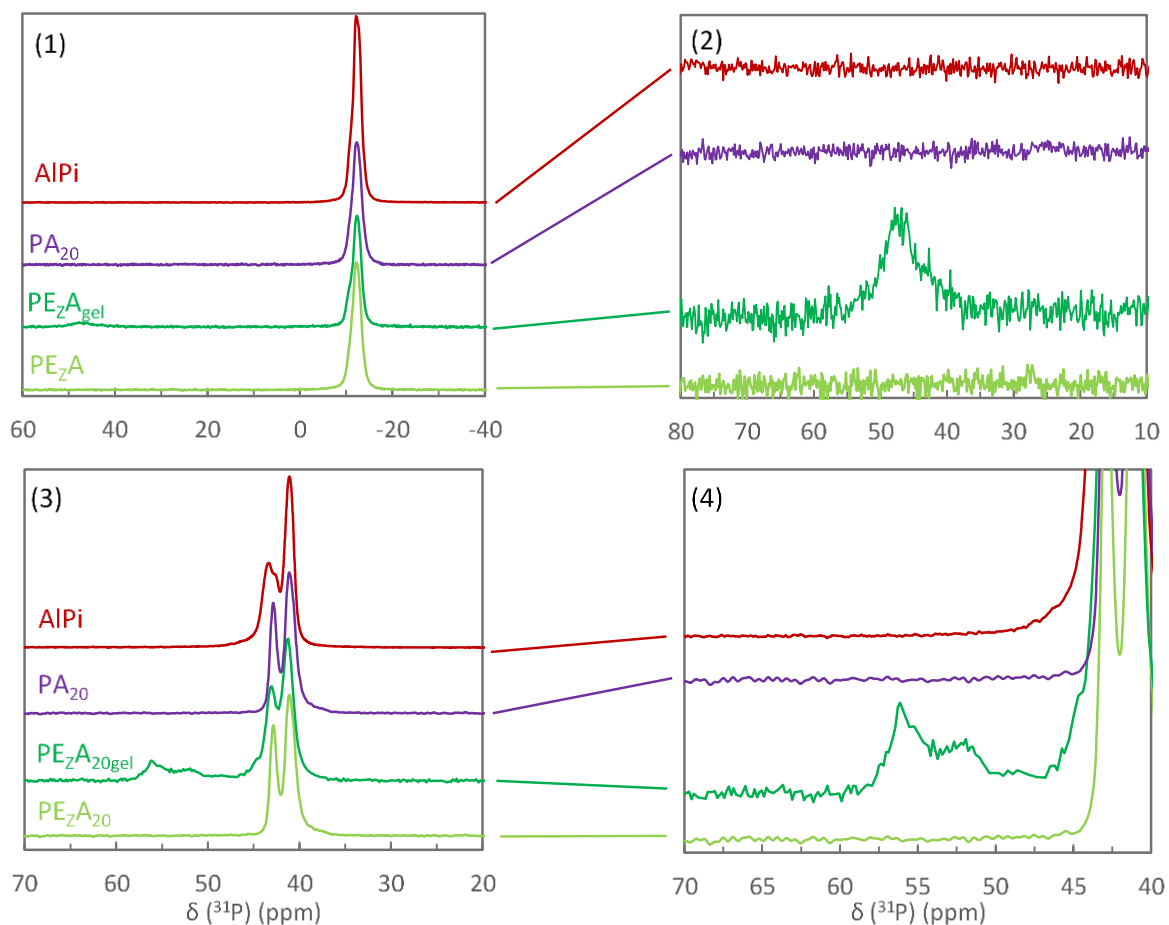


Figure 45 : ^{27}Al ss RMN (1) and (2), ^{31}P ss RMN (3) and (4) spectra of AlPi, PA₂₀, PE_ZA₂₀ and PEZA_{20gel}; zoom on the new peak (right)

Demongeot et al.⁸¹ previously showed that Zn transesterification catalysts in vitrimers do not remain under their initial Zn(acac)₂ form, but undergo ligand exchanges to form active complexes structurally bonded to the network through alkoxide or carboxyl ligands. By analogy with this study, it is reasonable to assume that the Al³⁺ cation can undergo similar ligand exchanges and might also be structurally bonded to the vitrimer network (Figure 46).

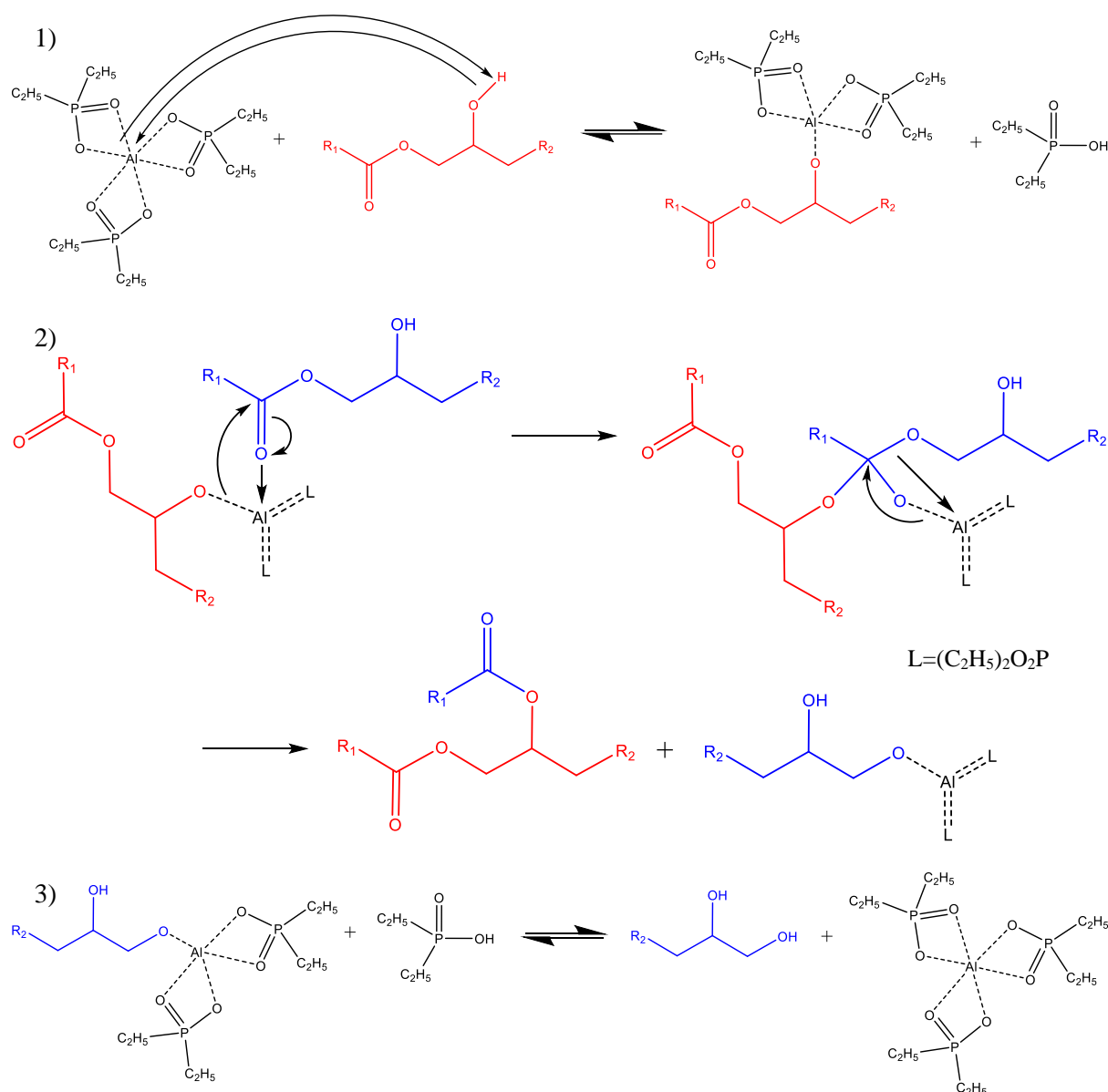


Figure 46 : Proposed mechanism of transesterification catalysed by aluminium phosphinate. (1) Formation of an alkoxide through the loss of a phosphinate ligand. (2) Transesterification between alkoxides and esters. (3) Reformation of the diol through proton exchange and recuperation of the phosphinate ligand.

In conclusion, we successfully obtained an AlPi-filled vitrimer with equivalent gel ratio than PE_Z. AlPi additive is thus not detrimental to cross-linking. Indeed, ³¹P and ²⁷Al ss NMR showed that some ligand exchanges may have occurred explaining the change in P and Al chemical environment, i.e. the phosphinate ligands may act as weak bases to deprotonate the β-hydroxyester, forming an alkoxide which will, in turn, either attack an ester group from the PBT backbone or serve as a ligand for Al³⁺. This statement can be put in perspective with the presence of solubilized aluminum and phosphorus in the EMPA analysis conducted on PE_ZA₂₀gel, proving that some AlPi is still present near the reaction centers and is able to participate in the ligand exchange reaction. The low intensity of the new peaks observed at 52-58 ppm on the ³¹P NMR and 47 ppm on the ²⁷Al NMR may be caused by the low

crosslinking density of the cross-linked network, limited by the number of reactive -COOH and -OH bonds. Thus, only low quantities of AlPi can interact with the matrix to effectively catalyze the transesterification reaction. This result may explain why a similar cross-linking degree was observed for PE_ZA compared with PE_Z. The catalytic role of AlPi will be studied more in details in Chapter 3.

2.3.3 Systems with ZnPi

The second FR additive tested is ZnPi. It was chosen because it is another phosphinate salts having the same metallic cation as the transesterification catalyst. This additive was tested at two loadings 10 wt.-% and 24 wt.-%, the latter corresponds to the same phosphorus molar loading as AlPi (4.8 wt.-%) The materials prepared are named compound PE_ZZ₁₀ and PE_ZZ₂₄. The evolution of the axial force is presented on Figure 47.

During reactive extrusion (Figure 47) for PZ₂₄, no rise in force is visible within the 8 minutes of reactive extrusion as in the case of PA₂₀ processing. For both FR compounds, on another hand, a rise in the force is recorded only one minute after the incorporation of the reactants until a stabilization at around 3700 N for PE_ZZ₁₀ and 2000 N for PE_ZZ₂₄ is reached after 5 min and 3.5min respectively. This rise indicate has previously that crosslinking occurs in both cases, but not the same extent. The gel ratios were calculated to ascertain this.

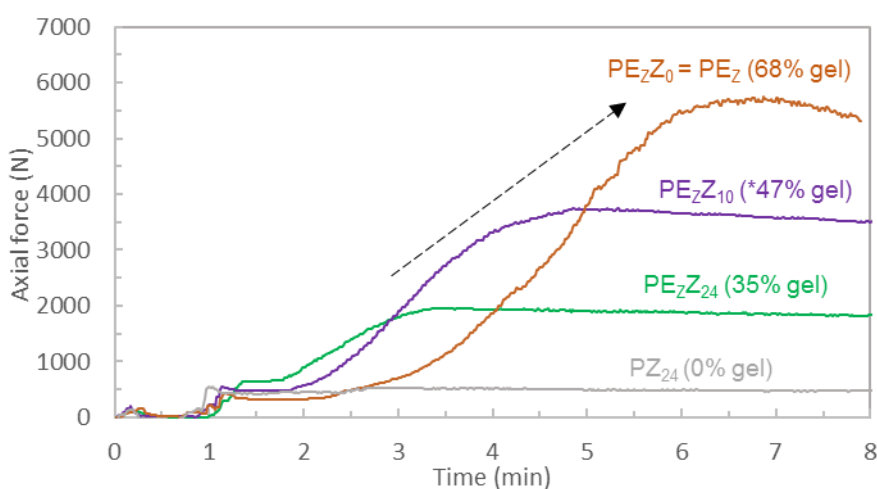


Figure 47 : Evolution of the axial force as a function of the residence time in the extruder in presence of ZnPi (270 °C, 60 rpm, N₂ flow)

Table 5 : Gel ratio and weight percentage of aluminum, phosphorus and zinc remaining in each cross-linked formulation based on elemental analysis. *Results for PE_ZZ₁₀ is an extrapolation from the values obtained for PE_ZZ₂₄.

Sample	Gel ratio (wt.-%)	Elemental composition (wt.-%)		FR _{calculated} (wt.-%)	FR _{expected} (wt.-%)
		Zn	P		
PE _Z Z ₁₀	*47 ±5	/	/	*9	10

PE _z Z ₁₀ gel	100	/	/	*4.9	-
PE _z Z ₂₄	34 ±3	5.71 ±0.06	4.33 ±0.10	21.5	24
PE _z Z ₂₄ gel	100	3.01 ±0.03	2.37 ±0.06	11.8	-
PE _z Z ₂₄ sol*	0	5.59 ±0.12	5.39 ±0.27	26.8	-

The obtained materials have gross gel ratios of 43 wt.-% for PE_zZ₁₀ and 31 wt.-% for PE_zZ₂₄. The quantities of phosphorus and zinc in PE_zZ₂₄ and its cross-linked counterpart PE_zZ₂₄gel are presented in Table 5, as well as the calculated amount of FR in the polymer and the gel fraction. Similarly to AlPi-filled polymer, the phosphorus content (4.33 wt.-%) in PE_zZ₂₄ is below the amount expected (4.8 wt.-%), as some of the volatile ZnPi powder may have been lost during the integration of the reactants in the extruder under N₂ flow. 2.37 wt.-% of phosphorus remains in the gel ratio. Once again, we considered only the amount of phosphorus to calculate the real concentration of FR inside the matrices. The calculated concentration of FR in PE_zZ₂₄ is 21.5 wt.-%, while it decreases to 11.8 wt.-% in PE_zZ₂₄gel. Thus, the calculated gel ratio for PE_zZ₂₄ is 34 wt.-%. For PE_zZ₁₀, the elemental analysis was not performed, consequently the gel ratio was calculating assuming a similar fraction of the FR remains in the soluble and insoluble fractions than the ones measured for PE_zZ₂₄. The loss of ZnPi due to the N₂ flow was also considered. The gel ratio was estimated at 47 wt.-%. Nevertheless, the vitrimer with 10 wt.-% of ZnPi presents a higher gel ratio than the one with 24 wt.-%. These results confirm that with lower amounts of ZnPi added to the vitrimer system, a higher cross-linking density is obtained (ratio ZnPi:Zn(acac)₂ of 48:1 in PE_zZ₁₀ and 140:1 in PE_zZ₂₄) (Table 2). In addition, it has to be noticed that the gel ratio of PE_zZ₂₄ is twice lower than the one obtained for PE_zA₂₀ even if both systems have similar weight and molar phosphorus loadings.

To understand the difference of behavior of both materials containing two similar phosphinate salts, different characterizations were performed on PE_zZ₂₄. First, microscopic observation of the sample and the distribution of the flame retardant (FR) in both PE_zZ₂₄ and PE_zZ₂₄gel samples were performed using an EPMA. Firstly, on the PE_zZ₂₄ microscopy, a lot of small holes are visible. A decomposition of a component of the formulation or a reaction between them could have led to evolution of gaseous species, but ZnPi starts degrading above 400°C²²⁰. Besides, the P and Zn elemental analyses show that this additive is still present in the same quantity. Then, phosphorus and zinc elemental mappings show no visible agglomerates at this scale neither in PE_zZ₂₄ nor in PE_zZ₂₄gel. This is consistent with previous studies on PET-ZnPi compounds^{220,221}. The fact that the additive melts during the processing facilitates the solubilization of the additive in the matrix.

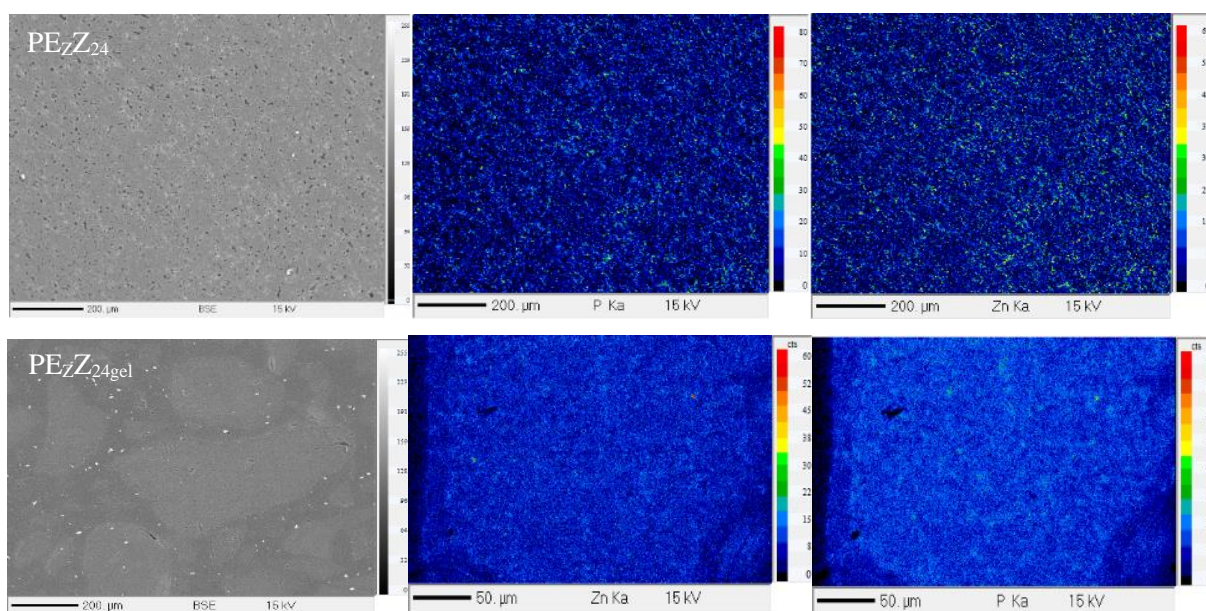


Figure 48 : EPMA microscopy of $PE_{zZ_{24}}$ and $PE_{zZ_{24}gel}$. The $PE_{zZ_{24}gel}$ EPMA was conducted on crygrinded pellets, hence the different scales for the Zn and P mappings.

As for the $PE_{zA_{20}}$ material, ^{31}P and ^{13}C ss NMR characterization have been performed on the material. Figure 49 and Figure 50 presents the spectra obtained for ZnPi, $PE_{zZ_{24}}$ and $PE_{zZ_{24}gel}$. $PE_{zA_{20}gel}$ spectrum is added for comparison purpose. In $PE_{zZ_{24}}$, the ^{31}P peaks characteristic of ZnPi are observed at 45.2, 46.9, 52.9 and 53.6 ppm. Surprisingly, the gel fraction of this material presents a radically different spectrum with a main peak at 55.3 ppm presenting a shoulder at 55.9 ppm. The environment of the phosphorus is consequently completely changed. The chemical shift at which the peaks are observed corresponds to the one also observed for the gel part of $PE_{zA_{20}}$. It is reasonable to assume that diethylhypophosphorus acid is also formed. In this case, all the ZnPi in the gel was modified during the preparation of the materials. The presence of the characteristic bands of the diethyl group (between 20 and 24 ppm for the CH_2 and around 6 ppm for CH_3) is detected on the ^{13}C NMR spectrum, showing the integrity of the phosphinate. A shift from 6.6 ppm for $PE_{zZ_{24}}$ to 5.9 ppm for $PE_{zZ_{24}gel}$ is however observed. Regarding the signal of CH_2 , four peaks are observed in ZnPi at 21.2, 21.9, 22.2 and 22.8 ppm. In contrast, $PE_{zZ_{24}}$ exhibits only two peaks at 21.9 and 22.8 ppm, while the gel shows signals at 21.2 and 22.2 ppm. It is hypothesized that the observed shift is related to the change in the carbon environment, with the phosphorus atoms initially bonded with zinc diethylphosphine being now present in the form of diethylhypophosphorus acid.

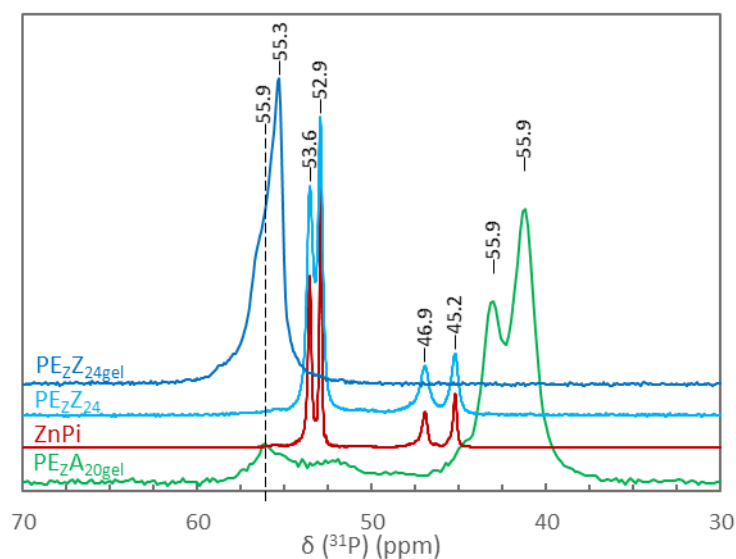


Figure 49 : ^{31}P ss RMN spectra of ZnPi, PE_zZ_{24} , $\text{PE}_z\text{Z}_{24\text{gel}}$ and $\text{PE}_z\text{A}_{20\text{gel}}$. The curves were normalized considering the higher intensity peaks of each sample.

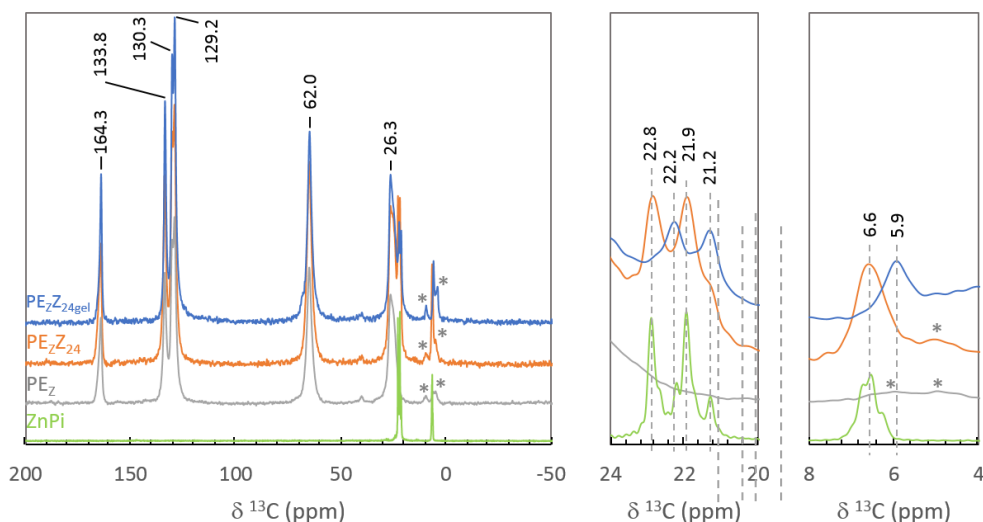


Figure 50 : ^{13}C ss NMR spectra of ZnPi, PE_zZ_{24} , $\text{PE}_z\text{Z}_{24\text{gel}}$ (* rotation bands)

ATR-FTIR spectra were conducted to compare the structure of ZnPi, PE_zZ_{24} as well its gel fractions. The C-O-CH band of the oxirane group is still visible at 915 cm^{-1} for all samples, gel fractions included, as previously explained by the stoichiometry. The O-H stretching band at 3500 cm^{-1} is relatively intense for PE_zZ_{24} indicating numerous O-H groups are present in the PE_zZ_{24} formulation, but significantly decrease in the gel fraction. The absorption band corresponding to the ZnPi at 770 , 1058 , 1140 and 2880 cm^{-1} are still present in the cross-linked material. Those peaks are of significantly lower intensity for the gel fraction, which is explained by the lower amount of ZnPi present in the insoluble fraction (Table 5). However, the bands at 2880 and 1058 cm^{-1} have nearly disappeared, which may suggest that the structure of the ZnPi left in the insoluble fraction has changed.

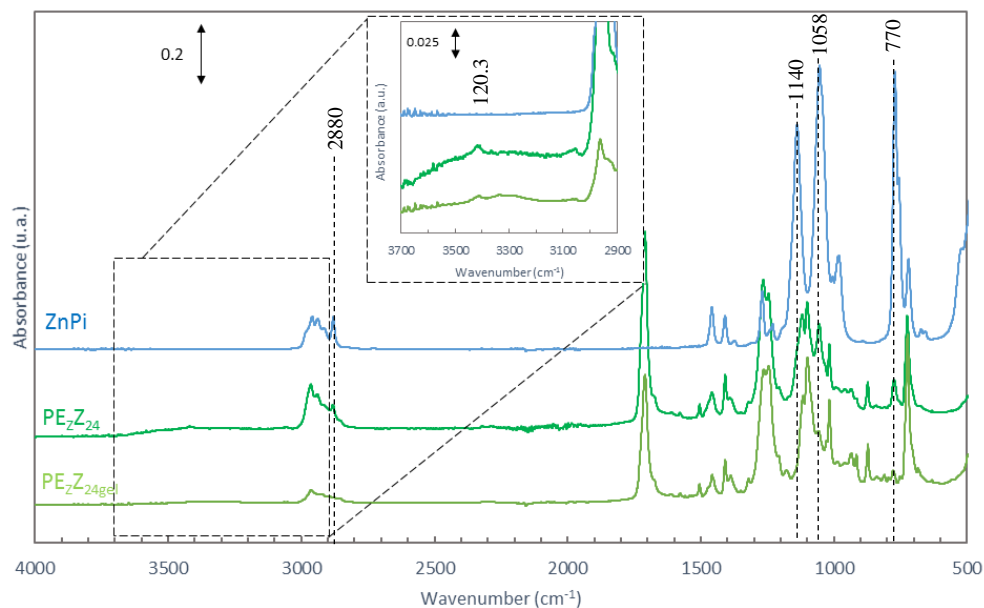


Figure 51 : IR spectra of PE_zZ_{24} , PE_zZ_{24gel} and $ZnPi$

In conclusion, the addition of $ZnPi$ during the synthesis of a PBT vitrimer leads to a significant decrease of the cross-linking degree, with a gel ratio divided by two compared with pristine vitrimer (35 wt.-% for PE_zZ_{24} vs 69 wt.-% for PE_z). Also, with a fusion temperature below the processing temperature of PBT, $ZnPi$ melts, facilitating the dissolution of the salt within the PBT matrix. Differences in the chemical composition of the material were observed when conducting the NMR analysis on the gel fraction of PE_zZ_{24} . New peaks appeared at 55.9 and 55.3 ppm for ^{31}P ss NMR, characteristic of diethylhypophosphorus acid, as well as at 22.2, 21.9 and 5.9 ppm for ^{13}C , indicating change of the chemical environment around the carbons constituting the diethyl groups. Those results are consistent with ligand exchanges occurring between the zinc diethylphosphinate and the vitrimer matrix. FTIR analysis, on the other hand, did not give conclusive information on chemical modifications. Hence, the $ZnPi$ additive impacts the formation of a cross-linked network by participating in the ligand exchange and subsequent bond-exchange dynamics.

2.3.4 System with HM1100

Contrary to $AlPi$ and $ZnPi$, HM1100 is an amorphous poly(methylphosphonate) presenting a glass transition temperature measured at $97^{\circ}C$. In this case, a blend of two polymers is consequently performed. This P containing polymer was tested at different loadings and with different amounts of epoxy and catalyst.

2.3.4.1 Different weight loading with the same amount of epoxy and catalyst

The first formulations were synthesized either at the same phosphorus loading than $AlPi$ and $ZnPi$ (4.8 wt.-%) or at the same weight loading as $AlPi$. Formulations containing 44 wt.-% and

20 wt.-% of HM1100 were consequently prepared. In these formulations, the catalyst and epoxy ratio was identical than the ones considered for the phosphinate salts formulations. These formulations were named PE_ZH₄₄ and PE_ZH₂₀.

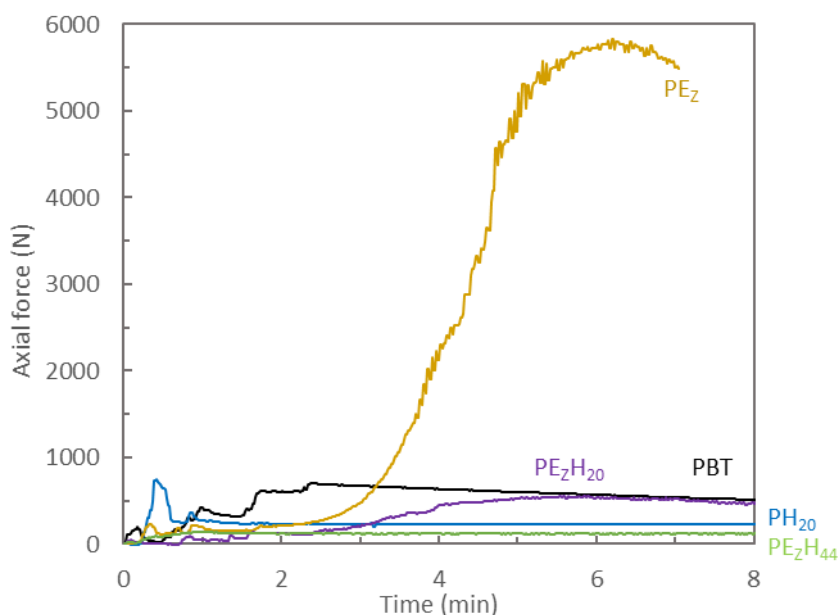


Figure 52 : Evolution of the axial force as a function of the residence time in the extruder in presence of HM1100 (270 °C, 60 rpm, N₂ flow)

The evolution of the axial force during the extrusion for these materials and the reference thermoplastic PH₂₀ is presented in Figure 52. When extrusion is performed with only PBT and HM1100, the axial force remains low and constant, as expected for a thermoplastic compound (PH₂₀). For PE_ZH₄₄, contrary to what was expected, no rise in viscosity occurs within 8 minutes. Besides, the sample dissolves completely in HFIP, with no gel fraction measured. For PE_ZH₂₀, the viscosity seems to slightly increase at 3 minutes, but it stabilizes rapidly and remains low. This rise in viscosity may be attributed to the formation of a few cross-linking bonds, however, those bonds are not enough to obtain a sufficiently cross-linked compound, as the gel ratio remains near zero. Compared to previous systems, it seems that HM1100 prevents the vitrimer network formation.

PE_ZH₄₄ and PH₂₀ exhibit a double glass transition temperature. The first glass transition (T_{g1}) occurs at 51.1°C and 45°C respectively, and is related to the glassy transition of the PBT. Those values are higher compared to previously studied formulations PA₂₀ (39.7°C) and PZ₂₄ (42.6°C). The second glass transition occurs at 97°C for both PE_ZH₄₄ and PH₂₀, and is attributed to HM1100. Usually, a double glass transition in a polymer blend is a consequence of immiscibility²²². The presence of 44 wt.-% HM1100 in PE_ZH₄₄ increases T_{g1} by 12°C compared with pristine PBT, while 20 wt.-% HM1100 in PH₂₀ increases T_{g1} by 6°C. Those results may imply that a small amount of HM1100 may have reacted with the PBT or epoxy, increasing the

degree of compatibilization between both polymers²⁰⁴. PE_ZH₂₀, on the other hand, exhibits a single glass transition at 58.5°C.

SEM and EPMA analyses were performed to observe the blends morphologies. The phosphorus mapping of the materials is depicted in Figure 53, along with three images of the materials captured at increasing magnifications ranging from x1500 to x45000 illustrated in Figure 54. The phosphorus elemental mapping for PE_ZH₄₄ shows the incompatibility between the two polymers. There are domains with HM1100 and domains with PBT. On the SEM pictures, the two polymer domains are very distinct. One appears smooth and uniform while the other is rough and irregular due to inclusions of the first phase (particle like domains). These inclusions are even more observable at high magnifications. DSC analyses confirmed this conclusion since two glass transition temperatures are observed for this material (respectively at 51.1 and 96.6°C), the second glass transition being on par with the glass transition of HM1100 (97°C). For the formulation containing only 20 wt.-% of HM1100 (no epoxy and no catalyst), the EPMA mapping shows also significant concentration of HM1100 in agglomerates, while the rest of the polymer is comparatively poor in HM1100 (Figure 53). In the continuous phase (PBT), HM1100 appears as smooth particles (shown by EDS phosphorus mapping). The poor adhesion between the polyphosphonate and the PBT phase is however visible at very high magnification (Figure 54). In this case, two T_g were measured at 45.2 and 97.1°C confirming the presence of two non-compatibilized phases. The material PE_ZH₂₀ displays a homogeneous repartition of the phosphorus on the EPMA mapping. No phase separation nor particles is observed at x1500 and x15000 magnification. Small particles well integrated in the matrix are however visible at x45000. These are much smaller than for the two other materials and their adhesion with the matrix seems good. This tends to demonstrate that HM1100 is in this case compatibilized with the PBT main phase.

PE_ZH₄₄

PH₂₀

PE_ZH₂₀

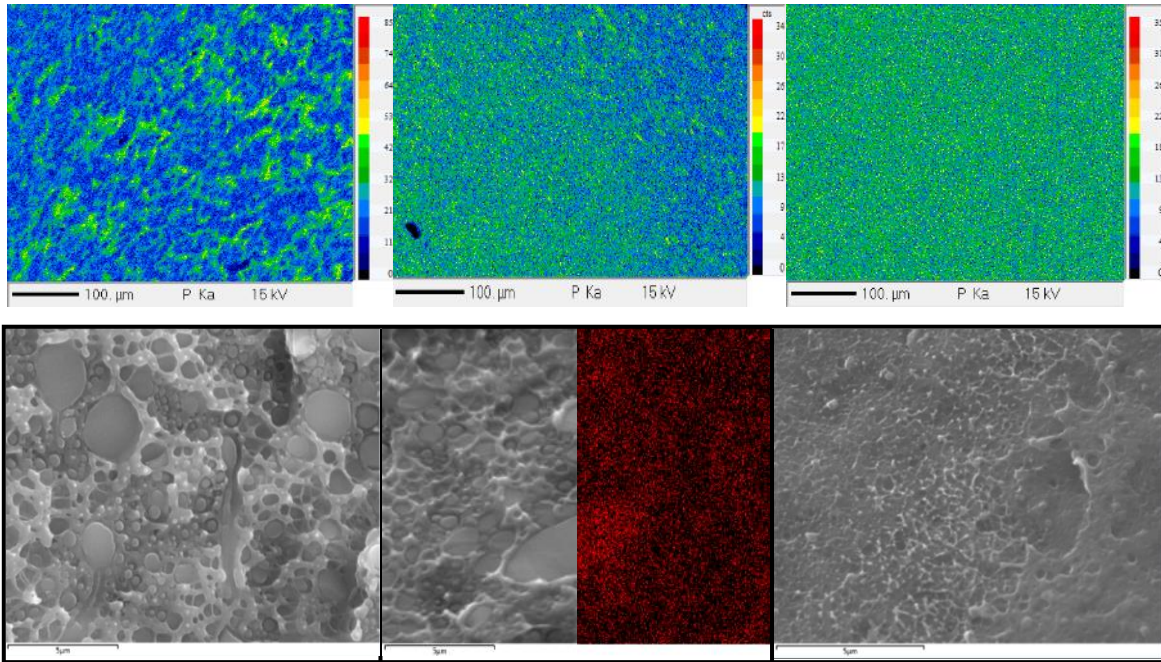


Figure 53 : Phosphorus EPMA analysis conducted on PE_zH₄₄ (left), PH₂₀ (middle) and PE_zH₂₀ (right)

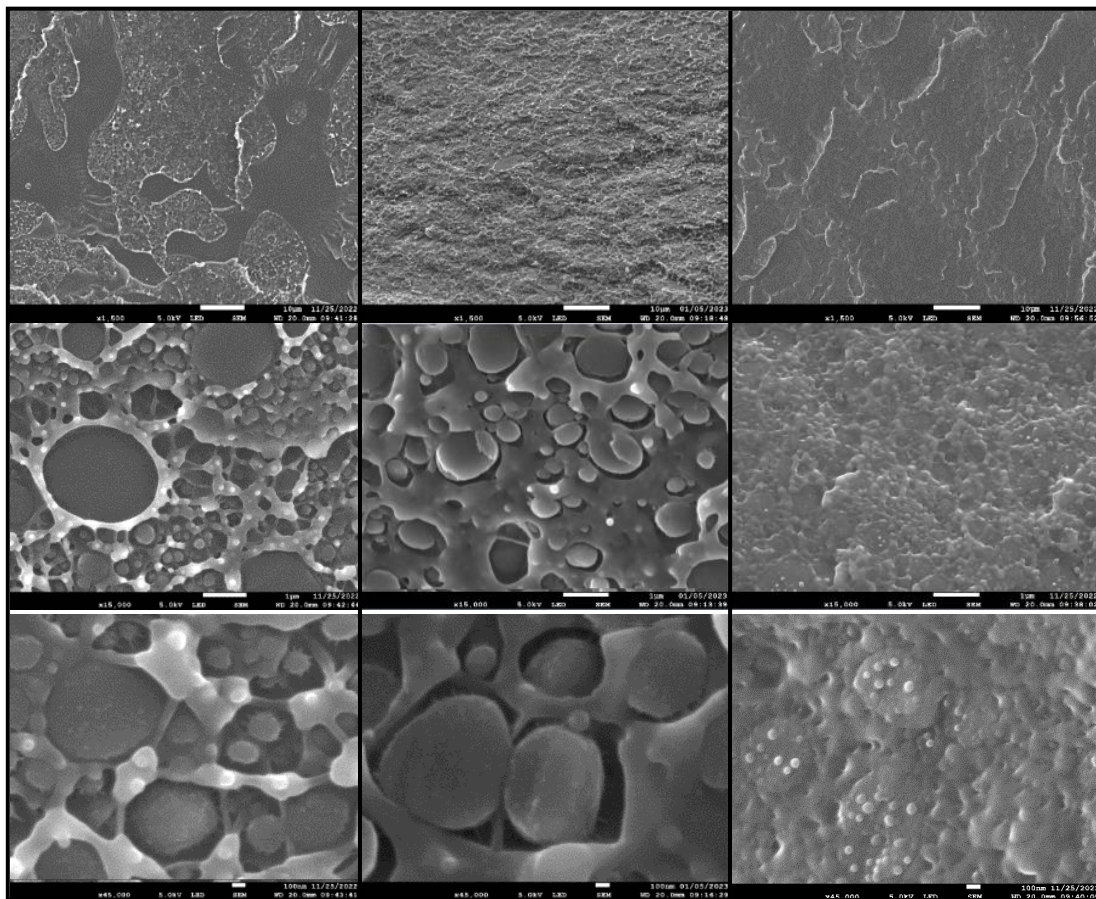


Figure 54 : SEM imagery conducted on PE_zH₄₄ (left), PH₂₀ (middle) and PE_zH₂₀ (right), and at magnifications of x1500 (top), x15000 (middle) and x45000 (bottom)

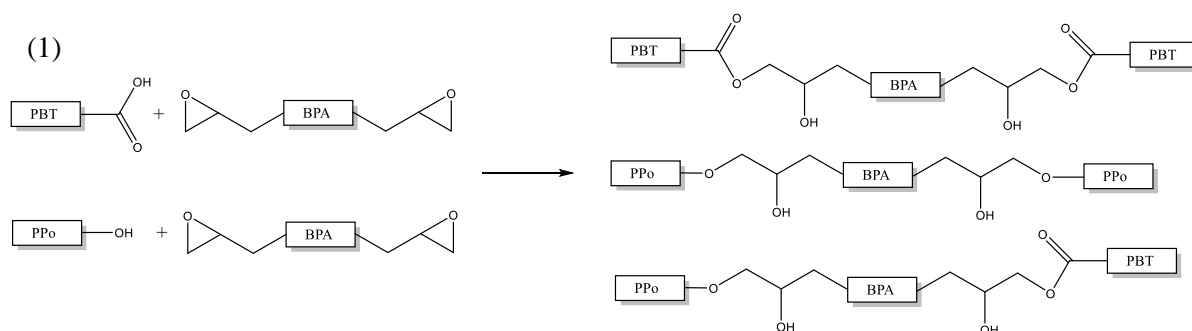
The addition of the standard amount of reactant (epoxy and catalyst) to PBT in the presence of 44 wt.-% or 20 wt.-% HM1100 did not result in a material with a significant degree of cross-linking.

Furthermore, PBT and HM1100 formed an incompatible melt in PH₂₀ and PE_ZH₄₄, exhibiting two distinct phases. However, in the case of PE_ZH₂₀, the two materials were fully be compatibilized, as a single T_g was measured. This suggests that the presence of epoxy may serve as a compatibilizer, promoting the compatibility between PBT and HM1100.

2.3.4.2 PBT-epoxy-polyphosphonate chemical interaction

In the last part, no vitrimer was obtained with HM1100 even in presence of epoxy and catalyst. It has been demonstrated that the PBT and HM1100 polymers in PH₂₀ and PE_ZH₄₄ formulations are incompatible with each other. Indeed, the torque during synthesis remains low, even inferior to pristine PBT, two T_g were measured and phase segregation is visible through microscopy imagery. However, when used at 80 wt.-% PBT /20 wt.-% polyphosphonate ratio in presence of epoxy, compatibilization occurs. This compatibilization leads to higher axial force than the non-compatibilized mixture, a single T_g, barely visible nodules of polyphosphonate and no interface separation between the two polymers.

The role of epoxy resin as a reactive compatibilizer has been reported in the literature. For example, it has been used to compatibilize PBT/polyamide-6 blends^{223,224}. Generally, the reactive compatibilization with multifunctional epoxy is due to formation of a copolymer of both component of the blend. In our case, it would imply that PBT-epoxy-polyphosphonate copolymer are formed. Figure 55 presents the possible reaction between PBT, HM1100 and the epoxy. The reaction of epoxy and PBT is well known and is the starting point of the synthesis of PBT vitrimers. Epoxy solubilizes in PBT and react preferentially with the carbonyl group as the kinetically favored reaction. The reaction of epoxy with polyphosphonate is not reported, however a patent reports a polyester which can chemically react with a phosphonate compound²⁰⁴. To do so, they blended PBT with polyphosphonate (Nofia HM1100), and a nucleating agent (for example sodium-based) or a polymerization catalyst used for polyester synthesis. The obtained copolymer is obtained when an aromatic ester of the phosphonate chain end becomes chemically attached to a carbonyl group of the PBT. In our case, this reaction may be promoted by the Zinc(II)(acetylacetonate) as it is an efficient polymerization (i.e. transesterification) catalyst (Figure 56).



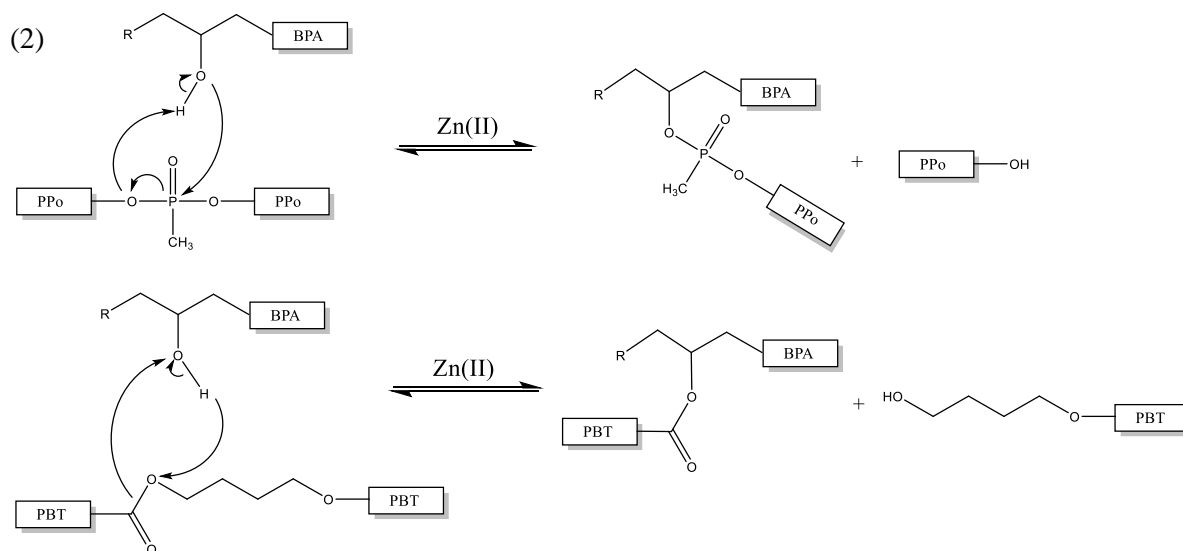


Figure 55 : Reaction between PBT, epoxy (DGEBA) and HM1100 (polyphosphonate, PPO). (1) Chain extension and (2) transesterification in presence on Zn(II) catalyst
BPA = bisphenol-A

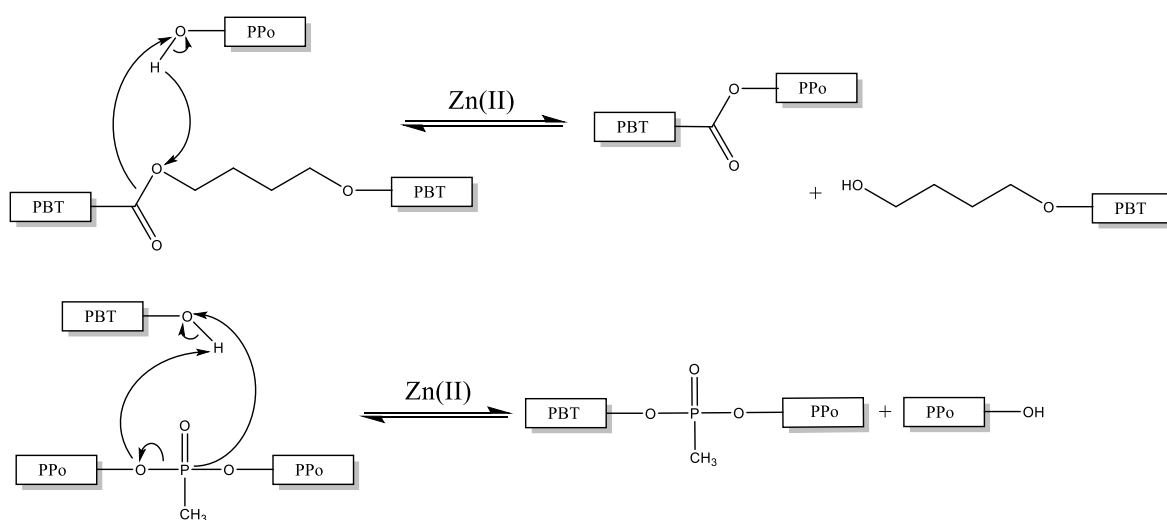


Figure 56 : Proposed transesterification reaction between PBT and HM1100 (polyphosphonate, PPO) in presence of the Zn(II) catalyst.

³¹P and ¹³C ss NMR characterization have been performed on HM1100, PE_ZH₄₄ and PE_ZH₂₀, and their respective spectrum are presented in Figure 58 and Figure 57. PE_Z spectrum is added for comparison purpose. In both PE_ZH₂₀ and PE_ZH₄₄, the ³¹P peak corresponding to the main chain aromatic ester structure of a phosphonate polymer²⁰⁴ is observed at 23.8 ppm. However, it seems that the peaks shift slightly toward higher chemical shifts for PE_ZH₄₄ and PE_ZH₂₀ compared to HM100. A new, low-intensity peak also appears at 48.2 ppm. This shift and new peak suggest a chemical environment change for the phosphorus atoms within the blend. According to the patent US 10,836,909 B2²⁰⁴, a reaction can occurs between a phosphonate chain end carbonyl group of a polyester or its esters groups, leading to the formation of a new aromatic ester of phosphonate. A new peak can then be observed in ³¹P NMR between 38 to 60 ppm.

The ^{13}C NMR spectra, on the other hand, presents the characteristic peaks of PBT, as well as the characteristic peaks of HM1100 at 10.9, 31.0, 41.0, 120.3, 127.8 and 148.3 ppm. A barely visible peak is visible at 153.5 ppm for PE_zH_{44} and PE_zH_{20} . It could be attributed to epoxy. If a reaction had occurred between the phosphonate and the PBT (end chain or ester groups), a peak around 120-122 ppm could be observed²⁰⁴. It is not the case here.

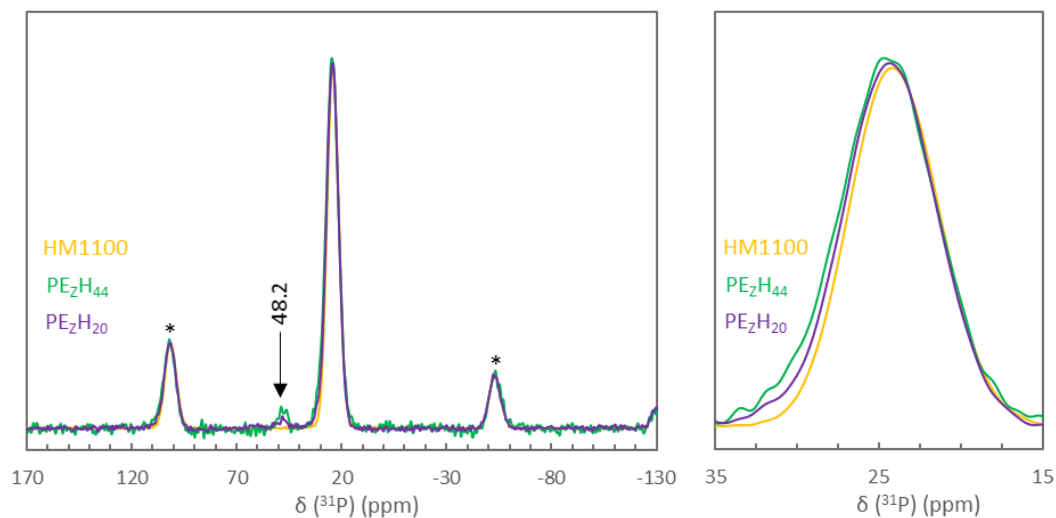


Figure 57 : ^{31}P ss RMN spectra of the HM1100 formulations. Right: Zoom on the main band. The curves were normalized considering the highest intensity peak of sample HM1100. (* rotation bands)

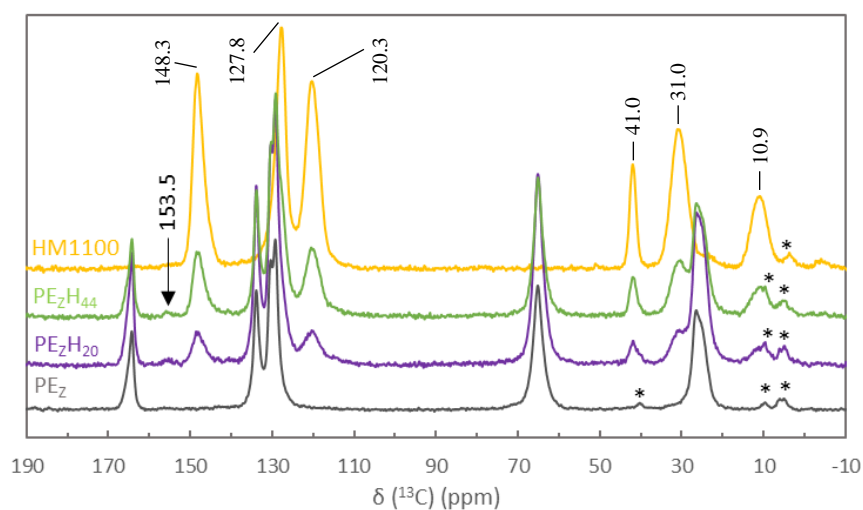


Figure 58 : ^{13}C ss NMR spectra of the H1100 formulations, HM1100 and PE_z . (* rotation bands)

The IR analyses do not show any specific bands highlighting reaction between the components.

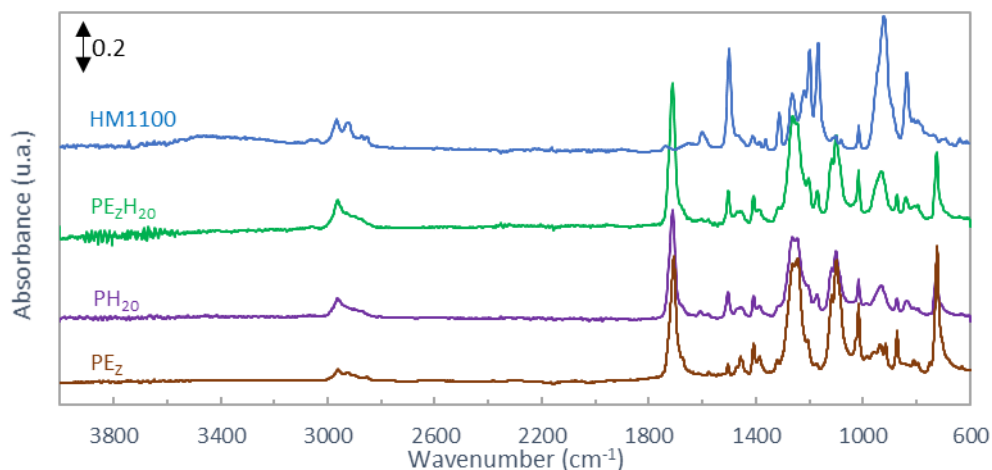


Figure 59 : IR spectra of PE_zH_{20} , PH_{20} , HM1100 and PE_z

The study of the chemical interaction occurring within the HM1100-filled vitrimer is complex to conduct. A very subtle chemical shift was observed for the peak corresponding to the aromatic chain structure of the phosphonate, and a low-intensity peak was observed 48.2 ppm. According to the analyses done it is difficult to conclude on the reactivity between PBT and HM1100.

2.3.4.3 20wt-% HM1100 with different amounts of epoxy and catalyst

With the previous formulation tested, compatibilization was observed but not crosslinking. Additional materials were consequently prepared with 20 wt.-% of HM1100 in order to see if a vitrimer can be obtained. Two hypotheses could explain the lack of bond exchange reactions leading to crosslinking. First, a decrease of the kinetic of the reaction caused by the presence of the FR could happen, as it was the case for nanoparticle inclusions in vitrimer matrix (see Chapter 1). Secondly, an insufficient quantity of epoxy could prevent the formation of the network. Consequently, the following formulations were prepared: $PE_{5Z}H_{20}$ was prepared with 5 times the original amount of catalyst, while in $P5E_zH_{20}$, 5 times the original amount of epoxy was used. Finally, $P5E_{5Z}H_{20}$ was synthesized with both 5 times the amount of catalyst and 5 times the amount of epoxy. Quantities for each formulation are shown in Table 2, while the evolution in the axial force during extrusion is shown in Figure 60.

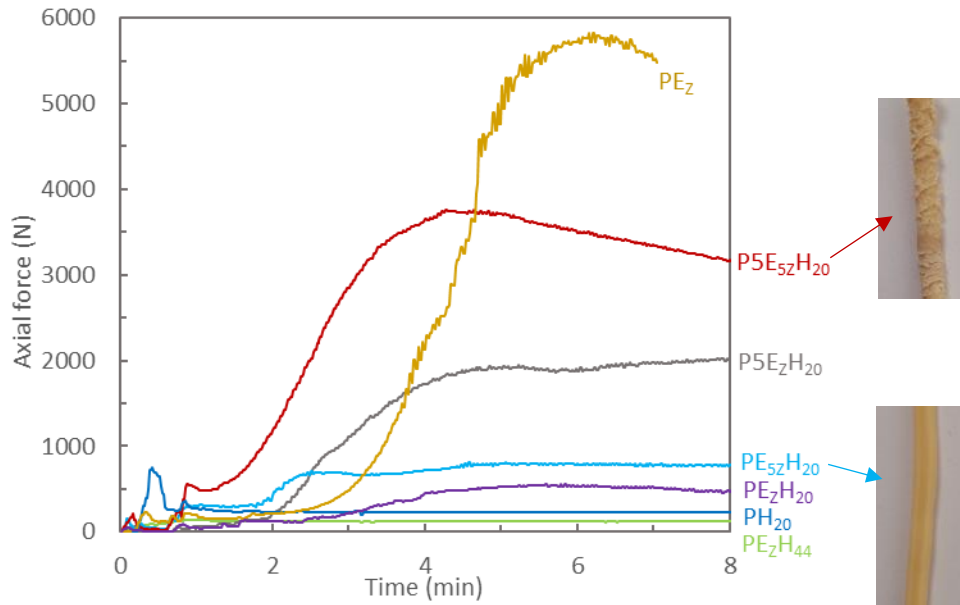


Figure 60 : Evolution of the axial force as a function of the residence time in the extruder in presence of HM1100. (270 °C, 60 rpm, N2 flow)

When increasing five times the amount of transesterification catalyst (0.55:1 [catalyst]/([OH]+[COOH])), the small rise in viscosity occurs faster, within 2.5 minutes. However, the final force remains low, around the same values as PE_zH_{20} and the gel ratio is nearly equal to zero.

On the contrary, when increasing five times the quantity of epoxy (10:1 [epoxy]/([OH]+[COOH])), a rise in viscosity is observed. A plateau is achieved at 5 minutes at around 2000 N. Gel measurements confirm the presence of a gel fraction of 42 wt.-%. It shows that the hindering effect of HM1100 could be overtaken by increasing the quantity of reactants. However, this value is much lower than what could be expected with the amount of epoxy added to the system. Indeed, in the previous part, with only a 2:1 [epoxy]/([OH]+[COOH]) ratio, a 68 wt.-% cross-linked PBT-vitrimer was obtained.

When increasing both epoxy and catalyst quantity five times, a very fast rise in viscosity occurs, starting only 1 minute after the addition of the reactants, and stabilizing after 4 minutes. The excess quantity of epoxy combined with a higher amount of catalyst has a beneficial effect on the kinetics, as the reactions occur much faster than with any other previous system, despite the presence of HM1100. However, like for sample $P5E_zH_{20}$, most epoxies did not promote cross-linking during the extrusion (Figure 60), and the gross amount of gel fraction was measured at 61 wt.-%. Elementary analysis (Table 6) confirms the presence of a significant amount of phosphorus in the gel fraction. The real gel fraction was then calculated at 62 wt.-%.

Table 6 : Weight percentage of phosphorus and zinc remaining in P5E_{5Z}H₂₀ based on elementary analysis. The calculated amount of FR in the formulation was obtained from the amount of phosphorus measured. *Results obtained from Equation 5.

Sample	Gross gel ratio (wt.-%)	Elemental composition (wt.-%)		FR _{calculated} (wt.-%)	FR _{expected} (wt.-%)
		Zn	P		
PE _Z H ₄₄	0	-	-	-	-
PE _Z H ₂₀	0	-	-	-	-
PE _{5Z} H ₂₀	0	-	-	-	-
P5E _Z H ₂₀	42 ± 4	-	-	-	-
P5E _{5Z} H ₂₀	61.5 ± 5	0.130 ± 0.003	1.91 ± 0.05	17.7	20
P5E _{5Z} H _{20gel}	100	0.160 ± 0.004	1.82 ± 0.05	16.8	-
P5E _{5Z} H _{20sol} *	0	0.063 ± 0.003	2.06 ± 0.10	19.0	-

³¹P and ¹³C ss NMR characterization have been performed on the newly synthesized P5E_{5Z}H₂₀, as well as its gel fraction. The main peak, initially observed at 23.8 ppm, significantly shift to 25.7 ppm for P5E_{5Z}H₂₀ and 27.3 ppm for P5E_{5Z}H_{20gel}. The intensity of the new peak at 48.2 ppm previously observed for PE_ZH₂₀ is also more visible. Those results are evidence of the modification of the phosphorus atom environment.

Two new peaks appeared at 153.5 and 114.4 ppm on the ¹³C spectrum of both samples. The last peak was not visible for PE_ZH₂₀. In addition, a shoulder at 68.1 ppm is visible on the peak at 65 ppm. These peaks are due to the epoxy.

For the formulation P5E_{5Z}H₂₀, some modifications are observed but not well understood. Reactivity of phosphonate with carboxylic end chains or epoxy is highly probable. However, the conducted analyses did not provide enough information to draw a conclusion regarding whether the reaction results in the formation of Phosphonate-PBT, Phosphonate-Epoxy-PBT or a mix of both. Indeed the components of the blend have very similar chemical structures. Transesterification can potentially be occurring in both cases.

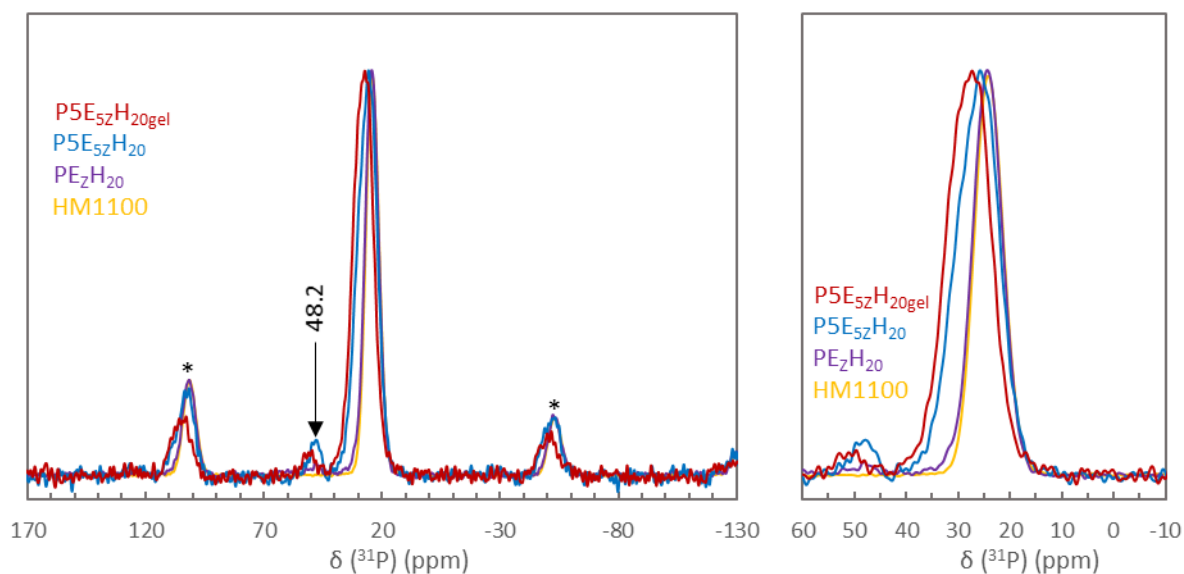


Figure 61 : ^{31}P ss RMN spectra of the HM1100 formulations. Right: Zoom on the main bands. The curves were normalized considering the highest intensity peak of sample HM1100. (* rotation bands)

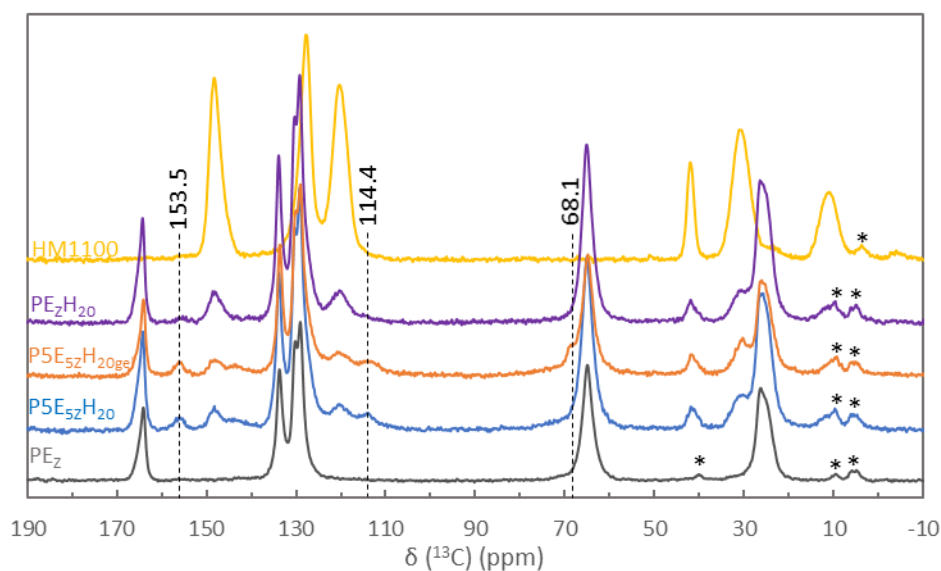


Figure 62 : ^{13}C ss NMR spectra of the H1100 formulations, HM1100 and PEz. (* rotation bands)

The IR spectra of the different formulations are very similar. The most striking differences are the presence of two peaks present only in the gel of P5E_{5z}H₂₀. These peaks are located at 890 and 680 cm⁻¹. They have not been identified yet. In addition, the comparison P5E_{5z}H₂₀ and P5E_{5z}H_{20gel} also evidence the presence of HM1100 in higher concentration in the gel. The peaks at 1168 and 1200 cm⁻¹ are indeed more intense in the gel part.

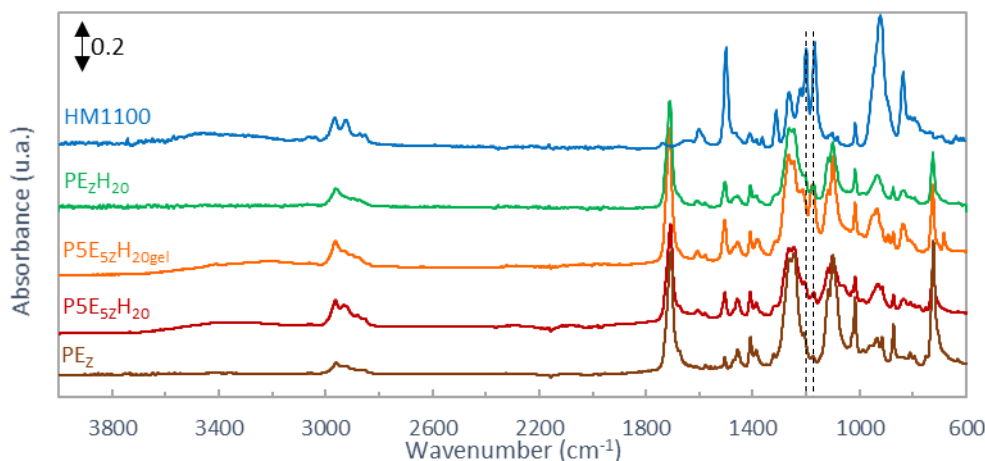


Figure 63 : IR spectra of PE_zH_{20} , PH_{20} , $HM1100$ and PE_z

All materials exhibit a single T_g around $58-60^\circ\text{C}$, whether they possess a measurable cross-linked fraction or not. This implies that the addition of the reactants helps in obtaining a homogeneous repartition of $HM1100$ in the systems. Besides, the formation of a cross-linked network does not greatly affect glass transition temperature, as samples with high cross-linking content ($P5E_zH_{20}$ and $P5E_{5z}H_{20}$) and samples with very low cross-linking content (PE_zH_{20} and $PE_{5z}H_{20}$) exhibit roughly the same T_g .

Figure 64 presents Zn and P mapping of $P5E_{5z}H_{20}$ obtained by EPMA, the selected pictures being representative of the observations conducted on the whole sample. As seen previously for PE_zH_{20} , $HM1100$ in $P5E_{5z}H_{20}$ is quite well compatibilized with the PBT matrix, as a single T_g (58.5°C) was observed by DSC.

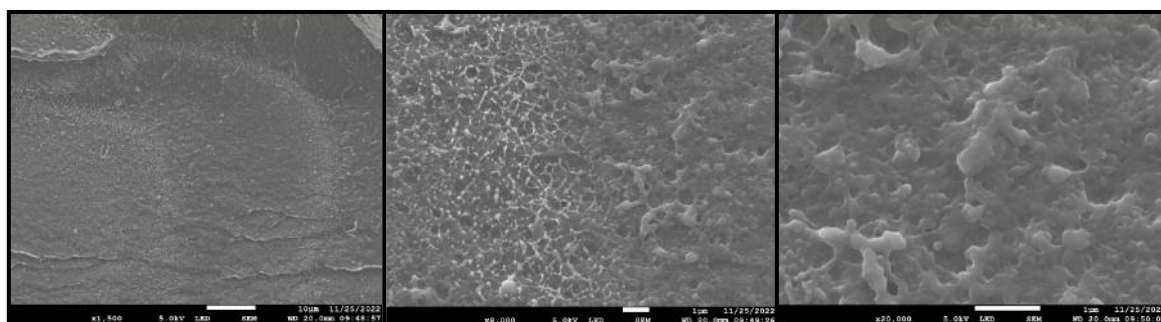


Figure 64 : SEM imagery conducted on $P5E_{5z}H_{20}$ at magnifications of $\times 1500$ (left), $\times 8000$ (middle) and $\times 20000$ (right)

Subsequent P and Zn cartography analysis was performed on the sample (Figure 65), revealing the presence of agglomerates that contained both P and Zn elements simultaneously. Zn and P profiles, along the lines presented on the mappings, were additionally carried out on the sample. Profile 1 and 2 go through $HM1100$ agglomerates (high phosphorus concentration), as well as the polymer matrix for which agglomerates are not visible ($HM1100$ is micro-dispersed). For both profiles, the Zinc is present in high concentration exclusively where the

HM1100 agglomerates are located, as it is otherwise distributed in low concentration in the polymer matrix. The mapping shows the zinc catalyst is segregated within the oligomeric methylphosphonate phase.

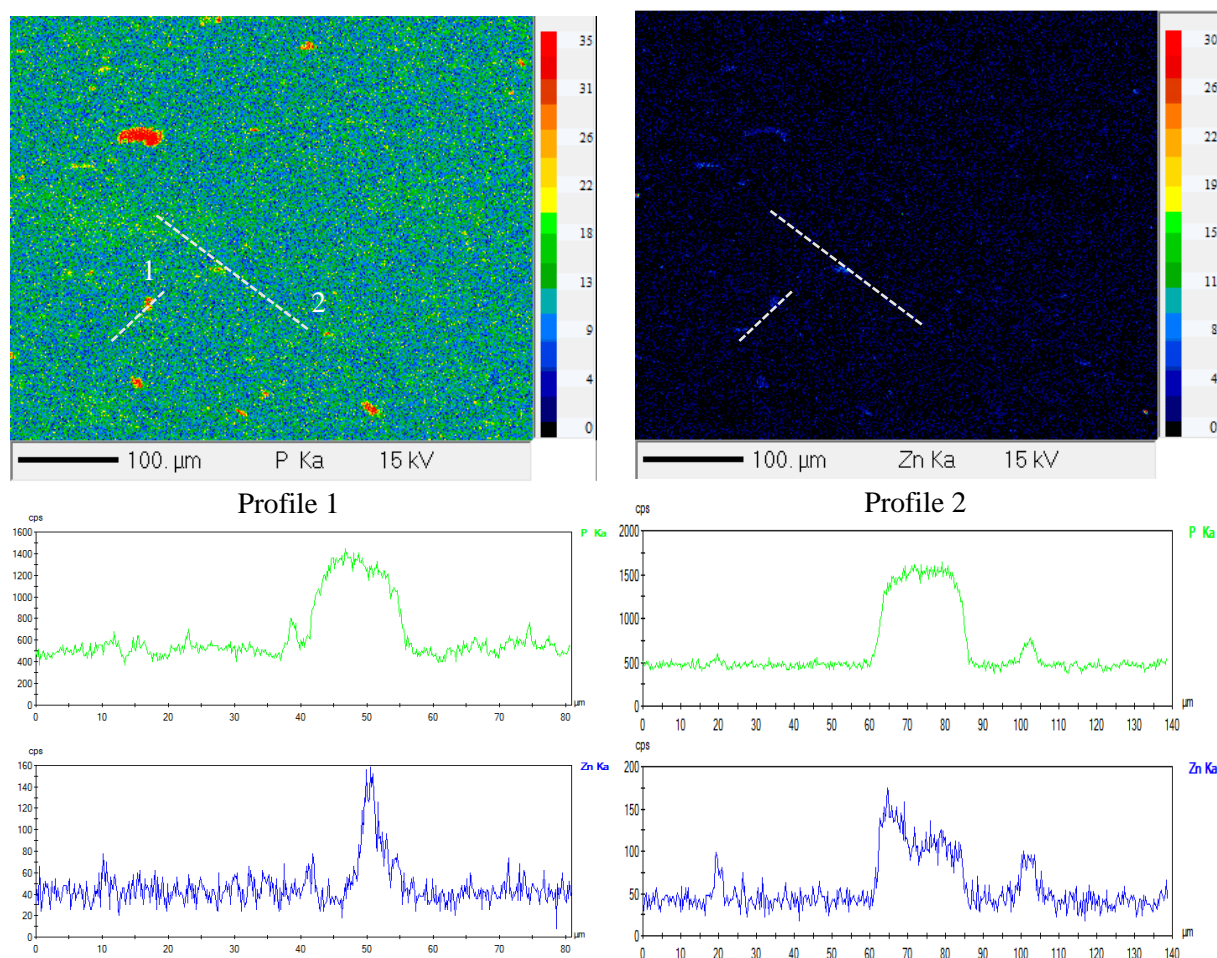


Figure 65 : Up: Mappings of phosphorus and zinc on the $P5E_{5Z}H_{20}$ sample. Down: Profiles of the phosphorus and zinc

The addition of five times the amount of reactant (epoxy and catalyst) to the vitrimer is a solution to achieve a cross-linked HM1100-filled material, with a cross-linking degree of 62 wt.-% obtained for $P5E_{5Z}H_{20}$. In addition, the ^{31}P ss NMR chemical shifts previously observed at 23.8 ppm for $PE_{ZH_{20}}$ are more evident for the cross-linked material, shifting up to 25.7 ppm for $P5E_{5Z}H_{20\text{gel}}$, and the new peak observed at 48.2 ppm exhibit a higher intensity. This change in the environment around the phosphorus atom, resulting from the peak shift and new peak, supports the hypothesis of the formation of a PBT-epoxy-HM1100 copolymer. Also, the segregation of the catalyst within the oligomeric methylphosphonate phase seen by EPMA tends to indicate that epoxy is the main factor influencing the formation of the copolymer. However, no clear conclusion can be drawn on whether PBT-epoxy-HM1100 or PBT-HM1100 are formed during reactive extrusion. Supplementary studies conducted on model-molecules may help to conclude on this topic.

In conclusion, our results demonstrate that the incorporation of HM1100 into the epoxy-based vitrimer matrix requires a significant amount of epoxy (8 wt.-%) and a catalyst to achieve effective cross-linking, whereas in the absence of HM1100, a lower amount of epoxy is sufficient to induce cross-linking. This suggests that the presence of HM1100 acts as a cross-linking inhibitor, necessitating specific conditions to achieve an adequate cross-linked structure.

2.4 Characterization of the relaxation behavior of the cross-linked systems

We previously developed cross-linked PBT-systems with flame-retardant additives, based on the same process used for synthesizing a PBT vitrimer through the addition of a diepoxy and a transesterification catalyst. Depending on the chemical composition of the flame-retardant (i.e. aluminum or zinc metallic salt, phosphonate polymer), different cross-linking degrees were obtained. This part aims at characterizing if the synthesized cross-linked materials effectively behave like vitrimers and will focus on the formulations containing 4.8 wt.-% P-content (PE_ZA₂₀ and PE_ZZ₂₄), and the most promising H1100 formulation (P5E_{5Z}H₂₀).

2.4.1 Relaxation of cross-linked vs thermoplastic systems

As explained in Chapter 1, vitrimers exhibit a unique relaxation behavior originating from the dynamic cross-links, as bond-exchange reactions lead to a rearrangement of the network. In the specific case of cross-linked PBT, bond-exchange reactions can only occur above T_m , as the crystalline structure hinders local chain motion, hindering the clustering of reactive centers, thereby impeding exchange reactions. Concerning flame-retardant additives, AlPi remains in a solid form up to 350°C, ZnPi melts at 200°C and HM1100 is an amorphous material with a T_g of 97°C. Stress-relaxation experiments were conducted in the temperature range between 230 and 270°C, which is sufficiently higher than the highest T_m registered for the formulations (216°C for PE_Z), assuring that no crystalline structure remains. All materials were previously injected into a 25 mm*1.6 mm diameter mold, highlighting their reprocessable nature. Figure 66 compares the stress relaxation behavior at 250°C of all cross-linked materials (PE_Z, PE_ZA₂₀, PE_ZZ₂₄ or P5E_{5Z}H₂₀) and their thermoplastic references (PBT, PA, PZ, PH20). All thermoplastic materials totally relax in very short times, with relaxation decreasing by a factor of 100 within 0.1 s for PBT. On the other hand, the total relaxation of the cross-linked materials occurs in several seconds. As classic cross-linked PBT materials do not completely relax stress^{198,225}, those relaxation behaviors can be attributed to transesterification reactions promoting bond-exchange reactions, leading to a rearrangement of the cross-linked network adapting to the new stress.

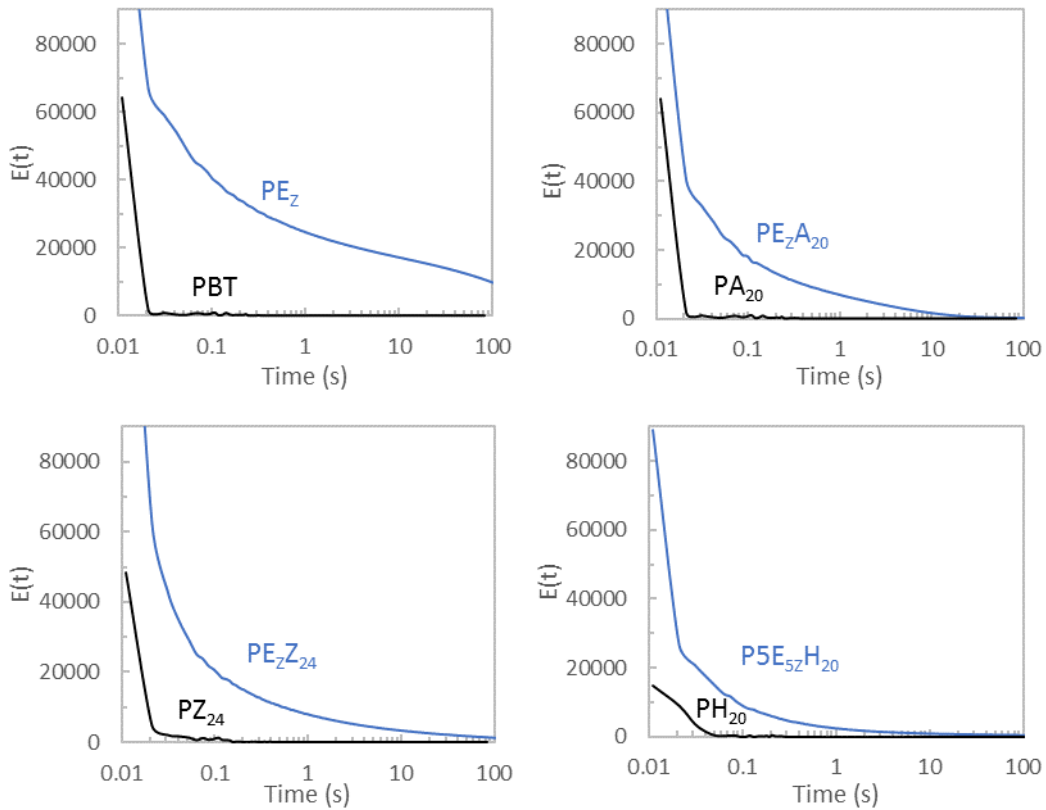


Figure 66: Relaxation behavior of all cross-linked samples compared with thermoplastic reference ($T=250^{\circ}\text{C}$)

2.4.2 First method: the Maxwell model

In the first method, the relaxation curves were analysed using a method widely shared in the literature that considers an ideal viscoelastic of the material. In this case, the Maxwell model for relaxation can be applied and relaxation behavior is described using an exponential function (Equation 8), with characteristic relaxation time (τ) defined as the $1/e$ value (37%) of the normalized stress^{30,60,89}.

$$\text{Equation 8} \quad \frac{\sigma}{\sigma_0} = \frac{G}{G_0} = \exp\left(-\frac{t}{\tau}\right)$$

Most studies conducted on vitrimer materials, independently of the type of chemistry used, applied this method to quantify the performance of the newly synthesized systems. This is also the case of most papers focusing on the synthesis of vitrimer based on thermoplastic backbones. The value of zero-shear viscosity, G_0 , is commonly plotted as *the* value of relaxation modulus recorded at 1s after the beginning of the test ($G_0 = G(1\text{s})$).

Figure 67 presents the normalized stress-relaxation times curves obtained for PE_z , PE_zA_{20} , PE_zZ_{24} and $\text{P5E}_{5z}\text{H}_{20}$. PE_z , PE_zA_{20} present significant temperature-dependent decrease of relaxation on the whole range of temperature, while this behavior is less visible for PE_zZ_{24} and $\text{P5E}_{5z}\text{H}_{20}$.

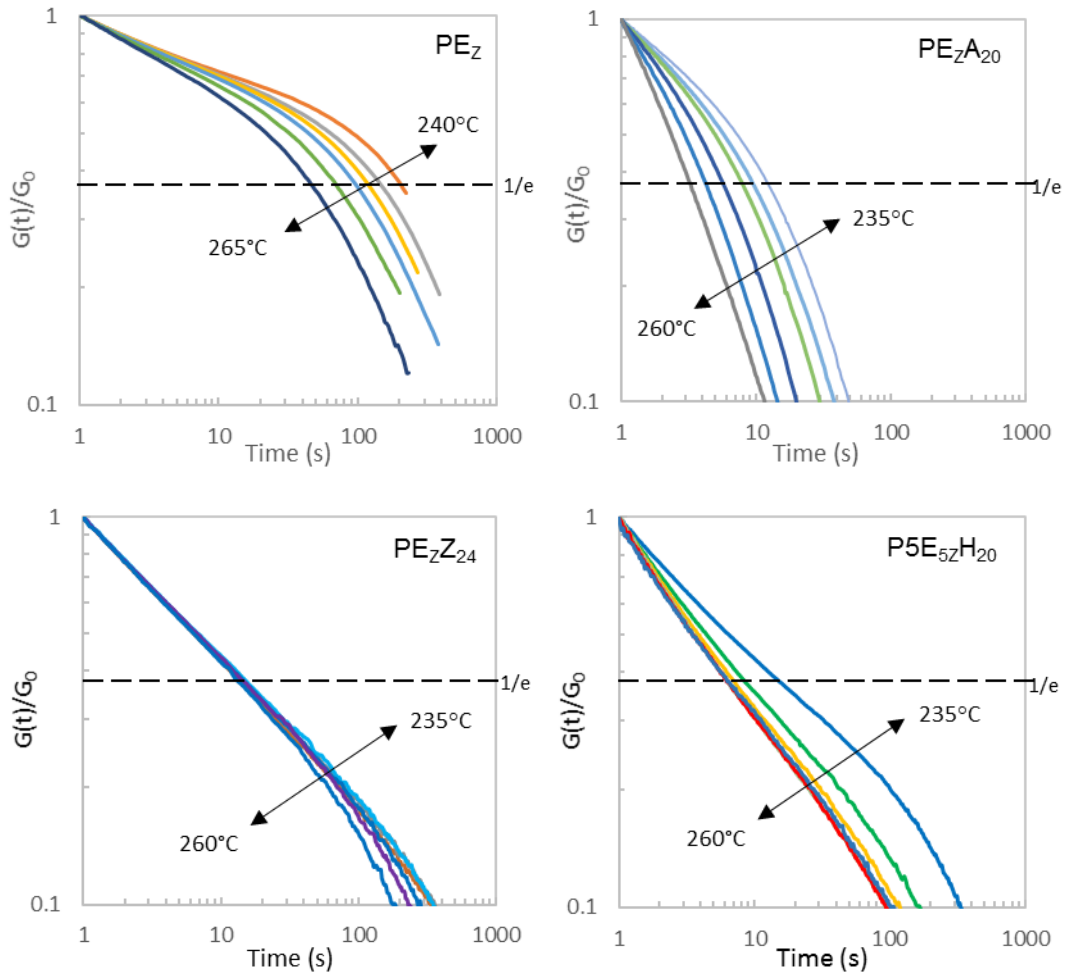


Figure 67 : Normalized stress-relaxation curves between 235 and 265°C for PE_Z, PE_ZA₂₀, PE_ZZ₂₄ and P5E_{5z}H₂₀ at 1% deformation, considering $G_0 = G(1s)$

Usually, associative covalent adaptable networks exhibit shorter relaxation times with increasing temperatures⁴. In the case of vitrimer, those relaxation times are governed by the chemical nature of the bond-exchange reactions, cross-linking density^{22,98,226} and the presence of filler³⁵. This temperature-dependency relaxation behavior follows the Arrhenius law (Equation 9).

Equation 9
$$\tau = \tau_0 \exp\left(\frac{-E_a}{RT}\right)$$

The evolution of the characteristic relaxation time versus temperature obtained for our materials are plotted in Figure 68 and Table 7.

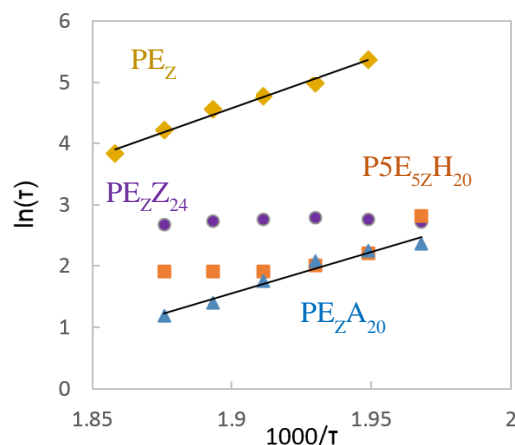


Figure 68 : Characteristic relaxation times for PE_z , PE_zA_{20} , PE_zZ_{24} and $P5E_{5Z}H_{20}$, as a function of inverse of temperature. The Arrhenius law is verified if all dots can be merged by passing through a straight line.

Table 7 : Characteristic relaxation times at 240, 250 and 260°C obtained for each cross-linked formulation. An activation energy was found for PE_z and PE_zA_{20}

Sample	Activation energy (kJ.mol ⁻¹)	Relaxation times (s)			R ²
		240°C	250°C	260°C	
PE_z	133	211	118	68	0.986
PE_zA_{20}	112	10	5	4	0.9669
PE_zZ_{24}	/	16	16	16	/
$P5E_{5Z}H_{20}$	/	9	7	7	/

Relaxation times of PE_z decrease with temperature following an Arrhenius-type temperature-dependency, with an activation energy of 140 kJ.mol⁻¹, which is on par with the values found in the literature^{5,34} for PBT vitrimer using this method. 1/e value of relaxation is reached in 211 s at 240°C, 118 s at 250°C and 68 s at 260°C, which is much higher than relaxation times obtained under 0.1s for PBT.

The PE_zA_{20} relaxation also follows an Arrhenius law, with a lower activation energy of 112 kJ.mol⁻¹, thus exhibiting a vitrimer behaviour. However, compared with PE_z vitrimer, PE_zA_{20} relaxation times is tenfold lower, reaching 1/e value of relaxation in 10 s at 240°C, 5 s at 250°C and 4 s at 260°C respectively. Usually, the addition of filler tends to impact relaxation behavior by increasing relaxation times. For example, Legrand and Soulié-Ziakovic showed that twice longer times are necessary to obtain relaxation for a 25 wt.-% filled silica/epoxy-acid vitrimer system compared to its pristine counterpart³⁵. This unique result may imply that ALPi plays an active role during transesterification reactions.

Stress-relaxation experiments conducted for compound PE_zZ_{24} do not show any evolution of relaxation time toward temperature, which is relatively constant at around 16 seconds.

For P5E_{5Z}H₂₀, two distinct behaviors are observed. From 235 to 245°C, the material exhibits a decreasing relaxation time with temperature. From 250°C and further up, relaxation times also reach a plateau.

By using this first method, PE_ZA₂₀ relaxation time exhibits an Arrhenius behavior while the two other flame-retarded systems, PE_ZZ₂₄ and P5E_{5Z}H₂₀ do not relax like usual vitrimer despite their cross-linked nature and ability to be reshaped by injection. The cross-linked materials were assimilated as ideal viscoelastic materials following the Maxwell model for relaxation. This model may not be relevant here considering the complex relaxation modes found for our systems. Indeed, in our case, the materials are only partially crosslinked networks. A more suitable model was consequently tested.

2.4.1 Stress-relaxation behavior of partially cross-linked systems

Originally, dynamic cross-linked materials classified as vitrimer by Leibler and coworkers in 2011 were synthesized following a thermoset approach. Through the reactions of bi- or tri-functional monomers, they obtained highly cross-linked networks presenting one-step relaxation behavior⁴. However, in the case of partially cross-linked dynamic systems, relaxation occurs radically differently. The presence of a non-negligible thermoplastic fraction leads to complex relaxation behavior. Raw stress-relaxation curves of PEZ are reported in Figure 69-1. The material exhibits a mixed network relaxation type. Based on the relaxation of PEZ, a model curve from the relaxation modulus of a partially cross-linked thermoplastic-based vitrimer was plotted in Figure 69-2 and compared with the relaxation of a fully cross-linked vitrimer. A steep decrease of the relaxation modulus is observed under 0.1 seconds (similar to the relaxation modulus found for thermoplastic references materials in Figure 66) and concerns the relaxation of the strict thermoplastic fraction composed of polymer chains which do not share any cross-linked bonds with neighboring chains. An intermediate phase follows. $G(t)$ decreases lightly due to the relaxation of network defects, like partially cross-linked polymer chains. Depending on the number of network defects and the kinetic of the bond-exchange reactions, this transition step may last for several seconds. The relaxation of a fraction of the cross-linked network may also occur in this period. Several studies report the presence of such a step^{5,34,59} for partially cross-linked thermoplastic-based vitrimer, with the slope depending on the molecules involved. Finally, for higher durations, relaxation of the cross-linked network occurs, leading to a slow decrease of the relaxation modulus until total relaxation of the material. On the other hand, for fully cross-linked materials, no evolution of $G(t)$ is usually observed^{4,30,60} within the first seconds. As a result, the initial relaxation value of zero-shear viscosity (G_0) is often attributed to $G(1s)$.

Fully cross-linked materials usually exhibit G_0 values which only slightly vary with increasing temperatures²²⁷, as the bond-exchange reactions are the only parameters driving the

temperature-dependency of the zero-shear viscosity. However, for PE_Z, the relaxation modulus decreases significantly with increasing temperature, due to the thermo-dependent relaxation of both the thermoplastic²²⁸ and the dynamic cross-linked fraction⁵.

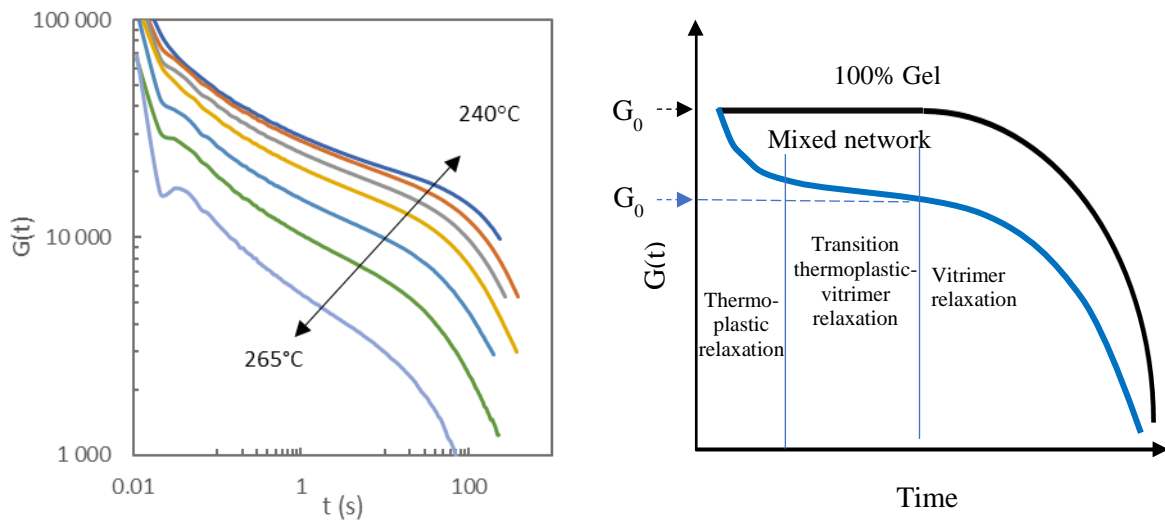


Figure 69 : (1) Stress-relaxation curves of PE_Z under 1% deformation. (b) Model curve of an incomplete cross-linked network (blue curve), compared with a 100% cross-linked network (black curve).

On a side note, the relaxation curves shown in this study correspond to the temperatures where good relaxation behaviors were obtained. As mentioned earlier in this chapter, the reactive extrusion process was stopped after a maximum level of internal pressure was reached, hence the systems may not be fully equilibrated at the end of the process. This explains why at lower temperatures, especially from 230 to 240°C, some systems were still curing inside the Rheometer. Besides, when relaxation was performed at higher temperatures (above 260 to 270°C depending on the material), the samples started to exhibit a different relaxation behavior attributed to secondary reactions leading to the formation of permanent cross-links. Significant degradation could also occur at even higher temperatures, as samples were tested up to 290°C. To the best of our knowledge, no studies concerning the effect of in-situ side-reaction occurring inside a Rheometer were studied, and the overwhelming majority of the papers only exhibit normalized stress relaxations, and not the real shape of the relaxation curves, thus possibly hiding important information.

In the following part, we will apply another model to analyze the stress-relaxation behavior of the cross-linked materials.

2.4.2 Second method: the Kohlrausch-Williams-Watts (KWW) model

Recent studies implemented another model by experimenting with relaxation on transient vitrimers possessing hybrid networks^{227,229–235}. For example, it was used in the case of cross-

linked polymer composed of only a fraction of the network able to perform dynamic bond-exchange reactions^{229,230,235}, or combining both vitrimer and dissociative networks²²⁷. Experimental data were fitted with the Kohlrausch-Williams-Watts (KWW) model^{229,231} with Origin software. This model uses a stretched exponential function and is presented in Equation 8. It consists in adding a fitting parameter β , which simulates the degree of elongation of the exponential function with time ($0 < \beta \leq 1$). A value of 1 means that the material behaves like an ideal viscoelastic material by perfectly following the Maxwell relaxation model. However, low β values is an indication of the material behaving like a less ideal Maxwell material, implying numerous relaxation modes.

$$\text{Equation 10} \quad \frac{\sigma}{\sigma_0} = \frac{G}{G_0} = \exp\left(-\left(\frac{t}{\tau^*}\right)^\beta\right)$$

G_0 value was obtained by fitting the curve using the KWW model between curve domains chosen appropriately, when relaxation of the cross-linked network effectively occurs. For our materials, the domains considered were the following: from 30 seconds for PE_Z, PE_ZZ₂₄ and P5E_{5Z}H₂₀, and from 3 seconds for PE_ZA₂₀ as the material relaxes stress much faster in presence of AlPi. G_0 value was obtained from the fitting model, and a global fitting parameter β was shared over all temperature ranges for all curves of the same formulation. Raw relaxation curves of PE_Z, PE_ZA₂₀, PE_ZZ₂₄ and P5E_{5Z}H₂₀ as well as their respective fitting model curves are presented in Figure 71. Complementary data obtained from those fits (G_0 , and Tau) are presented in Appendix 2. For a stretched exponential decay, the characteristic relaxation time, $\langle \tau \rangle$, is obtained from Equation 11, where Γ is the gamma function^{229,231,236–238}.

$$\text{Equation 11} \quad \langle \tau \rangle = \frac{\tau^* \Gamma(1/\beta)}{\beta}$$

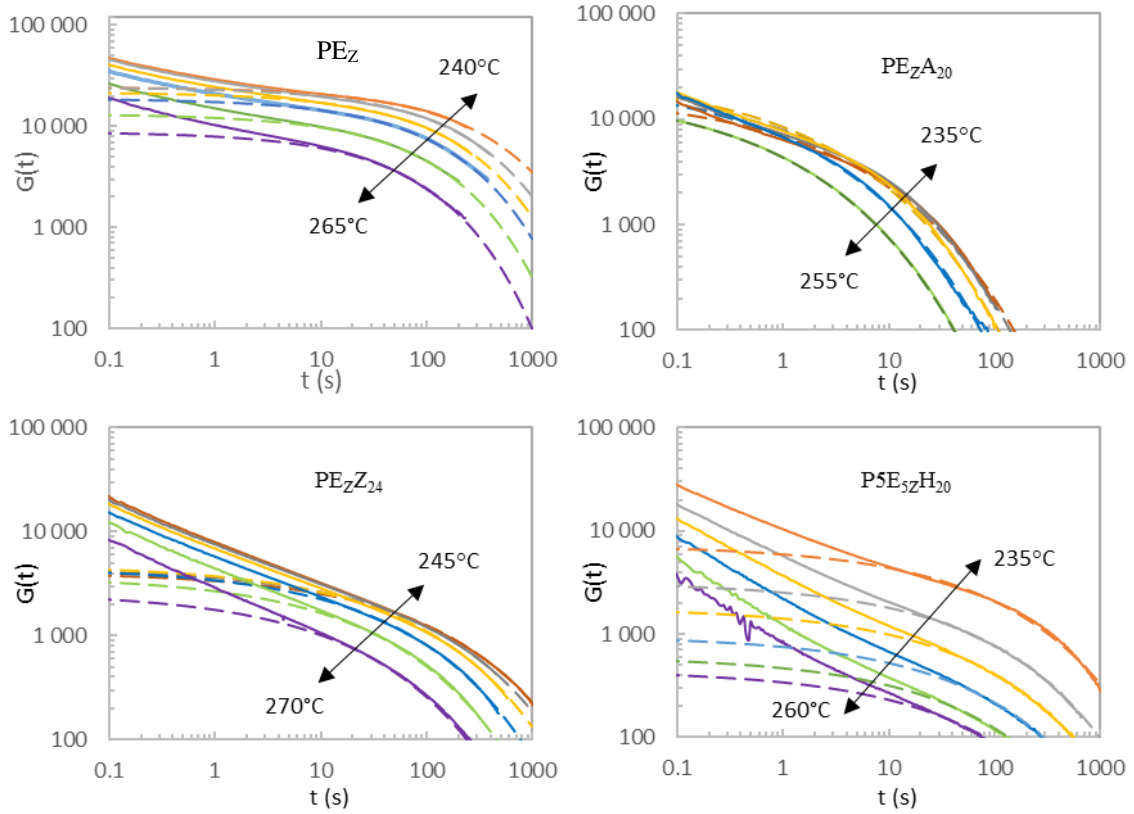


Figure 70 : KWW model fit for the stress-relaxation curves of PE_z, PE_zA₂₀, PE_zZ₂₄ and P5E_{5z}H₂₀ (solid line = experimental data, dotted line = fit data)

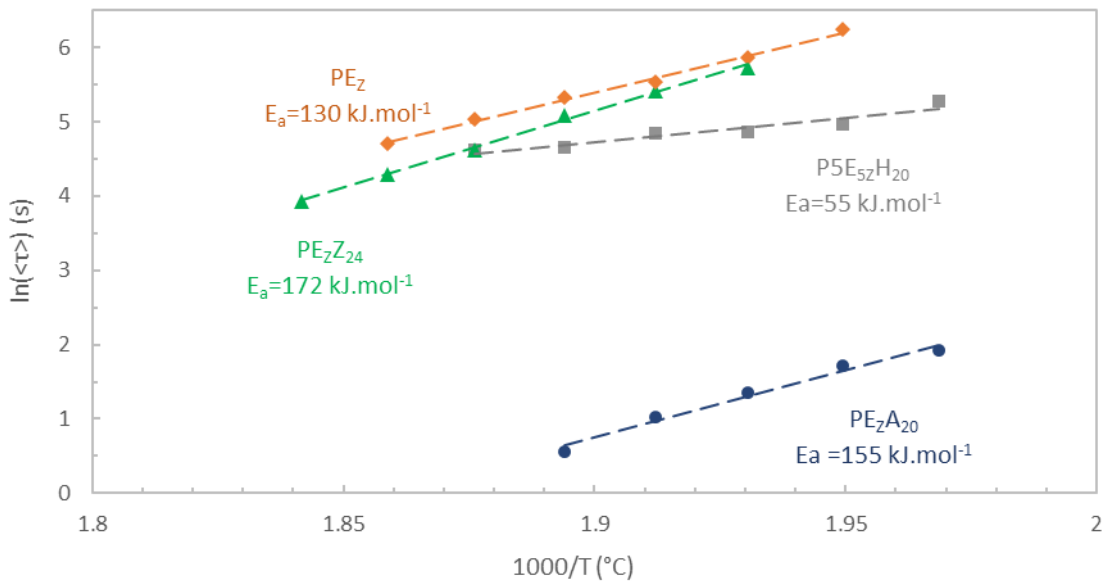


Figure 71 : Variation of the stress relaxation time versus inversed temperature

Table 8 : Stress relaxation data for all formulations

Sample	Activation energy	$\langle\tau\rangle$ at 250°C (s)	Beta	R ²
PE _Z	130	252	0.54	0.986
PE _Z A ₂₀	155	2.61	0.34	0.981
PE _Z Z ₂₄	172	224	0.41	0.997
P5E _{5Z} H ₂₀	55	127	0.39	0.898

PE_Z presents a broad relaxation behavior, with a relatively low beta parameter (0.54), indicating the presence of numerous relaxation modes and confirming that the application of a Maxwell model is not ideal in the case of partially cross-linked materials. Compared to the results obtained from the first method, longer relaxation times were obtained, at 250°C (252 s compared with 118s found by using the previous method). Interestingly, activation energy is still similar to the one obtained from the first method.

Upon adding 24 wt.-% ZnPi, beta value decreases to 0.41, as the addition of fillers in the matrix adds complexities to the relaxation behaviors. From previously measured gel ratios, PE_ZZ₂₄ exhibits the lowest cross-linking density. Moreover, faster relaxation rates were measured compared with PE_Z on the whole temperature range. This result is consistent with the findings of Zhou et al., where reducing the cross-link density has a comparable effect to increasing the temperature³⁴. Compared to thermoset-based vitrimer, for which lower cross-linking density has an inverse impact on relaxation times, the cross-linking density of thermoplastic-based vitrimer is relatively low, allowing for greater mobility of polymer chains at even lower cross-linking densities.

The relaxation behavior of the materials upon adding AlPi or HM1100 is more complex. In the case of PE_ZA, relaxation effectively occurs between 235 and 255°C, with a higher activation energy of 152 kJ.mol⁻¹.K⁻¹ and a lower β value of 0.34. AlPi demonstrates an exceptionally rapid relaxation behavior, with an average relaxation time ($\langle\tau\rangle$) of under 3 seconds at 250°C. In comparison, PE_Z or PE_ZZ₂₄ exhibit relaxation times in the range of hundreds of seconds (Appendix 2).

For HM1100 compound, the low fitting parameter ($R^2 < 0.9$) betrays phenomena occurring inside the matrix with increasing temperature. The relaxation shapes of the curves radically differ between 235 and 260°C. In this case, applying a single β value for all curves may show its limits. Indeed, when experimental data were independently fitted, the β parameter effectively decreased from 0.54 at 235°C to 0.24 at 260°C. The addition of epoxy in excess during the formation of P5E_{5Z}H₂₀ may lead to side reactions, like self-polymerization and the formation of non-dynamic cross-links.

The beta parameter obtained for each material (from 0.54 to 0.34) shows that the relaxation of the material significantly derives from an ideal Maxwell model, especially upon the incorporation of the additives. Besides, defining the zero-stress viscosity (G_0) at $G(1s)$ for all materials is not relevant in the case of vitrimer with a significant thermoplastic fraction, as the numerous relaxations modes hinder the

formation of a stable G_0 plateau. Here, we proposed a new method to find G_0 by fitting the relaxation curves using a KWW model. In theory, a vitrimer exhibit similar relaxation behavior at each temperature. As a result, we chose to attribute a global β value over the temperature range studied for each material. However, the presence of a thermoplastic fraction leads to a drift in relaxation behavior at higher temperatures (over 270°C in our case), for which the β value may decrease significantly. In addition, the curve fitting bounds for the KWW model were defined considering the overall aspect of the curve, but a better method to define those bounds needs to be implemented. The amelioration of this model may be an opportunity for future work.

2.4.3 Conclusion on stress-relaxation

This study shows that both phosphinate-filled vitrimer could totally relax stress. When AlPi is added to the system, promising relaxation behavior were registered, as the materials is able to fully relax stress in seconds instead of minutes. For PE_ZZ₂₄, even if the addition of the fusible flame-retardant lead to a decrease of the cross-linking degree, the material could still relax stress and exhibit an activation energy on par with the one observed for PE_Z.

The formulation of PBT-vitrimers with HM1100 as additive presented challenges compared to other materials. Achieving a sufficient level of cross-linking could only be accomplished by drastically increasing the quantity of reagents. Additionally, P5E_{5Z}H20 did not follow a clear Arrhenius law, despite total relaxation of the network.

2.5 Thermal and crystalline characterization of the materials

After highlighting the relaxation behavior of the materials, we studied the impact of the cross-linked network formation on the thermal characteristics of the vitrimer through DSC and TGA. DRX was conducted to see if cross-linking could lead to a modification of the crystalline structure of PBT.

2.5.1 Pristine PBT vitrimer system

We studied the impact of the cross-linked network formation on the thermal characteristics of the vitrimer. DSC experiments were conducted on the pristine PBT matrix and PE_Z vitrimer. Second heating curves are shown in Figure 72 and data obtained from the curves are summarized in Table 9. A 6°C increase in T_g is visible for the vitrimer material, due to cross-linked bonds. PBT exhibits a double melting peak (T_{m1} at 215°C and T_{m2} at 225°C), usually attributed to melting, recrystallization of crystals (perfection of crystals)^{239,240} and/or two populations in crystalline thickness. The thicker crystals (perfected) melt at higher temperatures. In the case of the cross-linked material, only a single melting peak is visible at $T_m = 218^\circ\text{C}$, intermediate between the two melting peaks of pure PBT. Crystallinity decreases between PBT

(35.5%) and PE_Z (31.5%). Those results are in agreement with a previous study⁵ related to the impact of the cross-linking ratio on PBT vitrimer crystallinity. Indeed, it was established that for high cross-linked materials (>50 wt.-% gel ratio), cross-linking leads to a decrease of crystallinity^{5,88} of PBT vitrimer. To further study the impact of the formation of the vitrimer network on the partially cross-linked materials, the gel and soluble part of PE_Z, respectively PE_{Zgel} and PE_{Zsol}, were also analyzed. PE_{Zsol} exhibits roughly the same T_g as PBT, as well as a double-crystallization peak. PE_{Zgel} depicts the same T_g as PE_Z, while a lower T_m of 210°C is measured, as well as a significant decrease in crystallinity, reaching only 26%. Equivalent values obtained for T_g between PE_Z and PE_{Zgel} highlight the concurring effects between a decrease in crystallinity, which tends to decrease T_g²⁴¹, and higher cross-linking concentration, which increases T_g.

Table 9: Thermal characteristics of the pristine PBT vitrimer

Abbreviation	T _{g1}	T _{m1}	T _{m2}	ΔH _m	T _c	ΔH _c	X _c	%Gel
PBT	39.5 ±1.2	215.4 ±1.2	225 ±1.8	51.0 ±0.8	191.4 ±2.1	51.3 ±1.8	36 ±1	0
PE _Z	47.1 ±0.9	217.2 ±1.3		44.7 ±1.2	185.4 ±1.2	46.5 ±1.0	32 ±1	68 ±4
PE _{Zgel}	47.4 ±0.6	210.2 ±2.5		36.7 ±1.4	173.5 ±32	37.2 ±1.2	26 ±1.0	100
PE _{Zsol}	40.4 ±0.5	212.1 ±1.0	223 ±1.1	48.6 ±1.2	189.7 ±1.3	49.2 ±0.9	35 ±1	0

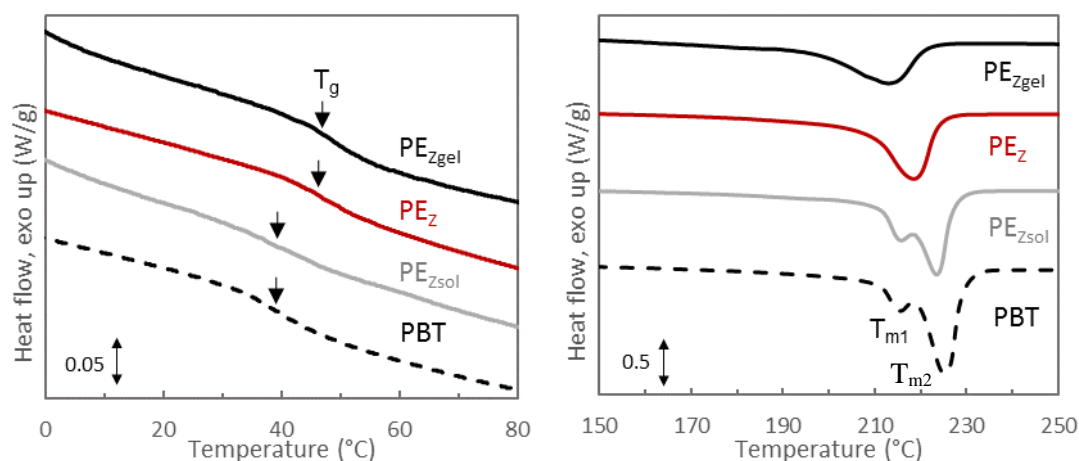


Figure 72: DSC thermograms recorded at a heating and cooling rate of 20°C.min⁻¹ for compounds PBT, PE_Z, PE_{Zsol} and PE_{Zgel}

Wide-angle X-ray diffraction was used on the four DSC samples to probe the crystal structure at room temperature. The normalized spectra were obtained by dividing the local intensity by the total measured intensity ($I/\text{Sum}(I)$), and are shown in Figure 73. All samples

present strong diffraction peaks at 15.8° , 16.9° , 20.2° , 22.9° and 24.7° , assigned to the [011], [010], [110], [100] and [111] planes which characterizes the α -crystal structure of PBT^{242,243}. This indicates that cross-linking does not alter the crystal structure of the PBT matrix. Zhou and coworkers studied the crystal structure of a PBT/glycerol vitrimer obtained by solid-state polymerization, and also observed the same α -crystal structure³⁴.

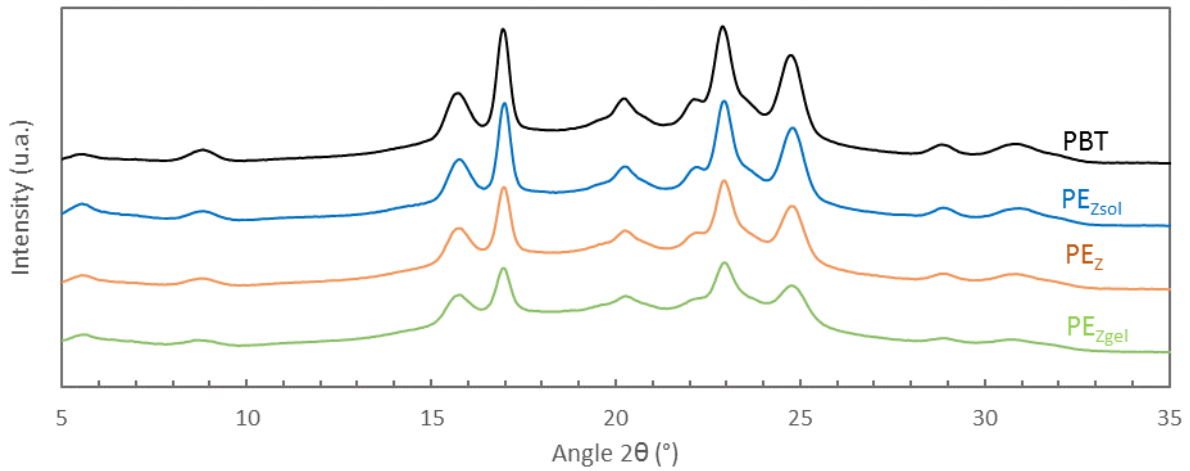


Figure 73 : WAXD diffractogram of the pristine PBT formulations

The decomposition behavior registered by TGA analysis (Figure 74) is roughly similar between PBT and PE_Z, with a one-step degradation between 350 and 450°C. PBT is widely considered a low-charring polymer²¹³, consistent with the low residue of 4.5% measured. The vitrimer sample exhibits a slightly higher char residue of 5.5%, linked with its cross-linked nature²⁴⁴. Similar results have been observed in the literature for PBT- and PBS-vitrimer^{61,91}.

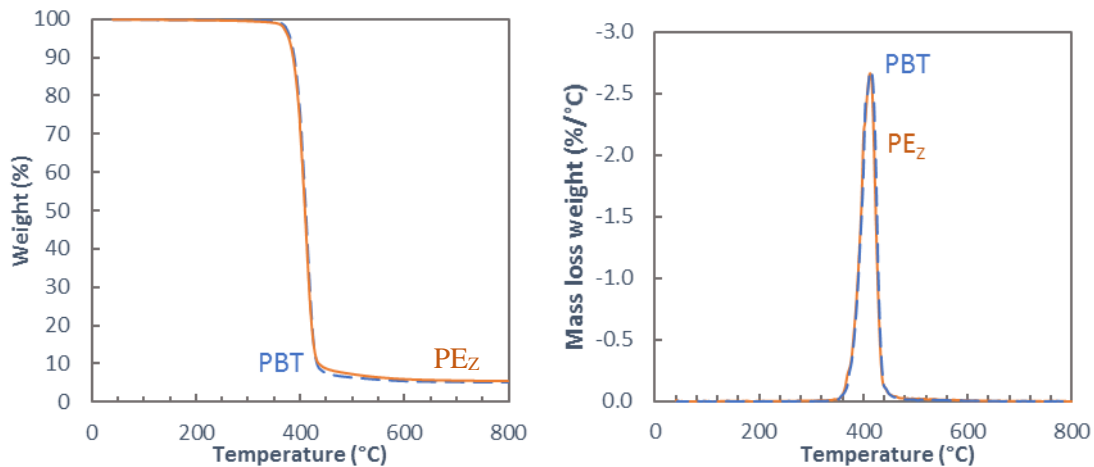


Figure 74 : TG and DTG of PBT and PE_Z under nitrogen flow with a heating rate of $20^\circ\text{C}\cdot\text{min}^{-1}$

2.5.2 20 wt.-% AlPi filled formulations

AlPi DSC curve is given in Figure 75, and the peaks attributed to the presence of AlPi for each formulation are presented in Table 10. AlPi is a non-fusible salt that exhibits three endothermic peaks. The first peak, centered around 41-43°C, has a very low enthalpy of 2.6 J.g⁻¹. The presence of a second peak in the range of 160-185°C, with an enthalpy of 25 J.g⁻¹, is related to a reversible crystal-crystal phase transition. The third peak is attributed to a second indistinct phase transition and is observed in the temperature range of 215-240°C, with an enthalpy of 7.5 J.g⁻¹. The low enthalpy first peak is not visible in the thermograms of PA₂₀ and PE_ZA₂₀. The second one is observed in a temperature range where it does not overlap with PBT signals; however, it could impact the measurement of the crystallinity for PBT vitrimer if the T_m of the latter is significantly decreased. The third peak is really closed to the melting peaks of PBT. However, since it has a very low intensity, it is considered that it will not significantly influence the results from the DSC thermograms in this study.

Table 10: details of the signals due to AlPi on the DSC curves of each formulation. The ΔH are the enthalpies of phase transition.

Abbreviation	T ₁ (°C)	ΔH_1	T ₂ (°C)	ΔH_2	T ₃ (°C)	ΔH_3
AlPi	42.5	2.6	171	25	230	7.5
PA ₂₀	/	/	172.8 ±0.7	3.7 ±0.8	/	/
PE _Z A ₂₀	/	/	173.5 ±0.5	3.7 ±0.4	/	/
PE _Z A ₂₀ gel	/	/	/	/	/	/
PE _Z A ₂₀ sol	/	/	173.6 ±0.5	6.6 ±0.6	/	/

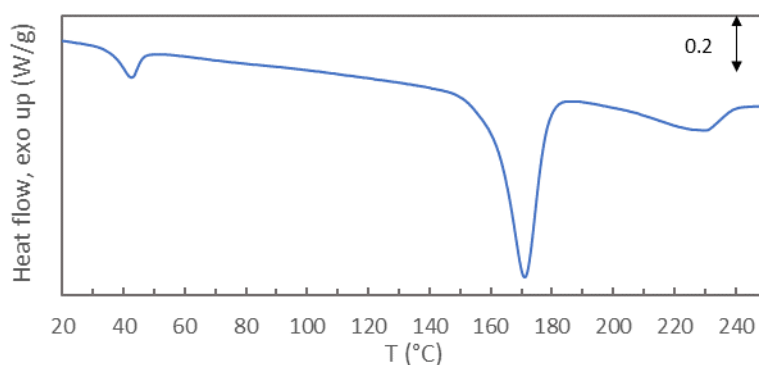
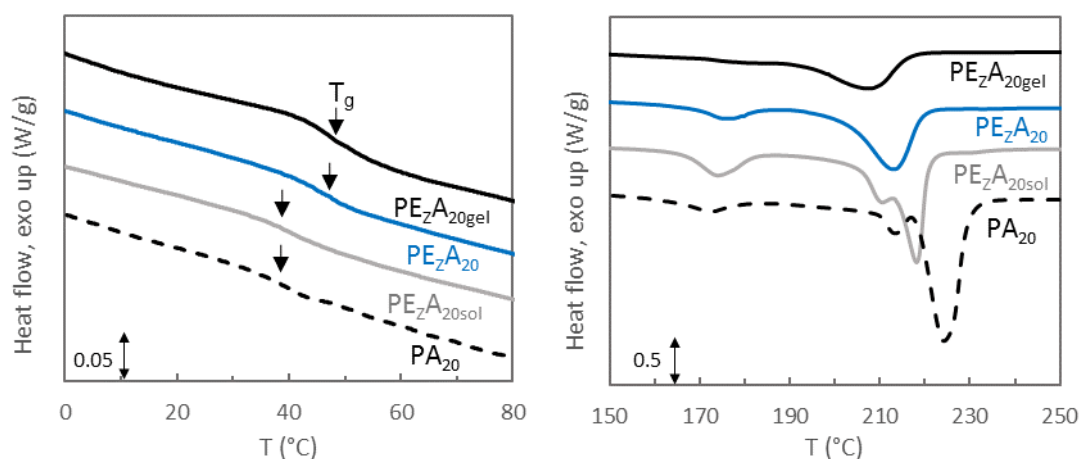


Figure 75: 2nd heating ramp DSC thermogram of AlPi

The results of experiments for samples PA₂₀, PE_ZA₂₀, PE_ZA₂₀gel and PE_ZA₂₀sol are reported in Table 11 and Figure 76. Crystallinity ratios were calculated by taking into account the amount of additives in each formulation (Equation 2, Equation 5 and Equation 6 in part 2.2.3).

Table 11: Thermal characteristics of the PBT matrix from the formulations filled with 20 wt.-% AlPi

Abbreviation	T_{g1}	T_{m1}	T_{m2}	ΔH_m	T_c	ΔH_c	X_c	%Gel
PBT	39.5 ± 1.2	215.4 ± 1.2	225 ± 1.8	51.0 ± 0.8	191.4 ± 2.1	51.3 ± 1.8	36 ± 1	0
PA ₂₀	39.7 ± 0.7	213.5 ± 0.7	224.5 ± 1.0	36.8 ± 1.5	190.9 ± 0.7	42.3 ± 1.3	32 ± 2	0
PE _Z A ₂₀	45.8 ± 1.2	213 ± 1.3	/	21.1 ± 1.7	172.0 ± 3.4	/	18 ± 2	69 ± 3
PE _Z A _{20gel}	46.3 ± 0.8	209.1 ± 1.1	/	/	161.7 ± 0.8	/	/	100
PE _Z A _{20sol}	41.1 ± 0.9	210 ± 0.7	218 ± 0.5	27.2 ± 0.6	180.0 ± 0.5	30.5 ± 0.8	29 ± 1	0

Figure 76 : DSC thermograms recorded at a heating and cooling rate of $20^{\circ}\text{C}\cdot\text{min}^{-1}$ for compounds PA₂₀, PE_ZA_{20sol}, PE_ZA₂₀ and PE_ZA_{20gel}

PA₂₀ exhibits a similar melting behavior as PBT, with two melting peaks at 213.5°C and 223.2°C and a T_g of 39.7°C with a slight decrease of crystallinity (32 % for PA₂₀ versus 36 % for PBT). This 4% reduction is on par with results obtained by Köppler et al¹⁹⁶ for a 20wt.-% AlPi-filled PBT. This slight reduction of crystal content is in good agreement with the slight decrease of T_c between PBT and PA₂₀ which shows that the addition of AlPi tends to reduce the crystallization rate of PBT. PE_ZA₂₀ sample exhibits a T_g similar to PE_Z at around 46°C, higher than PA₂₀, due to the stiffening effect provided by the cross-linked network. It is worth noticing that AlPi particles, on their own, do not increase T_g . As for PE_Z, PE_ZA₂₀ presents a single PBT melting peak at around 213°C but the crystallinity radically decreases to 18%, which is around 40% less than PA₂₀. A reduction of crystallinity was also observed between PBT and PE_Z but it was much more modest. In order to go further, PE_ZA_{20gel} and PE_ZA_{20sol} was also analyzed. PE_ZA_{20gel} exhibits a melting temperature at 208°C, i.e. lower than PE_ZA₂₀ and in the similar range of the second melting peak of AlPi, preventing the calculation of the crystallinity of PE_ZA_{20gel}. However, its peak area is smaller than for PE_ZA₂₀ indicating of lower crystallinity of this part, as already observed for PE_{Zgel} in comparison with

PE_Z. PE_ZA_{20sol} presents a clearly distinctive behavior from PA₂₀. The material exhibits a slightly higher T_g at 41°C, similar to PA₂₀ and a twin-melting peak located at temperature lower than PA₂₀. The signal around 170°C on the DSC curve of the soluble part of the vitrimer (Figure 76) is more intense than for the gel part and the PE_ZA₂₀. This result reveals that the concentration of AlPi is higher in this fraction, as confirmed by the elemental analysis of PE_ZA_{20sol} (33.7wt.-% versus 18.3wt.-% in PA₂₀). The enthalpy of AlPi in both PA₂₀ and PE_ZA₂₀ is 3.7 J.g⁻¹. However, it rises to 6.6 J.g⁻¹ for PE_ZA_{20sol} confirming that the concentration of AlPi in PE_ZA_{20sol} is 1.5 times in comparison to the average concentration. Taking into account the real amount of AlPi present in the soluble fraction, the calculated crystallinity ratio is 29%, slightly lower than PE_ZA₂₀ but much higher than its gel part.

WAXD experiments conducted on AlPi, PA₂₀, PE_ZA_{20sol}, PE_ZA₂₀ and PE_ZA_{20gel} are reported in Figure 77. AlPi presents a distinctive high intensity peak at 2θ ≈ 9.0° and others peaks in the same 2θ range as the one characteristics of the crystalline phase of PBT. All polymer samples present diffraction peaks which can be attributed to both the crystalline phases of PBT and AlPi.

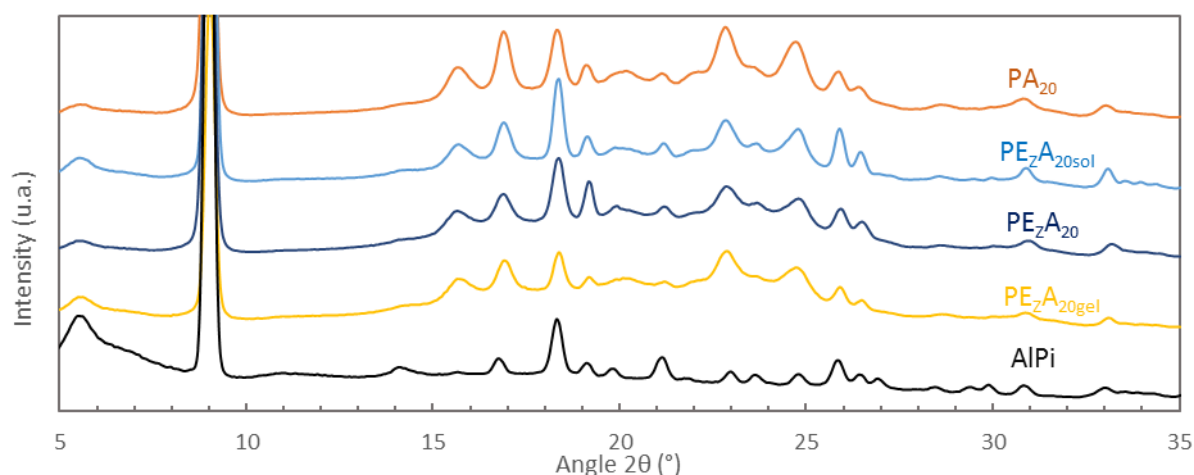


Figure 77: WAXD diffractogram for AlPi and compounds PA₂₀, PE_ZA_{20sol}, PE_ZA₂₀ and PE_ZA_{20gel}.

TGA and DTG curves recorded under nitrogen for AlPi, PA₂₀ and PE_ZA₂₀ are presented in Figure 78. The decomposition of pure AlPi is usually considered condition-dependent^{157,158}. In our case, the decomposition of AlPi follows a one-step between 420 and 500°C attributed to the vaporization of the phosphinate salt. A relatively limited char residue was measured at 15%. Braun et al. conducted extended TG analysis and found that this vaporization occurs for small sample mass and high heating rates, which is consistent with our TGA conditions (20°C/min and sample mass of 5-10mg)¹⁵⁸. Under more classic conditions (like a fire scenario), AlPi is expected to decompose at lower temperatures through scission of the phosphinic acid, leading to higher char content¹⁵⁸.

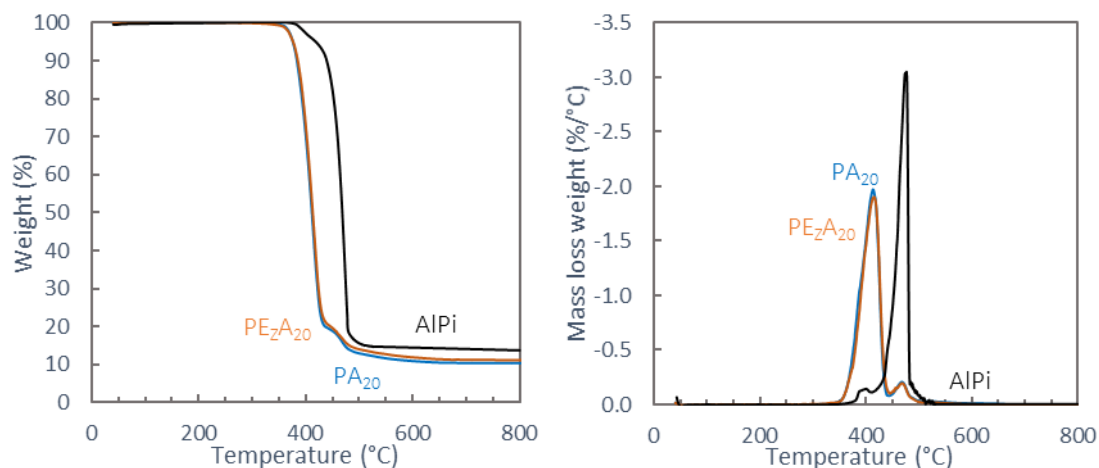


Figure 78: TG and DTG of AlPi, PA₂₀ and PE_ZA₂₀ under nitrogen flow with a heating rate of 20 °C.min⁻¹

The addition of AlPi to the polymer matrix leads to a two-steps decomposition process. The first one (main decomposition), attributed to the degradation of PBT, occurs between 350°C and 440°C, leading to an 80 % mass loss. A second minor decomposition step occurs between 450 and 500°C. In comparison with PBT, the addition of 20 wt.-% of AlPi leads to an increase of about 7 % of the residue, with a total residue measured at 11 % for PA and 12 % for PE_ZA. AlPi is known to act in the gas phase but also in the condensed phase to some extent with the formation of a transitory residue stabilized by phosphorus that eventually decomposes at higher temperatures^{196,245}. Whether the material is cross-linked or thermoplastic, the same decomposition pathway is followed, thus the presence of the cross-linked network does not lead to enhanced thermal stability.

2.5.3 PBT+ZnPi system

ZnPi is a metallic salt that presents different thermograms in DSC on the first and second heating ramp (Figure 79). During the first heating ramp a single, high enthalpy endothermic melting peak ($H_{m1}=27 \text{ J.g}^{-1}$) is visible in the range of 200-220°C, according to the manufacturer. On the second heating ramp, and for further cooling/heating cycles, two other endothermic peaks are observed, one at 108°C and the main one at around 137°C. Those peaks exhibit a much lower enthalpy ($H_2=1.1 \text{ J.g}^{-1}$ and $H_3=6 \text{ J.g}^{-1}$). Studies conducted by A. Vannier during her PhD²²⁰ showed that after several days at room temperature, recrystallization of ZnPi occurs, until reaching a thermo-dynamically stable phase with a single melting temperature at around 215°C. In our case, considering the second heating cycle, ZnPi will not have enough time to recrystallize, so its melting peaks will not affect the enthalpy measurements of the formulations.

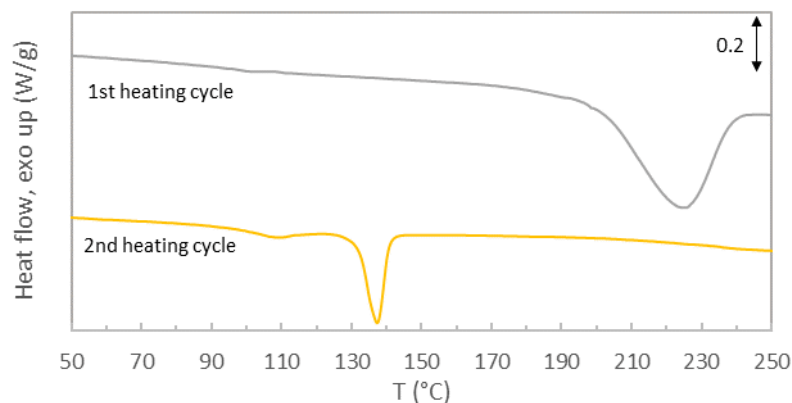


Figure 79: DSC thermogram of the 1st and 2nd heating ramp of ZnPi.

DSC results obtained for the ZnPi-filled polymers (PA, PE_ZA, PE_ZA_{gel} and PE_ZA_{sol}) are reported in Table 12 and Figure 80.

Table 12: Thermal characteristics of the formulations filled with 24 wt.-% ZnPi. Crystallinity was obtained depending on the amount of additive left in the matrixes (Table 5), using Equation 1 to 5.

Abbreviation	T _g	T _{m1}	T _{m2}	ΔH _m	T _c	ΔH _c	X _c	%Gel
PBT	39.5 ±1.2	215.4 ±1.2	225 ±1.8	51.0 ±0.8	191.4 ±2.1	51.3 ±1.8	36 ±1	0
PZ ₂₄	42.6 ±0.6	214.2 ±0.6	223.2 ±0.5	37.2 ±0.4	189.0 ±0.3	38.2 ±0.7	33.8 ±0.4	0
PE _Z Z ₂₄	45.1 ±0.6	220.1 ±0.3		35.1 ±0.9	193.1 ±0.5	36.2 ±0.8	31.9 ±0.8	34 ±3
PE _Z Z ₂₄ gel	45.4 ±0.8	211.2 ±0.8		31.9 ±0.8	186.2 ±1.6	33.9 ±1.1	25.8 ±0.5	100
PE _Z Z ₂₄ sol	43.2 ±0.4	211.3 ±0.5	216.5 ±0.3	28.5 ±0.7	187.5 ±5	31.5 ±0.9	27.8 ±0.7	0

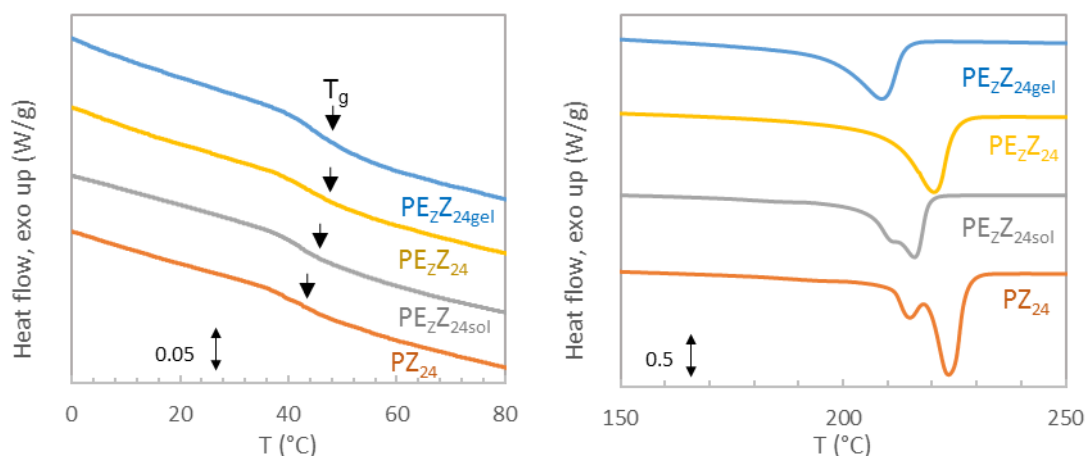


Figure 80: DSC thermograms recorded at a heating and cooling rate of 20°C.min⁻¹ for compounds PZ, PE_ZZ₂₄sol, PE_ZZ₂₄ and PE_ZZ₂₄gel. The curves were shifted vertically for clarity.

The addition of ZnPi in PBT slightly increases the T_g (T_g (PBT)~ 40°C / T_g (PZ₂₄)~ 43°C) and decreases the crystallinity, similar to the crystallinity decrease observed with the addition of

AlPi (PA₂₀). Similar results have been reported on a 80wt.-% PET/20wt.-% ZnPi, with a slight reduction of crystallinity (by 2%)⁷². The double melting peak of PBT is still present with similar melting temperature ($T_{m1}=215^{\circ}\text{C}$ and $T_{m2}=224^{\circ}\text{C}$). The T_g of the partially cross-linked PE_ZZ₂₄ exhibits an increase of only 3°C compared to PZ₂₄. Note that in the case of both PE_Z and PE_ZA₂₀, the T_g increase was more pronounced (6°C increase due to cross-linking). A similar tendency could be found with the decrease of crystallinity, with only 1% decrease for PE_ZZ₂₄ compared with PZ₂₄. It is assigned to a much lower cross-linking degree of PE_ZZ₂₄ compared to PE_Z and PE_ZA₂₀ (34 wt% versus 68-69wt%).

PE_ZZ₂₄'s cross-linking ratio of 34%, twice lower than the previous cross-linked formulations, implies that a smaller amount of diepoxy effectively reacted with the PBT backbone. Besides, one can notice a crystallization temperature of PE_ZZ₂₄ higher than for PZ₂₄ (193°C vs 189°C). This might indicate that a part of the diepoxy species which has not reacted with the PBT chains or ZnPi would play a nucleating role.

As previously conducted, in order to further understand the structure of PE_ZZ₂₄, the thermal behavior of PE_ZZ_{24sol} and PE_ZZ_{24gel} was analysed. However, the results are slightly confusing, in particular regarding the melting behaviour of PE_ZZ_{24sol} and PE_ZZ_{24gel} which is in both case lower than for the PE_ZZ₂₄. Additional investigations are needed to explain this unexpected result.

WAXD experiments conducted on ZnPi, PZ₂₄, PE_ZZ_{24sol}, PE_ZZ₂₄ and PE_ZZ_{24gel} are depicted in Figure 81. The phosphinate salt exhibit a complex diffractogram, with numerous peaks in the same 2θ range as for PBT α phase. Similarly to the diffraction results found for AlPi-filled polymers, all polymer samples depict diffraction peaks corresponding to both the crystal structures of ZnPi and the α -crystal structure on PBT-vitrimer sample. The peak located at around 10.5° , attributed to ZnPi, displays a radically lower intensity for the cross-linked compounds (PE_ZZ₂₄ and PE_ZZ_{24gel}). This change in intensity, observed especially for the cross-linked materials, can be put in perspective with the former ss NMR studies which suggested the presence of diethylhypophosphorus acid originating from the separation of a phosphorus ligand from the ZnPi. Therefore, the crystalline structure of ZnPi is affected, which may explain the lower peak intensity observed for the vitrimer compounds.

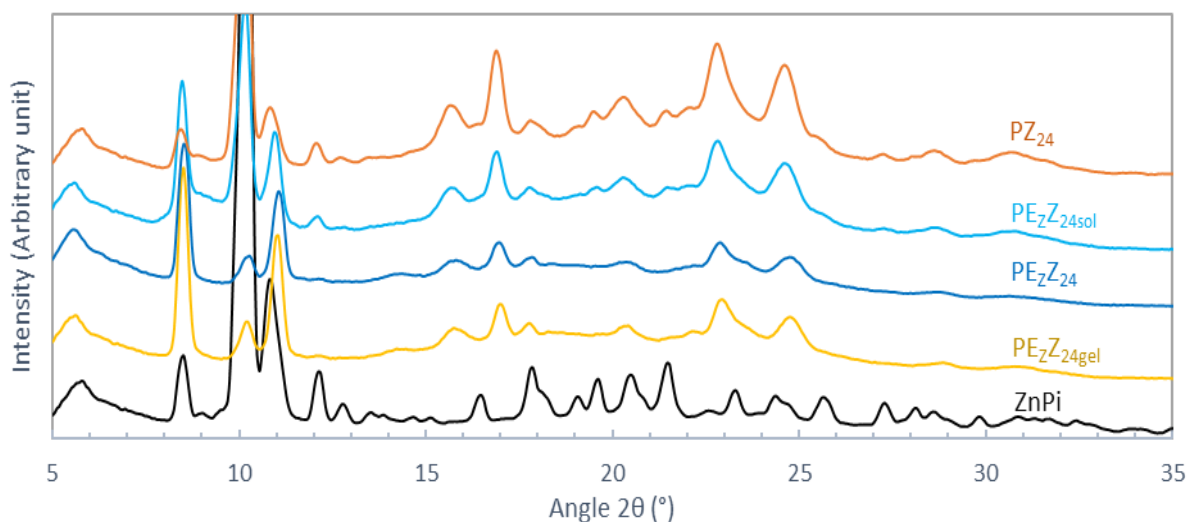


Figure 81 : Left: WAXD diffractogram for ZnPi and compounds PZ_{24} , $PEzZ_{24sol}$, $PEzZ_{24}$ and $PEzZ_{24gel}$.

Figure 82 presents TG curves of ZnPi, PZ_{24} and $PEzZ_{24}$ conducted under nitrogen, as well as their respective derivative, DTG. The thermal degradation of ZnPi occurs in one step, from 400 to 560°C, with a final residue of 34%. During the decomposition, phosphonic acids, phosphinate salts, benzoate, ethane and carbon dioxide are formed¹⁵⁸. While this result is consistent with previous studies^{220,221,247}, Reuters et al. reported a two-step decomposition of zinc phosphinate salts, with a first decomposition occurring at lower temperatures, between 350 to 440°C^{158,248}. It then appears that the decomposition step of zinc phosphinate is condition-dependent, similarly to aluminum phosphinate. When 24 wt.-% ZnPi is added to the PBT matrix, a first decomposition step is visible between 330 to 430°C, similar to pristine PBT. A second decomposition step is also visible at higher temperatures, from 430 to 470°C, and slightly overlaps the first decomposition step. During the first step, the sample loses approximately 80% of its mass, while 11% is lost during the second decomposition, with a final of 8% remains at 800°C. Braun et al. observed a much smaller second decomposition step, as well as no significant increase in residue for PBT/GF30 wt.-%/ZnPi20 wt.-% samples compared with pristine equivalent¹⁵⁸. In our case, both higher ZnPi concentration and higher polymer fraction may explain those differences observed. The cross-linked material $PEzZ_{24}$ behaves similarly during the first decomposition, but exhibits a broader second decomposition step, ranging from 430 to 480 corresponding to more transitory residue. A slightly higher final residue at 9% is obtained, explained by the tendency of cross-linking compounds to promote a slightly higher charring effect⁹¹. Overall, the cross-linked nature of the polymer does not give significant improvement in degradation behavior.

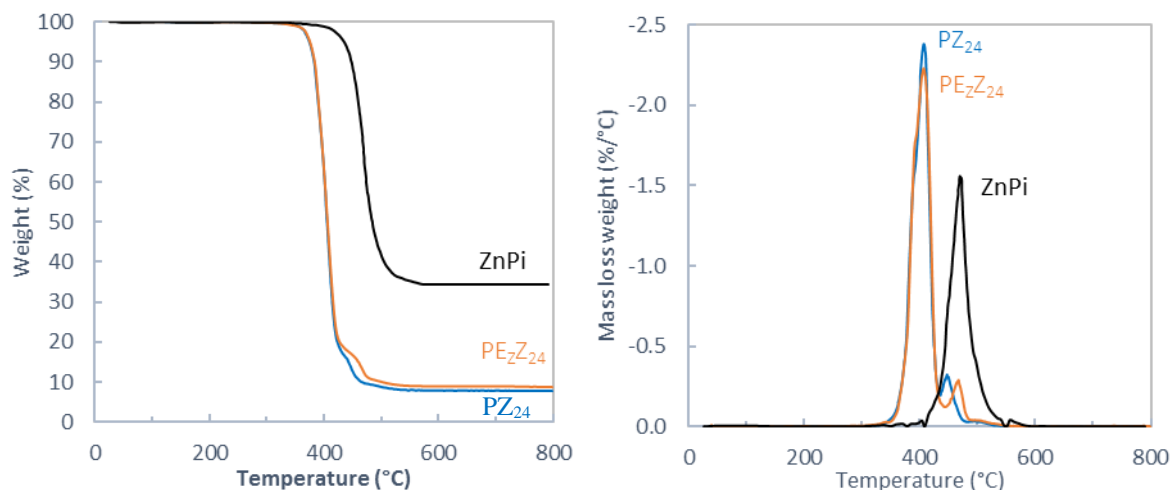


Figure 82 : TG and DTG of ZnPi, PZ₂₄ and PE_ZZ₂₄ under nitrogen flow with a heating rate of 20 °C.min⁻¹

2.5.4 PBT+HM1100 system

DSC experiments have been conducted on the thermoplastic reference PH₂₀, of the cross-linked reference P5E_{5Z}H₂₀ as well as PE5_{Z5}H_{20gel} and PE5_{Z5}H_{20sol}, respectively the gel and soluble part of this cross-linked reference, with values reported in Table 13. Thermograms of the materials are shown in Figure 83.

Table 13: Thermal characteristics of the PBT matrix from the formulations filled with HM1100

	T _{g1}	T _{g2}	T _{m1}	T _{m2}	ΔH _m	T _c	ΔH _c	X _c	%Gel
PBT	39.5 ±1.2	/	215.4 ±1.2	225 ±1.8	51.0 ±0.8	191.4 ±2.1	51.3 ±1.8	36 ±1	0
HM1100	99.3 ±0.2	/	/	/	/	/	/	/	0
PH ₂₀	45.2 ±0.6	97.4 ±0.7	211.7 ±0.4	221.4 ±0.5	35.0 ±0.6	180 ±0.2	37.9 ±0.8	31 ±1	0
P5E _{5Z} H ₂₀	58.5 ±0.7	/	213.2 ±1.0		32.2 ±0.4	185.3 ±0.5	35.2 ±0.6	28 ±1	62 ± 5
P5E _{5Z} H _{20sol}	51.4 ±0.3	/	206.4 ±0.3	215.7 ±0.3	39.3 ±0.5	183.9 ±0.4	41.5 ±0.4	34 ±1	0
P5E _{5Z} H _{20gel}	58.2 ±0.4	/	202.0 ±0.3		23.5 ±0.5	172.8 ±0.8	26.1 ±0.7	21 ±1	100

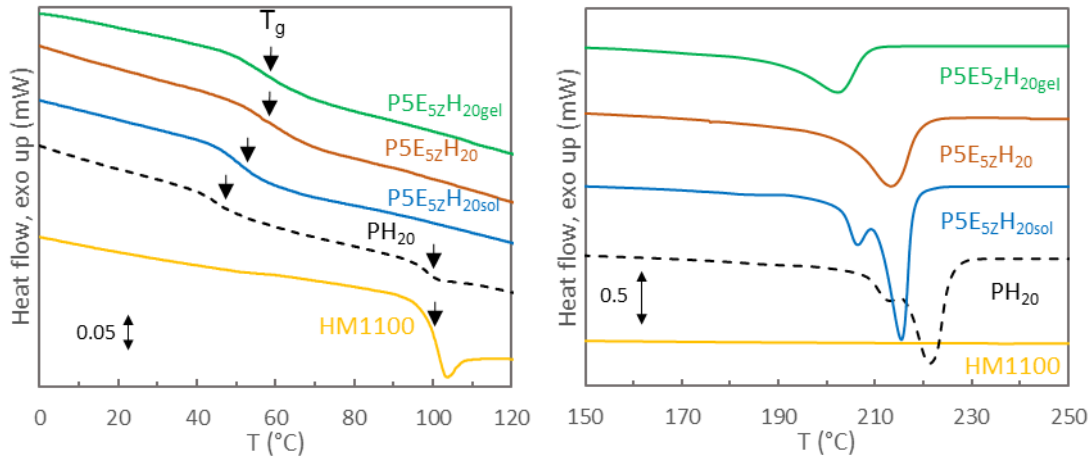


Figure 83 : DSC thermograms recorded at a heating and cooling rate of $20^{\circ}\text{C}\cdot\text{min}^{-1}$ for compounds PH, $\text{P5E}_{5z}\text{H}_{20\text{sol}}$, $\text{P5E}_{5z}\text{H}_{20}$ and $\text{P5E}_{5z}\text{H}_{20\text{gel}}$. The curves were shifted vertically for clarity.

PH_{20} has a crystallinity of 31.2%, which is 4.2% lower than pristine PBT. The higher crystallinity ratios observed for PE_zH_{20} and $\text{PE}_{5z}\text{H}_{20}$ is attributed to nucleation effects promoted by the presence of unreacted epoxy⁸¹, as T_c also increases from 180°C to 186°C in the process. For high cross-linked compounds $\text{P5E}_z\text{H}_{20}$ and $\text{P5E}_{5z}\text{H}_{20}$, the nucleating effect is offset by cross-linking, which is clearly detrimental to crystallization. Especially, compound $\text{P5E}_{5z}\text{H}_{20}$, which has the highest cross-linked fraction, exhibits a lower crystallinity at 27.9%. Logically, $\text{P5E}_{5z}\text{H}_{20\text{gel}}$ has the lowest crystallinity of all samples at 20.7%.

WAXD experiments were conducted on PH_{20} , $\text{P5E}_{5z}\text{H}_{20}$, $\text{P5E}_{5z}\text{H}_{20\text{gel}}$ and $\text{P5E}_{5z}\text{H}_{20\text{sol}}$. HM1100 , as an amorphous polymer, is characterized by a broad halo between 13° and 25° (without diffraction peaks) and is not represented in the Figure 84. The α -crystal structure of pristine PBT is conserved for all 4 samples, with strong diffraction peaks observed at 15.9° , 16.9° , 20.1° , 22.8° and 24.6° respectively.

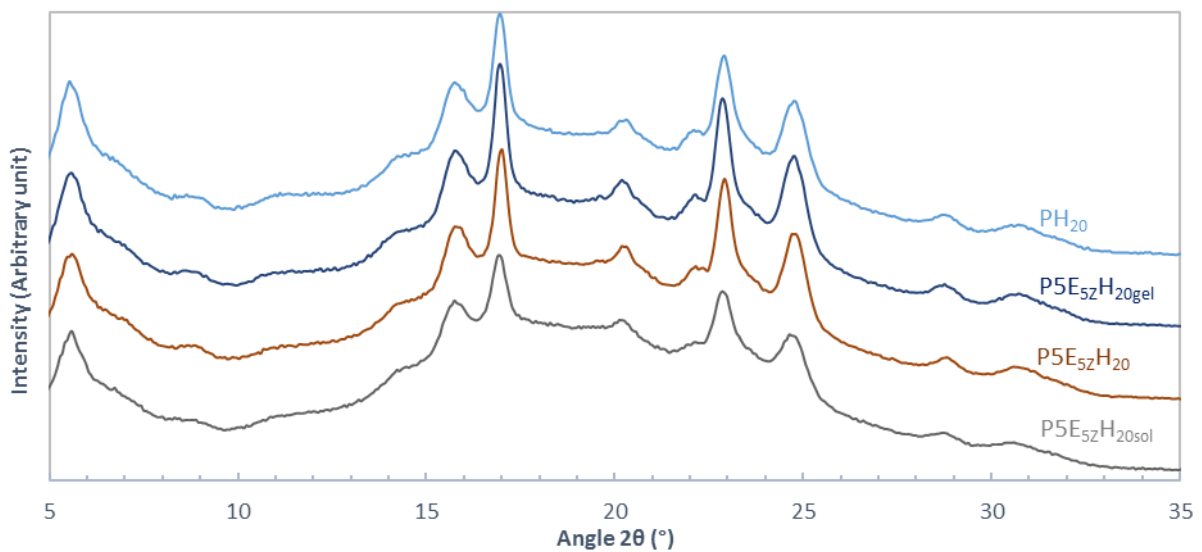


Figure 84: WAXD spectra for compound PH_{20} , $\text{P5E}_{5z}\text{H}_{20}$ as well as gel and soluble part of the latter.

The degradation behavior of HM1100, PH₂₀ and P5E_{5Z}H₂₀ were recorded by TGA and are presented in Figure 85. The polyphosphonate exhibits a single decomposition step occurring between 400 and 600°C. At 800°C, a significant residue of 23% is obtained. Compared with phosphinate salts, phosphonate alone promotes higher charring content due to the presence of a rich carbon environment provided by the aromatic groups. When mixed with the PBT matrix, similar decomposition steps occur for both materials. The first decomposition step caused by the degradation of the PBT matrix is followed by a second decomposition step at 480-560°C, linked with the decomposition of the polyphosphonate. Despite a phosphorus concentration of only 2.1 wt.-%, the amount of char residue is about 13 wt.-% for PH₂₀, and 15 wt.-% for P5E_{5Z}H₂₀, slightly higher than the previous results involving phosphinate salts. Consequently, while the addition of HM1100 increases the amount of residue, the decomposition behavior is not affected by the cross-linking of the material.

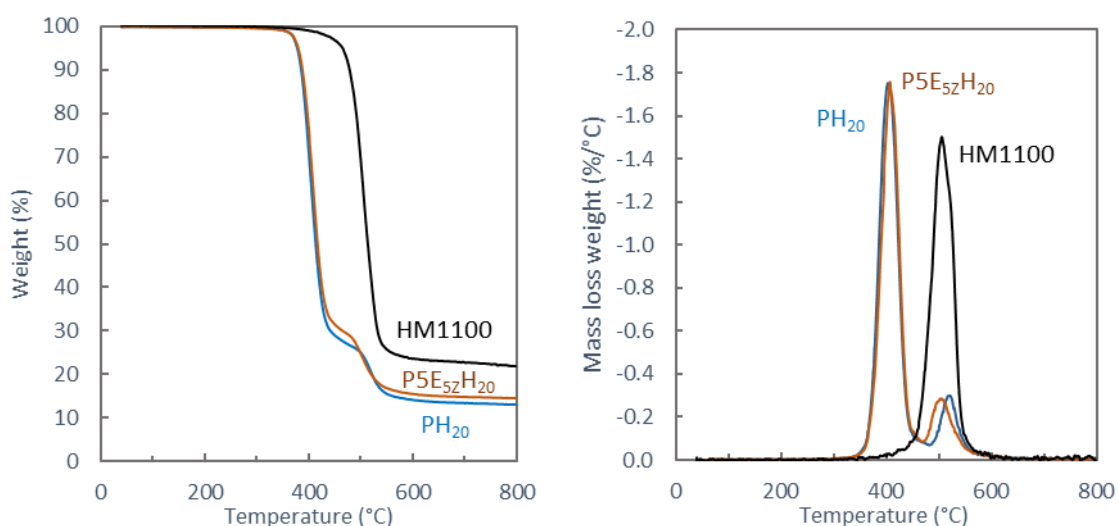


Figure 85 : TG and DTG of HM1100, PH₂₀ and P5E_{5Z}H₂₀ under nitrogen flow with a heating rate of 20 K.min⁻¹

2.5.5 Conclusion

The thermal and crystalline characterization of flame-retardant-filled PBT vitrimer has provided valuable insights into the properties of these materials. The differential scanning calorimetry (DSC) analysis conducted on the vitrimer materials as well as on their soluble and insoluble fractions revealed higher glass transition temperatures (T_g) associated with a stiffer network formed through partial cross-linking. However, a decrease in overall crystallinity was observed for the most cross-linked materials (especially the gel fractions), leading to notable impacts on the melting temperature (T_m) and crystallization temperature (T_c). Despite these changes, no significant difference in thermal stability was observed between the vitrimer compounds and thermoplastic references, indicating that the incorporation of cross-links did not compromise the overall thermal stability of the material. Additionally, no variation in the crystalline phase was observed among the vitrimer materials, as they

all exhibited the alpha-crystalline structure characteristic of PBT. These findings provide valuable knowledge about the thermal and crystalline behavior of filled semi-crystalline thermoplastic-based vitrimer.

2.6 Conclusion

In this chapter, a study of the formation of a cross-linked vitrimers in the presence of flame-retardant additives was conducted. The vitrimer system was composed of a commercial PBT, a diepoxy (DGEBA) and a transesterification catalyst ($\text{Zn}(\text{acac})_2$) and eventually a flame retardant additive. Three commercial flame-retardants were considered: two commercial phosphinates – aluminum phosphinate (Exolit OP1230) and zinc phosphinate (Exolit OP950) –and a polyphosphonate (Nofia HM1100).

The first part focused on the synthesis of cross-linked compounds in the presence of flame-retardants. The evolution of the axial force monitored during the reactive extrusion process and the measurement of the gel fractions were used as a first approach as marker of the formation of a cross-linked network. It was demonstrated that the addition of 20wt.-% loading of AlPi, enough to theoretically obtain fire retardant efficiency, during the synthesise of the vitrimers does not affect its formation. AlPi-filled formulation (PEzA_{20}) exhibited similar cross-linking fraction compared with pristine PBT-vitrimer (PEz) (around 70%). The characterization of the dispersion of the FR in the materials shows the presence of AlPi in the form of particles of around 20 μm , but also the presence of a fraction of homogeneously dispersed flame-retardant in the gel fraction. Solid-state NMR (^{13}C , ^{27}Al and ^{31}P) reveal a modification of the environment of both the phosphorous and the aluminum but no modification of the carbon environment in the gel fraction of the material. These analyses highlight the formation of a small fraction of diethylphosphinic acid. It was thus proposed that the Al^{3+} most probably interacts with the carboxylates in the same way as the Zn^{2+} based transesterification catalyst.

The addition of ZnPi during the processing of the vitrimer matrix is not as simple, and in this case the addition of this additive at 10 or 24wt% is detrimental to the network formation. The gel ratio decreases with an increasing additive content. ^{31}P NMR analysis showed that only diethylphosphinic acid remained in the gel fraction.

The last system with HM1100 is also complex. Indeed, in this case, the blend of PBT and HM1100 is incompatible. No measurable gel fractions could be obtained in the presence 20 or 44wt.-% of HM1100 with the content of epoxy and catalyst used to synthesize the PBT vitrimer, demonstrating the inhibition of the network formation due to such additive. It was however show that the compatibility between the two polymers is improved in presence of epoxy. For PEZH_{44} , even if the two polymers are segregated in two domains, nodules of HM1100 are observed in the PBT phase but no nodule of PBT in H1100. In PEzH_{20} , the nodules of HM1100 are much smaller and the interface barely visible. It was suggested that epoxy most likely play the role of a reactive compatibilizer and is consumed to form a copolymer PBT-Epoxy-HM1100 or PBT-HM1100 rather than to create the network. An optimization of the HM1100-

polymer formulation to obtain an effectively cross-linked material was then performed by multiplying by five the amount of epoxy, the amount of catalyst or both simultaneously. It was thus possible to conclude that increasing the amount of catalyst content alone does not enable significant crosslinking whereas the amount of epoxy played a major role in the increase of gel content.

In the second part, the cross-linked formulation dynamics was characterized by stress-relaxation experiments. The relaxation of the materials was analyzed following two distinct methods. The study showed that all materials did not follow a classic Maxwell model as they do not behave like ideal viscoelastic fluids due to their partially crosslinked structures. The use of a Kohlrausch-Williams-Watts model was much more appropriate in our case. The addition of FRs had various consequences on the relaxation behavior of the synthesized materials. Both ZnPi and AlPi-filled formulations follow an Arrhenius-like relaxation type confirming that these materials are vitrimers. However, the presence of AlPi also significantly decreased relaxation times, from 118s for PE_Z to 5s for PE_ZA₂₀ at 250°C. On the other hand, the HM1100-filled formulation could totally relax in the studied temperature range but did not display a clear Arrhenius-type tendency.

The last part of this chapter investigated the properties of the crosslinked materials. All of them exhibit lower crystallinity and a single melting peak compared with their thermoplastic references. However, all materials kept the α -crystalline structure of pristine PBT. TGA experiments did not show a significant effect on the degradation behavior of the presence of cross-linked networks compared with thermoplastic equivalents.

The next chapter will focus on the optimization and characterization of the AlPi-filled vitrimer system. This study falls within the second part of the project, consisting in developing an effective flame-retarded PBT vitrimer and studying its pertinence for application in Electronic and Electric applications.

Chapter 3 - Evaluating the performance of aluminum phosphinate as flame-retardant and transesterification catalyst

3.1. Introduction

The previous chapter dealt with the addition of commercially available flame-retardants during the synthesis of a PBT-vitrimer. Starting with the exact same composition as the one used to prepare the non-FR vitrimer, using epoxy and the Zn-based transesterification catalyst, we compared several cross-linked PBT systems filled with flame-retardants and studied the effect of those flame-retardants on the dynamics of the bond-exchange reactions. Of all the systems studied, aluminum phosphinate shares complex interactions with the vitrimer matrix, allowing very fast bond-exchange reactions to occur. This raises the obvious question: to what extent does aluminum phosphinate influence the formation of the cross-linked network? Is aluminum an effective transesterification catalyst? Could it be used without the Zn-based catalyst to obtain vitrimers? What about the properties of these vitrimers (flame-retardancy, mechanical behavior, ageing)?

To answer those questions, in the first part, AlPi-filled vitrimer will be synthesized, without the addition of the Zn-based catalyst. Stress-relaxation experiments will allow us to further understand the interaction of those materials. Also, microscopy and NMR analysis will be performed to understand the nature of the interactions of AlPi with the cross-linked system.

In the second part, the performance of the material will be discussed. The mechanical behavior will be studied through tensile tests both at room temperature and slightly below the melting temperature. Chapter 1 provides strong evidence that aluminum phosphinate is one of the most effective commercially available flame-retardants for PBT, commonly used for E&E applications²¹⁶. The flame-retardant performances of FR vitrimers will be evaluated and compared with the equivalent FR thermoplastics using a fire reaction test used for E&E materials evaluation (UL-94 test). The pertinence of turning PBT into vitrimer will also be evaluated through ageing experiments. Thermal ageing and immersion scenario will be conducted on both the vitrimer and thermoplastic equivalents and subjected to fire test. The last part of this chapter examines the benefits provided by AlPi on the viscosity of the final material by proposing the synthesis of novel vitrimers through continuous reactive extrusion.

3.2. Experimental

3.2.1. Material description

All the raw materials utilized in this chapter have been introduced previously (for more information, see Chapter 2 p.2.2.1). This includes the PBT polymer grade, the DGEBA epoxy resin, aluminum acetylacetonate as flame-retardant, and HFIP as solvent.

3.2.2. Material processing

The processing of the materials was done following the same protocol as in Chapter 2, *i.e.* using a 15cm³ DSM micro-explorer under nitrogen flux, keeping a volume of reactants at 10 cm³, introducing premixed components (PBT and AlPi previously dried at 80°C overnight) and processing at 270°C and 60 rpm. The torque was recorded as a function of the residence time during each test. After 8 minutes, the formulations were extracted. The formulation names have been set as in Chapter 2. Quantities of reactants added for each formulation are presented in Table 14. Materials containing various amounts of AlPi have been prepared without the use of the Zn-based transesterification catalyst. The stoichiometric ratios were kept identical to the ratio [epoxy]/([OH]+[COOH]) at 2:1. These materials will be compared to materials already prepared in Chapter 2 (in gray in the table). Specimens for the fire, rheology and mechanical tests were prepared using a DSM Xplore 12 cm³ Laboratory Injection-Molding Machine. The injection temperature was set to 270°C and the mold temperature to 100°C.

Table 14: List of the different formulations

Abb.	Mass of components (g)				Ratio [catalyst]/([OH]+[COOH]) and [AlPi]/([OH]+[COOH])
	PBT (P)	DGEBA (E)	Zn(acac) ₂ (Z)	AlPi (A)	
PBT	12 (100wt%)				-
PE _Z	11.7 (98wt%)	0.23 (1.9wt.-%)	0.021 (0.18wt.-%)		0.11:1
PA ₂₀	9.5 (80wt%)			2.41 (20wt.-%)	-
PE _Z A ₂₀	9.5 (78wt%)	0.19 (1.6wt.-%)	0.017 (0.14wt.-%)	2.41 (20wt.-%)	Zn: 0.11:1 AlPi: 0.11:1
PEA _{0.26}	11.7 (98wt%)	0.23 (1.9wt.-%)		0.031 (0.26wt.-%)	- 0.11:1
PEA _{0.52}	11.7 (98wt%)	0.23 (1.9wt.-%)		0.062 (0.52wt.-%)	- 0.22:1
PEA ₁	11.5 (97wt%)	0.23 (1.9wt.-%)		0.12 (1wt.-%)	- 0.43:1
PEA ₁₀	10.6 (88wt.-%)	0.21 (1.8wt.-%)		1.20 (10wt.-%)	- 4.3:1
PEA ₁₅	10.0 (83wt.-%)	0.20 (1.7wt.-%)		1.81 (15wt.-%)	- 6.4:1
PEA ₂₀	9.5 (78wt.-%)	0.19 (1.6wt.-%)		2.41 (20wt.-%)	- 8.6:1

3.2.3. Characterization methods

Part of the characterization techniques used in this chapter was identical as in the previous one (see Chapter 2 p.2.2.3 for more details). It includes:

- the gel ratio measurement, determined after solubilization of the non-crosslinked part in HFIP and quantification of the FR content thanks to elemental analyses (phosphorus content) ;

- the thermal analysis (TGA and DSC), conducted using a heating rate of 20°C/min under nitrogen flow ;
- the isothermal stress relaxation experiments (with data further analysed only using the Kohlrausch-Williams-Watts (KWW) model) ;
- SEM and EPMA analyses ;
- the ³¹P, ¹³C and ²⁷Al ss NMR analyses.

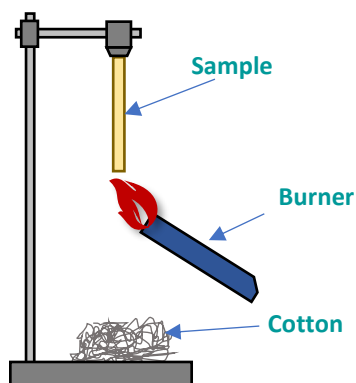
To complement the characterization of the materials, three additional analyses were performed.

Swelling ratio. The samples were immersed in HFIP for 3 days under stirring, following a similar protocol used for the separation of gel and soluble fractions. Subsequently, the swollen materials were promptly extracted from the solvent. Image analysis was performed using ImageJ software by comparing the visible surface area of the samples before and after swelling.

Rheology. Dynamic shear measurements were conducted using an Anton Paar MCR 301 Rheometer equipped with a 25mm diameter plate geometry with a gap of 1.5mm. Frequency sweeps from 0.01 to 100 rad/s were performed between 230 and 250°C.

Mechanical testing. Uniaxial tensile tests were performed using an INSTRON 4466 apparatus on 1.5 mm thick, injected ISO-527-2 dogbone-shaped samples with an effective length of 35mm. The tensile machine was fitted with a heating oven capable of reaching temperatures exceeding 300°C. The samples were initially secured in the clamps at room temperature before heating. The spacing between the clamps was then adjusted to accommodate with the thermal expansion of the material before initiating the tensile test. A constant speed of 1 mm/min (quasi-static regime) was applied. From 5 to 10 samples were tested for each formulation to ensure repeatability.

Fire test. UL-94 tests were conducted with a Fire Technology equipment on injected 125mm*12mm*1.6mm bar samples, following the procedure defined in the standard IEC 60695-11-10. Each specimen is fixed on a testing holder as presented in Figure 86, positioned at a sample-to-cotton distance of 30 ± 0.5 cm. A 20 mm high blue Bunsen burner flame is applied to the free end of the specimen for 10s and then removed. Time of burning is recorded (t_1). If the sample is extinguished before the clamp, the burner is applied a second time and the flaming time is measured again (t_2).



Criteria conditions	V-0	V-1	V-2
After flame time for each individual specimen t1 or t2	≤10s	≤30s	≤30s
Total after flame time for any condition set (t1 plus t2 for the 5 specimens)	≤50s	≤250s	≤250s
After flame plus afterglow time for each individual specimen after second flame application (t2+t3)	≤30s	≤60s	≤60s
After flame or afterglow of any specimen up to the holding clamp	No	No	No
Cotton indicator ignited by flaming particles or drops	No	No	Yes

Figure 86 : Schematic view of a UL-94 standard test and criteria conditions for each classification. A material that fails to reach V-2 classification is usually referred to as NR (not rated).

The test was instrumented with an IR camera (FLIR model X6540sc) calibrated from 20°C to 1500°C and equipped with a specific filter (opacity of 60%) eliminating the wavelength corresponding with the flame and decomposition gazes. Thus, the camera can measure the temperature both at the surface of the sample and of the flaming and non-flaming drops. The material emissivity was set at 1 for all measurements. Figure 87 shows an example of a picture filmed by the thermal camera. BOX 1 was positioned to measure the evolution of maximum temperature during the burning of the bar sample, while BOX 2 was positioned around the cotton to measure the evolution of the temperature of the drips, which could eventually lead to the inflammation of the cotton. The weight of the samples before and after the test was measured as well as the weight of the drops (scale placed under a pan containing the cotton). The setup is shown in Figure 87.

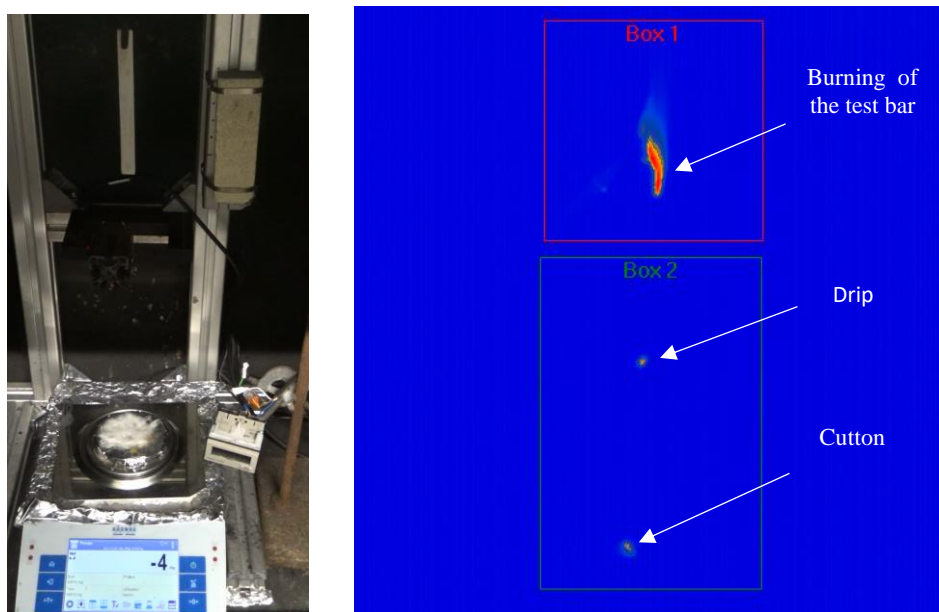


Figure 87 : Left : UL-94 setup, with a high precision weighting scale positioned under the testing bar to record the total mass of the drops ; Right : Position of the temperature recording boxes of the FTIR camera, with box 1 recording the max temperature of the testing bar around the burner, and box 2 recording the max temperature of the drops

Figure 88 illustrates the typical temperature curves obtained during temperature recording for both the materials and the drops. In this test, the temperature recording begins before the application of the flame on the materials, resulting in the observation of a plateau. It is important to note that the temperature at which the plateau is observed does not reflect the actual temperature of the sample. This discrepancy arises due to the setup of the temperature profile, which provides temperature readings only within the range of 100°C to 600°C. Consequently, if the temperature falls below 100°C, the profile indicates it as 100°C.

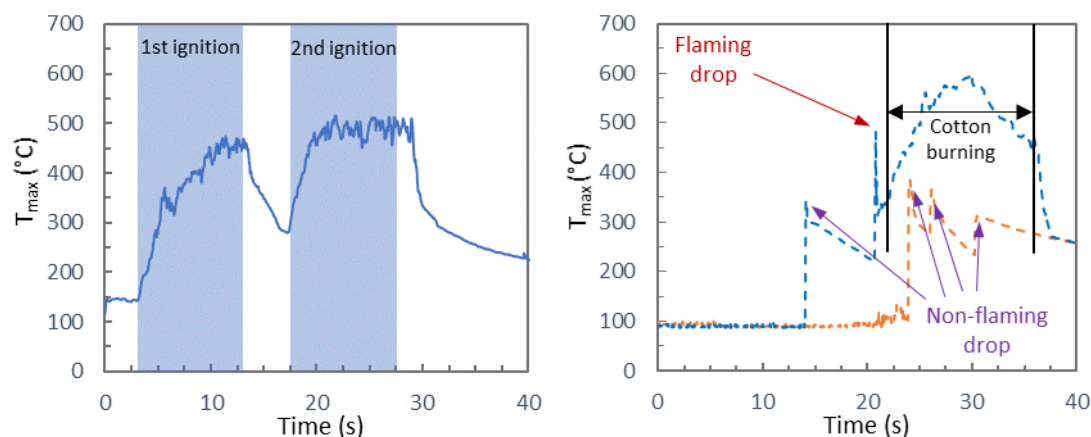


Figure 88 : Left : Typical temperature curve obtained from measuring the temperature at the surface of the UL-94 specimen. Right : Typical curves obtained from measuring the drops.

Upon the application of the burner to the materials, a rapid increase in temperature is observed in the recorded data. The flame is maintained for a duration of 10 seconds before being removed. Subsequently, depending on the scenario, the sample may either continue burning or extinguish. In the case of extinguishment, the temperature experiences a noticeable drop. The first inflammation time refers to the duration between flame application and flame extinction, subtracting the 10-second maintenance period. This behavior is consistently observed across the experiments.

Continuous reactive extrusion. The extruder used to carry out the cross-linking reaction was a co-rotative twin-screw extruder Process 11 from Thermo Scientific with a screw diameter, D , of 11mm and a length-to diameter ratio, L/D , of 40. The screw design was composed of two mixing zones composed of kneading blocks, promoting both melting of the polymer and mixing with the reactants (Figure 89). At the end of the extruder, the pumping zone was equipped with a pressure sensor ($P_{max} < 100$ Pa). Both pressure and torque were carefully monitored to prevent blockage of the extruder due to the high viscosity promoted by cross-linking.

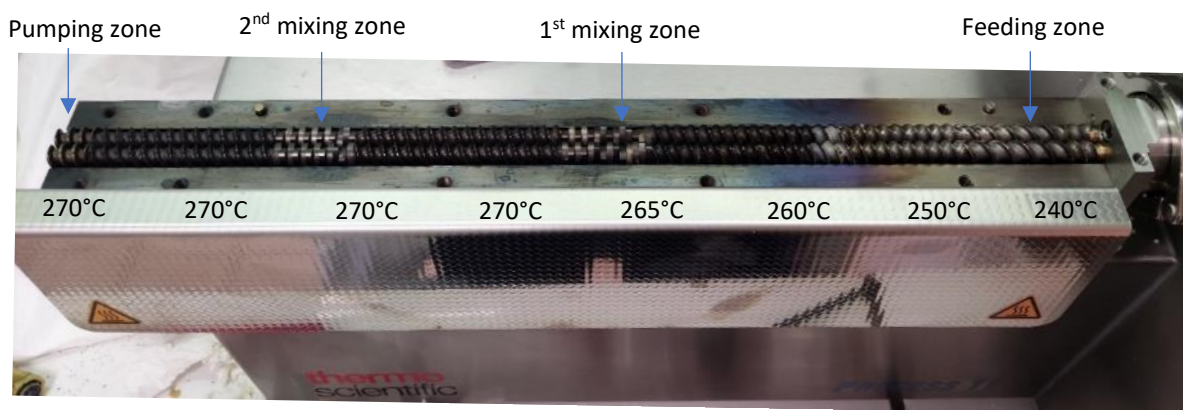


Figure 89 : Screw profile and temperature parameters of the extruder*

3.2.4. Ageing scenarios

The comprehensive review of Ferry et al. describes the influence of environmental ageing on the flaming behavior of flame-retardants in various polymers²⁴⁹. Out of the six ageing sources identified, temperature and moisture are the most pertinent with E&E applications. Two ageing procedures were consequently used.

Thermal ageing: A total of five UL-94 samples were subjected to thermal exposure by placing them in a ventilated oven set at a temperature of 70°C for a duration of 7 days (referred to as 7d70°C). Following this thermal exposition period, the samples were carefully taken out from the oven and transferred to a desiccator for further testing in UL-94 and subsequent characterization. This specific conditioning regime was chosen to align with the sample preparation and conditioning procedures described in the UL-94 standards.

Immersion in water test: Five UL94 tests were immersed together in a 3-liter distilled water bath that was thermoregulated at 50°C for a duration of 30 days (referred to as 30d50°Cwater). Following this ageing process, the samples were taken out of the water bath, dried using paper, and weighed. Subsequently, they were placed in an oven overnight at 80°C to ensure complete drying. Once dried, the samples were weighed again to assess weight changes.

3.3. Synthesis of materials without the Zn—transesterification catalyst

The previous chapter showed that the incorporation of AlPi has an impact on the crosslinking kinetic and the dynamics of the bond exchange reactions of a PBT vitrimer. It is consequently reasonable to assume that it acts as a co-catalyst during the formation of the vitrimer network. This section aims at verifying this and at characterizing the properties of the obtained materials.

3.3.1. Reactive extrusion

The materials were prepared without the Zn-catalyst but with different loadings of AlPi. Lower loadings were tested to ensure the presence of AlPi in a catalyst concentration in the material (0.26 wt.-%, 0.52 wt.-%, and 1 wt.-%), while higher loadings were used to achieve fire performances (10 wt.-%, 15 wt.-%, and 20 wt.-%). The formation of a crosslinked network was initially confirmed by monitoring the evolution of axial force during processing and quantifying the gel ratio.

The evolution of the torque during the reactive extrusion of the different formulations is reported in Figure 90 and Table 15. In all formulations, an initial increase in the axial force is observed, eventually reaching a plateau value. The specific plateau value and the time required to reach it vary depending on the amount of AlPi used. This indicates that cross-linking occurs even in the absence of the Zn-based catalyst, suggesting that AlPi is capable of promoting cross-linking on its own.

When extrusion is performed with AlPi added in the same molar quantity as $\text{Zn}(\text{acac})_2$ in PE_Z (PEA_{0.26}), the force slowly increases, reaching 4000 N after more than 16 minutes of residence time in the extruder. Compared with PE_Z, the time to reach the plateau when using AlPi instead of $\text{Zn}(\text{acac})_2$ is much longer showing that AlPi is a less efficient cross-linking catalyst. Increasing the amount of AlPi in the formulation enables to speed up the network formation up to a certain loading. Indeed, the maximum force is reached at 15 minutes for PEA_{0.56}, at 9 minutes for PEA₁, then at 6-7 min for PEA₁₀, PEA₁₅, and PEA₂₀. The optimum loading of AlPi as catalyst of transesterification is between 1 and 10 wt.-%. Above this loading, no significant variation in the maximum axial force is observed. This lack of difference can be attributed to the excessive amount of AlPi, indicating that the formulation is already well-saturated with catalysts. The maximum force achieved for all the AlPi-filled formulations (reaching up to 5000 N) is consistently lower than the one observed previously for PE_Z (up to 6000 N). This disparity can be attributed to a lower melt viscosity when AlPi is present, rather than indicating a less crosslinked network. The gel ratio, which will be discussed in the following paragraph, provides further evidence regarding the level of crosslinking achieved in the materials.

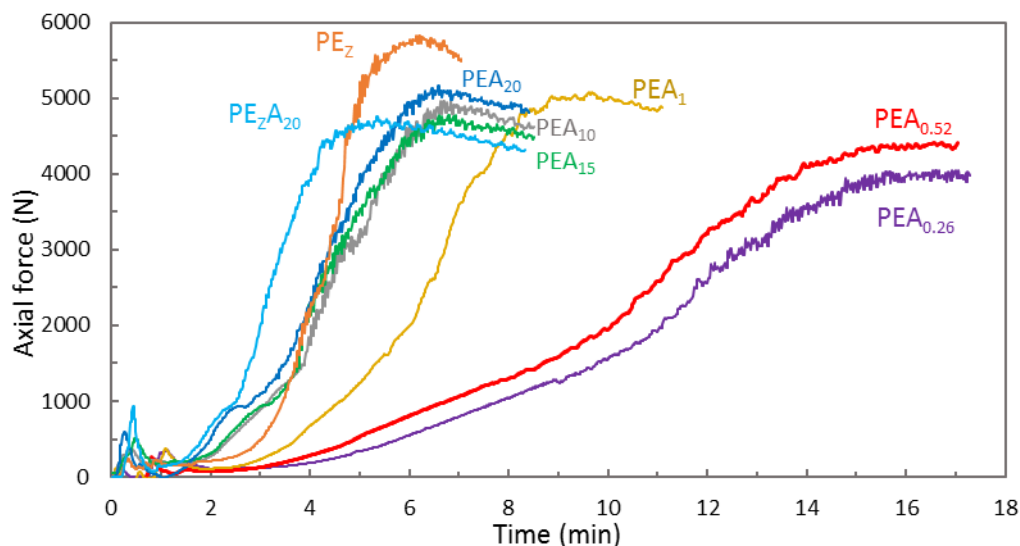


Figure 90 : Evolution of the axial force as a function of residence time for PBT/Epoxy systems with various amount of AlPi

Table 15 : Summary of the parameters extracted from the curves and gel ratio for these materials (PAF = peak of axil force).

AlPi (wt.-%)	PAF (N)	t (PAF) (min)	Gross gel ratio (wt.-%)	Final ratio (wt.-%)
0.26	4000	16	72 ±3	-
0.52	4400	15	71 ±2	-
1	5000	9	71 ±3	-
10	4700	6.5	67 ±3	-
15	4700	6.5	64 ±3	-
20	5000	6.5	62 ±4	68 ±4

The gross gel ratios (including the fraction of non-solubilized AlPi) of the formulations were measured (Table 15). At low FR loading, *i.e.* 0.26, 0.56 and 1wt.-%, the gross gel ratio of the materials is around 70% but with 10, 15 and 20 wt.-% of AlPi, slightly lower values are obtained (64 to 67 wt.-%). This is due to the presence of the fraction of FR maintained in the gel part that cannot be neglected anymore. For these three materials, the gel ratio has to be corrected as explained in the experimental part. Elemental analyses have to be performed to quantify the FR loading in the gel and then a final gel value can be calculated. This has only been done for PEA₂₀ as this is the materials of interest to have the best FR properties.

Elemental analysis was conducted on the extruded PEA samples and their insoluble fraction (PEA_{gel}) to quantify the amount of aluminum and phosphorus present. Those results are reported in Table 16. Based on the initial amount of phosphorus content in AlPi, it appears that only 18 wt.-% AlPi instead of 20 wt.-% remains in the material at the end of the extrusion process. A similar result was already reported in the previous chapter for PE_zA₂₀ and explained by the processing conditions. Considering the amount of AlPi left in the insoluble fraction, the

final fraction of polymer materials remaining in the gel is about 68%, similar to the fraction obtained for PE_Z (68%) and PE_ZA₂₀ (69%) in the previous chapter.

Table 16 : Weight percentage of Aluminum and Phosphorous remaining in PEA compound, based on elementary analysis.

Sample	Al (wt.-%)	P (wt.-%)	FR _{calculated}	FR _{expected}
PEA ₂₀	1.25 ± 0.02	4.28 ± 0.02	17.8	20
PEA ₂₀ gel	0.71 ± 0.01	2.49 ± 0.01	10.4	

This part shows that AlPi catalyzes the transesterification reaction but in a less efficient way than Zn(acac)₂. To perform the crosslinking in a time frame similar to that for Zn(acac)₂, a loading between 1 and 10wt% is necessary. However, at this loading the FR performances will not be high enough for the E&E applications. In addition, the incorporation of 20wt.-% of FR has no detrimental effect on the vitrimer network formation. The majority of the analyses that follow will focus on this specific material exclusively.

The crosslinking density was appreciated thanks to swelling tests. Figure 91 presents the aspect of PE_Z and PEA₂₀ before and after swelling in HFIP. Image analysis showed that a swelling ratio of approximately 700% and 600% could be observed for PE_Z and PE_ZA₂₀ respectively. All synthesized crossed-linked materials exhibited similar swelling ratios. This high swelling ratio indicates that, despite a high gel ratio of 68 wt.-%, the cross-linking density is low⁶¹.

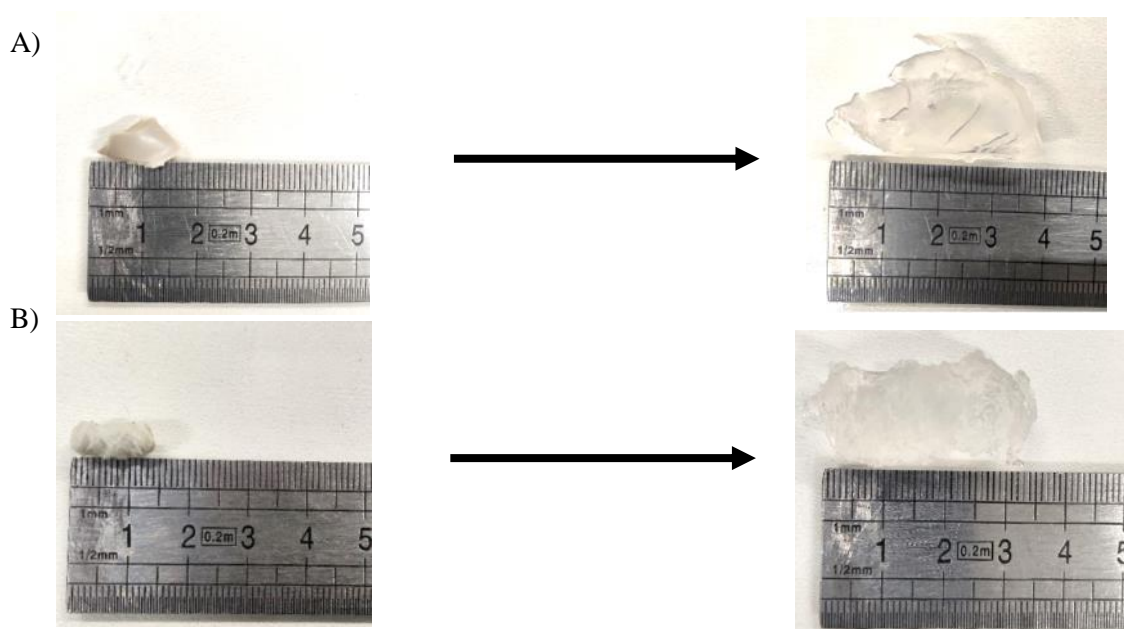


Figure 91 : Sample image before (left) and after (right) swelling in HFIP for 4 days at room temperature for A) PE_Z, B) PEA₂₀.

3.3.2. Thermal characterization of the materials

The thermal characterization of the previously discussed materials has been performed by DSC. The results are presented in Table 17. Glass transition temperature (T_g), melting and crystallization temperature (T_m , T_c) as well as corresponding enthalpy (ΔH_m and ΔH_c) are listed in Table 17. Crystallinity was calculated by considering only the fraction of PBT. Cross-linking modifies the molecular structure of PBT by chemically bonding adjacent polymer chains together. The reduced degree of mobility and chain regularity are detrimental to the formation of crystals for cross-linked compounds, as shown by the decrease of T_c and the crystal content. While this reduction in crystallinity tends to have a negative effect on the rigidity of the polymer structure, cross-linking promotes the reverse effect, leading to a higher T_g for all cross-linked compounds. Indeed, PEA_{0.26} and PEA₂₀ exhibit a 6°C higher T_g than pristine PBT, similarly than the results found for PE_Z in the previous chapter. PEA₂₀ behaves in the same way as PE_ZA₂₀ (Chapter 2), as the presence of AlPi which induces a decrease of T_c and T_m compared to PE_Z. From an industrial point of view, the slight decrease in T_m can be seen as a positive effect as the material can be processed at lower temperatures, thus requiring less energy to shape the material using similar processing techniques compared with pristine PBT.

Table 17 : Thermal characteristics of the materials measured by DSC

Sample	T_g (°C)	T_{m1} (°C)	T_{m2} (°C)	ΔH_m (J/g)	T_c (°C)	ΔH_c (J/g)	χ_c (%)
PBT*	39.5 ± 1.2	215.4 ± 1.2	225 ± 1.8	51.0 ± 0.8	191.4 ± 2.1	51.3 ± 1.8	36 ± 1
PE _Z *	47.1 ± 0.9	217.2 ± 1.3		44.7 ± 1.2	185.4 ± 1.2	46.5 ± 1.0	32 ± 1
PA ₂₀ *	39.7 ± 0.7	213.5 ± 0.7	224.5 ± 1.0	36.8 ± 1.5	190.9 ± 0.7	42.3 ± 1.3	32 ± 1
PEA ₂₀	45.8 ± 1.2	213 ± 1.3		21.1 ± 1.7	172.0 ± 3.4	/	18 ± 1
PEA _{0.26}	45.7 ± 0.5	220.2 ± 0.6		42.8 ± 1.3	174.2 ± 0.7	44.8 ± 0.9	31 ± 1

*Results from Chapter 2

Table 18 displays the results of thermogravimetric analyses performed on the synthesized vitrimers, while Figure 6 presents the corresponding curves.

PEA_{0.26} does not present significantly higher residue yields at high temperatures compared to PBT, a conclusion previously raised from the PE_Z vitrimer from Chapter 2 and in the literature^{61,91}. Also, both T_{onset} and T_{MLR} are roughly similar, implying that the cross-linked network does not delay degradation.

PEA₁₀, PEA₁₅ and PEA₂₀ present higher residue yield than PE_Z due to the presence of AlPi. Also, an increased amount of AlPi has a beneficial effect on residue yield (12.5% for PEA₂₀, 10.5% for PEA₁₅, and 9% for PEA₁₀). These materials exhibit a slightly lower onset temperature (T_{onset}) compared to PEA_{0.26} or PE_Z. The TG curve comparison between PA and PEA with 10%, 15%, and 20% weight ratios reveals that all materials exhibit the same onset temperature (T_{onset}) at $348 \pm 5^\circ\text{C}$. Additionally, the temperature at the maximum rate of mass loss remains consistent at $420 \pm 10^\circ\text{C}$ across all the

materials, regardless of their cross-linked nature. These values are similar to those of pristine PBT, indicating comparable thermal behavior between the different formulations.

These analyses show that no significant difference is observed in the thermal behavior between the vitrimers and thermoplastic equivalents.

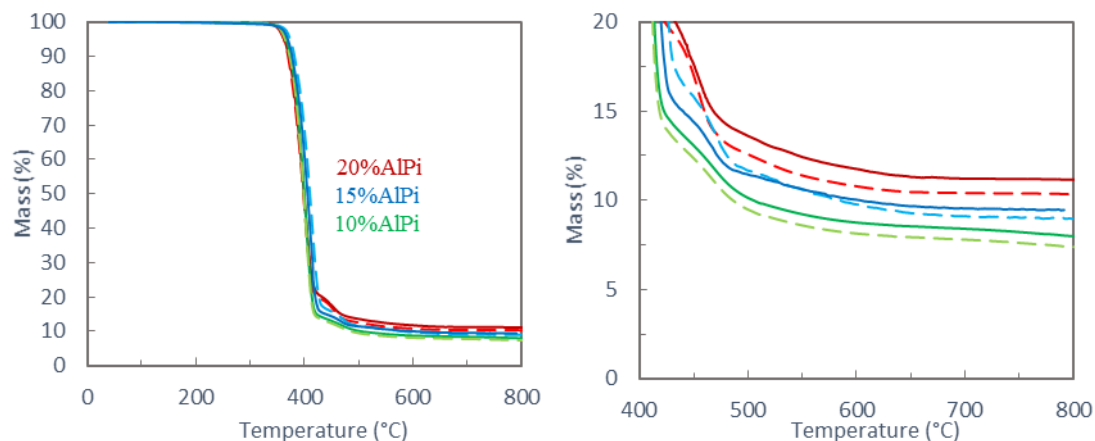


Figure 92 : TG of PEA (full line) and PA (dotted lines) at various AlPi concentrations (20°C/min, N₂ flow). Right: Zoom on the residue

Table 18 : TGA results for PBT and vitrimer formulations

	T _{onset} * (°C)	T _{MLR} ** (°C)	Residue yield at 800°C (wt.-%)
PBT	362 ± 4	418 ± 3	4.2 ± 0.4
PEZ	364 ± 3	415 ± 4	5.5 ± 0.6
PEA _{0.26}	364 ± 3	415 ± 5	5.3 ± 0.5
PA ₁₀	351 ± 4	420 ± 10	8.5 ± 0.5
PA ₁₅	350 ± 5	420 ± 10	10.2 ± 0.6
PA ₂₀	347 ± 5	420 ± 10	11.1 ± 0.5
PEA ₁₀	350 ± 5	420 ± 10	9.2 ± 0.5
PEA ₁₅	348 ± 4	420 ± 10	10.7 ± 0.4
PEA ₂₀	348 ± 5	420 ± 10	12.2 ± 0.5

* T_{onset} : Onset temperature degradation

** T_{MLR} : Temperature at maximum mass loss rate

3.3.3. Rheological behavior

The vitrimer nature of the aforementioned materials was characterized by stress-relaxation experiments between 235 and 265°C, *i.e.* in the molten state. The curves were treated considering the Kohlrausch-Williams-Watts (KWW) model for relaxation. Zero-shear viscosity (G₀) and characteristic stress-relaxation times (τ* and < τ >) are presented in Appendix 2, and were obtained from the fitted curves using Origin software, with a β parameter (defining the stretched exponential) shared between each curve. Both raw curves and fitted relaxation curves are presented in Figure 93.

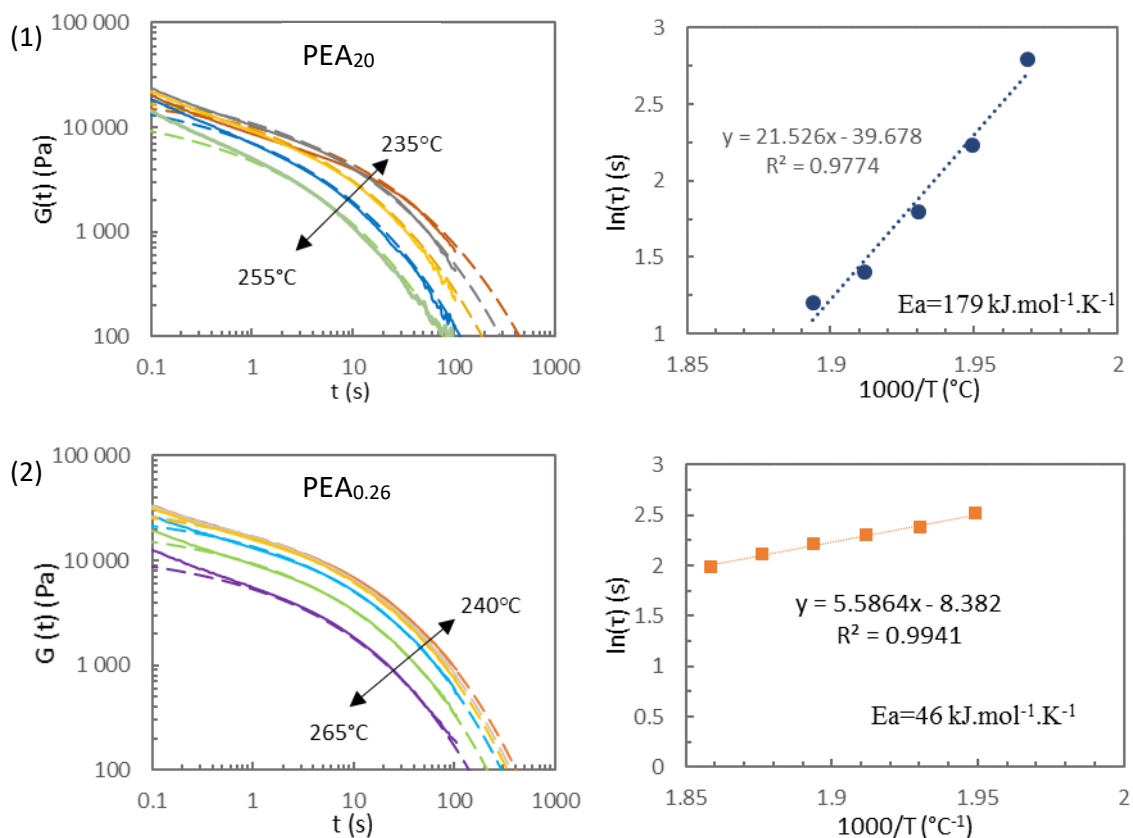


Figure 93 : Raw (full lines) and fitted (dotted lines) stress-relaxation curves for PEA₂₀ (1) and PEA_{0.26} (2). Arrhenius graph (left).

All materials behave like partially dynamic cross-linked materials, similar to the results obtained in the previous chapter, with the relaxation of the network defects occurring at shorter times (below 1 second in most cases). PEA₂₀ exhibits an activation energy of 179 kJ.mol⁻¹ and a relaxation time of 4.1 s at 250°C. Those results are slightly different from the results of PEZ_{A20} in the previous chapter (152 kJ.mol⁻¹ and relaxation time of 2.6 s at 250°C). For fast relaxing materials, it may be complex to precisely determine relaxation times and activation energy as the relaxation of the thermoplastic fraction also occurs in this time frame. However, by strictly looking at relaxation times, the presence of 20 wt.-% AlPi significantly sped up the bond-exchange reactions.

Lower relaxation times are also obtained when AlPi is added in catalytic quantities, with a relaxation time measured at 10 s at 250°C. This result proves the involvement of AlPi as a transesterification catalyst. However, it depicts a surprisingly lower activation energy of 47 J.mol⁻¹ compared to PEA. The difference in activation energies between PEA_{0.26} and PEA₂₀ is unexpected. Usually, the addition of a higher amount of catalysts in a system tends to lower the activation energy barrier needed to form the reactive intermediate²². However, the activation energy values indicate how sensitive a process is to temperature changes, rather than providing information about the absolute kinetics of the process²³¹. If it is reasonable to consider that AlPi

totally solubilizes in the gel part of PEA_{0.26}, the presence of numerous agglomerates in PEA₂₀ may involve complex interactions with the matrix, hence the unexpected differences observed in activation energies.

The rheological behavior of the formulations was also characterized by oscillatory frequency sweep experiments conducted in the molten state. Samples PE_Z, PEA₂₀, PE_ZA₂₀ and thermoplastic equivalents PBT and PA₂₀ were tested in the linear viscoelastic regime (low strain amplitude of 1%). A frequency range of 10² to 10⁻² Hz was applied to the materials at a temperature of 250°C. The results are presented in Figure 94.

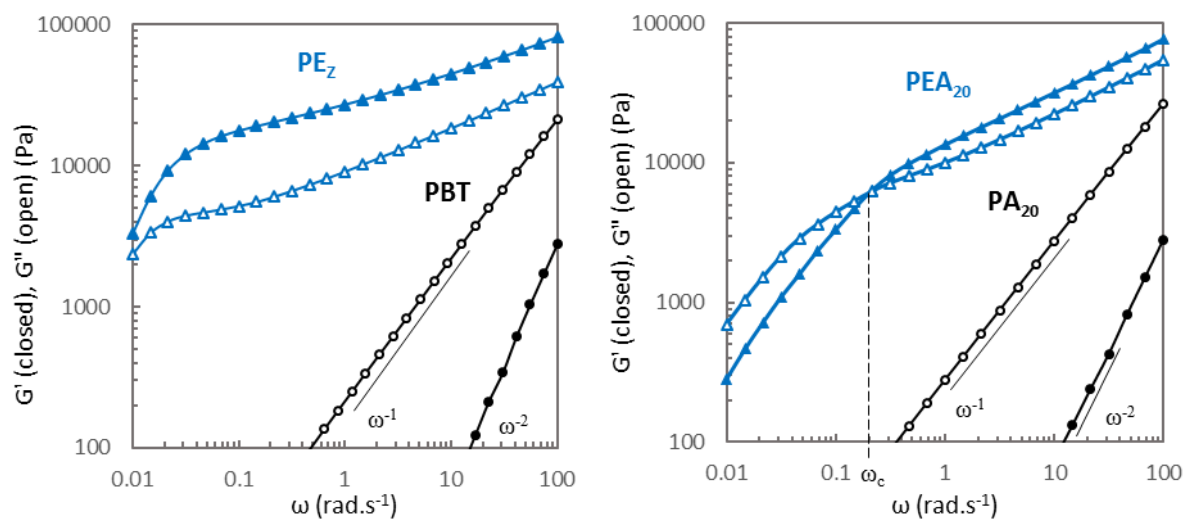


Figure 94 : Angular frequency dependence of storage modulus G' and loss modulus G'' at 250°C for PBT and PE_Z (left), PA₂₀ and PEA₂₀ (right)

At 250°C, both pristine PBT and PA exhibit higher loss moduli ($G'' > G'$) in the entire frequency range, characteristic of a nonentangled polymer. The viscosity of both thermoplastics is in their terminal regime³⁴, where $G'(\omega) \sim \omega^1$ and $G''(\omega) \sim \omega^2$. As expected, the addition of AlPi does not radically change the overall viscosity of the melt, as PA₂₀ has a viscosity of 265 Pa.s⁻¹, compared with 215 Pa.s⁻¹ calculated for PBT.

Classic cross-linked materials, formed by permanent covalent bonds, exhibit a frequency-independent storage modulus (G')⁸⁶. On the other hand, both vitrimer samples exhibit frequency-dependency values for storage moduli G' and loss moduli G'' owed to their covalent adaptable network. PE_Z exhibits higher viscous modulus for the whole frequency range, with an extrapolated crossover value below 10⁻² rad.s⁻¹. This result is in accordance with previous stress-relaxation experiments (Chapter 2), which measured a relaxation time of 145 seconds at 250°C for PE_Z. At higher epoxy loadings and the same temperature range, the PBT vitrimer obtained by Demongeot et al. exhibited a better-defined elastomeric plateau linked with higher relaxation times⁵.

For PEA₂₀ compounds, the storage modulus is higher than the loss modulus at higher frequency ranges. However, despite having the same relative amount of epoxy as PE_Z, PEA₂₀ reaches crossover

point much sooner at $\omega_c = 0.21 \text{ rad.s}^{-1}$ ($\sim 5 \text{ s}$), which is in good agreement with the value of approximately 4.1 s obtained via stress relaxation.

The stress relaxation tests previously conducted are best suited for materials with relaxation times exceeding a minute or even hours. However, due to the short relaxation time of PEA₂₀, this method becomes less accurate in determining its characteristic relaxation time. Therefore, additional tests were conducted on PEA₂₀ at 230 and 240°C (Figure 95) using an isothermal frequency oscillation method. Crossover shifts to higher frequencies with higher temperatures, while high storage modulus is conserved at higher frequencies. The time to reach crossover value could be implemented in an Arrhenius graph^{34,45}, and similar activation energy of 176 kJ.mol⁻¹ was found compared with stress-relaxation experiments (179 kJ.mol⁻¹). Although those results are promising, extra sweep strain tests conducted at other temperatures would be necessary to definitely validate this method.

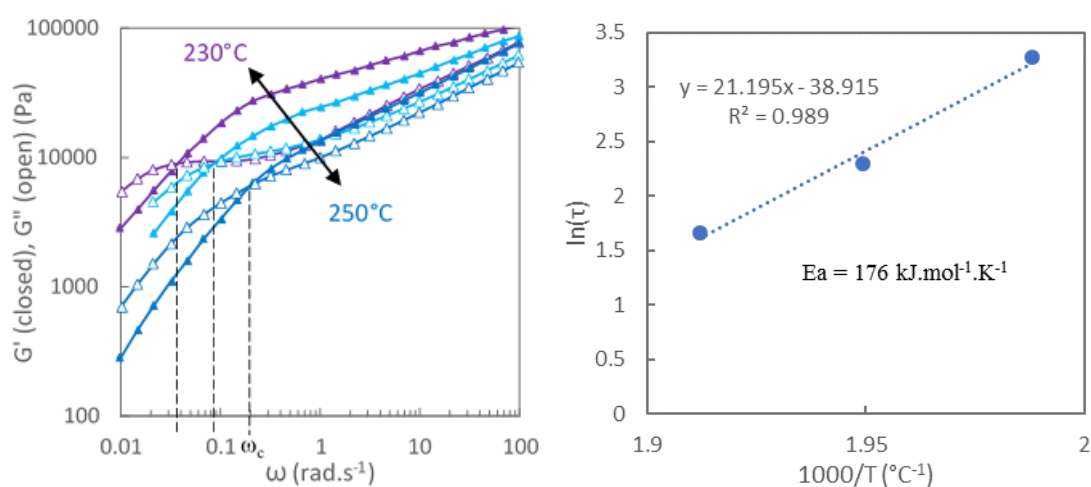


Figure 95 : Left: Angular frequency dependence of storage modulus G' and loss modulus G'' at different temperatures for PEA₂₀, crossover frequency indicated by dotted lines. Right: Characteristic relaxation times for PEA₂₀, obtained from the crossover frequency ν , in function of inverse of temperature.

3.3.4. Impact of the vitrimer network on the FR dispersion and structure

As demonstrated previously, AlPi acts as a catalyst in the bond exchange reaction of the PBT-vitrimer network. It is consequently not an inert additive. SEM and Microprobe analysis have first been performed on cross-sections of the extruded PEA₂₀ and its gel fraction PEA_{20gel} (Figure 96 and Figure 97).

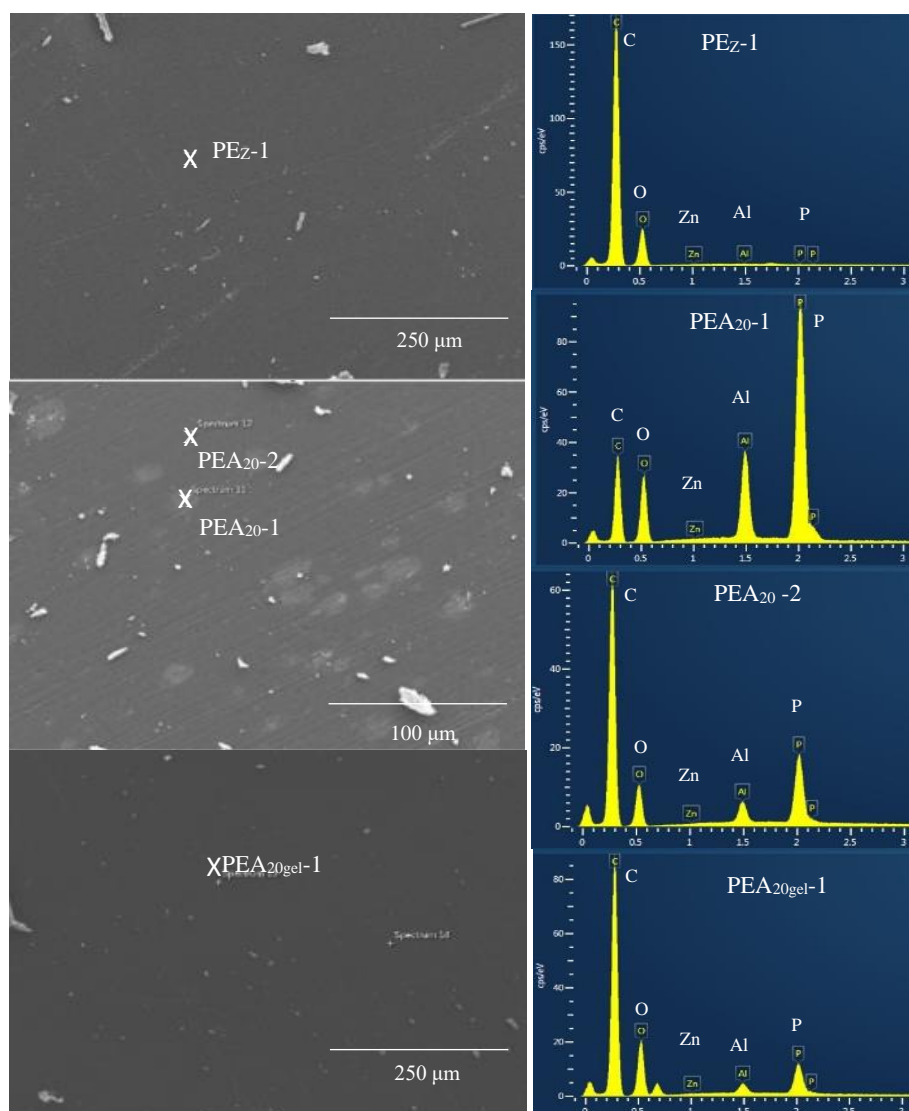


Figure 96 : SEM of PEZ, PEA₂₀, PEA_{20gel} and their respective EDX chemical analysis.

PEZ presents a high carbon and oxygen concentration at its surface, with no presence of catalyst particles. On the one hand, particles containing at the same time P and Al are visible in PEA₂₀, and can be attributed to the presence of FR. Their diameters range from a few μm to up to 20 μm, which is within range of the particle size given by the supplier. On the other hand, chemical analyses were also performed on point PEA₂₀-2 and PEA_{20gel}-1, where no particles were visible. The presence of P and Al is also observed outside of the AlPi agglomerates. It implies that a fraction of aluminum phosphinate is dissolved in the vitrimer matrix. The presence of both Aluminum and Phosphorus in the gel fraction of PEA₂₀ is also confirmed (point PEA_{20gel}-1). EPMA mapping presented in Figure 97 confirmed that P and Al are homogeneously distributed in the sample. This result should be put into perspective with the concentration of Al and P obtained from the elementary analysis (Table 16). Indeed, around 10.4 wt.-% AlPi is still present in the gel fraction in a diffused form.

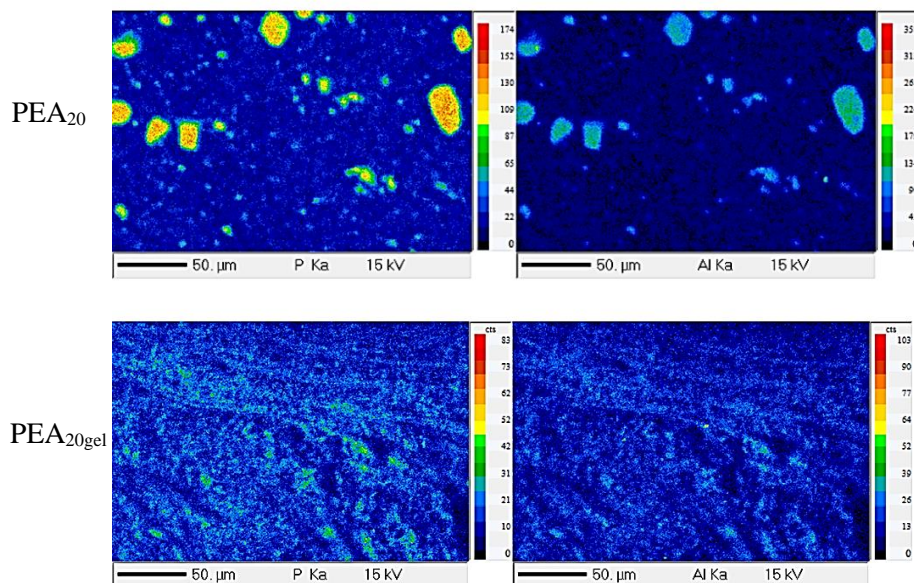


Figure 97 : Phosphorus (left) and Aluminum (right) EDMA mapping of PEA and PEA_{gel}

Those results thus demonstrate that AlPi was partially solubilized in the PBT/epoxy mixture, leading to the homogeneous dispersion of Al and P in the gel fraction of the vitrimer. The presence of AlPi in a solubilized form may play a crucial role in promoting ligand exchange and the formation of intermediates to trigger transesterification. It is also reasonable to assume that AlPi in PEA_{0.26} was only present in a soluble state. The following part will be dedicated to determining to what extent the chemical environment around the solubilized fraction of AlPi may have evolved.

²⁷Al and ³¹P NMR analyses were performed on PEA₂₀ and its respective gel fraction (PEA_{20gel}) to see the modification of the chemical environment around the aluminum and phosphorous atoms. The obtained spectra are presented in Figure 98. On this graph, the results obtained for PE_ZA₂₀ (Chapter 2) were also superimposed. The comparison between the materials prepared with and without the use of Zn-catalyst during the reactive extrusions shows similar environments of P and Al in the formulations. The gel fraction of PEA_{20gel} exhibits the same new peak that appeared for PE_ZA_{20gel}, at around 52-58ppm for ³¹P analyses. It had been attributed to the formation of diethylphosphinic acid. Consequently, a new peak appeared at 47ppm for ²⁷Al analyses which was explained by the ligand exchange of Al³⁺ that interact with the matrix to catalyse transesterification reactions.

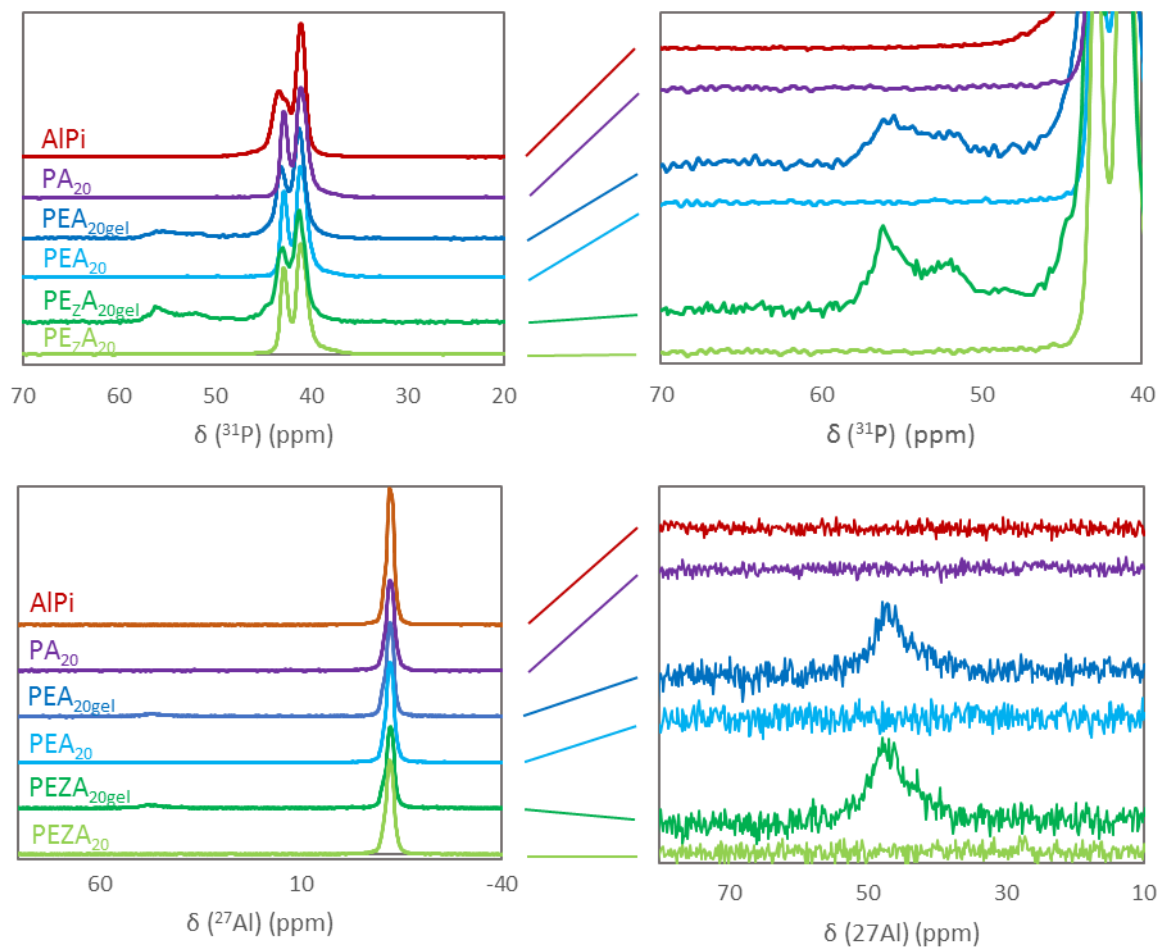


Figure 98 : ^{31}P and ^{27}Al RMN spectrum of AlPi, PA₂₀, PEA₂₀, PEA_{20gel}, PEZA₂₀ and PEZA_{20gel}. Right: zoom on the new peaks

3.4. Evaluation of the performances of the AlPi-based vitrimer

3.4.1. Resistance to creep

PEA₂₀ presents a high activation energy (E_a) compared with PE_Z. This is an advantage to prevent or minimize creep at service temperatures, while still allowing for flow at elevated temperatures without causing decomposition⁴⁴. In the following part, the dimensional stability of both vitrimer samples was analysed. Well-dried PBT, PEA₂₀ and PE_Z samples were injected at 270°C. To ensure adequate filling of the entire mold, a high mold temperature of 120°C was employed, specifically targeting the PE_Z material due to its high viscosity at elevated temperatures. The obtained coin-shaped samples were then placed in an oven at 250°C (molten state) under air atmosphere. Figure 99 shows pictures of the samples after 0min, 3min, 10min and 30min. All materials eventually darken due to oxidation taking place, as no anti-oxidants were added during the extrusion process.

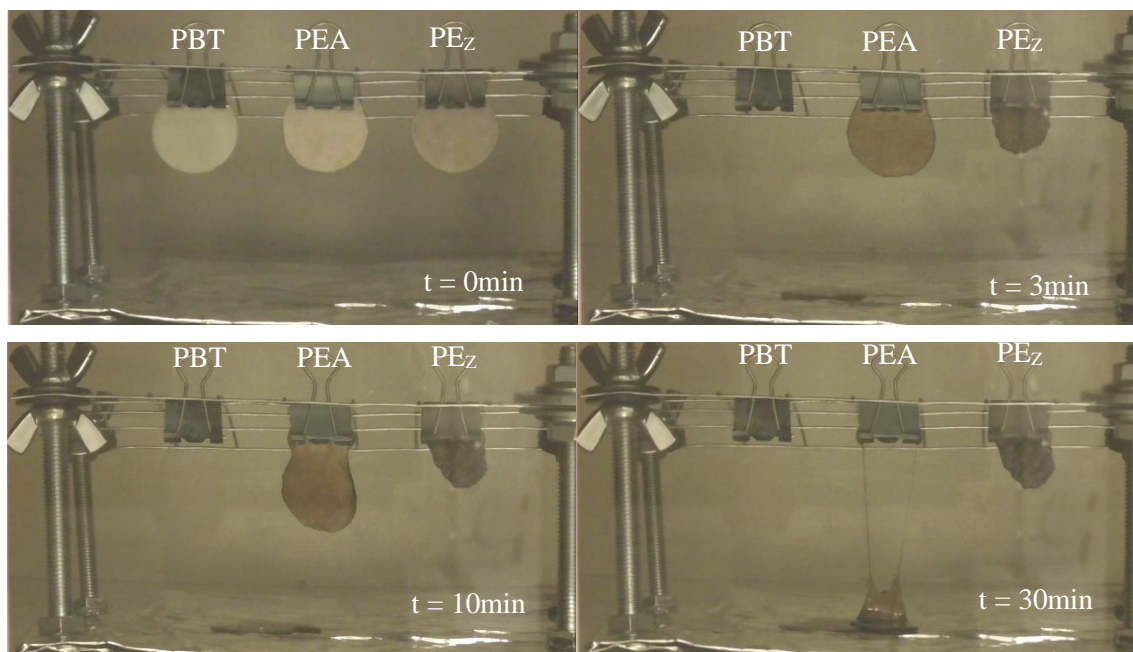


Figure 99 : Picture of injected polymer samples in the oven at 250°C at various times

In less than 3 min, all materials become more or less transparent. This is linked to the melting of the crystals in the PBT vitrimers. In the case of PBT, this melting is accompanied by a total loss of dimensional stability: the low degree of entanglement does not prevent the sliding of the macromolecular chains relative to each other, leading to the sample flowing from the clamp. An approximation of the strain rate of this material can be calculated using the potential energy formula, $\epsilon \sim \rho gh$, with ϵ the gravitational stress applied to the sample, ρ the density of PBT (1.31 g.cm^{-3} at 250°C), g the gravitational acceleration (10 N.kg^{-1}) and h the height of the coin-shaped sample (25mm). All samples undergo a stress of around 300Pa. As the measured melt viscosity of PBT at 250°C is around 215 Pa.s, a shear rate $\dot{\gamma} = \sigma/\eta$ of 1.4 s^{-1} is obtained (with σ the shear stress), leading to a fast-flowing behavior. Since PA₂₀ has the same melt viscosity as PBT, its behavior should be similar.

In under 3 min, PE_Z behaves radically differently. It exhibits a strong shrinking tendency and does not flow under 30 min. This shrinkage phenomenon has already been reported in the work of Dr. Capelot²⁵⁰ for injected Epoxy/Fatty acid vitrimer matrices and would be related to residual stresses in the injected samples. It can be explained as follow. In the case of an injection molded sample, the material undergoes a fast shaping/cooling cycle. Injection cooling times for a thermoplastic PBT are around 5s to decrease temperature from 270°C to 120°C ²⁵¹. However, the viscous flow of the vitrimer network is limited by the kinetics of the chemical reactions. While stress-relaxation experiments showed that thermoplastic PBT blends totally relaxes stress in under a second, PE_Z needs several minutes to relax. During the injection cycle, the vitrimer materials consequently do not have time to fully relax which induced residual stress in the sample, causing the shrinkage.

To check this point, vitrimer materials prepared by reactive extrusion were reshaped into coin-shaped samples. One sample was shaped through injection molding using parameters similar to those

described above, while the other sample underwent compression molding at 250°C under 10 tons pressure for 5 minutes of post-curing (2.5 times the relaxation time). Both samples were placed in an oven at 250°C and pictures were taken at 0 and 30 min (Figure 100). As expected, the sample that underwent a longer post-curing step maintained its dimensional stability over the 30-minute period. In contrast, the injected sample exhibited shrinkage, thus demonstrating the possibility of fully post-curing formed PBT vitrimers. This observation helps to explain why, in the literature, the (re)shaping of vitrimers has primarily been limited to compression molding. To address the issue of shrinkage, Demongeot et al.⁵ and Farge et al.⁹¹ have introduced an alternative method. Instead of preparing crosslinked materials through reactive extrusion, they utilized a rapid extrusion process to create a mixture of the reactants. Subsequently, a post-curing step was performed within a mold to effectively crosslink the matrix into a specific shape. This method offers the advantage of using low-viscosity materials for shaping purposes. Demongeot et al. demonstrated that a PBT vitrimer processed with a post-curing step could maintain its dimensional stability over a 30-minute period at 250°C.

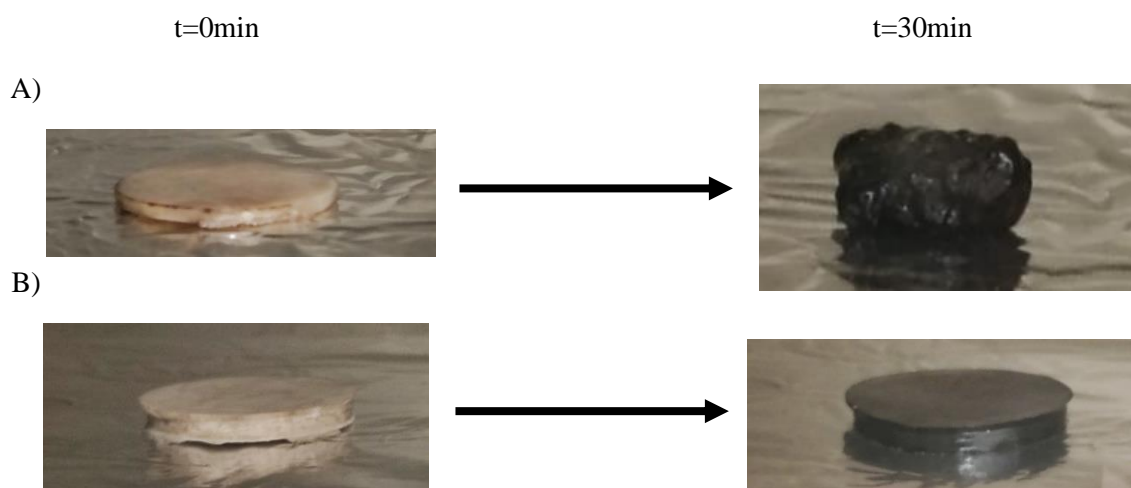


Figure 100 : Picture of fully reacted pristine PBT vitrimer in a oven at 250°C. A) PE_Z sample after an injection-molding step; B) PE_Z sample after a 5 minute post-curing step in a press at 250°C

PEA₂₀ exhibits the most interesting behavior. Indeed, no shrinkage is observed, which indicates that the stress undergone by the material during injection molding was relaxed prior to placing the sample in the oven. This is not surprising considering the relaxation time of PEA₂₀ of around 5 seconds at 250°C, which is a hundred times faster than PE_Z (Chapter 2). PEA₂₀ is able to relax the stress induced by injection molding fast enough, leading to this unique behavior. However, while the material keeps a relative dimensional stability for three minutes at 250°C, it starts to slowly elongate afterward, until eventually flowing from the clamp within 30 min. As relaxation and viscosity are intrinsically linked, fast relaxation also implies a lower viscosity, leading to the earlier flowing of PEA₂₀ compared to PE_Z.

3.4.2. Mechanical characterization

The mechanical behavior of the PE_Z and PEA₂₀ vitrimer, as well as their reference thermoplastic equivalent PBT and PA₂₀, was studied by uniaxial tensile testing at room temperature. All materials were injected after an overnight drying step at 80°C. For filled compounds, the broken samples from the first tensile tests were then grinded into 1mm powder, dried and injected again into tensile bars in order to evaluate the mechanical behavior of recycled samples. All results are presented in Table 19, Figure 101 and Figure 102.

Table 19 : Mechanical Properties of both PE_Z and PEA vitrimer, as well as their thermoplastic equivalents. The presence of the "r" before the sample name indicates that the material was recycled.

Sample name	Young's modulus (MPa)	Tensile strength (MPa)	Elongation at break (%)
PBT	1320 ± 90	48 ± 3	Up to 400
PE _Z	1750 ± 120	60 ± 4	12 ± 2
PA ₂₀	1600 ± 100	38 ± 4	3.8 ± 0.5
rPA ₂₀	1640 ± 70	33 ± 3	2.3 ± 0.3
PEA ₂₀	2150 ± 100	55 ± 5	3.7 ± 0.3
rPEA ₂₀	2110 ± 90	38 ± 10	2.1 ± 0.6
PA _{20/160}	227 ± 9	12 ± 1	27 ± 5
rPA _{20/160}	234 ± 19	11 ± 1	16 ± 3
PEA _{20/160}	339 ± 20	23 ± 2	50 ± 8
rPEA _{20/160}	306 ± 11	14 ± 1	14.0 ± 2

On Figure 101, a necking and ductile behavior, including a cold drawing region, occurs for PBT. This classic semi-crystalline thermoplastic behavior leads to a high elongation at break reaching up to four times its initial length²⁵². On the other hand, PE_Z exhibit a less ductile behavior with a stress at break of around 10% and a homogeneous plastic deformation characterized by a strain hardening step after the yield stress. The Young's modulus E defining the stiffness of a material is about 1.3 GPa for PBT at room temperature. This value is expected for a polymer at a temperature below its T_g. Note that an increase of 30% is measured for PE_Z compared to PBT. These results show the major impact of the cross-linked nature of PE_Z on Young's modulus, even though the crystallinity of PE_Z is lower than that of PBT and on the strain at break which is drastically reduced.

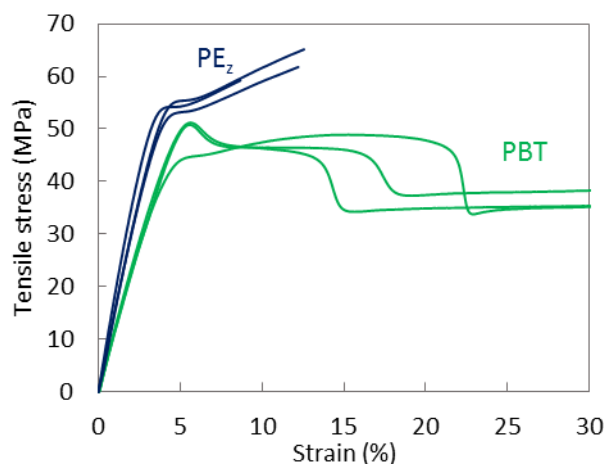


Figure 101 : Left: Stress-strain curve obtained by tensile test at room temperature for PBT and PE_z. Right: Picture of PBT dog-bone sample during uniaxial tensile test, exhibiting a heterogeneous deformation.

When AlPi is added to the systems, the Young's modulus increases by around 20% for PEA₂₀ compared to PE_z, and for PA₂₀ compared to PBT. Note that PEA₂₀ exhibits the highest Young's modulus of all tested samples with a value of 2150 MPa, showing the complementary effect of cross-linking and fillers on overall rigidity. However, both AlPi-filled matrices exhibit brittle-like behavior with low tensile strength and low elongation at break. Note that in the case of both PEA₂₀ and PA₂₀, no neck is visible as rupture occurs too rapidly. In addition to the higher stiffness of AlPi particles compared with pristine thermoplastic or vitrimer matrices, micro-scaled particles have usually bad interfacial adhesion with the matrix promoting the formation of micro cracks leading to a higher brittleness of PA₂₀ and PEA₂₀ compared with PE_z. Upon recycling, no major change occurs: both materials keep their stiffness although a slight decrease of the tensile strength and a strain at break. This phenomenon can be attributed to thermal degradation as revealed by the slightly darker color of the recycled dog-shaped samples.

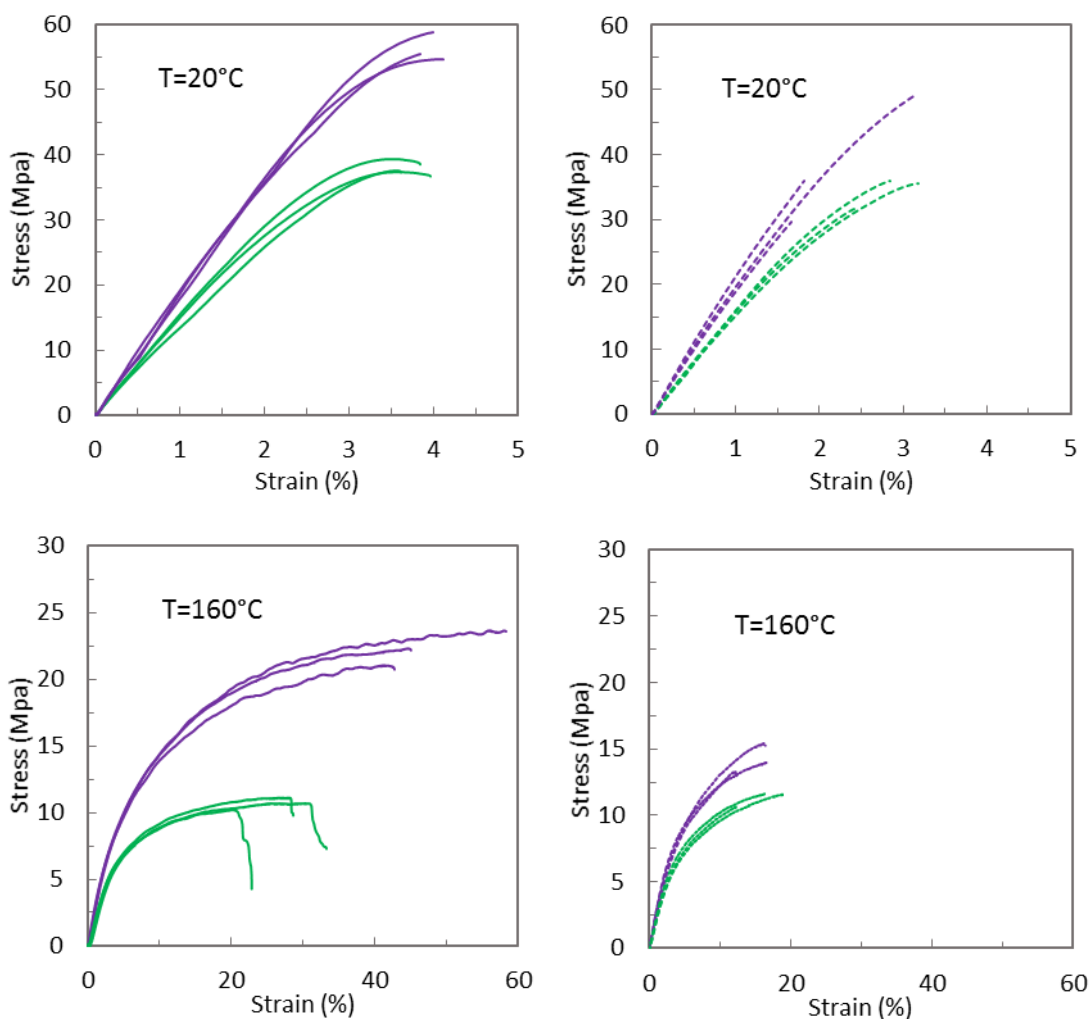


Figure 102 : Stress-strain curves of the AlPi-filled vitrimer at 20 and 160°C. Left: PA₂₀ (green) and PEA₂₀ (purple) samples; Right: recycled PA₂₀ (green) and PEA₂₀ (purple) samples.

The mechanical behavior of AlPi-filled vitrimers has also been investigated at temperature well above T_g , *i.e.* at 160°C. This temperature has been selected because it is below the melt temperature of PBT (210-225°C). As expected, in comparison with the previous values measured at room temperature, the Young's Modulus and the tensile strength significantly decrease at high temperature whereas an improvement of elongation at break is observed. However, we obtain the same classification as that obtained at room temperature: $E_{PA_{20}} < E_{PEA_{20}}$ and a significantly higher tensile strength for the vitrimer sample is observed. Elongation at break is also improved for PEA₂₀ (50%) compared with PA₂₀ (27%). Once recycled, a decrease of the stress level and the strain at break is observed attributed to the thermal degradation occurring during the reprocessing. Also, PEA₂₀ exhibited uniform strain distribution throughout the entire specimen and was able to undergo plastic deformation without necking (Figure 103-left). The same phenomenon was reported by Farge et al. for pristine PBT vitrimer^{91,92}. They observed a drawing effect associated with uniform deformation. On the other hand, PA₂₀ breaks immediately as soon as necking occurs (Figure 103-right). Thus, at 160°C, PEA₂₀ exhibits both better elongation at

break and dimensional stability than its thermoplastic counterpart, thanks to the strain-hardening effect resulting from the cross-linking of the vitrimer network.

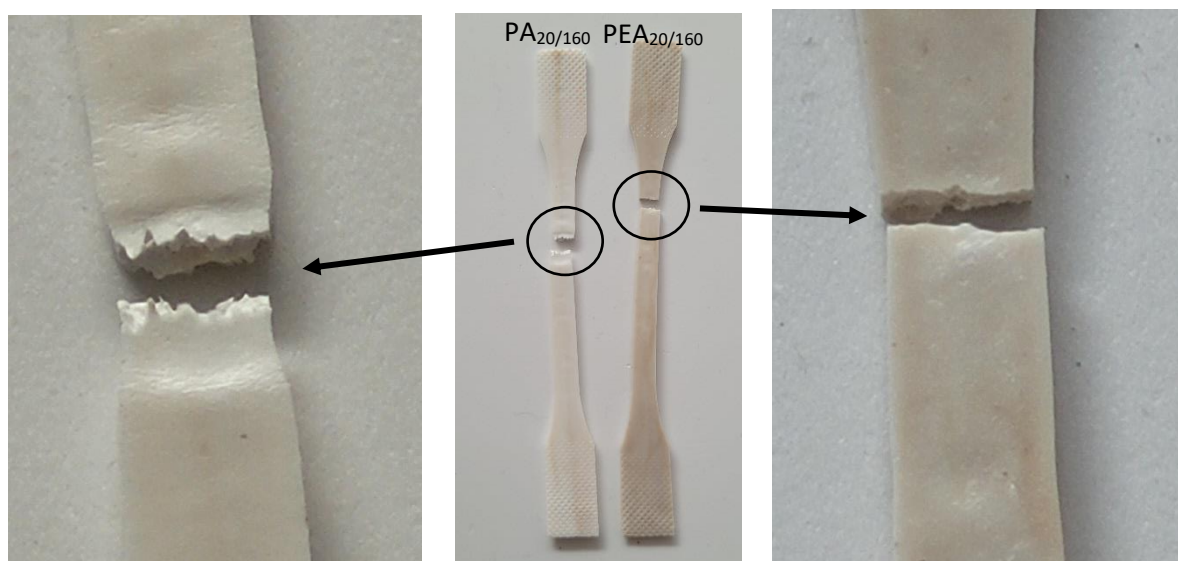


Figure 103 : Pictures of dog-bone samples after tensile test at 160°C. A beginning of drawing with strong strain localization (necking) is visible for compound PA (left), while no strain localization appears for PEA_{20/160}.

3.4.3. Flame-retardancy of AlPi-filled vitrimer

Previously in this chapter, we showed the good performance of AlPi as a transesterification catalyst and synthesized a material presenting a fast relaxation. As referred to the bibliographic part of this thesis, PBT is usually used for E&E applications. This field requires fire performances that are mainly evaluated using UL-94 vertical plastic flammability standards. UL-94 test, as a classification test, gives information on the flaming time of a material subjected to an ignition source and whether the drops can ignite a cotton placed under the tested sample. In this test, V-1 and V-0 ratings (low flaming time and no burning drops) are required to meet E&E legislation.

However, this test is a pass or fail test that does not give valuable and quantitative pieces of information to understand the reaction to fire behavior of the materials. To get more inside on this, an instrumentation of the UL94 test can be set up. Dupretz et al. implanted thermocouples in the bar-shaped polymer samples to measure the temperature gradient inside PA-6 and PA-6/GF formulations during a UL-94 test²⁵³. Hu et al. complemented this method by coupling thermocouples and filtered IR camera to measure the temperature of dripping parts of PBS and PBS/DOPO materials²⁵⁴.

In this work, the UL94 test was instrumented with an IR camera and a balance placed under the cotton. The maximum temperature during the burning was measured on the bar sample

and on the drops which could eventually lead to the inflammation of the cotton. All results are presented in Table 20.

Table 20 : UL-94 results for PBT and PBT-vitrimer as well as AlPi-filled vitrimer with various loading ratios and thermoplastic equivalents

Sample	Rating	t ₁ (s)	t ₂ (s)	T _{max} surface (°C)	Samples dripping	Drops		Burning Cotton
						Number	T _{max} (°C)	
PBT	NR ¹	Burn ²	/	460 ±15	5 / 5	>50	500 ±100	Yes
PE _Z	NR ¹	5 ± 2	Burn ²	460 ±15	5 / 5	>50	500 ±50	Yes
PA ₂₀	V0	0	1 ± 1	520 ±10	5 / 5	3 ± 2	320 ±25	No
PEA ₂₀	V0	0	1	520 ±10	1 / 5	1	335 ±20	No
PA ₁₅	V0	0	1	515 ±1	5 / 5	3 ± 1	370 ±20	No
PEA ₁₅	V0	0	1	515 ±10	3 / 5	1 ± 1	360 ±25	No
PA ₁₀	V2	0	2 ± 2	495 ±10	5 / 5	6 ± 2	440 ±30	Yes
PEA ₁₀	V2	0	2 ± 1	495 ±10	5 / 5	3 ± 1	420 ±15	Yes

¹Not rated

²Burning to the clamp

Both references without FR, PBT and PE_Z, are not rated in the test. PBT burns from the first application of the flame and does stop whereas the PE_Z extinguishes rapidly after the first inflammation. However, it burns to the clamp after the second application of the burner. They extensively burn up to the clamp with intense flaming and dripping. Figure 104 shows the temperature evolution versus time on the samples during the experiments. It increases rapidly and reaches 460°C, above the degradation temperature of PBT. The temperature of the numerous drips was not shown for clarity reasons. Figure 105 shows pictures PBT, PE_Z, PA₂₀ and PEA₂₀ samples after the tests. For PBT and PE_Z, the burning was stopped by immersion in water of the sample before the end of the test to have samples left for visual observation. PBT bottom sample exhibit a triangle shape, characteristic of a high-flowing material. PE_Z, on the other hand, seems to retract upon burning. This result is consistent with the shrinking behavior previously observed when placed in an oven at 250°C, since the material relaxes the stress accumulated during the injection process. This shrinking behavior, however, does not prevent the material from intensely burning, as both materials exhibit similar time to totally burn to the clamp (110s for PE_Z vs 100s for PBT).

At 10% loading, both PA₁₀ and PEA₁₀ have a V-2 rating. Very short flaming times are recorded on both burner applications but dripping systematically occurs for all the tested samples. During the first flame exposure, dripping occurs at the end of the test for PA₁₀, while PEA₁₀ does not exhibit dripping behavior. However, during the second flame application, both PA₁₀ and PEA₁₀ show dripping, which ultimately leads to the ignition of the cotton, as visually observed in Figure 18. According to the literature, Gallo et al. obtained a better V-1 rating for a PBT-10wt.-%AlPi²¹⁶. We attribute this different result to the use of another grade of AlPi

(OP1230 compared with OP1240 in those papers), as well as a possible lower amount of AlPi effectively present in our materials linked with processing conditions. Indeed, Brehme et al. obtained a V-2 rating with 6.3wt.-% AlPi^{196,245}. Also, both materials exhibit similar maximum temperatures at 495°C. The maximum dripping temperature exceeds 420°C, which is in the same range as the auto ignition temperature of cotton (407-439°C)²⁵⁵. This similarity in temperature could potentially explain the observed behavior, even if the droplet may no longer be ignited upon reaching the cotton.

At 15 and 20 wt.-% loadings, all samples are rated V-0 and no inflamed dripping occurs. Both vitrimer materials stand out compared to thermoplastics thanks to their reduced dripping (only 3 on 5 samples drip for PEA₁₅ and 1 on 5 for PEA₂₀ compared to 5 on 5 for PA₁₅ and PA₂₀). This difference can be attributed to the variation in the melt viscosity of the samples. Indeed, the overall melt viscosity of PA₂₀ is similar to PBT (265 Pa.s for PA₂₀ vs 215 Pa.s for PBT at 250°C) whereas for PEA₂₀, higher melt viscosity is obtained thanks to crosslinking. This higher melt viscosity is beneficial for keeping a relative dimensional stability of the material upon burning, leading to a reduced number of samples dripping. Besides, shrinkage is observed for vitrimer whereas the thermoplastics elongate significantly (Figure 105). This non-dripping behavior was also found for PBT/GF/AlPi samples¹⁵⁷, as glass fiber promotes an anti-dripping effect¹⁹². In addition, the drops' temperature decreases with increasing loading of AlPi (430°C for 10wt.-%, 360°C for 15wt.-%, and 340°C for 20 wt.-%). As the decomposition temperature of PBT is above 360°C, a value reached only for PA₁₀ and PEA₁₀, which may explain the presence of inflamed drops soon extinguished before touching the cotton. As reviewed in the first part of this manuscript, aluminum phosphinate acts mainly in the gas phase. Its thermal decomposition generates radicals that will interact with the flame radicals and quench them. At 10 wt.-% of AlPi not enough radicals are produced to effectively decrease the temperature of the drops contrary to 15 and 20 wt.-%. For both thermoplastics and vitrimer loaded with more than 10wt.-% of FR, AlPi effectively prevent the formation of flaming drops, as the maximum dripping temperature was measured at around 330°C, far below the decomposition temperature of PBT.

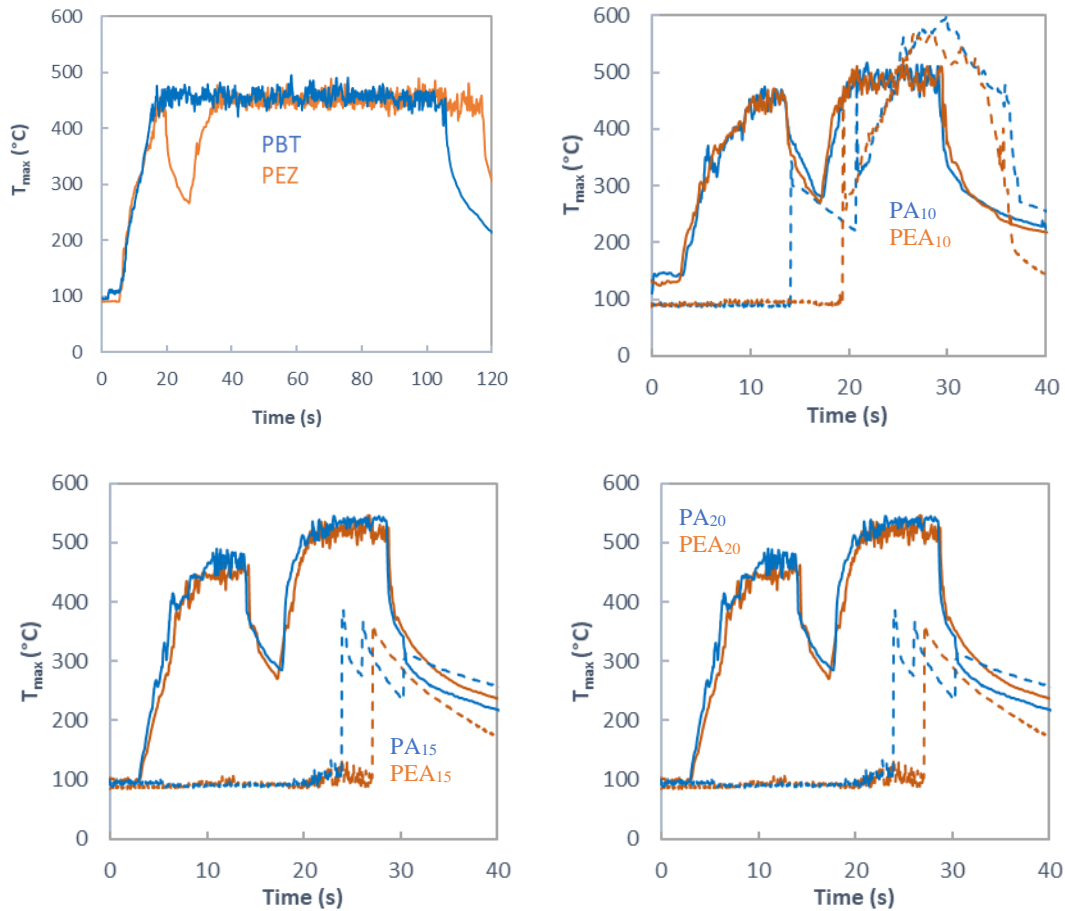


Figure 104 : Thermal evolution recorded using an IR camera of the test bar (full line) and the drops (dotted lines) for PA10, PEA10, PEA15, PA15, PA20 and PEA 20



Figure 105 : UL94 samples of PBT and PEZ (combustion stopped to observe the samples) and before and after test for PA₂₀ and PEA₂₀.

Figure 106 presents the mass loss of the samples after the fire test. It highlights that the vitrimer materials experience lower mass loss compared to the thermoplastics at all loadings. This is in agreement with the difference observed in the dripping behavior of the materials. Thermoplastics with lower melt viscosity tend to exhibit greater dripping, resulting in higher mass loss during the fire test. The mass loss is significantly reduced when comparing PA₁₀ and PEA₁₀, with a difference of 63%.

Similarly, there is a 58% reduction in mass loss between PA₁₅ and PEA₁₅, and a 48% reduction between PA₂₀ and PEA₂₀. These findings indicate that the greater the dripping tendency of a formulation, the larger the difference between the thermoplastic and vitrimer in terms of mass loss during the fire test.

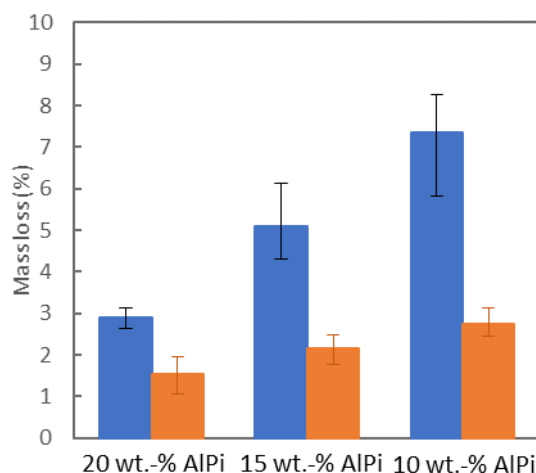


Figure 106 : Mass loss during UL-94 tests for PA (blue) and PEA (orange) at different AlPi loadings

3.4.4. Behavior upon ageing

To assess the suitability of a flame retarded vitrimer system compared to thermoplastics for long terms applications, both materials were aged in the same conditions and then analysed. Two ageing conditions were chosen as explained in section 3.2.3 and applied to PA₂₀ and PEA₂₀ : a thermal ageing (7d70°C) and a immersion scenario (30d50°Cwater). UL-94 results of those experiments are presented in Table 21 and thermal evolution in Figure 107.

Table 21 : UL-94 results for PEA₂₀ and PA₂₀ after ageing

Sample	Rating	t1/t2 (s)	T _{max} surface (°C)	Sample dripping	Drops		Burning cutton
					Number	T _{max} (°C)	
PA ₂₀	V0	0 / 1 ± 1	520 ±10	5 / 5	1 ± 1	320 ±25	No
PA ₂₀ 7d70°C	V0	0 / <1	485 ±15	5 / 5	3 ± 1	340 ±40	No
PA ₂₀ 30d50°C water	V0	0 / <1	505 ±15	5 / 5	6 ± 2	350 ±40	No
PEA ₂₀	V0	0 / 1	520 ±10	1 / 5	1	335 ±20	No
PEA ₂₀ 7d70°C	V0	0 / <1	490 ±20	0 / 5	0	*	No
PEA ₂₀ 30d50°Cwater	V0	0 / 1	505 ±10	0 / 5	0	*	No

*No dripping

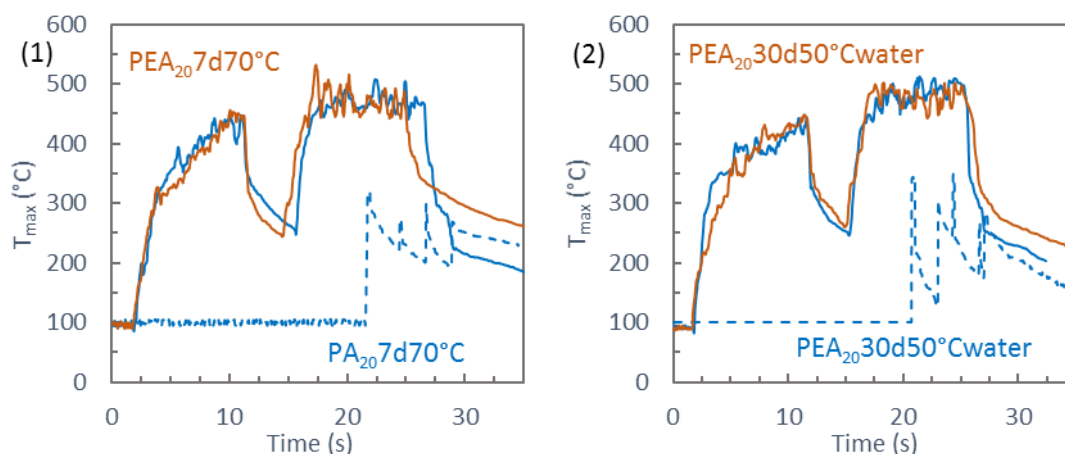


Figure 107 : Thermal plot of the test bar (full line) and the drips (dotted lines) for (1) PA_{7d70°C} and PEA_{7d70°C}, (2) PEA_{30d50°Cwater} and PA_{30d50°Cwater}, recorded by the FTIR camera

Upon conditioning at 7d70°C, the reference material PA₂₀ achieves a V-0 classification despite the sample dripping. This result is different from the V-1 classification obtained by Dr Jeremy Louisy²⁵⁶ during his PhD for a PBT/25%GF/20%AlPi, but a relatively high combustion time (>10 seconds) was observed in his case. The addition of glass fiber is usually an important factor to prevent dripping, however because of their high thermal conductivity the fibers are prone to promote longer burning²⁵³. In the case of PEA, V-0 rating is also achieved but no dripping occurs, confirming the beneficial effect of the higher viscosity of the material toward dripping behavior. After immersion scenario, both materials obtain a V-0 classification. However, the dripping behavior of PA₂₀ also increases, reaching an average of 6 drips per sample, while still no dripping occurs for PEA₂₀. Once again, both thermoplastic and vitrimer materials exhibit similar thermal evolution upon ignition (Figure 107), and dripping temperature for PA₂₀ below the decomposition temperature of PBT (<360°C).

Following the flaming test, the average mass loss for each ageing scenario was measured. Figure 108 presents the total mass loss, the mass loss through dripping and the mass loss in the gas phase, obtained as the difference between the two former results. It appears that dripping is the sole factor leading to the global mass loss, as mass loss measured in the gas phase remains stable for all ageing conditions and materials (2 wt.-%). The thermoplastic material exhibits a great sensibility over ageing, as mass loss through dripping increased from 1% to 5% for 7d70°C ageing, and up to 10% for immersion scenario. On the other hand, PEA₂₀ does not drip whatever the ageing condition. The next part will aim to explain the origin of these observed differences in ageing.

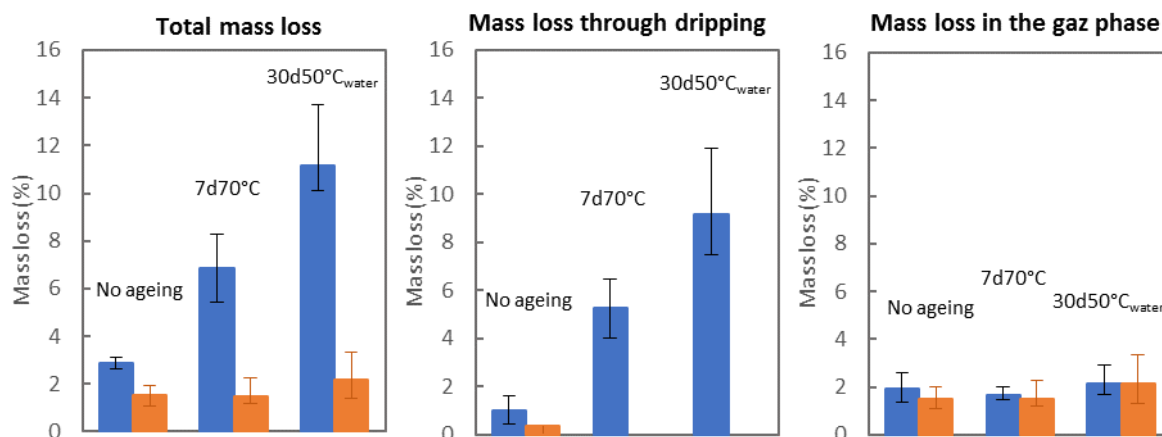


Figure 108 : Mass loss for PA (blue) and PEA (orange) for each ageing scenarios

The main effect of thermal aging on flame-retardants is the potential migration and subsequent exudation of low-molecular-weight additives²⁵⁷. In the presence of water, flame-retardants can also undergo degradation²⁵⁸. To investigate these effects, Electron Probe Micro Analysis (EPMA) was performed at the edge of the vitrimer and thermoplastic counterparts under two aging conditions (Figure 109). The EPMA results indicate that the aluminum phosphate (AlPi) particles appear smaller and more sparsely distributed for the immersion scenario in both materials, as well as for the thermal aging of PEA₂₀7j70°C. This suggests that a portion of the AlPi may have migrated during thermal aging or been solubilized during immersion scenario. Elementary analysis was conducted on the aging water to confirm these assumptions. Phosphorus concentrations of 0.33 mg/L for PA₂₀30d50°C_{water} and 0.36 mg/L for PEA₂₀30d50°C_{water} were obtained. When compared with the total mass of AlPi contained in five aged UL-94 samples (3.5g AlPi with %P=24), it is apparent that only 0.5 wt.-% of AlPi has migrated into the water in both cases. This result can be attributed to the properties of aluminum diethylphosphinate, a non-hygroscopic powder insoluble in water¹³⁵, and the low water uptake of PBT (0.5% in the saturated state²⁵⁹), which does not promote easy solubilization.

Thus, the findings from the EPMA imagery contradict the results obtained from the elementary analysis. The variations observed in the EPMA images may be linked to processing conditions and inadequate homogenization of AlPi within the material.

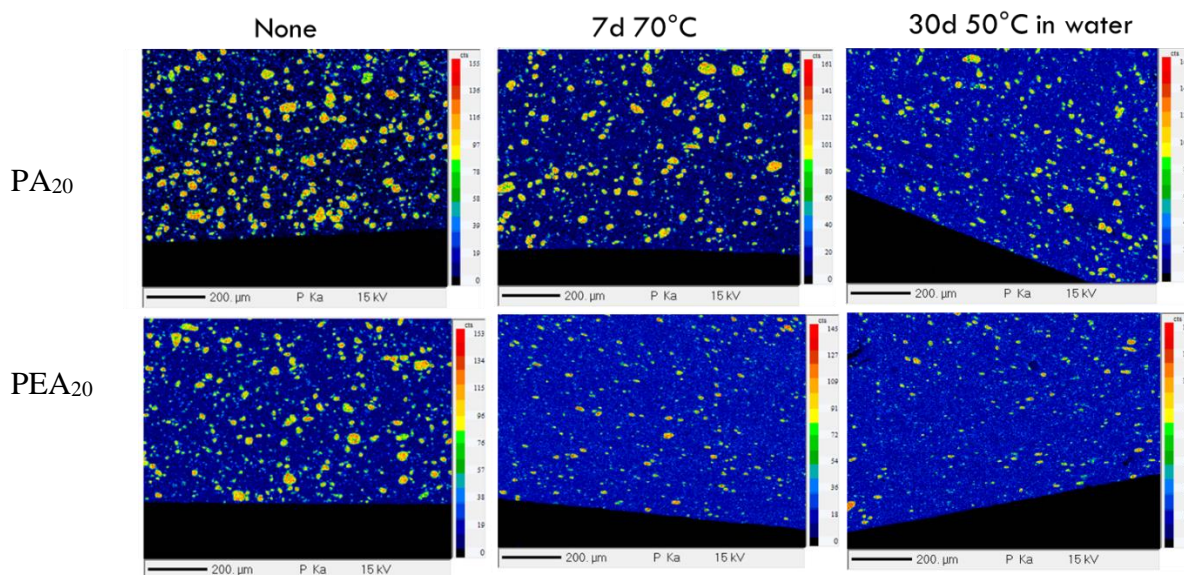


Figure 109 : Phosphorus EPMA mapping of the samples edge for PA₂₀ and PEA₂₀ after ageing experiments. Smaller particles of AlPi are observed for the vitrimer compounds as a fraction of AlPi was dissolved in the matrix during cross-linking.

Gel ratio was measured for the aged samples (Table 22). A significant reduction of the insoluble fraction was measured, especially in the case of immersion scenario. For instance, the raw gel ratio of PEA₂₀7d70°C decreases from 62% to 38%, and it drops even further to 14% for PEA₂₀30d50°Cwater. These low gel ratios may suggest a reduction in the degree of crosslinking.

Table 22 : Gross gel amount measured before and after ageing

Sample	Gross gel ratio (wt.-%)
PEA ₂₀	62 ± 4
PEA ₂₀ 7d70°C	38 ± 3
PEA ₂₀ 30d50°Cwater	14 ± 3

Despite the lower gel ratios, it is interesting to note that both aged vitrimer samples do not exhibit a flow behavior similar to their thermoplastic counterpart (Figure 110). Instead, they display a shrinking behavior similar to PEA₂₀ (Figure 105), even though PEA₂₀ has a significantly higher gel fraction.

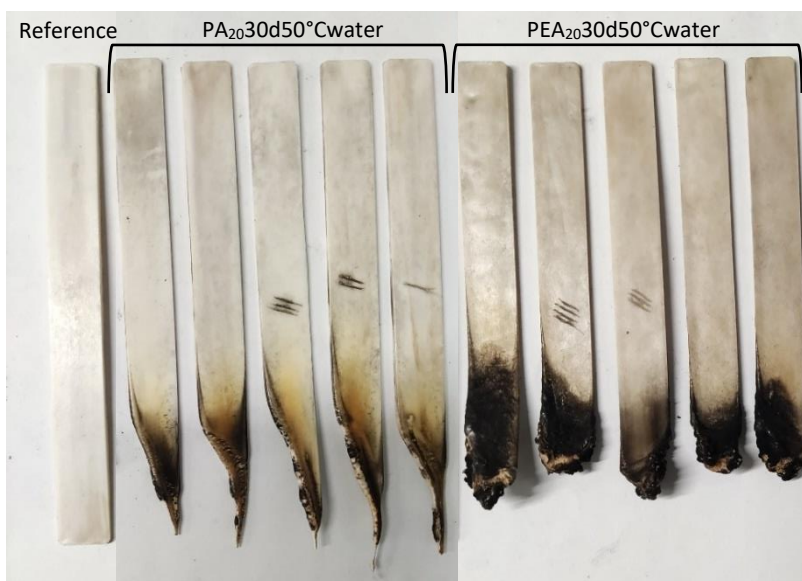


Figure 110 : Aspect of the samples aged in water after burning test. Similar results were obtained from the thermal aged samples.

The next section will focus on investigating why the aging conditions have resulted in a considerable reduction of the insoluble fraction in these materials. It is reasonable to assume that aluminum diethylphosphinate (AlPi) did not significantly degrade or undergo changes under both aging conditions due to its high thermal stability and non-hygroscopic nature. However, both thermal oxidation^{213,260–262} and hydrolysis^{263–266} can promote scissions or bond cleavage in PBT. Besides, breakage can also occur on the epoxies composing the crosslinking nodes (ester bonds). Those two possible consequences of ageing are illustrated in Figure 111.

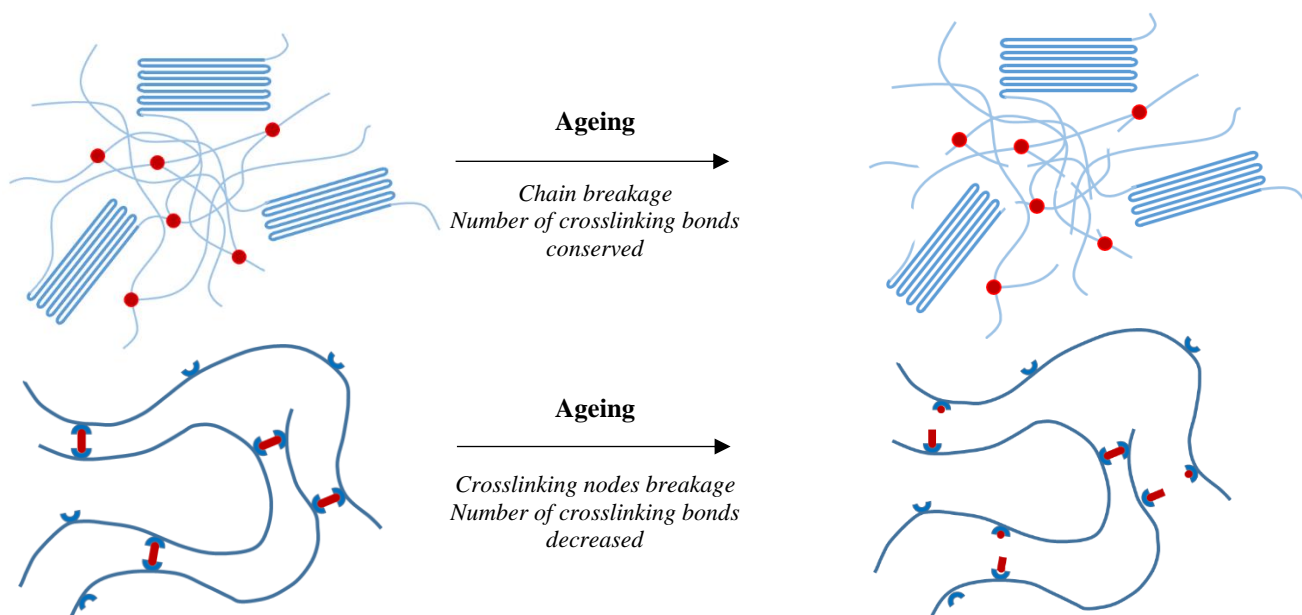


Figure 111 : Illustration of the two possible consequences of ageing on a PBT vitrimer. AlPi particles were not shown for clarity.

Water ageing is well known to promote the formation of hydrophilic carboxyl group formed due to chain breakage²⁶⁴⁻²⁶⁶. For example, when immersed in water for 30 days at a temperature 7°C above T_g , Bastioli and al. measured a significant drop of 30% of the molar mass of their PBT²⁶⁴. Literature report that thermal ageing can also promote chain length reduction through the production of unsaturated oligomers²⁶¹, however most papers reported some ageing tests conducted at higher temperatures (>140°C)^{213,260-262} than the ageing experiments we did in the present study. For epoxy resins, ageing studies conducted on epoxy-anhydride systems, also possessing numerous ester functions, show that significant degradation occurs at higher temperatures ($T > 70^\circ\text{C}$)²⁶⁷ and usually involves salty water²⁶⁸.

Based on this information, it is not possible to draw clear conclusions regarding the preferred mode of action of degradation, whether it involves chain scission or bond scission. To further understand the effects of ageing on the vitrimer, DSC experiments have been performed to evaluate the impact on the thermal properties of the material.

The first heating cycle of PEA₂₀, PA₂₀ and aged samples is reported in Figure 112 to see if any structural change occurred during thermal ageing and immersion scenario. T_g do not significantly evolves between aged and unaged samples. A supplementary melting endotherm, T_1 ($\Delta H_m \sim 1.3 \text{ J.g}^{-1}$) appears for all aged samples at temperature around 90-100°C, *i.e* above the ageing temperature. This result is rather common and has already been reported by Louisy for PBT/GF/AlPi samples aged after 7d at 70°C²⁵⁶, and Bastioli for PBT samples aged in water at 86°C²⁶⁴. This phenomenon corresponds to the melting of crystals produced during the ageing steps²⁶⁴. Moreover, one can observe an endothermic peak only for PA₂₀ at 200-210°C for both ageing conditions (T_2). The origins of this phenomenon remains unexplained and further experiments such as in-situ X-ray diffraction should be useful to clarify this event.

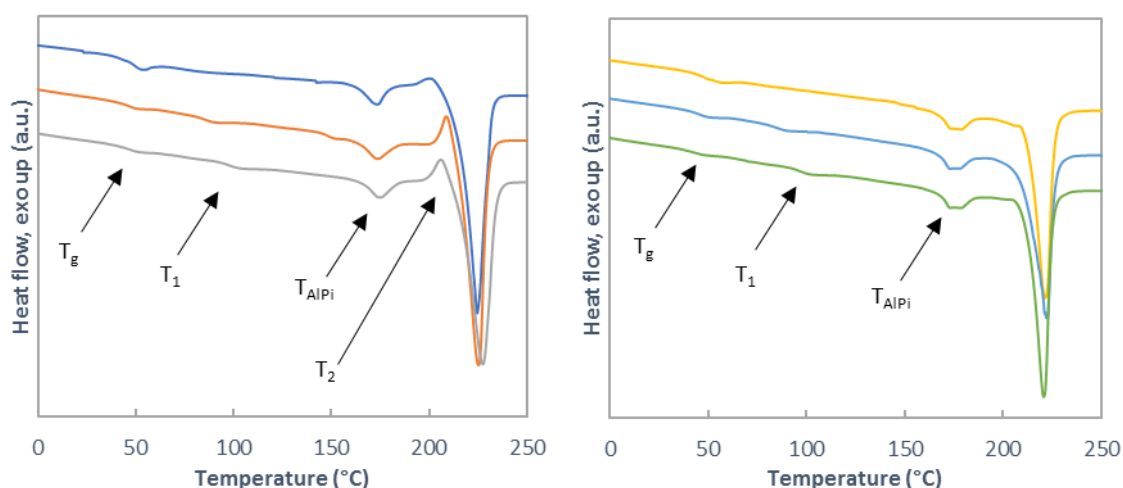


Figure 112 : DSC thermograms of the 1st heating cycle for pristine samples (upper curve), 7d70°C conditioning (middle curve) and 30d50°C water ageing (lower curve) of PA₂₀ (left) and PEA₂₀ (right) compounds. With T_g : glass transition temperature ; T_1 : Melting of crystals produced during the annealing/ageing tests ; T_{AlPi} : reversible crystal transition of AlPi; T_2 : unidentified exothermic peak

In the case of PA₂₀, the second heating cycle shows a slight decrease of T_g, going from 39°C (PA₂₀ and PA₂₀7d70°C) to 37°C (PA₂₀30d50°Cwater). However, such differences are within the measurement uncertainty range ($\pm 1^\circ\text{C}$). For the cross-linked compounds, T_g decreases from 46°C for PEA₂₀ to 44°C for PEA₂₀7d70°C and further to 41°C for PEA₂₀30d50°Cwater. The significant decrease in T_g for water aged samples can be attributed to both chain breakage and de-crosslinking processes.

During ageing, crystallites are usually considered as impermeable domains²⁶⁴, thus during immersion scenario, no diffusion of hydrolyzed molecules are to be expected in the crystalline region, so chain scission is expected to be exclusively located in the amorphous region of the polymer. For the vitrimers, this amorphous region is also where the dynamic crosslinks are segregated²⁶⁹. Thus, by applying fusion-crystallization cycles, the crosslinks are expected to reshuffle, leading to a randomized distribution of the cross-linking bonds. This homogenization of cross-linking bonds may help to better understand the impact of ageing on T_m, T_c and χ_c . To do so, a sequential heating/cooling protocol (Figure 113) was implemented for both all materials. The results are reported in Table 23. The thermograms of the heating and cooling cycles of the vitrimers are presented in Figure 114, as well as an overview of the melting and crystallization temperatures (T_m, T_c) measured as the maximum peak value, and the crystallinity of the vitrimer compounds.

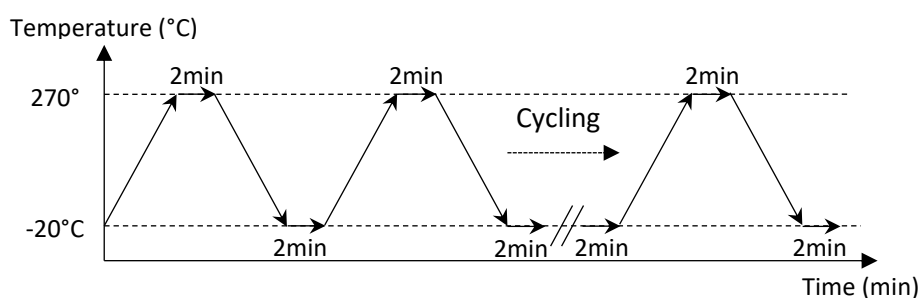


Figure 113 : DSC temperature protocol to study the effective of multiple heating/cooling ramp on the aged PA₂₀ and PEA₂₀ samples. Carried out at 20°C.min⁻¹ under N₂ flow.

Table 23 : Thermal characteristic of the samples on their 10th heating-cooling cycle. All values for the thermoplastic samples did not significantly evolved between the 2nd and the 10th heating cycle.

Sample	T _g (°C)	T _{m1} (°C)	T _{m2} (°C)	ΔH _m (°C)	T _c (°C)	ΔH _c (°C)	χ _c
PA ₂₀	39 ±1	212.2 ±0.8	224.3 ±0.6	38.6 ±1.7	188.8 ±0.3	42.2 ±0.9	34 ±2
PA ₂₀ 7d70°C	39 ±1	213.6 ±0.6	223.9 ±0.8	37.7 ±1.2	188.3 ±0.3	40.8 ±1.5	34 ±2
PA ₂₀ 30d50°Cwater	37 ±1	213.3 ±0.3	224.2 ±0.4	37.5 ±0.7	186.7 ±0.3	41.6 ±1.2	33 ±1
PEA ₂₀	46 ±1	210.5 ±0.8	/	21.4 ±0.9	169.5 ±0.3	31.4 ±0.7	19 ±1
PEA ₂₀ 7d70°C	44 ±1	211.9 ±0.6	/	21.8 ±0.8	170.7 ±0.3	31.9 ±0.9	19 ±1
PEA ₂₀ 30d50°Cwater	41 ±1	214.6 ±0.7	/	25.8 ±0.7	178.6 ±0.3	34.8 ±0.6	23 ±1

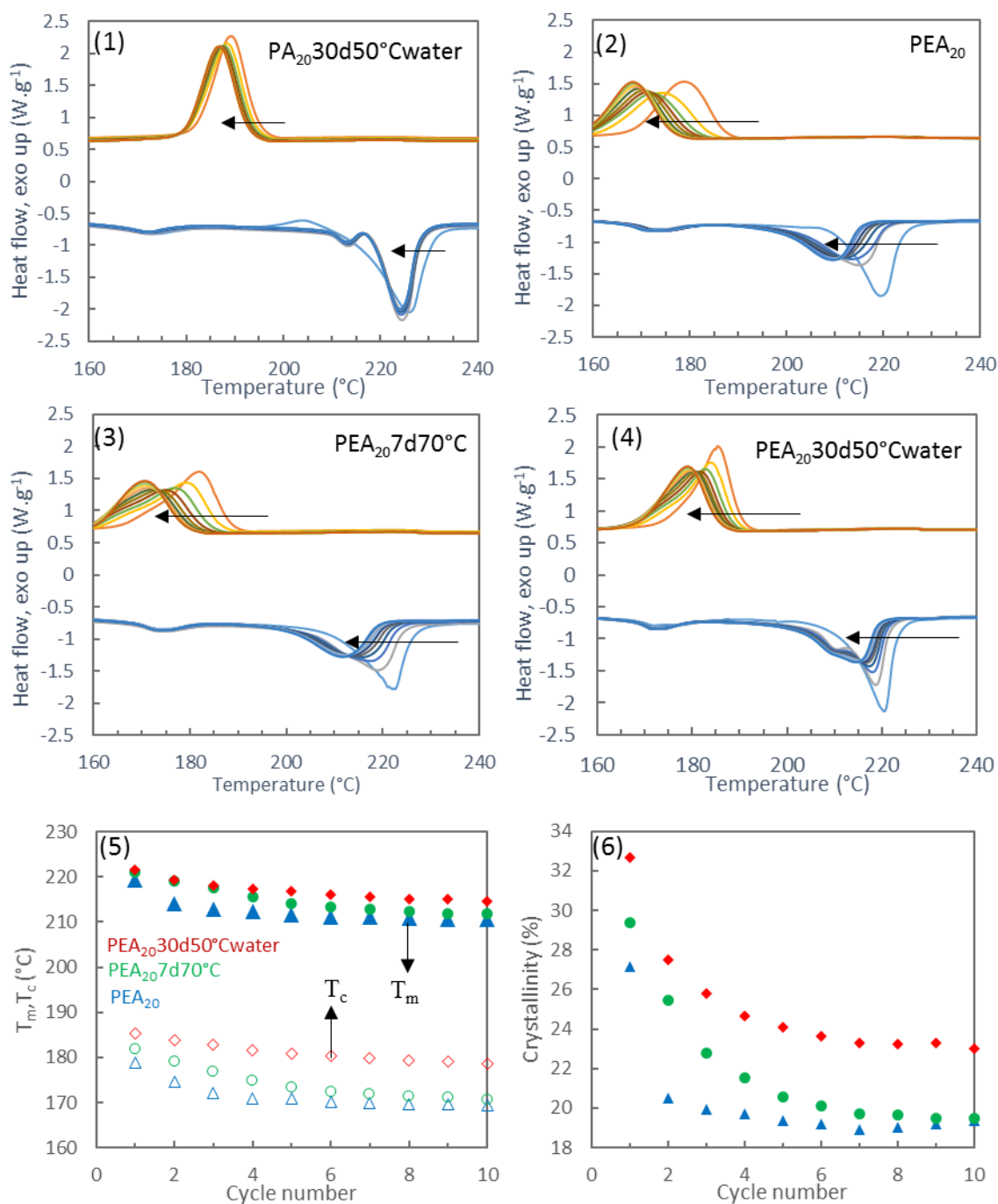


Figure 114 : DSC cooling and melting thermograms for (1) PA₂₀30d50°Cwater, (2) PEA₂₀, (3) PEA₂₀7d70°C and PEA₂₀30d50°Cwater. (5) T_c and T_m and (6) crystallinity for PEA₂₀ (blue), PEA₂₀7d70°C (green) and PEA₂₀30d50°Cwater (red)

For PA₂₀30d50°Cwater, the thermal properties, such as T_m, T_c, ΔH_m or ΔH_c did not significantly evolve beyond the first heating-cooling cycle (Figure 114). Moreover, thermograms of PA₂₀30d50°Cwater were similar to those obtained for PA₂₀ and PEA₂₀7d70°C. Also, no significant difference in thermal properties were obtained between pristine and aged thermoplastic samples (Table 23). This suggests that the two kinds of ageing did not induce significant changes in the molecular structure of the thermoplastic materials.

By contrast, all vitrimer melting and cooling peaks shift to lower temperature with increasing number of cycles (Figure 114). This result may suggest a subsequent reshuffling of the dynamic cross-links towards a statistic repartition in all the material. However, for all vitrimer compounds, T_m , T_c and ΔH_m seems to stabilize after around 5 heating-cooling cycles. After this stabilization, PEA_{20} and $PEA_{20}7d70^\circ C$ present similar thermal values. By contrast, $PEA_{20}30d50^\circ C$ water exhibits higher T_m and T_c , and presents a slightly higher crystallinity compared with PEA_{20} . As seen previously, the water aged thermoplastic reference, $PA_{20}30d50^\circ C$ water, did not exhibit significant changes compared to PA_{20} . Thus, this evolution may rather be caused by the lower degree of crosslinking than backbone PBT chain breakage. Indeed, if crosslinks are detrimental to the formation of crystals, the lower degree of crosslinking in the water aged vitrimer suggested by a raw gel ratio of 14 wt.-% has less impact on crystallinity.

Moreover, $PEA_{20}30d50$ water exhibit a complex melting behavior. At lower cycling number, it exhibits a poorly-defined two-melt peak, similar to the double-peak found for the thermoplastic equivalent PA_{20} . Then, for subsequent heating/cooling cycles, it exhibits a broader endotherm with a single melting peak similar to unaged PEA_{20} sample (Figure 114 and Table 23). This result may suggest a subsequent reshuffling of the dynamic cross-links toward a statistic repartition between broken, short polymer chains, and longer polymer chains previously located in the crystals, which did not suffer equivalently from degradation (Figure 115).

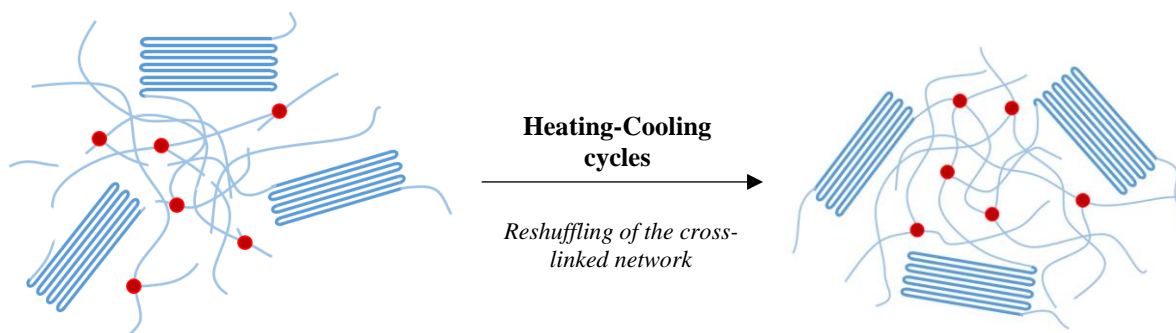


Figure 115 : Behavior of the dynamic cross-linked system after thermal ageing and subsequent heating step for $PEA_{20}30d50^\circ C$ water

In summary, no significant thermal differences were detected in the $7d70^\circ C$ aged vitrimer sample, despite a decrease in the cross-linked ratio from 62 wt.-% to 38 wt.-%. On the other hand, the water aged sample exhibited higher T_m , T_c and χ_c , attributed to its low degree of crosslinking. Mechanical tests such as DMA or tensile tests may provide additional information about the potential thermal degradation that occurred in the material. Being one of the first studies conducted on the ageing of thermoplastic-based vitrimer, it remains to be seen if the dynamic crosslinks may be more sensible to thermal or water ageing compared with traditional, non-dynamic crosslinks.

3.4.5. Upscaling PEA₂₀ vitrimer through continuous reactive extrusion

As mentioned in the first part of this manuscript, finding a continuous process to produce cross-linked vitrimer is the next milestone toward the full industrialization of this category of polymer. Currently, the most sought-after process is directly adapted from thermoplastic processing: continuous reactive extrusion (CRE). However, both the high viscosity of vitrimer in the molten state and relatively long reaction times needed (8 minutes by non-continuous reactive extrusion, NCRE) prevent effective cross-linking to occur inside the extruder without damaging the equipment. As detailed previously, Farge et al. developed a two-step process to effectively obtain fully cross-linked PBT-vitrimer while suppressing shrinking in the samples⁹¹. In this case, CRE could be considered as a preliminary mixing stage and the post-curing step implies keeping the sample at constant shape at high temperatures for several minutes, which greatly decrease the industrial application in terms of cadence. Another study report the synthesis of vitrimer especially designed to have high rate of chemical exchange involving vinylogous urethanes⁴⁵, with stress-relaxation times below 1s at processing temperature, compatible with CRE at low speed. Here, we propose a solution to synthesize PBT-vitrimer into a straightforward one-step CRE. This study aims at understanding the implications of the cross-linking reaction occurring inside an extruder, as well as studying the advantages of the fast-relaxing PEA compared with the references PBT-vitrimer, PE_Z. Well-dried PBT and DGEBA were previously mixed with either Zn(acac)₂ (PE_Z) or AlPi (PEA₂₀) and introduced in the extruder through a volumetric feeder (Figure 116).

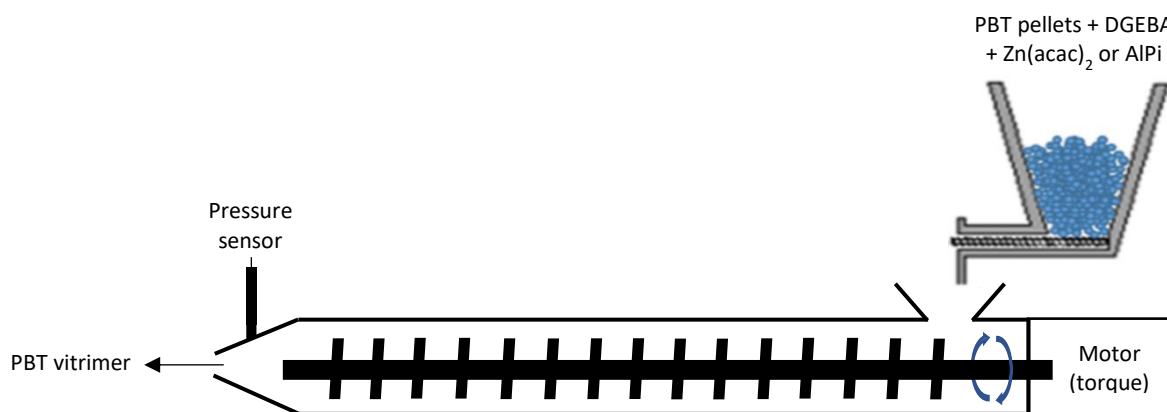


Figure 116 : Scheme of CRE with one-step reagent mixture feeding.

The proportions used for the formulations is presented in Table 24, Both pressure and torque are presented in Table 24, and were carefully monitored to prevent blockage of the extruder due to the high viscosity promoted by cross-linking. As feeding rate is the main parameter defining the residence time, a low feeding rate of 50 g/h was chosen to obtain an average residence time of 8 minutes. Experiments were conducted at 30 and 100 Rpm to study the impact of screw velocity on the reaction speed (Figure 117).

Table 24 : Operating conditions and registered parameters for the preparation of PBT vitrimer

	PBT (wt.-%)	DGEBA (wt.-%)	Zn(acac) ₂ (wt.-%)	AlPi (wt.-%)	Torque (Nm)	Die pressure (Bar)	Raw gel ratio (wt%)
PE _Z	97.8	2	0.2	/	35 ± 4	> 100	56 ± 5
PEA ₂₀	78.3	1.7	/	20	40 ± 2	50 ± 5	42 ± 4

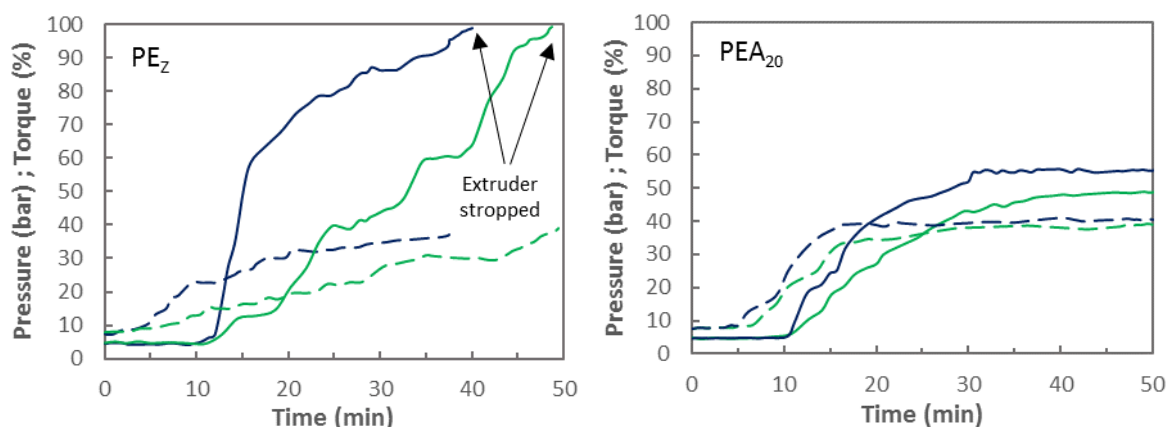


Figure 117 : Evolution of the torque (dotted line) and pressure (full lines) registered during CRE at 30 (green) and 100 (blue) Rpm

In all cases, the rise of both torque and pressure in the die, registered by the extruder, implies a rise in viscosity through the formation of a cross-linked network. This rise occurs at the same time for both screw speed, as in the presence of kneading blocks, residence time is only dependent on the feeding rate. On the other hand, the time toward network formation decrease with increasing mixing speed, as improved diffusion of the reactants and self-heating of the material accelerates the reaction rate. This reaction is also more visible for PE_Z, as die pressure eventually reaches maximum pressure value, stopping the motor. In the case of PEA₂₀, die pressure stabilizes at around 50 bar. For both materials and screw speed, the torque remains stable at 35 to 40 % of the motor, which indicates that most of the reaction occurs in the pumping zone, which may act as a curing step in the process. In regards with gel ratios, PE_Z exhibit a higher cross-linked fraction than PEA₂₀ (56% vs 42% considering raw gel ratios). Those results implies that a significant amount of epoxide did not react within the residence time, especially for PEA. Further tests would be necessary to conclude if the lower cross-linking degree is the only parameter explaining the difference of die pressure. Besides, an interesting outlook on this process would be to speed-up the reactions using a co-transesterification catalyst (like Zn(acac)₂), as previously seen by NCRE.

Figure 118 shows the visual aspect of the extrudate during CRE processing for various feeding ratios. The tests were implemented at a screw speed of 30 Rpm and at different feeding rates, from 200g/h to 50g/min, to understand the formation of the cross-linked network in regards to residence time. All PE_Z extrudates present a slightly yellowish aspect when equivalent material processed by NCRE had

showed a more pronounced grayish color (cf: Chapter 2). This implies that CRE processing promotes significantly less degradation than the laboratory-scaled extrusion process previously presented in this report despite the absence of a nitrogen flux. PEA exhibit a brighter white color, on par with the presence of 20wt% AlPi. At shorter residence times, the extrudate shares the aspect of a fully thermoplastic PBT material, with an average diameter equivalent with the diameter of the nozzle (1mm). At longer residence times, the diameter increases as rising viscosity prevents a proper flow of the material through the nozzle. With higher residence time, surface roughness increase, especially for higher cross-linked materials (PEZ, Figure 118). Those results are on par with the aspects of the material after passing through the die of the laboratory-scaled extruder from Chapter 2. This rough aspect are also found in crosslinked polymers, and are explained by the far greater relaxation time of the material compared with the shear rate imposed by the screw rotations, translated by an elastic memory effect⁴⁵.

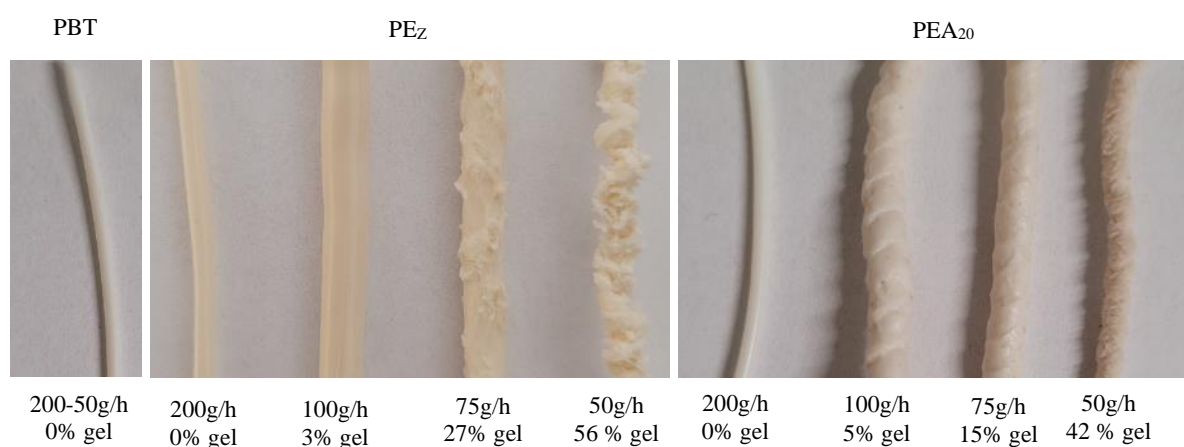


Figure 118 : Aspect of the extrudate for several feeding rates.

3.5. Conclusion

In this chapter, we report the successful synthesis of fireproof PBT-based vitrimers by reactive extrusion using aluminum phosphinate as both FR additive and transesterification catalyst. Gel content, elementary analysis and NMR studies proved that the aluminum (III) phosphinate salt can act as a transesterification catalyst without the presence of an other co-catalyst. Radically higher exchange rates at high temperature compared to pristine vitrimer was also reported, even when AlPi was added as in catalytic quantities (0.26wt.-%). Thermal analysis highlights a steep decrease in crystallinity for 20wt.-% filled vitrimers compared to PA₂₀, while its T_g is similar to unfilled PBT vitrimer formulations.

Expectedly, the very fast bond-exchange promoted by the presence of AlPi leads to a significant decrease in creep resistance in cases of temporary overheating above the melting point (3min at 250°C) compared with unfilled vitrimer (30 minutes at 250°C). However, compared to most vitrimer based on

thermoplastic precursors^{5,61,91}, the material could be processed through injection without exhibiting significant creep once heated above melt temperature, making it possible to bypass a post-curing step.

AlPi-filled vitrimer exhibits better mechanical performances compared to thermoplastic equivalent thanks to the cross-linked structure providing better rigidity. Interestingly, the plasticity development of the vitrimers studied showed a significant contrast with the filled thermoplastic reference, as revealed by the tensile tests conducted near the melting point. The vitrimer specimens were observed to deform plastically in a uniform manner without experiencing necking, indicating that the strain remained evenly distributed across the entire specimen.

Flame-retardancy of the flame-retarded vitrimer material did not intrinsically differ from the thermoplastic reference, with same V-0 classification shared for both materials at 20 wt.-% and 15 wt.-% loadings, and V-2 classification at 10 wt.-% loadings. The thermal stability did not give any significant difference on the degradation temperature between the two materials. However, the aspect of PEA₂₀ significantly differed from PA₂₀. Thanks to the higher melt viscosity of the vitrimer, the material keeps a relative dimensional stability upon burning, leading to lower dripping behavior while the thermoplastic easily flows.

During the ageing process, the differences in the flowing behavior upon burning became more pronounced, despite a significant decrease in the gel fraction for the vitrimer, particularly with immersion scenario (from 60 wt.-% to 15 wt.-% gross gel ratio). This decrease in gel fraction was attributed to chain breakage. Since chain breakage occurs only in the amorphous part of a semi-crystalline polymer, for the vitrimer, a rearrangement between broken (amorphous part) and unaffected polymer chains (crystalline phase) took place after several heating cycles, resulting in a more homogeneous distribution of cross-linking nodes towards broken and unaffected polymer chains. It is expected that similar phenomena occurred during UL-94 tests, allowing for the retention of the retraction behavior despite a lower degree of cross-linking.

Finally, tentative to upscale the production of cross-linked vitrimer by continuous reactive extrusion was conducted, obtaining 42wt.-% gel ratios at low feeding rates without risks of damaging the extruder thanks to the lower viscosity provided by the AlPi catalyst.

Whereas Chapters 2 and 3 investigated low cross-linked density vitrimer, it is also of interest to investigate the effect of FR in high cross-linked density system. Chapter 4 will thus focus on the addition of flame-retardant additives to epoxy-based vitrimer.

Chapter 4: Addition of flame-retardant additives to epoxy-based vitrimer

4.1 Introduction

Due to their excellent dimensional and chemical stability, mechanical and dielectric properties, epoxy resin (EP) has captured the largest market share as one of the most significant thermosetting polymers²⁷⁰. It is thus no coincidence that the first studies conducted on the synthesis of recyclable cross-linked materials were focused on systems based on epoxy precursors^{4,22}. However, the most industrially relevant approach to flame-retard epoxies revolves around adding flame retardant to reduce its flammability and improve its fire resistance. Very few studies have yet been reported on the sole addition of flame-retardant additives in vitrimer networks¹²². In order to dig deeper into this apparent oversight of traditional research, this chapter will focus on the synthesis of flame-retarded epoxy-based vitrimers through an additive approach. With the two previous chapters focusing on lowly cross-linked thermoplastic-based vitrimers, it becomes crucial to investigate the influence of flame-retardants on highly cross-linked epoxy-based vitrimers. Within this objective, two different systems were investigated.

In a first approach, the development of flame-retarded, recyclable epoxy resin coatings. Vitrimer was synthesized from a well-known mixture of DGEBA epoxy resin and fatty acid^{4,35,81}, to which a charring agent and a synergist compound were added. The recyclability of each formulation, as well as their performances as fire protective coating were assessed. The approach will focus on comparing the effectiveness of 9,10-dihydro-9-oxa-10-phosphaphenanthrene-10-oxide (DOPO) added to a Phenol-Novolac-epoxy/fatty acid system through two different pathway: a reactive approach in which the moiety is included in the polymeric chain and an additive approach where the DOPO is added as an additive. The impact of the two methods on cross-linking reaction and bond-exchange kinetics was analyzed by FTIR, isothermal relaxation and DMA. The properties of the materials were also studied through the analysis of the mechanical performances and flame-retardancy. After a presentation of the material and techniques used in this part of the work, the results obtained for both systems are successively discussed.

4.2 Experimental

4.2.1 Material description

The networks studied in this chapter are polycondensates formed by reactions between epoxy rings and acid functional groups beyond the gel point. The synthesis is carried out by polyaddition between a multi epoxy (Poly[(phenyl glycidyl ether)-co-formaldehyde]) or DGEBA) and a mixture of dimers and trimers of fatty acids (Pripol 1040). The stoichiometric ratio of 1:1 epoxy:acid is necessary to obtain a densely cross-linked system ratio with a maximized number of available hydroxyl function⁴. The chemical structures, acronyms and characteristics of the materials are presented in Figure 119.

Table 25 : List of the chemical components used in this study, their function and their main characteristics

Name	Grade (supplier)	Function	Characteristics
Pripol	Pripol 1040 (Croda)	Fatty acid	296 g.mol ⁻¹ COOH T _g = -35°C
Bisphenol-A Diglycidyl ether (DGEBA)	DER 332 (SIGMA-ALDRICH)	Epoxy	Purity >96% 170 g/Eq Functionality ~ 2 T _g = 5°C
Poly[(phenyl glycidyl ether)-co-formaldehyde]	Phenol Novolac epoxy resin (SIGMA-ALDRICH)	Epoxy	178 g/Eq Functionality ~3.1 T _g = 1°C
DOPO-9, 10-Dihydro-9-oxa-10-phosphaphenanthrene-10-oxide (DOPO)	POLYPHLOX 3742 (STRUKTOL)	Epoxy and flame-retardant	375 g/Eq 4 wt.-% P T _g = 24°C
Zn(II) acetate	(SIGMA-ALDRICH)	Transesterification catalyst	
9,10-Dihydro-9-oxa-10-phosphaphenanthrene 10-oxide	DOPO (GREENCHEM)	Flame-retardant	M _n =216 14.4 wt.-% P D < 400 μm
Ammonium Polyphosphonate (APP)	Exolit AP 422 (CLARIANT)	Flame-retardant (charring catalyst)	
Pentaerythritol (PER)		Synergist (char former)	

Concerning the coating-vitrimer, a FR formulation was selected using ammonium polyphosphate (as charring catalyst) and a pentaerythritol (as char former), with a 3:1 weight ratio since it is widely reported in the literature for such an application¹⁰⁻¹⁸¹. The objective of this part was not to develop new formulations but rather to study the effect of additives in such a system, thus a widely used formulation was considered. The list of the different formulations is reported in Table 26.

Table 26: List of the different formulations (in grams)

Name	Pripol	DGEBA	Zn(ac) ₂	PER	APP
E _z	20 (60.7 wt.-%)	11.5 (34.8 wt.-%)	1.5 (4.5 wt.-%)		
E _z PER	18 (54.4 wt.-%)	10.3 (31.5 wt.-%)	1.3 (4.1 wt.-%)	3.3 (10 wt.-%)	
E _z APP	14 (42.4 wt.-%)	8.0 (24.4 wt.-%)	1.0 (3.2 wt.-%)		9.9 (30 wt.-%)
E _z (APP+PER)	12 (36.4 wt.-%)	6.9 (20.9 wt.-%)	0.9 (2.7 wt.-%)	9.9 (30 wt.-%)	3.3 (10 wt.-%)

Concerning the DOPO-containing vitrimer, the formulations that have been prepared are listed in Table 27. A 1:1 epoxy/acid ratio was kept for all materials, considering the EEW (Epoxy Equivalent Weight) provided by the manufacturers.

Table 27 : List of the different formulations (in grams)

Name	Pripol	Novolac	Polyphlox	Zn(ac) ₂ (g)	DOPO
N _Z	20 (59.7 wt.-%)	12 (35.8 wt.-%)		1.5 (4.5 wt.-%)	
N _Z DOPO	17 (50.7 wt.-%)	10.2 (30.5 wt.-%)		1.3 (3.8 wt.-%)	5.0 (15 wt.-%)
Pol _Z	14.4 (43.0 wt.-%)		18.0 (53.7 wt.-%)	1.1 (3.3 wt.-%)	

4.2.2 Synthesis of flame-retarded epoxy vitrimer

The synthesis of flame-retarded epoxy vitrimer was achieved following three steps (Figure 119).

Solubilization of the catalyst in the fatty acid. As discussed in Chapter 1 of this manuscript, the exchange kinetics of acid/base systems are too slow to trigger a viscoelastic response at moderate temperatures. Thus, the use of a catalyst is required to speed up exchange reactions. The use of monomers as reactants leads to a highly cross-linked material, with numerous dynamic bonds. The amount of catalyst has to be comparatively higher than the quantity previously used for PBT vitrimer in order to effectively catalyze the reactions. In this study, Zn (II) acetate was preferred over the Zn(II) acetylacetonate from Chapters 2 and 3 thanks to its better solubility in acidic environments^{81,250}. The Zn(II) catalysts are widely known for promoting both esterification (with epoxy/acid reaction promoting cross-linking), and transesterification (thanks to β -hydroxyl ester/acid promoting bond-exchange reactions). Typically, 20g of Pripol 1040 was inserted in a round-bottom flask and heated at 100°C. 1.5g of Zn(ac)₂ was slowly added under stirring, then vacuum was applied. The temperature was then slowly increased up to 180°C. During this step, ligand exchange occurs. Acetate is substituted by carboxylate from pripol and acetic acid is released as already described in previous works⁴. Great care was taken during this step to prevent any complications. If the ligand exchange proceeds too rapidly, the significant production of acetic acid may give rise to the excess formation of bubbles and emulsion. This, in turn, can lead to an overflow of the reaction mixture.

Mixing with epoxy and FRs. The accurate amounts of epoxy and FRs were added to the previous {Pripol+Zn(II)} mixture using an electric agitator equipped with a PTFE rod mixer. As both the epoxy resins and pripol present a high viscosity at room temperature, mixing was performed at 100°C for several minutes to obtain a better homogeneity.

Curing. Obtained blends were poured into square-shaped 10x10mm iron molds sandwiched between Teflon fabrics in a hydraulic press under 50kN for 15h at temperatures ranging from 130°C (for all E_Z based systems) to 180°C depending on the mixture. N_Z was cured at 180°C, while Pol_Z and N_ZDOPO resin were both cured at 160°C. When used as a coating, the mixtures (1mm thickness) were deposited on well-sanded 10*10 cm² steel plates before curing in a oven at 130°C for 15 hours.

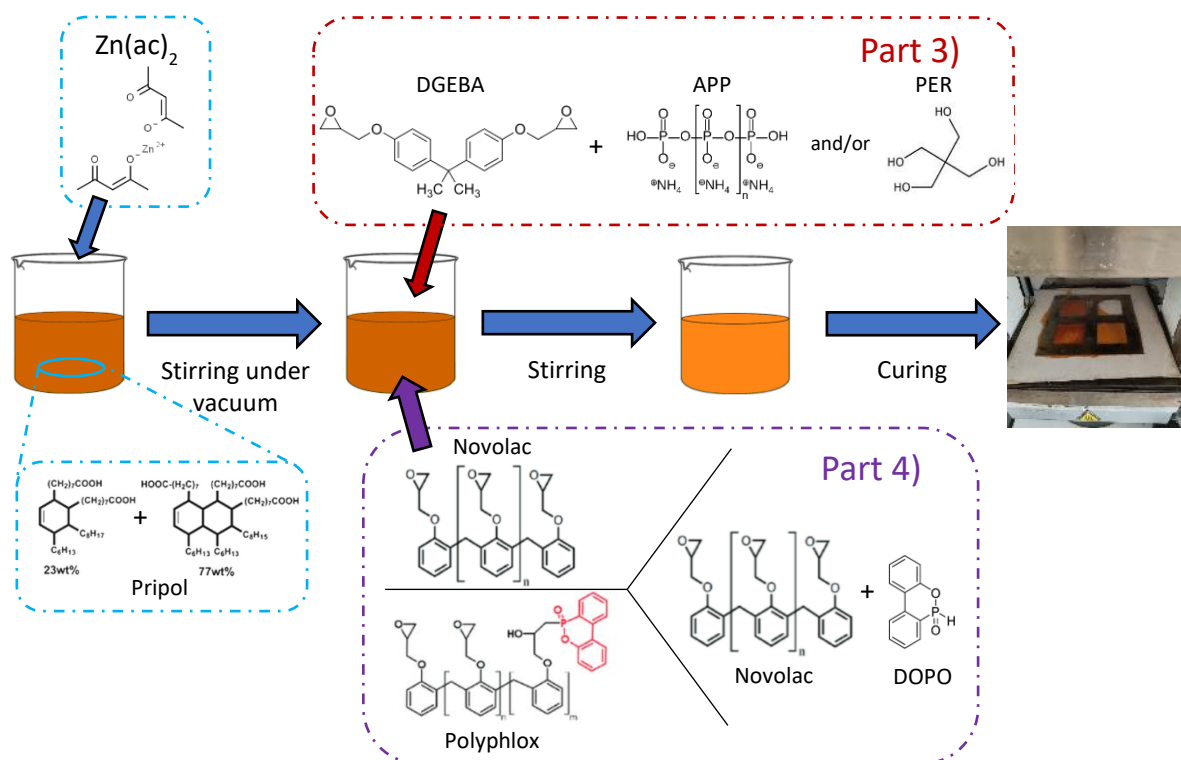


Figure 119 : Synthesis of flame-retarded vitrimer from part 3) and 4) of this chapter

4.2.3 Characterization

Thermal analysis. Differential scanning calorimetry (DSC) analyses were performed using a Discovery DSC from TA Instrument under nitrogen ($50 \text{ mL}\cdot\text{min}^{-1}$). Temperature and heat flow were calibrated with a high-purity indium sample using standard procedures. Aluminum pans and lids were used but the crucible was not hermetically sealed. The sample (5 mg) was heated from -40 to 180 °C at 20 °C/min, held at 180 °C for 2 min, then cooled to -40 °C at 20 °C/min, held at -40 °C for 2 min, and finally heated to 180 °C at 20 °C/min. Thermogravimetric analyses (TGA) were realized in alumina pans using a TG 209 F1 Libra apparatus from NETZSCH under nitrogen flow ($20 \text{ mL}/\text{min}$). A purge of 60 min at 40 °C was carried out before heating the sample (around 10 mg, powder) from 40 to 800 °C at a heating rate of 20 °C/min.

Quantification of the insoluble fraction. 200 mg of each formulation (m_0) were immersed in 20 mL of HFIP for 4 days under stirring at room temperature and filtered using a Büchner funnel. The insoluble gel fraction collected on the filter was dried for 4 days at room temperature and then weighed (m_{gel}). The gel ratio was obtained using Equation 12. As no elementary analysis was conducted on the gel fraction, only raw gel fractions were considered (Equation 12). As all fillers used in this chapter are soluble in HFIP, the cross-linked fraction is probably under-estimated for filled materials (for more detail, see Chapter 2, part 2.2.3) because a fraction of the filler may have solubilized instead of the polymer.

Equation 12

$$\%gel = 100 \times \frac{m_{gel}}{m_0}$$

FTIR spectroscopy. Fourier Transform Infrared Spectroscopy (FTIR) was conducted to investigate the chemical composition of the samples by using a Nicolet iS50 FTIR Spectrometer. Spectra were acquired by scanning the samples in the infrared region (4000-400 cm^{-1}) over a specified wavelength range. 32 scans were collected to improve the signal-to-noise ratio and ensure reliable data.

Electron probe microanalyzer. Phosphorus elemental analysis was performed by a Cameca SX100 electron probe microanalyzer (EPMA). The samples were embedded into epoxy resin, and polished with SiC polishing sheets from grade 80 up to grade 4000.

Mass loss cone calorimeter (MLC). MLC experiments were performed on a Fire Testing Technology (FTT) apparatus. The procedure involved exposing plates positioned horizontally and subjected to a radiative flux. Materials were tested with a flux of 50 $\text{kW}\cdot\text{m}^{-2}$ at 35mm from the resistances. 10x10 cm^2 surface samples with thicknesses varying from 1 to 3mm were positioned on a ceramic backing. Four thermocouples, located at the top of the chimney, were used to calculate the heat release rate. The calibration was conducted by burning methane (flow from 0 to 6.7 $\text{mL}\cdot\text{min}^{-1}$) to obtain a calibration curve of the heat release as a function of methane flow²⁷³. Before the test, the heat flux was blocked by a mechanical plate (shutter) preventing earlier degradation of the material. At the beginning of the test, the shutter was opened and an electric arc (igniter) was positioned to force the ignition of the degradation gases, and immediately removed afterward.

Dynamic mechanical analysis (DMA) and stress-relaxation experiments. Sweep temperature strain tests were conducted using a TA Instrument Q800 Rheometer in tensile mode on a 1.6mm thick sample, with a distance of 20mm between the grip. A constant frequency of 1Hz and a strain of 0.1% were used with a heating ramp of 10°C/min from -30°C to 150°C.

Stress-relaxation tests were conducted using the previous apparatus in tension mode, using the same sample size and distance between grips. Isothermal test was conducted with a strain coefficient of 1% at 160°C. The test was stopped when total relaxation of the material was reached, or after 10⁵ seconds.

Mechanical testing. Uniaxial tensile tests were performed using an INSTRON 4466 apparatus on 1.6 mm thick, compression-molded dogbone-shaped samples with an effective length of 25mm. A constant cross-head speed of 1 mm/min (quasi-static regime) was applied.

4.3 Flame-retarded vitrimer coatings

In this part the performance of epoxy-based vitrimer coatings with flame-retardant added through an additive approach was examined. A DGEBA/Pripol vitrimer system, whose performances have already been widely reviewed in the literature^{4,35,274,22}, was synthesized. This vitrimer exhibits poor mechanical performances due to the long chains of fatty acid (Pripol 1040) providing a low T_g (close to room temperature). However, its malleable nature makes it a promising candidate for intumescent coating for steel structures. This part will revolve around the synthesis of flame-retarded vitrimer coatings and the characterization of their fire performances through MLC.

4.3.1 Material aspect and recyclability

All samples exhibit the characteristic orange/yellow color originating from the fatty acid (Figure 120). Both E_z and E_z APP depict homogeneous and defect-free surfaces, with a slightly higher opacity for E_z (APP). Upon adding PER, white agglomerates are visible inside the material, as PER melts far above the processing conditions temperatures ($T_m \sim 200^\circ\text{C}$) and hardly dissolves in organic solvents. The visual aspect of E_z (APP+PER) sample also exhibits an homogeneously dispersed APP, while PER agglomerates are visible. All composites presented very high insolubility when immersed in HFIP at room temperature for 48h under gentle stirring, confirming their cross-linked nature. Due to their dynamic cross-linked nature, covalent bond reorganization may lead to a certain degree of solubility, as few small molecules or clusters can be dissolved, resulting in gel fraction below 100 wt.-%²⁵⁰. A raw gel fraction of 93% was obtained for E_z , 94% for E_z (APP), 95% for E_z (PER), and 91% for E_z (APP+PER). Moreover, no significant swelling is visible, confirming the highly cross-linked nature of the systems⁶¹.

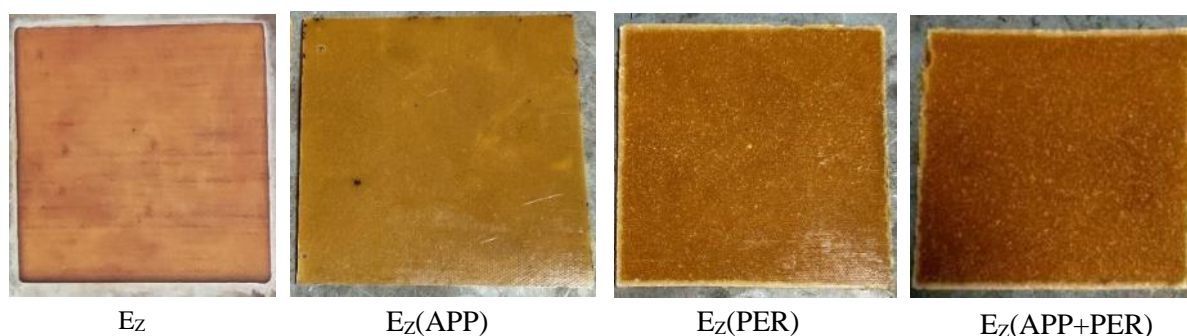


Figure 120 : Visual aspect of the flame-retarded vitrimer

The effect of the FR additives on the rigidity of the network was assessed by DSC (Figure 121). T_g decreases by 2°C upon the addition of 30wt% APP, and 8°C for 10wt% PER. The addition of the additives eventually decreases the density of the network, and lower density of cross-links is usually the main cause leading to a diminution of T_g . The steeper decrease upon adding PER may be linked with the presence of agglomerates further preventing cross-linking. Upon adding APP+PER, T_g further decreases by 10°C .

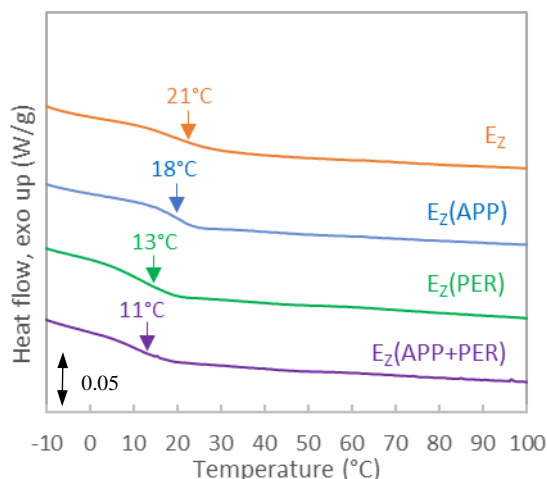


Figure 121 : DSC thermograms of the DGEBA-based vitrimer during the second heating ramp ($20^{\circ}\text{C}/\text{min}$, from -20 to 180°C). The curves were shifted vertically for clarity.

The recyclability of the materials was evidenced through reprocessing (Figure 122). All samples could be recycled after 15h at 130°C in the press. For similar vitrimer chemistry, Legrand et al. also obtained recyclable materials at 25wt% and 40wt% silica loadings³⁵. The long and flexible fatty acid chains of pripol 1040 lead to a robust network allowing for easy integration of particles without significantly hindering bond-exchange reactions. Figure 122 presents the aspect of the $E_z(\text{APP})$ sample before and after recycling. The irregular color pattern and transparency upon recycling is directly related to the average scale of the grinded pellets (2mm). Finer grinding (like cryogrinding) could help to obtain a better final aspect for recycled compounds.



Figure 122 : Recycling of EPOXY+APP plate

4.3.2 Performance of the flame-retarded vitrimer coatings

The synthesized vitrimers were used as protective coatings for metallic plates and their effectiveness as flame-retardant adhesives were assessed. The aspect of each formulation was similar to the ones previously obtained by compression molding and a good interfacial adhesion was obtained with the steel plate. To measure the effectiveness of such coatings as flame barrier, a thermocouple was

welded to the back of each plate. Mass loss cone experiments were then conducted to assess the performance of such coatings, with results reported in Table 28 and Figure 123.

Table 28 : Mass loss cone data of the epoxy vitrimer coatings

Formulation	pHRR (kW.m ²)	THR (MJ.m ²)	TTI (s)	TTFO (s)	Residue (wt%)	T _{plate, 500s} (°C)
E _Z	340 ± 12	27 ± 2	136 ± 8	240 ± 12	14 ± 4	542 ± 5
E _Z (APP)	149 ± 5	20 ± 1	120 ± 2	262 ± 8	42 ± 2	482 ± 2
E _Z (PER)	274 ± 7	29 ± 1	84 ± 2	200 ± 5	10 ± 1	548 ± 6
E _Z (APP+PER)	169 ± 18	19 ± 1	125 ± 7	296 ± 7	51 ± 9	487 ± 8

pHRR: peak Heat Release Rate ; THR: Total Heat Release Rate ; TTI: Tie To Ignition ; TTFO: Time To Flame Out

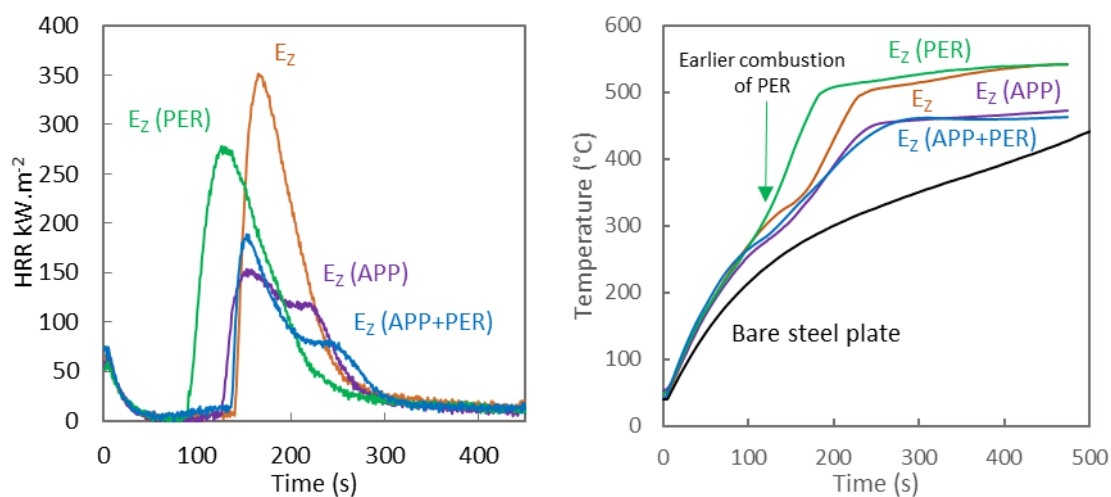


Figure 123 : Left: HRR profile of DGEBA samples (50 kW/m², 35mm); Right: Evolution of the temperature at the back of the plate, recorded by the thermocouple.

Pristine E_Z exhibit a time to ignition of 136s, with an sharp peak presenting a maximum of 340 kW.m⁻². It is followed by a rapid decrease of HRR, characteristic of a fast-burning material, with the total consumption of the polymer occurring within 240s. A similar aspect of the HRR curve is obtained upon the addition of 10wt% PER, but time to ignition is far lower than any other formulations. As PER degrades sooner than any other element of the matrix (degradation temperature assessed by TGA starts at 244°C²⁷⁵), it gives off flammable degradation gases before the vitrimer matrix, leading to sooner ignition. A 20% decrease in pHRR was measured, however total energy released by the combustion is similar to the pristine matrix.

Upon adding APP to the system, two decomposition steps are identifiable. Firstly, compared with E_Z, ignition starts a few seconds sooner and pHRR is reached at around the same speed. pHRR value is greatly reduced at 149 kW.m⁻². Secondly, this decrease of pHRR is followed by a plateau at around 80 kW.m⁻², before slowly decreasing as inflammation slowly stops. This behavior is characteristic of a charring phenomenon (Figure 124), forming a surface barrier protecting the material

from further degrading. Time To Flame Out is slightly increased, as the charring effect is inhomogeneously distributed at the surface of the sample, leaving some areas with moderate burning lasting for a longer time. Overall, the addition of APP flattens the curve, leading to a much lower THR (20 MJ.m^2) despite a slightly longer time to ignition.

Combining APP and PER gave similar results to APP alone, with similar THR, TTI, TTFO and residue. Upon degradation, a reaction occurs between APP and PER leading to the formation of a charred material^{181,182}. However, in the case of epoxy, the numerous thermally resistant aromatic groups leads to a high charring material^{270,276}. Thus, the introduction of PER as carbonizing agent^{181,182} do not significantly improves char formation. However, we observe a significant disparity in the charring yield for (APP+PER) formulation, registered at 51 ± 9 compared with 42 ± 2 upon adding APP only.

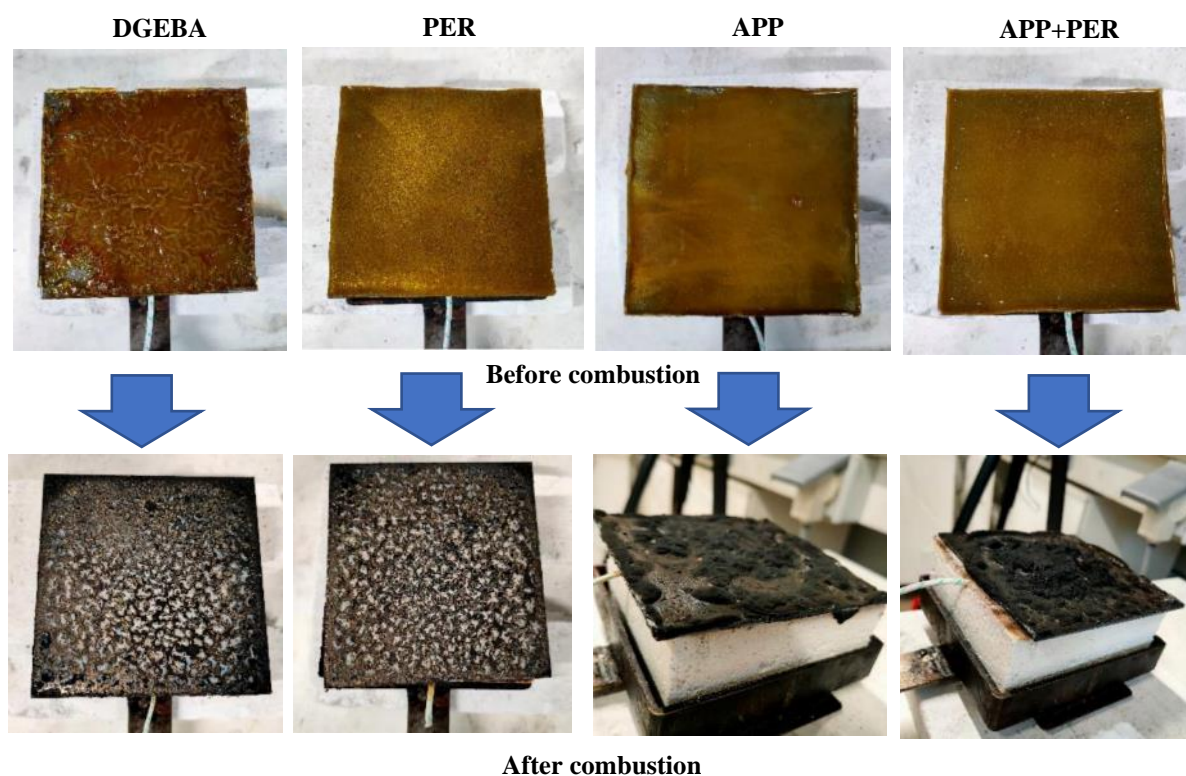


Figure 124 : Pictures of the plates before and after MLC test

Dealing with the fire protection of the steel, we show that when coated with E_z , the temperature recorded at the back of the plate stabilizes at 540°C after 400s. As expected, $E_z(\text{PER})$ coating exhibits similar results, with the earlier combustion due to the presence of PER leading to a plate temperature stabilizing at 540°C within 350s. Upon the addition of APP, the higher charring yield creates a protective barrier, which significantly decreases maximum plate temperature, which stabilizes at 450°C after 300s. The APP+PER formulation does not add significant improvement over the APP-only formulation. Those results need, however, to be compare with the value obtained for uncoated steel plate. In that case, the temperature reached after 500 s of exposure to the heat flux is around 450°C and linearly increases. It takes approximately 1000 seconds for the bare steel plate to reach similar temperatures, as no ignition

occurs on its surface. Additionally, the metallic surface reflects the radiative flux, which explains why it also takes longer to reach maximum temperature. So even if at 500 s, the temperature achieved for the virgin plate and the plates coated with APP-containing vitrimer are similar, the coating may preserve the fire protection at longer time.

4.3.3 Conclusion

This study demonstrates the possibility to synthesize effective recyclable, cross-linked flame-retardant coatings. Promising results were obtained, as the addition of 30wt% APP effectively shields a metallic plate from reaching high temperatures, with a maximum plate temperature decreased by 90°C. The addition of PER, alone or as synergist, did not show any significant improvements.

To complete this work, it would be interesting to investigate how the addition of fillers affects the relaxation performance of the vitrimer materials. Studying the reparability of the coating in case of scratch is also of high interest since it could improve the lifespan of future intumescent coatings.

4.4 Comparing DOPO in reactive or additive way

As a second approach, DOPO was considered as a flame retardant for epoxy. In this field, a few paper report the use of 9,10-dihydro-9-oxa-10-phosphaphenanthrene-10-oxide (DOPO) as flame-retardant moieties in vitrimer systems^{42,63,277,278} (see Chapter 1 for more details). It systemically encompasses a preliminary step, involving the chemical modification of a curing agent by grafting DOPO. This modified curing agent is then reacted with other monomers, leading to the synthesis of flame-retarded vitrimer networks. Even if the objective of this PhD work is to investigate the effect of flame retardant additives on vitrimer dynamics, we will consider in this part a comparison of the effectiveness of the reactive and additive approaches, as DOPO will be incorporated either reactively or as an additive to enhance the flame retardancy of the material (Figure 125). The objectives include assessing thermal stability, fire and mechanical properties. The effect on network structure, cross-linking density and curing behavior will also be investigated. The results should contribute to a better understanding of the role of DOPO in the vitrimer networks.

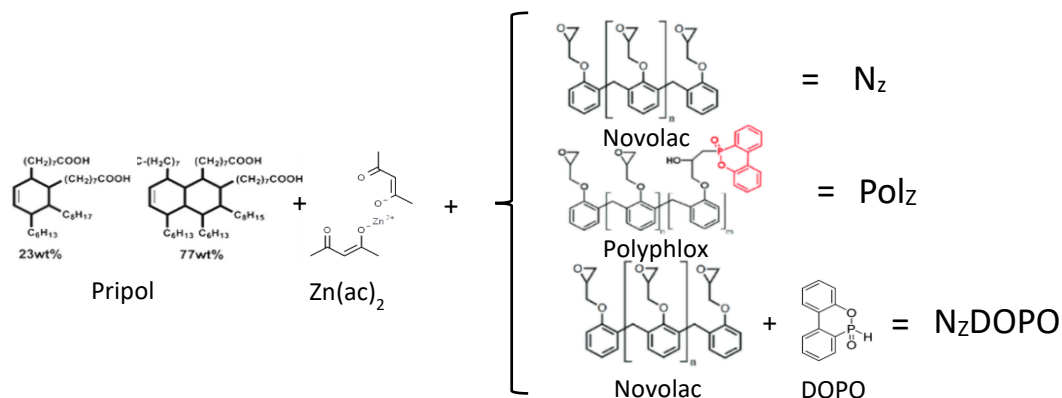


Figure 125 : Formulations studied in this part. Nz: reference formulation. Polz: formulation with DOPO incorporated reactively. NzDOPO: formulation with DOPO incorporated as an additive.

4.4.1 Characterization of the DOPO-based vitrimers

FTIR spectroscopy was conducted on each formulation before (prepolymers) and after curing (Figure 126). For prepolymer samples, the peaks can be observed at 1240 cm^{-1} , 1510 cm^{-1} , 2920 cm^{-1} , 914 cm^{-1} and 1710 cm^{-1} , which corresponds to the C-O stretching vibration peak, benzene ring stretching vibration peak, alkyl stretching peak, oxirane group and carboxylic acids, respectively^{42,81,276,279}.

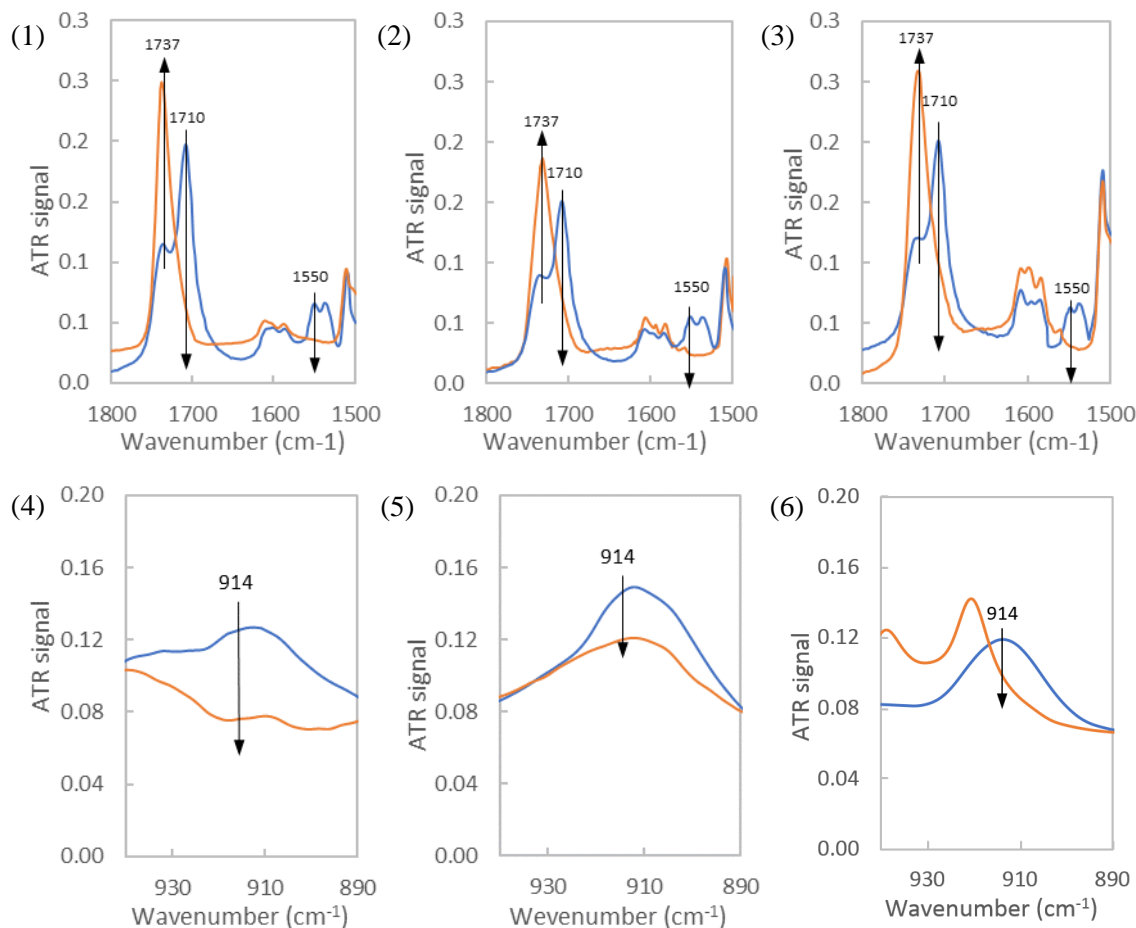


Figure 126 : FTIR spectra of Nz ((1),(4)) Polz ((2),(5)) and NzDOPO ((3),(6)) around the carbonyl ($1800\text{-}1500\text{ cm}^{-1}$) and epoxy ($940\text{-}890\text{ cm}^{-1}$) regions, before (blue) and after (orange) curing in the press for 15 hours.

After curing (Figure 126), total disappearance of the carboxylic acids was observed at 1710 cm^{-1} for all formulations, while the C=O stretching of the ester groups is responsible for the increase of the signal observed at 1737 cm^{-1} . However, it is worth noting that a signal at 1737 cm^{-1} was already present in all tested formulations before the curing process, even in the absence of any ester groups. For Polz and Nz, stretching vibration associated with carboxylates bonded with Zn^{2+} (1550 cm^{-1}) also disappear after curing, confirming the formation of Zn- β -hydroxyester anions^{66,81}, as Zn^{2+} is not bonded to a carboxylate anymore. The disappearance of the stretching vibration of the oxirane function at 914 cm^{-1} for Nz is usually indicative of the reaction of the oxirane group of the epoxy functions demonstrating the formation of the network. For Polz, significant fractions of oxirane groups did not react during curing since a peak is still visible at 914 cm^{-1} after curing even if its intensity decreases. This result could

potentially be attributed to the steric hindrance caused by the DOPO moiety, which isolates some of the epoxy groups and makes them less reactive towards the carboxylic acids for ester formation (Figure 127).

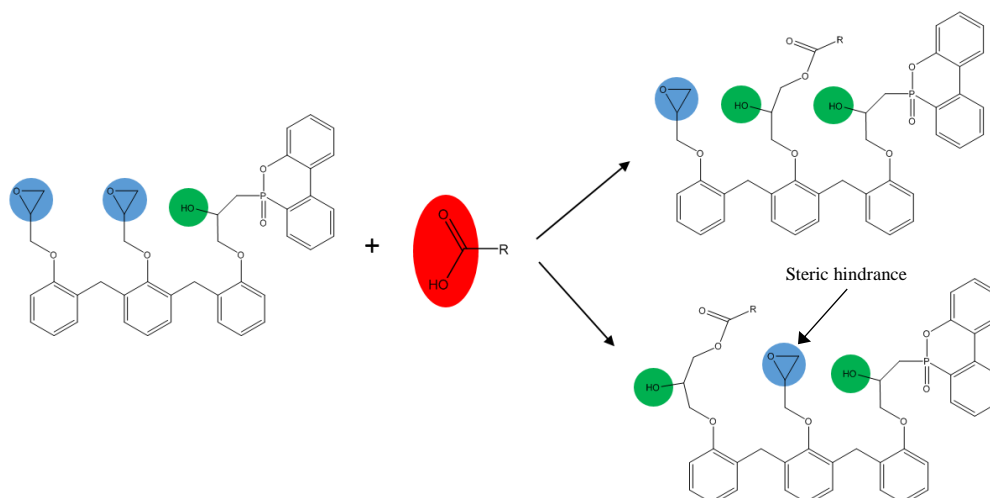


Figure 127 : Possible esterification reaction between polyphlox resin and carboxylic acid from the fatty acid. In function of the first epoxy group to react, steric hindrance may decrease the reactivity of the other epoxy group. Polyphlox was presented with an epoxy functionality of two for clarity.

For NzDOPO, total consumption of the epoxy groups is observed, with the apparition of new peaks at 940cm^{-1} and 920cm^{-1} that were not assigned. DOPO may also react directly with the carboxylic acids present in the fatty acids^{188,280}. However, the COOH groups of fatty acids and the P-H groups of DOPO are considered more reactive towards epoxies. This competition can lead to the formation of different compounds:

- With fatty acids, reaction with the epoxy leads to the formation of an ester group and an alcohol, capable of participating in transesterification exchange reactions
- With DOPO, the formation of a DOPO group covalently linked to the novolac epoxy (similar to polyphlox) may occur. This reaction only results in the formation of an OH group, thus no dynamic ester is formed. The hypothesis of DOPO reacting with esters would not be considered as a primary focus due to its lower reactivity compared to epoxy compounds.

Due to the 1:1 epoxy/acid stoichiometry, if DOPO effectively reacts with epoxy during curing, it will lead to a decrease in cross-linking density. This occurs because the DOPO reaction consumes some of the available epoxies, thereby limiting their availability to participate in cross-linking with carboxylic acids.

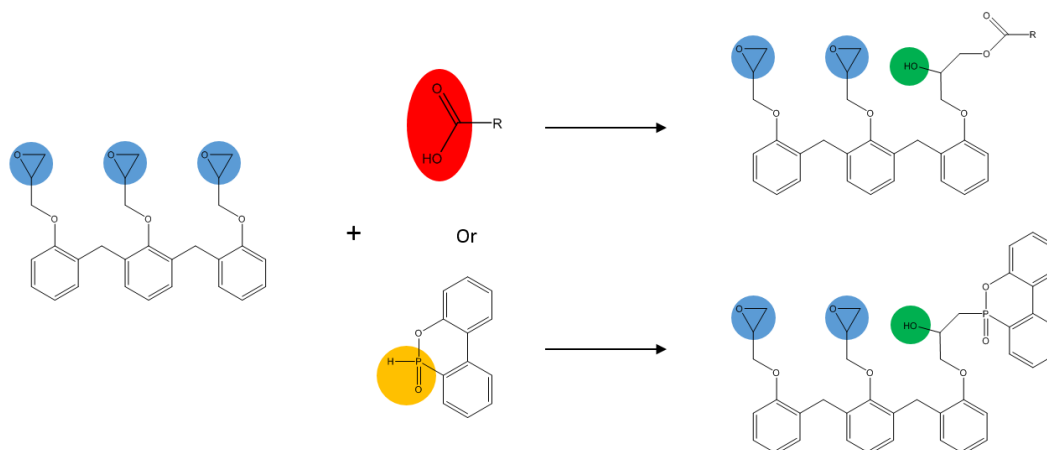


Figure 128 : Competition between the ester groups of the fatty acids and the highly reactive P-H bonds during the epoxy ring-opening reaction. Novolac was presented with functionality of three for clarity.

For all cured samples, a broad -OH stretching vibration is observed in the region 3500–3200 cm^{-1} , due to the opening of the epoxies forming pendant hydroxyl functions⁸¹. The remaining OH groups may still react by esterification with free carboxylic acids to form supplementary esters. However, this reaction usually takes longer times (several hours to days), due to the low reactivity of bare OH groups⁵.

The insoluble fraction of the vitrimer was measured. Raw gel ratios of 98%, 93% and 86% were obtained for N_z , Pol_z and N_zDOPO respectively. These high gel fractions are characteristic of highly cross-linked vitrimers. The lower gel fraction observed in sample N_zDOPO may be attributed to a lower cross-linking density and solubilization of a fraction of the DOPO.

EPMA mapping was carried out in order to study the dispersion of DOPO in both materials. Indeed, since the objective of this part of the work is to compare the reactive versus the additive approach, it is crucial to determine if it is the case. Figure 129 clearly shows that P is homogeneously dispersed in the case of Pol_z whereas particles of different sizes (varying from 10 to 150mm) are visible for N_zDOPO . Those results thus confirm that the material present two different dispersion of the DOPO moieties within the material.

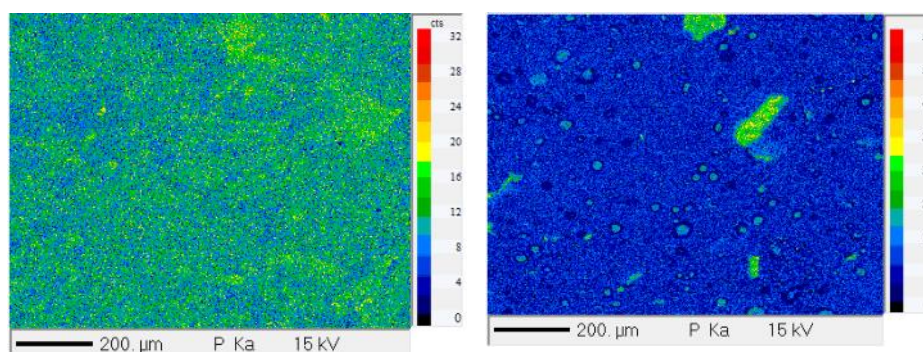


Figure 129 : Phosphorus EDMA mapping of Pol_z (left) and N_zDOPO (right)

4.4.2 Impact of recyclability of the DOPO-based vitrimer

The shape-memory and recyclability properties provided by exchangeable bonds are often detailed and praised in the literature. In our case, the recyclability of the materials was assessed by milling and reshaping the materials using similar processing conditions than those used during the synthesis (15h, 160°C for Polz and NzDOPO or 180°C for Nz). The milling was provided by a cryogenic grinding, allowing to reach micrometer-sized powder without degrading the material. All materials exhibited defect-free surfaces, and no significant color change was observed (Figure 130).

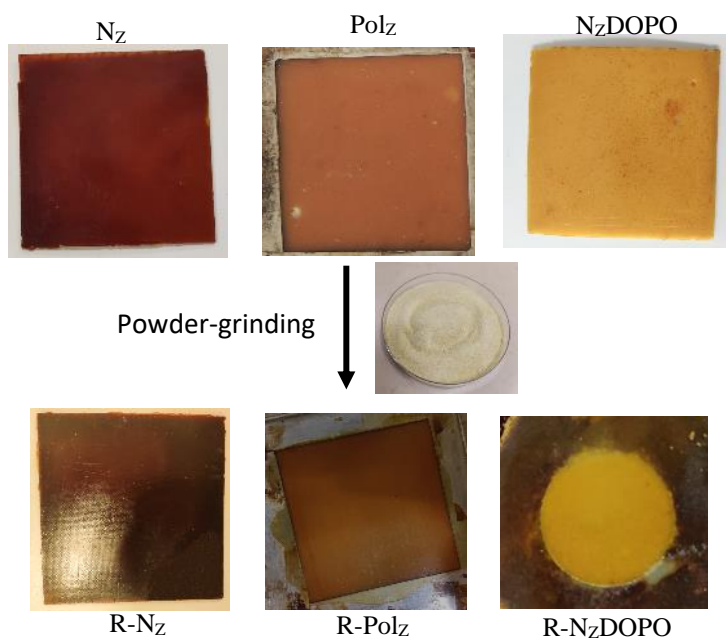


Figure 130 : Aspect of the different formulations before and after recycling.

The recycled materials, R-Nz, R-Polyz and R-PzDOPO, were then analyzed by FTIR and compared to their pristine counterpart (Figure 131). The initial structure of the material is conserved, as no modification or chemical degradation is observed.

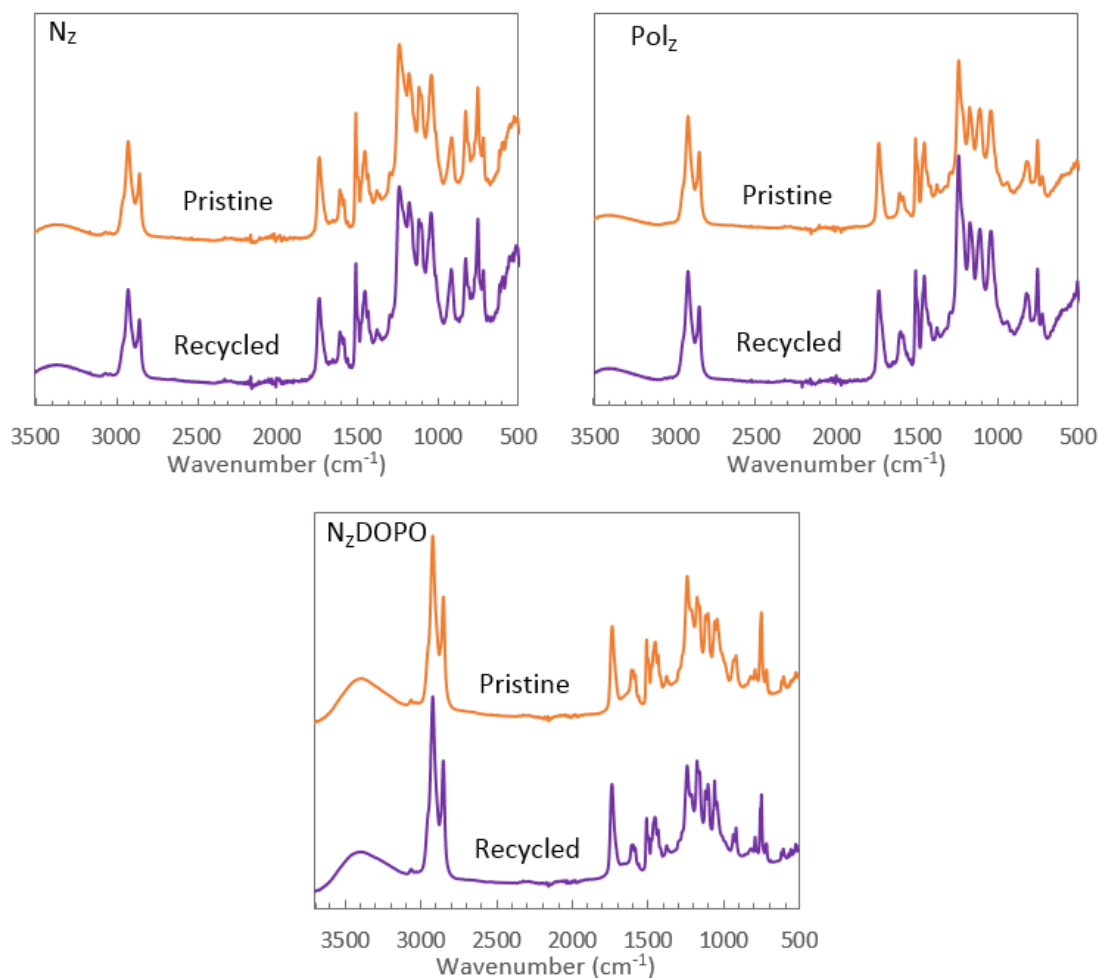


Figure 131 : FTIR spectra of the three formulations before and after recycling

To further study the effect of recyclability on cross-linking density, DSC and TGA experiments were conducted on the three materials and their recycled equivalent. The results are reported in Figure 132.

For pristine components, T_g of 29°C, 36°C and 25°C were measured for Nz, Polz and NzDOPO respectively. Compared to the previous work of this chapter as well as in the literature³⁶, the use of Novolac epoxy provides a significant increase of the matrix overall stiffness compared with DGEBA ($T_g = 21^\circ\text{C}$). The higher T_g value of Polz is due to the presence of the pendent DOPO group of the polyphlox. The rigid and bulky structure of DOPO restricts the molecular motion and consequently increases the overall stiffness of the network. Both R-Nz and R-Polz exhibited similar T_g than their pristine counterpart, implying that the number of cross-links is conserved upon recycling and no significant degradation occurred. On the other hand, 4°C higher T_g was obtained for R-NzDOPO. This should be explained by the fact that if the original sample is not fully cured, a further curing step may lead to esterification between the OH groups formed during curing and free carboxylic acids. This point could be further investigated by performing DSC measurements at different isothermal durations.

Regarding the thermal stability of the materials (Figure 16, right), all materials exhibited roughly equivalent characteristic temperature, with a T_{onset} of 300°C (320°C for NzDOPO) and a T_{Max}

(Temperature at which maximum weight loss is observed) at around 470°C. The presence of DOPO only slightly increased the high temperature residual mass. At 800°C, the residue yield is 8 ± 1 % for N_Z, 13 ± 0.5 % for Pol_Z and 14 ± 0.8 % for N_ZDOPO. DOPO mainly acts in the gas phase mechanism through the formation of free radicals PO[•] and HPO[•] to quench H⁺ and OH⁺ radicals formed during combustion¹⁷¹. However, the phosphorus elements can also lead to dehydration and char formation⁴², increasing the overall residue yield.

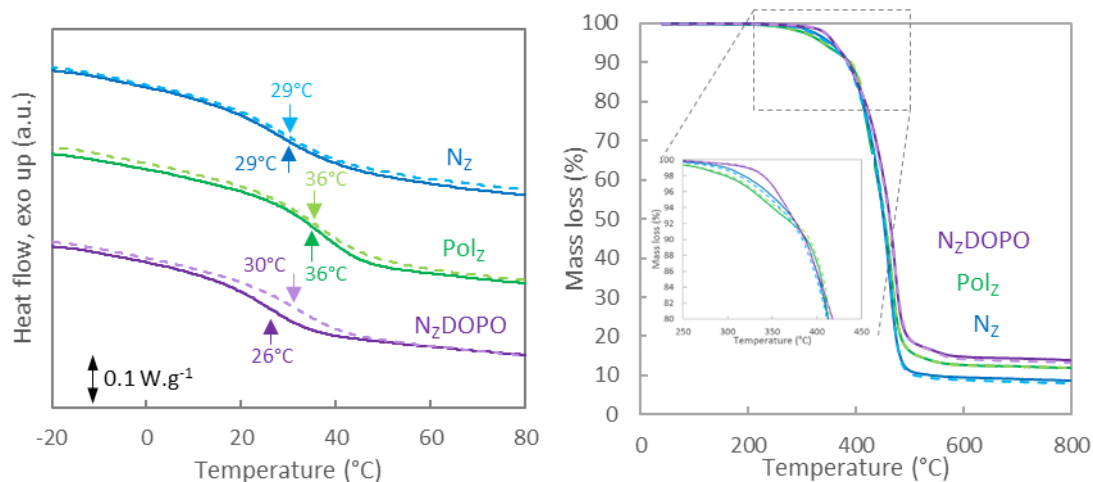


Figure 132 : DSC (left) and TGA (right) thermograms of the vitrimer compounds after synthesis (full lines) and after recycling (dotted lines)

Those results thus show that the recycling of the vitrimer-based system does not affect the thermal stability of the materials neither the structure (except in the case of N_ZDOPO).

4.4.3 Rheological and mechanical behavior of DOPO-based vitrimers

Stress relaxation measurements and dynamic mechanical analysis (DMA) were conducted to evaluate the rheological and mechanical properties of the DOPO-based vitrimers.

Normalized stress-relaxation of the three materials was carried out at 160°C and is presented in Figure 133 (left). It is evident that both the N_Z and Pol_Z networks can fully relax stress and flow at a temperature higher than T_g. The slower relaxation of Pol_Z may be attributed to the lower cross-linking density of the network proved by the amount of unreacted oxirane groups as demonstrated by FTIR measurements. Moreover, it has to be noted that it takes a significant amount of time for both compounds to totally relax stress (>10⁴s) when compared to stiffer anhydride networks^{4,90,98}. The long chains of the Pripol fatty acids lead to a network with a relatively low density of cross-linking bond compared with epoxy-anhydride compounds, and as the opposite of the Pripol, the high stiffness provided by the Novolac epoxy limits the mobility of the long aliphatic-wielding chains.

For N_ZDOPO, on the other hand, total relaxation is not attained after 10⁵ seconds.

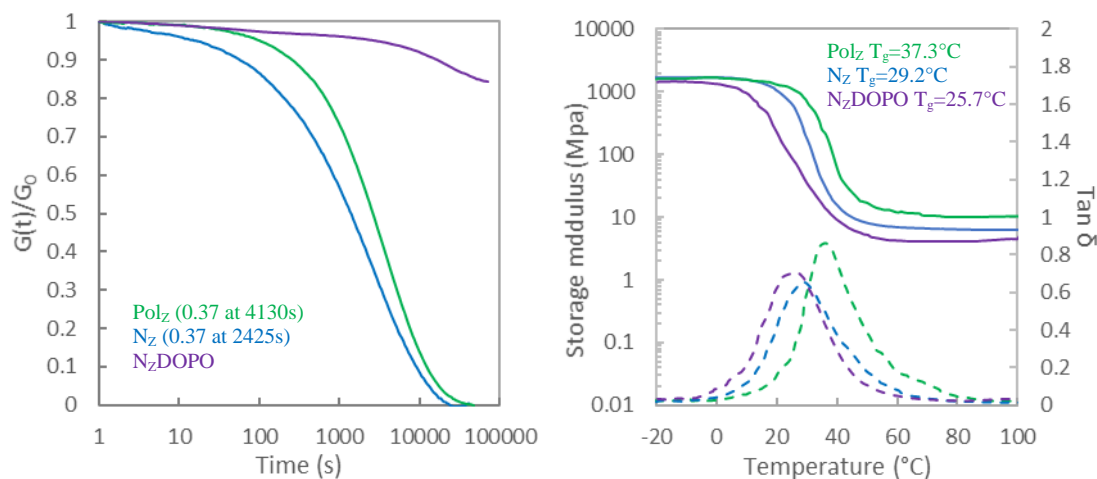


Figure 133 : Left: Normalized stress-relaxation at 160°C . Right: DMA analysis: storage modulus (full lines) and $\tan \delta$ (dotted lines)

The materials were also studied using thermomechanical analysis (DMA) (Figure 133 (right)). As previously observed using DSC, the DOPO groups of the Polz sample lead to a higher T_g of 37.3°C , however lower viscoelastic plateau is obtained (7 MPa) compared with Nz (11 MPa) due to the reduction of cross-link density⁴². On the other hand, a lower viscoelastic plateau was recorded for NzDOPO (4 MPa).

Finally, the mechanical performances of the vitrimer were further examined through tensile testing, with results reported in Table 29 and Figure 134.

Table 29 : Mechanical Properties of the synthesized and recycled vitrimer

Formulation	Young's modulus (MPa)	Stress at break (MPa)	Elongation at break (MPa)
Nz	360 ± 40	16.9 ± 1.1	28 ± 5
Polz	770 ± 60	25.9 ± 0.6	54 ± 9
NzDOPO	80 ± 30	9.1 ± 0.8	41 ± 5

Nz exhibit strain hardening during uniaxial deformation (Figure 134), which is usually an indication that the material is relatively brittle. However, elongation at break is higher at 26 % compared with what is usually obtained for brittle cross-linked epoxy-based vitrimer^{4,66} (<10 %). This phenomenon was attributed to the aliphatic chains of the fatty acid allowing a limited elasticity of the network. Besides, both Young's modulus (360 MPa) and stress at break (17 MPa) are significantly lower than values found in the literature for epoxy-anhydride vitrimer networks (>1 GPa and >50 MPa^{4,66}).

Polz exhibits a higher Young's modulus at 770 MPa due to the stiffening effect of the DOPO group. Unexpectedly, it also behaves radically differently than the previous formulations, with a hard tough plastic deformation combined with pronounced necking and ending with a strain-hardening effect usually found for semi-crystalline polymers. The combination of DOPO groups leads to a lower

functionality of the epoxy, which implies longer distance between each reticulation node, leading to better chain elongation and orientation.

N_zDOPO tensile curve exhibits a similar shape than N_z. However, it displays significantly weaker performances as Young's modulus is 5 times lower and stress at break is nearly divided by two, which can be explained supposing that this material has a lower cross-linking density.

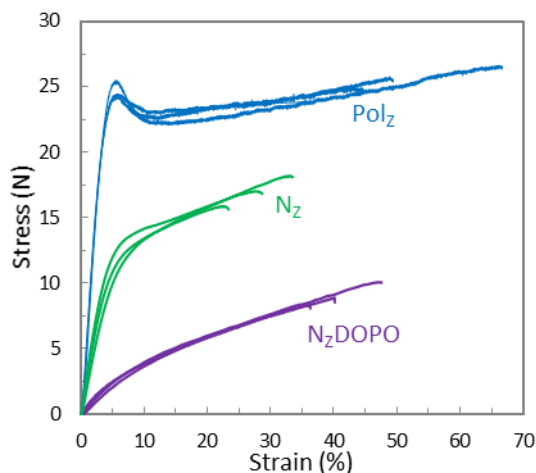


Figure 134 : Stress-stain curves of the DOPO-based vitrimer at 20°C

4.4.4 Flame-retardancy of DOPO-based vitrimers

Finally, cone calorimeter analyses were conducted to explore the behavior of the materials under conditions similar to a fire scenario. Square plates of approximately 100cm² with a thickness of 1.5mm or 3mm were exposed to an irradiative flux of 35kW/m². Time to Ignition, pHRR, THR, TTFO and residue after flame extinction were recorded and presented in Table 30 and Figure 135.

Table 30 : Mass loss calorimeter data for 1.5mm and 3mm samples

Formulation	pHRR (kW.m ²)	THR (MJ.m ²)	TTI (s)	TTFO (s)	Residue (wt%)
N _z 1.5mm	570 ± 5	49 ± 2	33 ± 2	240 ± 12	10 ± 1
Pol _z 1.5mm	461 ± 10	40 ± 2	33 ± 2	262 ± 8	14 ± 2
R-Pol _z 1.5mm	473 ± 11	39 ± 1	34 ± 1	190 ± 7	13 ± 1
N _z DOPO 1.5mm	450 ± 11	38 ± 1	33 ± 1	300 ± 40	15 ± 2
N _z 3mm	375 ± 7	66 ± 2	56 ± 2	440 ± 40	12 ± 1
Pol _z 3mm	259 ± 11	51 ± 1	56 ± 1	530 ± 50	19 ± 2

pHRR: peak Heat Release Rate ; THR: Total Heat Release Rate ; TTI: Tie To Ignition ; TFO: Time To Flame Out

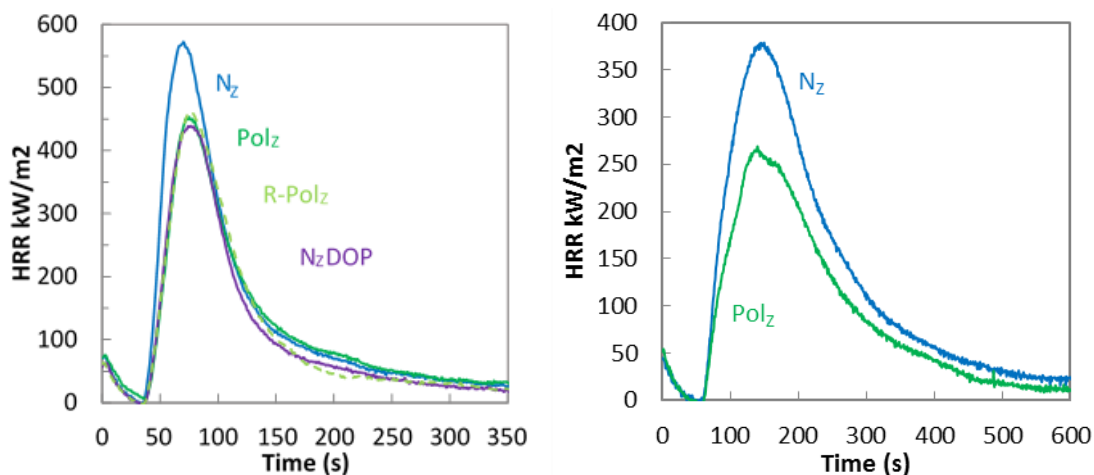


Figure 135 : HRR profile of NZ, PolZ, R-PolZ (dashed lies) and NZDOPO samples, for 1.5mm (left) and NZ and PolZ for 3mm (right) thickness samples. Heat flux of 50 kW/m² at 35mm from the resistance.

At 1.5mm thickness, all samples exhibit similar burning behavior, with a sharp peak right after ignition. The reference N_Z material exhibits a distinct HRR peak with a sharp value of 570 kW/m². After adding DOPO, the pHRR value evidently decreases by 19% for Pol_Z and 21% for DOPO. Those results indicate that DOPO can improve flame-retardancy of the cross-linked system. Meanwhile, the addition of the FR also decreases THR by 20% compared to N_Z, a value observed for both DOPO-containing formulations. In addition, it is noteworthy that all formulations share roughly the same time to ignition, implying that DOPO does not delay combustion. On a side note, R-Pol_Z also exhibits similar fire performances that its pristine counterpart, once again showing that recycling does not affect the performances of the materials.

On 3mm thickness samples, the effect of the DOPO-containing compound is also more significant, with a 31% decrease of pHRR observed for Pol_Z, while THR is reduced by 23%. Once again, TTI is not affected by the presence of DOPO. Interestingly, when MLC experiments are conducted on 3mm-thickness samples, overall pHRR values decrease significantly for both compounds. The investigation of thermally thicker samples also leads to an increase of the time to ignition, roughly doubled in our case compared to 1.5mm thickness samples (TTI of 56s vs 33s). The investigation of thermally thin samples can lead to more than just a decrease in the time to ignition and an influence on the peak of heat release^{281,282}. It may also result in significant mechanistic changes. Indeed, char yield residue is higher for thicker samples, implying that DOPO has a higher solid phase action. It is important to acknowledge that the heat flux applied to the surface of the sample during the cone calorimeter test may have varied due to sample swelling, resulting in a different thermal load than initially intended. Unfortunately, this parameter was not taken into consideration in the current study.



Figure 136 : Pictures of residue char for 3mm Novolac (left) and Polyphlox (left) after MLC test.

Pictures of the residual char after MLC tests are presented in Figure 136. During the test, after opening the shutter, the vitrimer plates swelled significantly due to the accumulations of decomposition gazes, until the char structure breaks up. Apart from the obvious color change, the residue of N_z is composed of a very delicate, three-dimensional, cellular structure, while the Pol_z residue (as well as the DOPO residue), exhibited a thicker structure and a higher mechanical resistance. Li et al.⁴² conducted SEM images on a similar DOPO-epoxy flame-retarded system, and observed that their char framework becomes more dense and cohesive with increasing amounts of DOPO. This suggests that the incorporation of DOPO into the material can create a safeguarding layer that can postpone the release of heat during combustion. This effect is however significantly reduced in our case, as yield residue only increased by up to a third in the presence of DOPO due to the low thickness of the sample (3mm).

4.4.5 Conclusion

The comparison between the addition of DOPO in an additive or a reactive way during the synthesis of a Novolac-epoxy vitrimer network has provided valuable insights into the material's properties and performance. The results demonstrate that when DOPO is added as an additive, its reactivity with the epoxies competes with the epoxy-acid esterification, leading to a hindered ester formation and a reduced potential for transesterification. In contrast, when DOPO is already bonded to the epoxy resin before curing, a sufficient amount of ester is formed, facilitating the total relaxation of the network. This reactive addition of DOPO results in a stiffer network and improved mechanical properties, including increased elongation at break, higher Young's modulus, and stress at break compared to the reference Novolac sample. On the other hand, the addition of DOPO as an additive resulted in poor mechanical performance. Interestingly, no significant difference was observed in term of flame-retardancy behavior between both methods, as similar degradation patterns were observed through ATG and cone calorimeter analysis. Importantly, all the material's performances, including chemical, mechanical and fire behavior were retained even after recycling, highlighting the promising potential for sustainable applications of these vitrimer networks.

4.5 Conclusion

The synthesis of flame-retarded epoxy-based vitrimer through an additive approach is the next step toward commercial relevancy for this new category of materials. We successfully synthesized a vitrimer coating a standard intumescent formulation. Promising flame-retardancy and metallic plate shielding performances were obtained without affecting recyclability. Then, we investigated the effect of a highly flame-retardant (DOPO) either added already bonded to the epoxy (reactive approach), or added in the monomer mixture before curing (additive approach). We demonstrated that through the additive approach, DOPO was still keen to fastly react with the oxirane groups, depriving the material of available epoxies to form esters with the fatty acid. The obtained material was low densely cross-linked, mechanically weak, recyclable but unable to efficiently relax stress. On the other hand, synthesizing a DOPO-flame-retarded material through the reactive approach showed better mechanical and fire performances compared to pristine materials without sacrificing the ability to relax stress. However, both materials exhibited similar fire performances. These results offer a starting point for considering the relevance of adding flame-retardant fillers to highly cross-linked vitrimer materials, considering that the reactivity of these fillers plays a crucial role in the synthesis of the materials, being more important than the quantity of filler added.

General conclusion

The primary idea behind the development of this thesis topic originated from the perceived lack of academic research interest in the flame-retardant properties of vitrimer materials. Recognizing the immense potential of combining flame-retardant capabilities with the dynamic and recyclable nature of vitrimers, this study aimed to address fire safety concerns while promoting the recycling and reprocessing of this class of materials. Indeed, to fully capitalize on the advantages and potential applications of flame-retardant vitrimer systems, further exploration and understanding are crucial. When considering flame retardancy achieved through the addition of flame retardant additives, a multitude of effects have to be taken into account. These effects were investigated and analyzed in this study.

Based on the literature review, transesterification is the most common bond-exchange reaction found in vitrimers thanks to the availability of numerous catalyst specifically designed for these reactions, as well as the widespread demand for tuning thermoset epoxy resins, for which esters are usually involved, into recyclable networks. Poly(butylene terephthalate) and epoxy-acid systems were selected as the materials of choice for this study due to their well-documented synthesis procedures and extensive literature reporting their properties and applications.

The first challenge consisted in proposing an efficient flame-retarded PBT system. To do so, the formation of a cross-linked vitrimer in the presence of flame-retardant additives was studied. Three commercial flame-retardants, aluminum phosphinate (AlPi), zinc phosphinate (ZnPi), and a polyphosphonate (HM1100), were incorporated into a vitrimer system composed of a commercial PBT, a diepoxy (DGEBA), and a transesterification catalyst ($\text{Zn}(\text{acac})_2$). It was found that the addition of 20wt.-% AlPi during the vitrimer synthesis did not affect its formation, resulting in a similar crosslinked fraction compared to pristine PBT-vitrimer. Microscopy and NMR analyses conducted on the insoluble phase of the material revealed that a fraction of the AlPi was homogeneously diluted inside the matrix. The addition of ZnPi at 10 or 24 wt.-%, however, was detrimental to the network formation, resulting in a decreased gel fraction. The gel fraction mainly contained diethylphosphinic acid instead of phosphinates, which implied that the chemical environment around the Phosphorus and Zinc was modified. The addition of HM1100 to the system using standard epoxy/catalyst proportions led to a compatibilization between the FR and PBT matrix, possibly linked with the formation of a PBT-Epoxy-HM1100 or PBT-HM1100 copolymer. However, significant gel fractions could only be obtained by increasing the amount of epoxy and catalyst.

Stress-relaxation experiments showed that the relaxation behavior of the materials deviated from the classic Maxwell model and instead followed a Kohlrausch-Williams-Watts model. The presence of AlPi or ZnPi indicated vitrimer behavior, while the HM1100-filled formulation did not display a clear Arrhenius-type tendency. All cross-linked materials exhibited lower crystallinity and a single melting peak compared to their thermoplastic counterparts but retained the α -crystalline structure of pristine PBT. TGA experiments did not show significant differences in degradation behavior compared to thermoplastic equivalents.

The aluminum-filled PBT vitrimer presented the best vitrimer performances and could be effectively synthesized without the need for any transesterification catalyst. The material kept similar thermal characteristics and kept significantly higher bond-exchanges rates compared to the pristine vitrimer, with relaxation times two decades shorter than PBT-vitrimers catalyzed with commonly used zinc or aluminum-based catalysts. The vitrimer demonstrated a decrease in creep resistance under temporary overheating above the melting point compared to the pristine vitrimer equivalent, but exhibited minimal creep when processed through injection. Mechanical testing showed that AlPi-filled vitrimers had better mechanical performance and rigidity compared to thermoplastic equivalents. The vitrimer specimens deformed uniformly without necking, indicating even strain distribution across the entire specimen near the melting point. Flame-retardancy classification (V-0 or V-2) of the vitrimer material did not differ significantly from the thermoplastic reference, but the vitrimer exhibited lower dripping behavior due to its higher melt viscosity. Upon aging, a decrease in gel fraction was observed for the vitrimer, particularly during water aging, attributed to chain breakage and de-crosslinking. However, the vitrimer retained its behavior and did not flow upon burning, while PBT showed increased dripping behavior. The dynamic structure of the cross-linked system allowed for the reshuffling of reticulation nodes, leading to better redistribution between aged and unaged polymeric chains. The lower viscosity provided by the AlPi catalyst lead was put into consideration for upscaling the vitrimer synthesis process through continuous reactive extrusion. A material with significant gel ratios (42wt.-%) at low feeding rates was obtained without risking damage to the extruder.

Finally, a recyclable epoxy resin coating was successfully developed using a standard intumescent formulation, achieving promising flame-retardant and metallic plate shielding performances while maintaining recyclability. Also, the pertinence of DOPO added through additive or reactive approach was assessed. DOPO as an additive readily reacts with the oxirane groups, depleting the available epoxies needed to form esters with the fatty acid. This resulted in a material with lower cross-link density, reduced mechanical strength, recyclability, and limited stress relaxation capability. In contrast, synthesizing a DOPO-flame-retarded material through the reactive approach demonstrated improved mechanical and fire performance compared to pristine materials, while retaining the ability to relax stress. However, both materials exhibited similar fire performance. These findings provide a starting point for considering the significance of incorporating flame-retardant fillers into highly cross-linked vitrimer materials. The reactivity of these fillers is of paramount importance in material synthesis, surpassing the mere quantity of filler added.

Overall, during this PhD work, it was shown that the investigation of reactive mechanisms between the added flame-retardant and vitrimer system is primordial in the comprehension of the network formation and performances. This research sets the foundation for future advancements and has the potential to classify the reactivity of fillers for each specific bond-exchange reaction that occur within vitrimers. Thus, in the future, various types of multi-functional fillers can be added judiciously to these systems.

In the case of PBT vitrimer, more studies should be led to assess the incorporation of glass fiber into the flame-retarded polymer and to see if glass fiber plays an antagonistic effect on cross-linking and relaxation behavior. Preliminary tests of reactive extrusion with glass fibers were inconclusive due to fiber degradation. However, the continuous extrusion process could be more fiber-friendly, allowing for their preservation.

References

- (1) OECD. *Global Plastics Outlook: Policy Scenarios to 2060*; OECD, 2022. <https://doi.org/10.1787/aa1edf33-en>.
- (2) Agarwal, S.; Gupta, R. K. Chapter 8 - The Use of Thermosets in the Building and Construction Industry. In *Thermosets (Second Edition)*; Guo, Q., Ed.; Elsevier, 2018; pp 279–302. <https://doi.org/10.1016/B978-0-08-101021-1.00008-3>.
- (3) Hamerton, I.; Kratz, J. Chapter 9 - The Use of Thermosets in Modern Aerospace Applications. In *Thermosets (Second Edition)*; Guo, Q., Ed.; Elsevier, 2018; pp 303–340. <https://doi.org/10.1016/B978-0-08-101021-1.00009-5>.
- (4) Montarnal, D.; Capelot, M.; Tournilhac, F.; Leibler, L. Silica-Like Malleable Materials from Permanent Organic Networks. *Science* **2011**, *334* (6058), 965–968. <https://doi.org/10.1126/science.1212648>.
- (5) Demongeot, A.; Groote, R.; Goossens, H.; Hoeks, T.; Tournilhac, F.; Leibler, L. Cross-Linking of Poly(Butylene Terephthalate) by Reactive Extrusion Using Zn(II) Epoxy-Vitrimer Chemistry. *Macromolecules* **2017**, *50* (16), 6117–6127. <https://doi.org/10.1021/acs.macromol.7b01141>.
- (6) Alabiso, W.; Schlögl, S. The Impact of Vitrimers on the Industry of the Future: Chemistry, Properties and Sustainable Forward-Looking Applications. *Polymers (Basel)* **2020**, *12* (8), 1660. <https://doi.org/10.3390/polym12081660>.
- (7) Pickering, S. J. Recycling Technologies for Thermoset Composite Materials—Current Status. *Composites Part A: Applied Science and Manufacturing* **2006**, *37* (8), 1206–1215. <https://doi.org/10.1016/j.compositesa.2005.05.030>.
- (8) Jiang, G.; Pickering, S. J.; Walker, G. S.; Bowering, N.; Wong, K. H.; Rudd, C. D. Soft Ionisation Analysis of Evolved Gas for Oxidative Decomposition of an Epoxy Resin/Carbon Fibre Composite. *Thermochimica Acta* **2007**, *454* (2), 109–115. <https://doi.org/10.1016/j.tca.2007.01.003>.
- (9) Piñero-Hernanz, R.; Dodds, C.; Hyde, J.; García-Serna, J.; Poliakoff, M.; Lester, E.; Cocero, M. J.; Kingman, S.; Pickering, S.; Wong, K. H. Chemical Recycling of Carbon Fibre Reinforced Composites in Nearcritical and Supercritical Water. *Composites Part A: Applied Science and Manufacturing* **2008**, *39* (3), 454–461. <https://doi.org/10.1016/j.compositesa.2008.01.001>.
- (10) Liu, Y.; Meng, L.; Huang, Y.; Du, J. Recycling of Carbon/Epoxy Composites. *Journal of Applied Polymer Science* **2004**, *94* (5), 1912–1916. <https://doi.org/10.1002/app.20990>.
- (11) McBride, M. K.; Worrell, B. T.; Brown, T.; Cox, L. M.; Sowan, N.; Wang, C.; Podgorski, M.; Martinez, A. M.; Bowman, C. N. Enabling Applications of Covalent Adaptable Networks. *Annu. Rev. Chem. Biomol. Eng.* **2019**, *10* (1), 175–198. <https://doi.org/10.1146/annurev-chembioeng-060718-030217>.
- (12) Brassinne, J.; Cadix, A.; Wilson, J.; van Ruymbek, E. Dissociating Sticker Dynamics from Chain Relaxation in Supramolecular Polymer Networks—The Importance of Free Partner! *Journal of Rheology* **2017**, *61* (6), 1123–1134. <https://doi.org/10.1122/1.4997594>.
- (13) Khan, A.; Ahmed, N.; Rabnawaz, M. Covalent Adaptable Network and Self-Healing Materials: Current Trends and Future Prospects in Sustainability. *Polymers* **2020**, *12* (9), 2027. <https://doi.org/10.3390/polym12092027>.
- (14) Adzima, B. J.; Aguirre, H. A.; Kloxin, C. J.; Scott, T. F.; Bowman, C. N. Rheological and Chemical Analysis of Reverse Gelation in a Covalently Cross-Linked Diels–Alder Polymer Network. *Macromolecules* **2008**, *41* (23), 9112–9117. <https://doi.org/10.1021/ma801863d>.
- (15) Elling, B. R.; Dichtel, W. R. Reprocessable Cross-Linked Polymer Networks: Are Associative Exchange Mechanisms Desirable? *ACS Cent. Sci.* **2020**, *6* (9), 1488–1496. <https://doi.org/10.1021/acscentsci.0c00567>.
- (16) Krishnakumar, B.; Sanka, R. V. S. P.; Binder, W. H.; Parthasarthy, V.; Rana, S.; Karak, N. Vitrimers: Associative Dynamic Covalent Adaptive Networks in Thermoset Polymers. *Chemical Engineering Journal* **2020**, *385*, 123820. <https://doi.org/10.1016/j.cej.2019.123820>.
- (17) Obadia, M. M.; Mudraboyina, B. P.; Serghei, A.; Montarnal, D.; Drockenmüller, E. Reprocessing and Recycling of Highly Cross-Linked Ion-Conducting Networks through Transalkylation Exchanges of C–N Bonds. *J. Am. Chem. Soc.* **2015**, *137* (18), 6078–6083. <https://doi.org/10.1021/jacs.5b02653>.

- (18) Luzuriaga, A. R. de; Martin, R.; Markaide, N.; Rekondo, A.; Cabañero, G.; Rodríguez, J.; Odriozola, I. Epoxy Resin with Exchangeable Disulfide Crosslinks to Obtain Reprocessable, Repairable and Recyclable Fiber-Reinforced Thermoset Composites. *Mater. Horiz.* **2016**, *3* (3), 241–247. <https://doi.org/10.1039/C6MH00029K>.
- (19) Cuminet, F.; Caillol, S.; Dantras, É.; Leclerc, É.; Ladmiral, V. Neighboring Group Participation and Internal Catalysis Effects on Exchangeable Covalent Bonds: Application to the Thriving Field of Vitriemer Chemistry. *Macromolecules* **2021**, *54* (9), 3927–3961. <https://doi.org/10.1021/acs.macromol.0c02706>.
- (20) Kaiser, S.; Novak, P.; Giebler, M.; Gschwandl, M.; Novak, P.; Pilz, G.; Morak, M.; Schlögl, S. The Crucial Role of External Force in the Estimation of the Topology Freezing Transition Temperature of Vitrimers by Elongational Creep Measurements. *Polymer* **2020**, *204*, 122804. <https://doi.org/10.1016/j.polymer.2020.122804>.
- (21) Hubbard, A. M.; Ren, Y.; Konkolewicz, D.; Sarvestani, A.; Picu, C. R.; Kedziora, G. S.; Roy, A.; Varshney, V.; Nepal, D. Vitriemer Transition Temperature Identification: Coupling Various Thermomechanical Methodologies. *ACS Appl. Polym. Mater.* **2021**, *3* (4), 1756–1766. <https://doi.org/10.1021/acsapm.0c01290>.
- (22) Capelot, M.; Unterlass, M. M.; Tournilhac, F.; Leibler, L. Catalytic Control of the Vitriemer Glass Transition. *ACS Macro Letters* **2012**, *1* (7), 789–792. <https://doi.org/10.1021/mz300239f>.
- (23) Denissen, W.; Winne, J. M.; Du Prez, F. E. Vitrimers: Permanent Organic Networks with Glass-like Fluidity. *Chemical Science* **2016**, *7* (1), 30–38. <https://doi.org/10.1039/c5sc02223a>.
- (24) Chen, M.; Zhou, L.; Wu, Y.; Zhao, X.; Zhang, Y. Rapid Stress Relaxation and Moderate Temperature of Malleability Enabled by the Synergy of Disulfide Metathesis and Carboxylate Transesterification in Epoxy Vitrimers. *ACS Macro Letters* **2019**, *8* (3), 255–260. <https://doi.org/10.1021/acsmacrolett.9b00015>.
- (25) Zhang, L.; Rowan, S. J. Effect of Sterics and Degree of Cross-Linking on the Mechanical Properties of Dynamic Poly(Alkylurea–Urethane) Networks. *Macromolecules* **2017**, *50* (13), 5051–5060. <https://doi.org/10.1021/acs.macromol.7b01016>.
- (26) Hendriks, B.; Waelkens, J.; Winne, J. M.; Du Prez, F. E. Poly(Thioether) Vitrimers via Transalkylation of Trialkylsulfonium Salts. *ACS Macro Letters* **2017**, *6* (9), 930–934. <https://doi.org/10.1021/acsmacrolett.7b00494>.
- (27) Huang, L.; Yang, Y.; Niu, Z.; Wu, R.; Fan, W.; Dai, Q.; He, J.; Bai, C. Catalyst-Free Vitriemer Cross-Linked by Biomass-Derived Compounds with Mechanical Robustness, Reprocessability, and Multishape Memory Effects. *Macromolecular Rapid Communications* **2021**, *42* (21), 2100432. <https://doi.org/10.1002/marc.202100432>.
- (28) Yang, Y.; Zhang, S.; Zhang, X.; Gao, L.; Wei, Y.; Ji, Y. Detecting Topology Freezing Transition Temperature of Vitrimers by AIE Luminogens. *Nat Commun* **2019**, *10* (1), 3165. <https://doi.org/10.1038/s41467-019-11144-6>.
- (29) Denissen, W.; De Baere, I.; Van Paepegem, W.; Leibler, L.; Winne, J.; Du Prez, F. E. Vinylogous Urea Vitrimers and Their Application in Fiber Reinforced Composites. *Macromolecules* **2018**, *51* (5), 2054–2064. <https://doi.org/10.1021/acs.macromol.7b02407>.
- (30) Denissen, W.; Rivero, G.; Nicolay, R.; Leibler, L.; Winne, J. M.; Du Prez, F. E. Vinylogous Urethane Vitrimers. *Adv. Funct. Mater.* **2015**, *25* (16), 2451–2457. <https://doi.org/10.1002/adfm.201404553>.
- (31) Zheng, N.; Hou, J.; Xu, Y.; Fang, Z.; Zou, W.; Zhao, Q.; Xie, T. Catalyst-Free Thermoset Polyurethane with Permanent Shape Reconfigurability and Highly Tunable Triple-Shape Memory Performance. *ACS Macro Lett.* **2017**, *6* (4), 326–330. <https://doi.org/10.1021/acsmacrolett.7b00037>.
- (32) Williams, M. L.; Landel, R. F.; Ferry, J. D. The Temperature Dependence of Relaxation Mechanisms in Amorphous Polymers and Other Glass-Forming Liquids. *J. Am. Chem. Soc.* **1955**, *77* (14), 3701–3707. <https://doi.org/10.1021/ja01619a008>.
- (33) Roylance, D. ENGINEERING VISCOELASTICITY. 37.
- (34) Zhou, Y.; Goossens, J. G. P.; Sijbesma, R. P.; Heuts, J. P. A. Poly(Butylene Terephthalate)/Glycerol-Based Vitrimers via Solid-State Polymerization. *Macromolecules* **2017**, *50* (17), 6742–6751. <https://doi.org/10.1021/acs.macromol.7b01142>.

- (35) Legrand, A.; Soulié-Ziakovic, C. Silica-Epoxy Vitrimer Nanocomposites. *Macromolecules* **2016**, *49* (16), 5893–5902. <https://doi.org/10.1021/acs.macromol.6b00826>.
- (36) Capelot, M.; Montarnal, D.; Tournilhac, F.; Leibler, L. Metal-Catalyzed Transesterification for Healing and Assembling of Thermosets. *J. Am. Chem. Soc.* **2012**, *134* (18), 7664–7667. <https://doi.org/10.1021/ja302894k>.
- (37) Lu, L.; Pan, J.; Li, G. Recyclable High-Performance Epoxy Based on Transesterification Reaction. *J. Mater. Chem. A* **2017**, *5* (40), 21505–21513. <https://doi.org/10.1039/C7TA06397K>.
- (38) Huang, J.; Zhang, L.; Tang, Z.; Wu, S.; Guo, B. Reprocessable and Robust Crosslinked Elastomers via Interfacial CN Transalkylation of Pyridinium. *Composites Science and Technology* **2018**, *168*, 320–326. <https://doi.org/10.1016/j.compscitech.2018.10.017>.
- (39) Yan, P.; Zhao, W.; Fu, X.; Liu, Z.; Kong, W.; Zhou, C.; Lei, J. Multifunctional Polyurethane-Vitrimers Completely Based on Transcarbamoylation of Carbamates: Thermally-Induced Dual-Shape Memory Effect and Self-Welding. *RSC Adv.* **2017**, *7* (43), 26858–26866. <https://doi.org/10.1039/C7RA01711A>.
- (40) Bakkali-Hassani, C.; Berne, D.; Admiral, V.; Caillol, S. Transcarbamoylation in Polyurethanes: Underestimated Exchange Reactions? *Macromolecules* **2022**. <https://doi.org/10.1021/acs.macromol.2c01184>.
- (41) Black, S. P.; Sanders, J. K. M.; Stefankiewicz, A. R. Disulfide Exchange: Exposing Supramolecular Reactivity through Dynamic Covalent Chemistry. *Chem. Soc. Rev.* **2014**, *43* (6), 1861–1872. <https://doi.org/10.1039/C3CS60326A>.
- (42) Li, X.; Zhang, J.; Zhang, L.; Ruiz de Luzuriaga, A.; Rekondo, A.; Wang, D.-Y. Recyclable Flame-Retardant Epoxy Composites Based on Disulfide Bonds: Flammability and Recyclability. *Composites Communications* **2021**, *25*, 100754. <https://doi.org/10.1016/j.coco.2021.100754>.
- (43) Lyon, G. B.; Cox, L. M.; Goodrich, J. T.; Baranek, A. D.; Ding, Y.; Bowman, C. N. Remoldable Thiol–Ene Vitrimers for Photopatterning and Nanoimprint Lithography. *Macromolecules* **2016**, *49* (23), 8905–8913. <https://doi.org/10.1021/acs.macromol.6b01281>.
- (44) Denissen, W.; Droesbeke, M.; Nicola, R.; Leibler, L.; Winne, J. M.; Du Prez, F. E. Chemical Control of the Viscoelastic Properties of Vinyllogous Urethane Vitrimers. *Nature Communications* **2017**, *8*. <https://doi.org/10.1038/ncomms14857>.
- (45) Taplan, C.; Guerre, M.; Winne, J. M.; Du Prez, F. E. Fast Processing of Highly Crosslinked, Low-Viscosity Vitrimers. *Materials Horizons* **2020**, *7* (1), 104–110. <https://doi.org/10.1039/c9mh01062a>.
- (46) Zhang, X.; Eichen, Y.; Miao, Z.; Zhang, S.; Cai, Q.; Liu, W.; Zhao, J.; Wu, Z. Novel Phosphazene-Based Flame Retardant Polyimine Vitrimers with Monomer-Recovery and High Performances. *Chemical Engineering Journal* **2022**, *440*, 135806. <https://doi.org/10.1016/j.cej.2022.135806>.
- (47) Lei, X.; Jin, Y.; Sun, H.; Zhang, W. Rehealable Imide–Imine Hybrid Polymers with Full Recyclability. *J. Mater. Chem. A* **2017**, *5* (40), 21140–21145. <https://doi.org/10.1039/C7TA07076D>.
- (48) Zhang, X.; Akram, R.; Zhang, S.; Ma, H.; Wu, Z.; Wu, D. Hexa(Eugenol)Cyclotriphosphazene Modified Bismaleimide Resins with Unique Thermal Stability and Flame Retardancy. *Reactive and Functional Polymers* **2017**, *113*, 77–84. <https://doi.org/10.1016/j.reactfunctpolym.2017.02.010>.
- (49) Zheng, P.; McCarthy, T. J. A Surprise from 1954: Siloxane Equilibration Is a Simple, Robust, and Obvious Polymer Self-Healing Mechanism. *J. Am. Chem. Soc.* **2012**, *134* (4), 2024–2027. <https://doi.org/10.1021/ja2113257>.
- (50) Schmolke, W.; Perner, N.; Seiffert, S. Dynamically Cross-Linked Polydimethylsiloxane Networks with Ambient-Temperature Self-Healing. *Macromolecules* **2015**, *48* (24), 8781–8788. <https://doi.org/10.1021/acs.macromol.5b01666>.
- (51) Wu, Y.; Yang, Y.; Qian, X.; Chen, Q.; Wei, Y.; Ji, Y. Liquid-Crystalline Soft Actuators with Switchable Thermal Reprogrammability. *Angewandte Chemie International Edition* **2020**, *59* (12), 4778–4784. <https://doi.org/10.1002/anie.201915694>.

- (52) Nishimura, Y.; Chung, J.; Muradyan, H.; Guan, Z. Silyl Ether as a Robust and Thermally Stable Dynamic Covalent Motif for Malleable Polymer Design. *J. Am. Chem. Soc.* **2017**, *139* (42), 14881–14884. <https://doi.org/10.1021/jacs.7b08826>.
- (53) Zych, A.; Pinalli, R.; Soliman, M.; Vachon, J.; Dalcanale, E. Polyethylene Vitrimers via Silyl Ether Exchange Reaction. *Polymer* **2020**, *199*. <https://doi.org/10.1016/j.polymer.2020.122567>.
- (54) Röttger, M.; Domenech, T.; Van Der Weegen, R.; Breuillac, A.; Nicolaÿ, R.; Leibler, L. High-Performance Vitrimers from Commodity Thermoplastics through Dioxaborolane Metathesis. *Science* **2017**, *356* (6333), 62–65. <https://doi.org/10.1126/science.aah5281>.
- (55) Breuillac, A.; Kassalias, A.; Nicolaÿ, R. Polybutadiene Vitrimers Based on Dioxaborolane Chemistry and Dual Networks with Static and Dynamic Cross-Links. *Macromolecules* **2019**, *52* (18), 7102–7113. <https://doi.org/10.1021/acs.macromol.9b01288>.
- (56) Caffy, F.; Nicolaÿ, R. Transformation of Polyethylene into a Vitramer by Nitroxide Radical Coupling of a Bis-Dioxaborolane. *Polymer Chemistry* **2019**, *10* (23), 3107–3115. <https://doi.org/10.1039/c9py00253g>.
- (57) Lu, Y.-X.; Guan, Z. Olefin Metathesis for Effective Polymer Healing via Dynamic Exchange of Strong Carbon-Carbon Double Bonds. *Journal of the American Chemical Society* **2012**, *134* (34), 14226–14231. <https://doi.org/10.1021/ja306287s>.
- (58) Lu, Y.-X.; Tournilhac, F.; Leibler, L.; Guan, Z. Making Insoluble Polymer Networks Malleable via Olefin Metathesis. *J. Am. Chem. Soc.* **2012**, *134* (20), 8424–8427. <https://doi.org/10.1021/ja303356z>.
- (59) Qiu, J.; Ma, S.; Wang, S.; Tang, Z.; Li, Q.; Tian, A.; Xu, X.; Wang, B.; Lu, N.; Zhu, J. Upcycling of Polyethylene Terephthalate to Continuously Reprocessable Vitrimers through Reactive Extrusion. *Macromolecules* **2021**, *54* (2), 703–712. <https://doi.org/10.1021/acs.macromol.0c02359>.
- (60) Brutman, J. P.; Delgado, P. A.; Hillmyer, M. A. Polylactide Vitrimers. *ACS Macro Letters* **2014**, *3* (7), 607–610. <https://doi.org/10.1021/mz500269w>.
- (61) Yin, Y.; Yang, J.; Meng, L. Preparation of Poly(Butylene Succinate) Vitramer with Thermal Shape Stability via Transesterification Reaction. *Journal of Applied Polymer Science* **2021**, *138* (39), 51010. <https://doi.org/10.1002/app.51010>.
- (62) Kar, G. P.; Saed, M. O.; Terentjev, E. M. Scalable Upcycling of Thermoplastic Polyolefins into Vitrimers through Transesterification. *J. Mater. Chem. A* **2020**, *8* (45), 24137–24147. <https://doi.org/10.1039/D0TA07339C>.
- (63) Chen, J.-H.; Lu, J.-H.; Pu, X.-L.; Chen, L.; Wang, Y.-Z. Recyclable, Malleable and Intrinsically Flame-Retardant Epoxy Resin with Catalytic Transesterification. *Chemosphere* **2022**, *294*, 133778. <https://doi.org/10.1016/j.chemosphere.2022.133778>.
- (64) Legrand, A. Nanocharges fonctionnelles pour Vitrimères et Catalyse. Chimie-Physique [physics.chem-ph]. Université Pierre et Marie Curie - Paris VI, 2016. Français. . NNT : 2016PA066427., 2016.
- (65) Builes Cárdenas, C.; Gayraud, V.; Rodriguez, M. E.; Costa, J.; Salaberria, A. M.; Ruiz de Luzuriaga, A.; Markaide, N.; Dasan Keeryadath, P.; Calderón Zapatería, D. Study into the Mechanical Properties of a New Aeronautic-Grade Epoxy-Based Carbon-Fiber-Reinforced Vitramer. *Polymers* **2022**, *14* (6), 1223. <https://doi.org/10.3390/polym14061223>.
- (66) Yue, L.; Guo, H.; Kennedy, A.; Patel, A.; Gong, X.; Ju, T.; Gray, T.; Manas-Zloczower, I. Vitramerization: Converting Thermoset Polymers into Vitrimers. *ACS Macro Lett.* **2020**, *9* (6), 836–842. <https://doi.org/10.1021/acsmacrolett.0c00299>.
- (67) Ji, F.; Liu, X.; Lin, C.; Zhou, Y.; Dong, L.; Xu, S.; Sheng, D.; Yang, Y. Reprocessable and Recyclable Crosslinked Polyethylene with Triple Shape Memory Effect. *Macromolecular Materials and Engineering* **2019**, *304* (3), 1800528. <https://doi.org/10.1002/mame.201800528>.
- (68) *Estérification*. Techniques de l'Ingénieur. <http://www.techniques.ingenieur.fr/base-documentaire/42329210-procedes-industriels-de-base-en-chimie-et-petrochimie/download/j5800/esterification.html> (accessed 2022-05-09).
- (69) Delahaye, M.; Winne, J. M.; Du Prez, F. E. Internal Catalysis in Covalent Adaptable Networks: Phthalate Monoester Transesterification As a Versatile Dynamic Cross-Linking Chemistry. *J. Am. Chem. Soc.* **2019**, *141* (38), 15277–15287. <https://doi.org/10.1021/jacs.9b07269>.

- (70) Altuna, F. I.; Pettarin, V.; Williams, R. J. J. Self-Healable Polymer Networks Based on the Cross-Linking of Epoxidised Soybean Oil by an Aqueous Citric Acid Solution. *Green Chem.* **2013**, *15* (12), 3360–3366. <https://doi.org/10.1039/C3GC41384E>.
- (71) Han, J.; Liu, T.; Hao, C.; Zhang, S.; Guo, B.; Zhang, J. A Catalyst-Free Epoxy Vitrimer System Based on Multifunctional Hyperbranched Polymer. *Macromolecules* **2018**, *51* (17), 6789–6799. <https://doi.org/10.1021/acs.macromol.8b01424>.
- (72) Han, J.; Liu, T.; Zhang, S.; Hao, C.; Xin, J.; Guo, B.; Zhang, J. Hyperbranched Polymer Assisted Curing and Repairing of an Epoxy Coating. *Industrial & Engineering Chemistry Research* **2019**. <https://doi.org/10.1021/acs.iecr.9b00800>.
- (73) Liu, T.; Zhang, S.; Hao, C.; Verdi, C.; Liu, W.; Liu, H.; Zhang, J. Glycerol Induced Catalyst-Free Curing of Epoxy and Vitrimer Preparation. *Macromolecular Rapid Communications* **2019**, *40* (7), 1800889. <https://doi.org/10.1002/marc.201800889>.
- (74) He, C.; Shi, S.; Wang, D.; Helms, B. A.; Russell, T. P. Poly(Oxime–Ester) Vitrimers with Catalyst-Free Bond Exchange. *J. Am. Chem. Soc.* **2019**, *141* (35), 13753–13757. <https://doi.org/10.1021/jacs.9b06668>.
- (75) Altuna, F. I.; Hoppe, C. E.; Williams, R. J. J. Epoxy Vitrimers with a Covalently Bonded Tertiary Amine as Catalyst of the Transesterification Reaction. *European Polymer Journal* **2019**, *113*, 297–304. <https://doi.org/10.1016/j.eurpolymj.2019.01.045>.
- (76) Hayashi, M. Dominant Factor of Bond-Exchange Rate for Catalyst-Free Polyester Vitrimers with Internal Tertiary Amine Moieties. *ACS Appl. Polym. Mater.* **2020**, *2* (12), 5365–5370. <https://doi.org/10.1021/acsapm.0c01099>.
- (77) Hayashi, M.; Inaba, T. Achievement of a Highly Rapid Bond Exchange for Self-Catalyzed Polyester Vitrimers by Incorporating Tertiary Amino Groups on the Network Strands. *ACS Appl. Polym. Mater.* **2021**, *3* (9), 4424–4429. <https://doi.org/10.1021/acsapm.1c00724>.
- (78) Delahaye, M.; Tanini, F.; Holloway, J. O.; Winne, J. M.; Prez, F. E. D. Double Neighbouring Group Participation for Ultrafast Exchange in Phthalate Monoester Networks. *Polym. Chem.* **2020**, *11* (32), 5207–5215. <https://doi.org/10.1039/D0PY00681E>.
- (79) Self, J. L.; Dolinski, N. D.; Zayas, M. S.; Read de Alaniz, J.; Bates, C. M. Brønsted-Acid-Catalyzed Exchange in Polyester Dynamic Covalent Networks. *ACS Macro Lett.* **2018**, *7* (7), 817–821. <https://doi.org/10.1021/acsmacrolett.8b00370>.
- (80) Tao, M.; Xue, L.; Sun, Z.; Wang, S.; Wang, X.; Shi, J. Tailoring the Synergistic Bronsted-Lewis Acidic Effects in Heteropolyacid Catalysts: Applied in Esterification and Transesterification Reactions. *Sci Rep* **2015**, *5* (1), 13764. <https://doi.org/10.1038/srep13764>.
- (81) Demongeot, A.; Mougner, S. J.; Okada, S.; Soulié-Ziakovic, C.; Tournilhac, F. Coordination and Catalysis of Zn²⁺ in Epoxy-Based Vitrimers. *Polym. Chem.* **2016**, *7* (27), 4486–4493. <https://doi.org/10.1039/C6PY00752J>.
- (82) De Hoe, G. X.; Zumstein, M. T.; Tiegs, B. J.; Brutman, J. P.; McNeill, K.; Sander, M.; Coates, G. W.; Hillmyer, M. A. Sustainable Polyester Elastomers from Lactones: Synthesis, Properties, and Enzymatic Hydrolyzability. *J. Am. Chem. Soc.* **2018**, *140* (3), 963–973. <https://doi.org/10.1021/jacs.7b10173>.
- (83) Kaiser, S.; Wurzer, S.; Pilz, G.; Kern, W.; Schlögl, S. Stress Relaxation and Thermally Adaptable Properties in Vitrimer-like Elastomers from HXNBR Rubber with Covalent Bonds. *Soft Matter* **2019**, *15* (30), 6062–6072. <https://doi.org/10.1039/C9SM00856J>.
- (84) Niu, X.; Wang, F.; Li, X.; Zhang, R.; Wu, Q.; Sun, P. Using Zn²⁺ Ionomer To Catalyze Transesterification Reaction in Epoxy Vitrimer. *Ind. Eng. Chem. Res.* **2019**, *58* (14), 5698–5706. <https://doi.org/10.1021/acs.iecr.9b00090>.
- (85) Guo, B.; Chan, C.-M. Chain Extension of Poly(Butylene Terephthalate) by Reactive Extrusion. *Journal of Applied Polymer Science* **1999**, *71* (11), 1827–1834. [https://doi.org/10.1002/\(SICI\)1097-4628\(19990314\)71:11<1827::AID-APP13>3.0.CO;2-7](https://doi.org/10.1002/(SICI)1097-4628(19990314)71:11<1827::AID-APP13>3.0.CO;2-7).
- (86) J. Kloxin, C.; N. Bowman, C. Covalent Adaptable Networks: Smart, Reconfigurable and Responsive Network Systems. *Chemical Society Reviews* **2013**, *42* (17), 7161–7173. <https://doi.org/10.1039/C3CS60046G>.
- (87) Zhou, Y.; Groote, R.; Goossens, J. G. P.; Sijbesma, R. P.; Heuts, J. P. A. Tuning PBT Vitrimer Properties by Controlling the Dynamics of the Adaptable Network. *Polymer Chemistry* **2019**, *10* (1), 136–144. <https://doi.org/10.1039/c8py01156g>.

- (88) Panagiotopoulos, C.; Porfyrus, A.; Korres, D.; Vouyiouka, S. Solid-State Polymerization as a Vitrimers Synthesis Tool Starting from Available Thermoplastics: The Effect of Reaction Temperature. *Materials* **2021**, *14* (1), 1–18. <https://doi.org/10.3390/ma14010009>.
- (89) Zhou, Y.; Goossens, J. G. P.; van den Bergen, S.; Sijbesma, R. P.; Heuts, J. P. A. In Situ Network Formation in PBT Vitrimers via Processing-Induced Deprotection Chemistry. *Macromolecular Rapid Communications* **2018**, *39* (19). <https://doi.org/10.1002/marc.201800356>.
- (90) Chen, J.-H.; An, X.-P.; Li, Y.-D.; Wang, M.; Zeng, J.-B. Reprocessible Epoxy Networks with Tunable Physical Properties: Synthesis, Stress Relaxation and Recyclability. *Chin J Polym Sci* **2018**, *36* (5), 641–648. <https://doi.org/10.1007/s10118-018-2027-9>.
- (91) Farge, L.; Hoppe, S.; Daujat, V.; Tournilhac, F.; Andre, S. Solid Rheological Properties of PBT-Based Vitrimers. *Macromolecules* **2021**, *54* (4), 1838–1849. <https://doi.org/10.1021/acs.macromol.0c02105>.
- (92) Farge, L.; Spiegel, R.; André, S.; Noûs, C.; Lainé, R.; Hoppe, S. Development of Plasticity in Vitrimers Synthesized from a Semi-Crystalline Polymer Using Injection Molding. *Journal of Polymer Science* **2022**, *60* (13), 1962–1975. <https://doi.org/10.1002/pol.20220062>.
- (93) Shechter, L.; Wynstra, J. Glycidyl Ether Reactions with Alcohols, Phenols, Carboxylic Acids, and Acid Anhydrides. *Ind. Eng. Chem.* **1956**, *48* (1), 86–93. <https://doi.org/10.1021/ie50553a028>.
- (94) Matějka, L.; Pokomý, S.; Dušek, K. Network Formation Involving Epoxide and Carboxyl Groups. *Polymer Bulletin* **1982**, *7* (2), 123–128. <https://doi.org/10.1007/BF00265462>.
- (95) Yu, K.; Taynton, P.; Zhang, W.; Dunn, M. L.; Qi, H. J. Reprocessing and Recycling of Thermosetting Polymers Based on Bond Exchange Reactions. *RSC Adv.* **2014**, *4* (20), 10108–10117. <https://doi.org/10.1039/C3RA47438K>.
- (96) Yang, H.; Yu, K.; Mu, X.; Wei, Y.; Guo, Y.; Qi, H. J. Molecular Dynamics Studying on Welding Behavior in Thermosetting Polymers Due to Bond Exchange Reactions. *RSC Adv.* **2016**, *6* (27), 22476–22487. <https://doi.org/10.1039/C5RA26128G>.
- (97) Yu, K.; Shi, Q.; Li, H.; Jabour, J.; Yang, H.; Dunn, M. L.; Wang, T.; Qi, H. J. Interfacial Welding of Dynamic Covalent Network Polymers. *Journal of the Mechanics and Physics of Solids* **2016**, *94*, 1–17. <https://doi.org/10.1016/j.jmps.2016.03.009>.
- (98) Yu, K.; Taynton, P.; Zhang, W.; Dunn, M. L.; Qi, H. J. Influence of Stoichiometry on the Glass Transition and Bond Exchange Reactions in Epoxy Thermoset Polymers. *RSC Adv.* **2014**, *4* (89), 48682–48690. <https://doi.org/10.1039/C4RA06543C>.
- (99) Liu, T.; Hao, C.; Wang, L.; Li, Y.; Liu, W.; Xin, J.; Zhang, J. Eugenol-Derived Biobased Epoxy: Shape Memory, Repairing, and Recyclability. *Macromolecules* **2017**, *50* (21), 8588–8597. <https://doi.org/10.1021/acs.macromol.7b01889>.
- (100) Yang, Y.; Urban, M. W. Self-Healing Polymeric Materials. *Chem. Soc. Rev.* **2013**, *42* (17), 7446. <https://doi.org/10.1039/c3cs60109a>.
- (101) Giebler, M.; Sperling, C.; Kaiser, S.; Duretek, I.; Schlögl, S. Epoxy-Anhydride Vitrimers from Aminoglycidyl Resins with High Glass Transition Temperature and Efficient Stress Relaxation. *Polymers* **2020**, *12* (5), 1148. <https://doi.org/10.3390/polym12051148>.
- (102) Liu, T.; Hao, C.; Zhang, S.; Yang, X.; Wang, L.; Han, J.; Li, Y.; Xin, J.; Zhang, J. A Self-Healable High Glass Transition Temperature Bioepoxy Material Based on Vitrimer Chemistry. *Macromolecules* **2018**, *51* (15), 5577–5585. <https://doi.org/10.1021/acs.macromol.8b01010>.
- (103) Huo, S.; Song, P.; Yu, B.; Ran, S.; Chevali, V. S.; Liu, L.; Fang, Z.; Wang, H. Phosphorus-Containing Flame Retardant Epoxy Thermosets: Recent Advances and Future Perspectives. *Progress in Polymer Science* **2021**, *114*, 101366. <https://doi.org/10.1016/j.progpolymsci.2021.101366>.
- (104) Laoutid, F.; Bonnaud, L.; Alexandre, M.; Lopez-Cuesta, J.-M.; Dubois, Ph. New Prospects in Flame Retardant Polymer Materials: From Fundamentals to Nanocomposites. *Materials Science and Engineering: R: Reports* **2009**, *63* (3), 100–125. <https://doi.org/10.1016/j.mser.2008.09.002>.
- (105) Alaei, M. An Overview of Commercially Used Brominated Flame Retardants, Their Applications, Their Use Patterns in Different Countries/Regions and Possible Modes of

- Release. *Environment International* **2003**, *29* (6), 683–689. [https://doi.org/10.1016/S0160-4120\(03\)00121-1](https://doi.org/10.1016/S0160-4120(03)00121-1).
- (106) Levchik, S. V.; Weil, E. D. Flame Retardancy of Thermoplastic Polyesters—a Review of the Recent Literature. *Polymer International* **2005**, *54* (1), 11–35. <https://doi.org/10.1002/pi.1663>.
- (107) Darnerud, P. O. Toxic Effects of Brominated Flame Retardants in Man and in Wildlife. *Environment International* **2003**, *29* (6), 841–853. [https://doi.org/10.1016/S0160-4120\(03\)00107-7](https://doi.org/10.1016/S0160-4120(03)00107-7).
- (108) Yang, H.; Song, L.; Tai, Q.; Wang, X.; Yu, B.; Yuan, Y.; Hu, Y.; Yuen, R. K. K. Comparative Study on the Flame Retarded Efficiency of Melamine Phosphate, Melamine Phosphite and Melamine Hypophosphite on Poly(Butylene Succinate) Composites. *Polymer Degradation and Stability* **2014**, *105*, 248–256. <https://doi.org/10.1016/j.polymdegradstab.2014.04.021>.
- (109) Köppl, T.; Brehme, S.; Pospiech, D.; Fischer, O.; Wolff-Fabris, F.; Altstädt, V.; Scharrel, B.; Döring, M. Influence of Polymeric Flame Retardants Based on Phosphorus-Containing Polyesters on Morphology and Material Characteristics of Poly(Butylene Terephthalate). *Journal of Applied Polymer Science* **2013**, *128* (5), 3315–3324. <https://doi.org/10.1002/app.38520>.
- (110) Könnicke, D.; Kühn, A.; Mahrholz, T.; Sinapius, M. Polymer Nanocomposites Based on Epoxy Resin and ATH as a New Flame Retardant for CFRP: Preparation and Thermal Characterisation. *J Mater Sci* **2011**, *46* (21), 7046–7055. <https://doi.org/10.1007/s10853-011-5673-7>.
- (111) Zhong, L.; Zhang, K.-X.; Wang, X.; Chen, M.-J.; Xin, F.; Liu, Z.-G. Synergistic Effects and Flame-Retardant Mechanism of Aluminum Diethyl Phosphinate in Combination with Melamine Polyphosphate and Aluminum Oxide in Epoxy Resin. *J Therm Anal Calorim* **2018**, *134* (3), 1637–1646. <https://doi.org/10.1007/s10973-018-7699-4>.
- (112) Shi, X.; Luo, S.; Du, X.; Li, Q.; Cheng, S. Improvement the Flame Retardancy and Thermal Conductivity of Epoxy Composites via Melamine Polyphosphate-Modified Carbon Nanotubes. *Polymers* **2022**, *14* (15), 3091. <https://doi.org/10.3390/polym14153091>.
- (113) Camino, G.; Costa, L.; Martinasso, G. Intumescent Fire-Retardant Systems. *Polymer Degradation and Stability* **1989**, *23* (4), 359–376. [https://doi.org/10.1016/0141-3910\(89\)90058-X](https://doi.org/10.1016/0141-3910(89)90058-X).
- (114) Puri, R. G.; Khanna, A. S. Intumescent Coatings: A Review on Recent Progress. *J Coat Technol Res* **2017**, *14* (1), 1–20. <https://doi.org/10.1007/s11998-016-9815-3>.
- (115) Feng, X.; Li, G. Versatile Phosphate Diester-Based Flame Retardant Vitrimers via Catalyst-Free Mixed Transesterification. *ACS Applied Materials and Interfaces* **2020**, *12* (51), 57486–57496. <https://doi.org/10.1021/acsami.0c18852>.
- (116) Zhou, L.; Zhang, G.; Feng, Y.; Zhang, H.; Li, J.; Shi, X. Design of a Self-Healing and Flame-Retardant Cyclotriphosphazene-Based Epoxy Vitrimer. *J Mater Sci* **2018**, *53* (9), 7030–7047. <https://doi.org/10.1007/s10853-018-2015-z>.
- (117) Mo, R.; Hu, J.; Huang, H.; Sheng, X.; Zhang, X. Tunable, Self-Healing and Corrosion Inhibiting Dynamic Epoxy–Polyimine Network Built by Post-Crosslinking. *J. Mater. Chem. A* **2019**, *7* (7), 3031–3038. <https://doi.org/10.1039/C8TA11546J>.
- (118) Taynton, P.; Yu, K.; Shoemaker, R. K.; Jin, Y.; Qi, H. J.; Zhang, W. Heat- or Water-Driven Malleability in a Highly Recyclable Covalent Network Polymer. *Advanced Materials* **2014**, *26* (23), 3938–3942. <https://doi.org/10.1002/adma.201400317>.
- (119) Liang, W.; Zhao, B.; Zhao, P.; Zhang, C.; Liu, Y. Bisphenol-S Bridged Penta(Anilino)Cyclotriphosphazene and Its Application in Epoxy Resins: Synthesis, Thermal Degradation, and Flame Retardancy. *Polymer Degradation and Stability* **2017**, *135*, 140–151. <https://doi.org/10.1016/j.polymdegradstab.2016.11.023>.
- (120) Yang, X.; Ke, Y.; Chen, Q.; Shen, L.; Xue, J.; Quirino, R. L.; Yan, Z.; Luo, Y.; Zhang, C. Efficient Transformation of Renewable Vanillin into Reprocessable, Acid-Degradable and Flame Retardant Polyimide Vitrimers. *Journal of Cleaner Production* **2022**, *333*, 130043. <https://doi.org/10.1016/j.jclepro.2021.130043>.
- (121) Lee, S.-H.; Shin, S.-R.; Lee, D.-S. Self-Healing of Cross-Linked PU via Dual-Dynamic Covalent Bonds of a Schiff Base from Cystine and Vanillin. *Materials & Design* **2019**, *172*, 107774. <https://doi.org/10.1016/j.matdes.2019.107774>.

- (122) Taynton, P.; Rubin, H.; MEYER, S.; Tobey, M.; Rognerud, E.; Sadowski, S. Vitrimers Containing Additives. US20220372273A1, November 24, 2022. <https://patents.google.com/patent/US20220372273A1/en?q=US20220372273> (accessed 2023-04-11).
- (123) Markwart, J. C.; Battig, A.; Urbaniak, T.; Haag, K.; Koschek, K.; Schartel, B.; Wurm, F. R. Intrinsic Flame Retardant Phosphonate-Based Vitrimers as a Recyclable Alternative for Commodity Polymers in Composite Materials. *Polymer Chemistry* **2020**, *11* (30), 4933–4941. <https://doi.org/10.1039/d0py00275e>.
- (124) Haag, K.; Deitschun, J.; Godlinski, D.; Zoellmer, V.; Koschek, K. On the Preservation of the Mechanical Integrity of Fiber Reinforced Composites with Integrated Functions; 2020.
- (125) Liu, Y.; Wang, B.; Ma, S.; Xu, X.; Qiu, J.; Li, Q.; Wang, S.; Lu, N.; Ye, J.; Zhu, J. Phosphate-Based Covalent Adaptable Networks with Recyclability and Flame Retardancy from Bioresources. *European Polymer Journal* **2021**, *144*, 110236. <https://doi.org/10.1016/j.eurpolymj.2020.110236>.
- (126) Feng, X.; Li, G. Catalyst-Free β -Hydroxy Phosphate Ester Exchange for Robust Fire-Proof Vitrimers. *Chemical Engineering Journal* **2021**, *417*, 129132. <https://doi.org/10.1016/j.cej.2021.129132>.
- (127) Wang, X.; Hu, Y.; Song, L.; Xing, W.; Lu, H.; Lv, P.; Jie, G. Flame Retardancy and Thermal Degradation Mechanism of Epoxy Resin Composites Based on a DOPO Substituted Organophosphorus Oligomer. *Polymer* **2010**, *51* (11), 2435–2445. <https://doi.org/10.1016/j.polymer.2010.03.053>.
- (128) Wu Klingler, W.; Rougier, V.; Huang, Z.; Parida, D.; Lehner, S.; Casutt, A.; Rentsch, D.; Hedlund, K. B.; Barandun, G. A.; Michaud, V.; Gaan, S. Recyclable Flame Retardant Phosphonated Epoxy Based Thermosets Enabled via a Reactive Approach. *Chemical Engineering Journal* **2023**, *466*, 143051. <https://doi.org/10.1016/j.cej.2023.143051>.
- (129) Ren, Q.-R.; Gu, S.; Liu, J.-H.; Wang, Y.-Z.; Chen, L. Catalyst-Free Reprocessable, Degradable and Intrinsically Flame-Retardant Epoxy Vitriimer for Carbon Fiber Reinforced Composites. *Polymer Degradation and Stability* **2023**, *211*, 110315. <https://doi.org/10.1016/j.polymdegradstab.2023.110315>.
- (130) Jin, S.; Qian, L.; Qiu, Y.; Chen, Y.; Xin, F. High-Efficiency Flame Retardant Behavior of Bi-DOPO Compound with Hydroxyl Group on Epoxy Resin. *Polymer Degradation and Stability* **2019**, *166*, 344–352. <https://doi.org/10.1016/j.polymdegradstab.2019.06.024>.
- (131) Chen, R.; Hu, K.; Tang, H.; Wang, J.; Zhu, F.; Zhou, H. A Novel Flame Retardant Derived from DOPO and Piperazine and Its Application in Epoxy Resin: Flame Retardance, Thermal Stability and Pyrolysis Behavior. *Polymer Degradation and Stability* **2019**, *166*, 334–343. <https://doi.org/10.1016/j.polymdegradstab.2019.06.011>.
- (132) Wu, Q.; Siqueira Curto Valle, R. de C.; Borges Valle, J. A.; Maesta Bezerra, F.; Meng, X.; Lis Arias, M. J. Recent Progress of DOPO-Containing Compounds as Flame Retardants for Versatile Polymeric Materials: Review. *World Journal of Textile Engineering and Technology* **2020**, *6*, 89–103. <https://doi.org/10.31437/2415-5489.2020.06.7>.
- (133) Wang, P.; Cai, Z. Highly Efficient Flame-Retardant Epoxy Resin with a Novel DOPO-Based Triazole Compound: Thermal Stability, Flame Retardancy and Mechanism. *Polymer Degradation and Stability* **2017**, *137*, 138–150. <https://doi.org/10.1016/j.polymdegradstab.2017.01.014>.
- (134) Zhang, L.; Wang, Q.; Jian, R.-K.; Wang, D.-Y. Bioinspired Iron-Loaded Polydopamine Nanospheres as Green Flame Retardants for Epoxy Resin via Free Radical Scavenging and Catalytic Charring. *J. Mater. Chem. A* **2020**, *8* (5), 2529–2538. <https://doi.org/10.1039/C9TA11021F>.
- (135) Goossens, J. G. P.; Kamps, J. H.; Van De Grampel, R. ENCAPSULATION OF FLAME RETARDANT AGENTS BY ATOMIC LAYER DEPOSITION FOR IMPROVED FLAME RETARDANT FORMULATIONS. EP4174124, May 3, 2023. <https://data.epo.org/publication-server/pdf-document/EP21205636NWA1.pdf?PN=EP4174124%20EP%204174124&iDocId=7102319&iepatch=.pdf> (accessed 2023-06-18).

- (136) Altuna, F.; Puig, J.; Hoppe, C. E.; Williams, R. J. J. REMOTE ACTUATION OF EPOXY NANOCOMPOSITES WITH FUNCTIONAL PROPERTIES. *An. Asoc. Quim. Argent.* **2018**, 22.
- (137) Yang, Y.; Pei, Z.; Zhang, X.; Tao, L.; Wei, Y.; Ji, Y. Carbon Nanotube-Vitrimer Composite for Facile and Efficient Photo-Welding of Epoxy. *Chemical Science* **2014**, 5 (9), 3486–3492. <https://doi.org/10.1039/c4sc00543k>.
- (138) Pei, Z.; Yang, Y.; Chen, Q.; Wei, Y.; Ji, Y. Regional Shape Control of Strategically Assembled Multishape Memory Vitrimers. *Adv. Mater.* **2016**, 28 (1), 156–160. <https://doi.org/10.1002/adma.201503789>.
- (139) Yang, Z.; Wang, Q.; Wang, T. Dual-Triggered and Thermally Reconfigurable Shape Memory Graphene-Vitrimer Composites. *ACS Appl. Mater. Interfaces* **2016**, 8 (33), 21691–21699. <https://doi.org/10.1021/acsami.6b07403>.
- (140) Poutrel, Q.-A.; Baghdadi, Y.; Souvignet, A.; Gresil, M. Graphene Functionalizations: Conserving Vitrimer Properties towards Nanoparticles Recovery Using Mild Dissolution. *Composites Science and Technology* **2021**, 216, 109072. <https://doi.org/10.1016/j.compscitech.2021.109072>.
- (141) Wang, Z.; Li, Z.; Wei, Y.; Ji, Y. Gold Nanospheres Dispersed Light Responsive Epoxy Vitrimers. *Polymers* **2018**, 10 (1), 65. <https://doi.org/10.3390/polym10010065>.
- (142) Vialle, G.; Prima, M. D.; Hocking, E.; Gall, K.; Garmestani, H.; Sanderson, T.; Arzberger, S. C. Remote Activation of Nanomagnetite Reinforced Shape Memory Polymer Foam. *Smart Mater. Struct.* **2009**, 18 (11), 115014. <https://doi.org/10.1088/0964-1726/18/11/115014>.
- (143) Puig, J.; Hoppe, C. E.; Fasce, L. A.; Pérez, C. J.; Piñeiro-Redondo, Y.; Bañobre-López, M.; López-Quintela, M. A.; Rivas, J.; Williams, R. J. J. Superparamagnetic Nanocomposites Based on the Dispersion of Oleic Acid-Stabilized Magnetite Nanoparticles in a Diglycidylether of Bisphenol A-Based Epoxy Matrix: Magnetic Hyperthermia and Shape Memory. *J. Phys. Chem. C* **2012**, 116 (24), 13421–13428. <https://doi.org/10.1021/jp3026754>.
- (144) Liu, Y.; Tang, Z.; Chen, Y.; Zhang, C.; Guo, B. Engineering of β -Hydroxyl Esters into Elastomer–Nanoparticle Interface toward Malleable, Robust, and Reprocessable Vitrimer Composites. *ACS Appl. Mater. Interfaces* **2018**, 10 (3), 2992–3001. <https://doi.org/10.1021/acsami.7b17465>.
- (145) Cusack, P. Novel Coated Fillers Enhance Flame-Retardant Properties. *Plastics, Additives and Compounding* **2007**, 9 (4), 26–29. [https://doi.org/10.1016/S1464-391X\(07\)70104-6](https://doi.org/10.1016/S1464-391X(07)70104-6).
- (146) Bartley, D. W.; Lawlor, T. J. Process for Making and Using Bisaryl Diphosphates. WO9835970A1, August 20, 1998.
- (147) Levchik, S. V.; Bright, D. A.; Alessio, G. R.; Dashevsky, S. Synergistic Action between Aryl Phosphates and Phenolic Resin in PBT. *Polymer Degradation and Stability* **2002**, 77 (2), 267–272. [https://doi.org/10.1016/S0141-3910\(02\)00058-7](https://doi.org/10.1016/S0141-3910(02)00058-7).
- (148) Mitschke, K.-H.; Schliebs, R. Production of High Viscosity Phosphoric and Phosphonic Acid Aryl Esters. US4212832A, July 15, 1980.
- (149) Klatt, M. D.; Gareis, B. D.; Yamamoto, M. Flammgeschützte Formmassen. DE19643280A1, April 23, 1998.
- (150) Klatt, M.; Heitz, T.; Gareiss, B. Flame-Proof Thermoplastic Moulding Materials. US6306941B1, October 23, 2001.
- (151) Van, D. S. P. a; Bos, M. L. M.; Roovers, W. a C.; Van, G. M.; Menting, H. N. a M. Halogen-Free Flame-Retardant Composition. US6767941B2, July 27, 2004.
- (152) Balabanovich, A. I.; Levchik, G. F.; Levchiky, S. V.; Engelmann, J. Fire Retardant Synergism Between Cyclic Diphosphonate Ester and Melamine in Poly(Butylene Terephthalate). *Journal of Fire Sciences* **2002**, 20 (1), 71–83. <https://doi.org/10.1177/0734904102020001201>.
- (153) Richardson, J.; Dellar, R. J. Flame Retardant Polymer Composition Containing Phosphonic Acid Salts. US4972011A, November 20, 1990.
- (154) Nass, B.; Wanzke, W. Synergistic Flameproofing Combination for Polymers. US6207736B1, March 27, 2001.
- (155) Jenewein, E.; Kleiner, H.-J.; Wanzke, W.; Budzinsky, W. Synergistic Flame Protection Agent Combination for Thermoplastic Polymers. US6365071B1, April 2, 2002.

- (156) Schlosser, E.; Nass, B.; Wanzke, W. Flame Retardant Combination for Thermoplastic Polymers I. US6547992B1, April 15, 2003.
- (157) Braun, U.; Schartel, B. Flame Retardancy Mechanisms of Aluminium Phosphinate in Combination with Melamine Cyanurate in Glass-Fibre-Reinforced Poly(1,4-Butylene Terephthalate). *Macromolecular Materials and Engineering* **2008**, *293* (3), 206–217. <https://doi.org/10.1002/mame.200700330>.
- (158) Braun, U.; Bahr, H.; Sturm, H.; Schartel, B. Flame Retardancy Mechanisms of Metal Phosphinates and Metal Phosphinates in Combination with Melamine Cyanurate in Glass-Fiber Reinforced Poly(1,4-Butylene Terephthalate): The Influence of Metal Cation. *Polymers for Advanced Technologies* **2008**, *19* (6), 680–692. <https://doi.org/10.1002/pat.1147>.
- (159) Yang, W.; Hu, Y.; Tai, Q.; Lu, H.; Song, L.; Yuen, R. K. K. Fire and Mechanical Performance of Nanoclay Reinforced Glass-Fiber/PBT Composites Containing Aluminum Hypophosphite Particles. *Composites Part A: Applied Science and Manufacturing* **2011**, *42* (7), 794–800. <https://doi.org/10.1016/j.compositesa.2011.03.009>.
- (160) Aufmuth, W.; Levchik, S. v.; Levchik, G. f.; Klatt, M. Poly(Butylene Terephthalate) Fire Retarded by 1,4-Diisobutylene-2,3,5,6-Tetraxydroxy-1, 4-Diphosphine Oxide. I. Combustion and Thermal Decomposition. *Fire and Materials* **1999**, *23* (1), 1–6. [https://doi.org/10.1002/\(SICI\)1099-1018\(199901/02\)23:1<1::AID-FAM660>3.0.CO;2-K](https://doi.org/10.1002/(SICI)1099-1018(199901/02)23:1<1::AID-FAM660>3.0.CO;2-K).
- (161) Klatt, M.; Gareiss, B.; Yamamoto, M. Flame-Proofed Moulding Materials. US6103797A, August 15, 2000.
- (162) Levchik, S. V.; Weil, E. D. A Review of Recent Progress in Phosphorus-Based Flame Retardants. *Journal of Fire Sciences* **2006**, *24* (5), 345–364. <https://doi.org/10.1177/0734904106068426>.
- (163) Weil, E. D.; Levchik, S. Flame Retardants for Plastics and Textiles: Practical Applications. *Flame Retardants for Plastics and Textiles: Practical Applications* **2009**, 1–297.
- (164) Suzuki, M.; Saiki, N. Flame-Retardant Resin Composition. US6133358A, October 17, 2000.
- (165) Wu, Q.; Lü, J.; Qu, B. Preparation and Characterization of Microcapsulated Red Phosphorus and Its Flame-Retardant Mechanism in Halogen-Free Flame Retardant Polyolefins. *Polymer International* **2003**, *52* (8), 1326–1331. <https://doi.org/10.1002/pi.1115>.
- (166) Yang, W.; Lu, H.; Tai, Q.; Qiao, Z.; Hu, Y.; Song, L.; Yuen, R. K. K. Flame Retardancy Mechanisms of Poly(1,4-Butylene Terephthalate) Containing Microencapsulated Ammonium Polyphosphate and Melamine Cyanurate. *Polymers for Advanced Technologies* **2011**, *22* (12), 2136–2144. <https://doi.org/10.1002/pat.1735>.
- (167) Balabanovich, A. I. The Effect of Melamine on the Combustion and Thermal Decomposition Behaviour of Poly(Butylene Terephthalate). *Polymer Degradation and Stability* **2004**, *84* (3), 451–458. <https://doi.org/10.1016/j.polyimdegradstab.2003.12.003>.
- (168) Levchik, G. F.; Grigoriev, Y. V.; Balabanovich, A. I.; Levchik, S. V.; Klatt, M. Phosphorus–Nitrogen Containing Fire Retardants for Poly(Butylene Terephthalate). *Polymer International* **2000**, *49* (10), 1095–1100. [https://doi.org/10.1002/1097-0126\(200010\)49:10<1095::AID-PI405>3.0.CO;2-B](https://doi.org/10.1002/1097-0126(200010)49:10<1095::AID-PI405>3.0.CO;2-B).
- (169) Pagliuca, A. Flame Retardant Material and a Cable Having a Cable Sheath Composed of the Same. US20110269888A1, November 3, 2011. <https://patents.google.com/patent/US20110269888/en> (accessed 2023-05-28).
- (170) Levchik, S.; Buczek, M. Epoxy Resin Composition Containing Reactive Flame Retardant Phosphonate Oligomer and Filler. WO2004044054A1, May 27, 2004. <https://patents.google.com/patent/WO2004044054A1/en> (accessed 2023-05-28).
- (171) Muriel, R.; Sebastian, W.; Manfred, D. Recent Developments in Halogen Free Flame Retardants for Epoxy Resins for Electrical and Electronic Applications. *Materials* **2010**, *3*. <https://doi.org/10.3390/ma3084300>.
- (172) Suihkonen, R.; Niemi, K.; Orell, O.; Honkanen, M.; Tang, L.; Zhang, H.; Zhang, Z.; Vuorinen, J. Performance of Epoxy Filled with Nano- and Micro-Sized Magnesium Hydroxide. *Journal of Materials Science* **2011**, *47*, 1480–1488. <https://doi.org/10.1007/s10853-011-5933-6>.
- (173) Matykiewicz, D.; Przybyszewski, B.; Stanik, R.; Czulak, A. Modification of Glass Reinforced Epoxy Composites by Ammonium Polyphosphate (APP) and Melamine Polyphosphate (PNA)

- during the Resin Powder Molding Process. *Composites Part B: Engineering* **2017**, *108*, 224–231. <https://doi.org/10.1016/j.compositesb.2016.10.003>.
- (174) Ciesielski, M.; Schäfer, A.; Döring, M. Novel Efficient DOPO-Based Flame-Retardants for PWB Relevant Epoxy Resins with High Glass Transition Temperatures. *Polymers for Advanced Technologies* **2008**, *19* (6), 507–515. <https://doi.org/10.1002/pat.1090>.
- (175) Zang, L.; Wagner, S.; Ciesielski, M.; Müller, P.; Döring, M. Novel Star-Shaped and Hyperbranched Phosphorus-Containing Flame Retardants in Epoxy Resins. *Polymers for Advanced Technologies* **2011**, *22* (7), 1182–1191. <https://doi.org/10.1002/pat.1990>.
- (176) Bourbigot, S.; Duquesne, S. Fire Retardant Polymers : Recent Developments and Opportunities. *Journal of Materials Chemistry* **2007**, *17* (22), 2283–2300. <https://doi.org/10.1039/B702511D>.
- (177) Li, Y.; Zheng, H.; Xu, M.; Li, B.; Lai, T. Synthesis of a Novel Phosphonate Flame Retardant and Its Application in Epoxy Resins. *Journal of Applied Polymer Science* **2015**, *132* (45). <https://doi.org/10.1002/app.42765>.
- (178) Zhao, B.; Liang, W.-J.; Wang, J.-S.; Li, F.; Liu, Y.-Q. Synthesis of a Novel Bridged-Cyclotriphosphazene Flame Retardant and Its Application in Epoxy Resin. *Polymer Degradation and Stability* **2016**, *133*, 162–173. <https://doi.org/10.1016/j.polymdegradstab.2016.08.013>.
- (179) Wang, J.-S.; Liu, Y.; Zhao, H.-B.; Liu, J.; Wang, D.-Y.; Song, Y.-P.; Wang, Y.-Z. Metal Compound-Enhanced Flame Retardancy of Intumescent Epoxy Resins Containing Ammonium Polyphosphate. *Polymer Degradation and Stability* **2009**, *94* (4), 625–631. <https://doi.org/10.1016/j.polymdegradstab.2009.01.006>.
- (180) Qu, H.; Wu, W.; Hao, J.; Wang, C.; Xu, J. Inorganic-Organic Hybrid Coating-Encapsulated Ammonium Polyphosphate and Its Flame Retardancy and Water Resistance in Epoxy Resin. *Fire and Materials* **2014**, *38* (3), 312–322. <https://doi.org/10.1002/fam.2182>.
- (181) Bourbigot, S.; Bras, M. L.; Delobel, R. Carbonization Mechanisms Resulting from Intumescence Association with the Ammonium Polyphosphate-Pentaerythritol Fire Retardant System. *Carbon* **1993**, *31* (8), 1219–1230. [https://doi.org/10.1016/0008-6223\(93\)90079-P](https://doi.org/10.1016/0008-6223(93)90079-P).
- (182) Bourbigot, S.; Le Bras, M.; Gengembre, L.; Delobel, R. XPS Study of an Intumescent Coating Application to the Ammonium Polyphosphate/Pentaerythritol Fire-Retardant System. *Applied Surface Science* **1994**, *81* (3), 299–307. [https://doi.org/10.1016/0169-4332\(94\)90287-9](https://doi.org/10.1016/0169-4332(94)90287-9).
- (183) Patrick Lim, W. K.; Mariatti, M.; Chow, W. S.; Mar, K. T. Effect of Intumescent Ammonium Polyphosphate (APP) and Melamine Cyanurate (MC) on the Properties of Epoxy/Glass Fiber Composites. *Composites Part B: Engineering* **2012**, *43* (2), 124–128. <https://doi.org/10.1016/j.compositesb.2011.11.013>.
- (184) Zhang, K.; Wu, K.; Zhang, Y.-K.; Liu, H.-F.; Shen, M.-M.; Hu, W. Flammability Characteristics and Performance of Flame-Retarded Epoxy Composite Based on Melamine Cyanurate and Ammonium Polyphosphate. *Polymer-Plastics Technology and Engineering* **2013**, *52* (5), 525–532. <https://doi.org/10.1080/03602559.2012.762520>.
- (185) Saba, N.; Jawaid, M.; Paridah, M. T.; Al-othman, O. Y. A Review on Flammability of Epoxy Polymer, Cellulosic and Non-Cellulosic Fiber Reinforced Epoxy Composites. *Polymers for Advanced Technologies* **2016**, *27* (5), 577–590. <https://doi.org/10.1002/pat.3739>.
- (186) Battig, A.; Markwart, J. C.; Wurm, F. R.; Scharrel, B. Hyperbranched Phosphorus Flame Retardants: Multifunctional Additives for Epoxy Resins. *Polym. Chem.* **2019**, *10* (31), 4346–4358. <https://doi.org/10.1039/C9PY00737G>.
- (187) Shi, Q.; Huo, S.; Wang, C.; Ye, G.; Yu, L.; Fang, Z.; Wang, H.; Liu, Z. A Phosphorus/Silicon-Based, Hyperbranched Polymer for High-Performance, Fire-Safe, Transparent Epoxy Resins. *Polymer Degradation and Stability* **2022**, *203*, 110065. <https://doi.org/10.1016/j.polymdegradstab.2022.110065>.
- (188) Bifulco, A.; Varganici, C.; Rosu, L.; Mustata, F.; Rosu, D.; Gaan, S. Recent Advances in Flame Retardant Epoxy Systems Containing Non-Reactive DOPO Based Phosphorus Additives. *Polymer Degradation and Stability* **2022**, *200*, 109962. <https://doi.org/10.1016/j.polymdegradstab.2022.109962>.
- (189) Perret, B.; Scharrel, B.; Stöß, K.; Ciesielski, M.; Diederichs, J.; Döring, M.; Krämer, J.; Altstädt, V. Novel DOPO-Based Flame Retardants in High-Performance Carbon Fibre Epoxy

- Composites for Aviation. *European Polymer Journal* **2011**, *47* (5), 1081–1089. <https://doi.org/10.1016/j.eurpolymj.2011.02.008>.
- (190) Yan, W.; Yu, J.; Zhang, M.; Wang, T.; Wen, C.; Qin, S.; Huang, W. Effect of Multiwalled Carbon Nanotubes and Phenethyl-Bridged DOPO Derivative on Flame Retardancy of Epoxy Resin. *J Polym Res* **2018**, *25* (3), 72. <https://doi.org/10.1007/s10965-018-1472-z>.
- (191) Rowles, W. Celanex Thermoplastic Polyester (PBT) — Properties, Design and Processing. *Materials & Design* **1986**, *7* (2), 89–94. [https://doi.org/10.1016/S0261-3069\(86\)80007-3](https://doi.org/10.1016/S0261-3069(86)80007-3).
- (192) Casu, A.; Camino, G.; Giorgi, M. D.; Flath, D.; Laudi, A.; Morone, V. Effect of Glass Fibres and Fire Retardant on the Combustion Behaviour of Composites, Glass Fibres–Poly(Butylene Terephthalate). *Fire and Materials* **1998**, *22* (1), 7–14. [https://doi.org/10.1002/\(SICI\)1099-1018\(199801/02\)22:1<7::AID-FAM623>3.0.CO;2-3](https://doi.org/10.1002/(SICI)1099-1018(199801/02)22:1<7::AID-FAM623>3.0.CO;2-3).
- (193) Vu-Khanh, T.; Denault, J.; Habib, P.; Low, A. The Effects of Injection Molding on the Mechanical Behavior of Long-Fiber Reinforced PBT/PET Blends. *Composites Science and Technology* **1991**, *40* (4), 423–435. [https://doi.org/10.1016/0266-3538\(91\)90032-K](https://doi.org/10.1016/0266-3538(91)90032-K).
- (194) Tjahjadi, M.; Gallucci, R. R. Tracking Resistance of Flame Retardant Glass Reinforced PBT; 1998; Vol. 2, pp 1168–1172.
- (195) Mohd Ishak, Z. A.; Leong, Y. W.; Steeg, M.; Karger-Kocsis, J. Mechanical Properties of Woven Glass Fabric Reinforced in Situ Polymerized Poly(Butylene Terephthalate) Composites. *Composites Science and Technology* **2007**, *67* (3), 390–398. <https://doi.org/10.1016/j.compscitech.2006.09.012>.
- (196) Köppl, T.; Brehme, S.; Wolff-Fabris, F.; Altstädt, V.; Schartel, B.; Döring, M. Structure–property Relationships of Halogen-Free Flame-Retarded Poly(Butylene Terephthalate) and Glass Fiber Reinforced PBT. *Journal of Applied Polymer Science* **2012**, *124* (1), 9–18. <https://doi.org/10.1002/app.34910>.
- (197) Miller, S. Macrocyclic Polymers from Cyclic Oligomers of Poly(Butylene Terephthalate). *Doctoral Dissertations Available from Proquest* **1998**, 1–253.
- (198) Schmitz, S.; Fischer, D. Radiation Cross-Linking of Plastics as a Finishing Process in Series Production. *VDI Berichte* **2020**, *2020* (2369), 197–206.
- (199) Li, J.; Tang, S.; Wu, Z.; Zheng, A.; Guan, Y.; Wei, D. Branching and Cross-Linking of Poly(Ethylene Terephthalate) and Its Foaming Properties. *Polym. Sci. Ser. B* **2017**, *59* (2), 164–172. <https://doi.org/10.1134/S1560090417020051>.
- (200) Levchik, S. Phosphorus-Based FRs. In *Non-Halogenated Flame Retardant Handbook*; John Wiley & Sons, Ltd, 2014; pp 17–74. <https://doi.org/10.1002/9781118939239.ch2>.
- (201) Kagumba, J.-P. L. X. S. L. Polymeric Flame Retardants for Reinforced Thermoplastic and Thermoset Resins. *Reinforced Plastics* **2021**. <https://doi.org/10.1016/j.repl.2017.11.016>.
- (202) Schmitt, T. E. Phosphonate Polymers, Copolymers, and Their Respective Oligomers as Flame Retardants for Polyamide Fibers. US20140308505A1, October 16, 2014. <https://patents.google.com/patent/US20140308505A1/en> (accessed 2022-11-30).
- (203) XIUDONG, S.; ZHIYUAN, L.; KEVIN, R. T. Flame Retardant Thermoplastic and Thermoset Compositions. WO2016090083A1, June 9, 2016. <https://patents.google.com/patent/WO2016090083A1/en> (accessed 2022-11-30).
- (204) Sun, X.; JEONG, Y.; LOUVARIS, P. Blends of Polyesters and Phosphonate Oligomers and Polymers. US10836909B2, November 17, 2020. <https://patents.google.com/patent/US10836909B2/en?q=16%2f162084> (accessed 2022-11-30).
- (205) *P-31 Phosphorus NMR Testing Services | NuMega Resonance Labs*. <https://www.numegalabs.com/p31.html> (accessed 2022-04-11).
- (206) Illers, K.-H. Heat of Fusion and Specific Volume of Poly(Ethylene Terephthalate) and Poly(Butylene Terephthalate). *Colloid & Polymer Sci* **1980**, *258* (2), 117–124. <https://doi.org/10.1007/BF01498267>.
- (207) Bikiaris, D. N.; Karayannidis, G. P. Chain Extension of Polyesters PET and PBT with Two New Diimidodiepoxides. II. *Journal of Polymer Science Part A: Polymer Chemistry* **1996**, *34* (7), 1337–1342. [https://doi.org/10.1002/\(SICI\)1099-0518\(199605\)34:7<1337::AID-POLA22>3.0.CO;2-9](https://doi.org/10.1002/(SICI)1099-0518(199605)34:7<1337::AID-POLA22>3.0.CO;2-9).

- (208) Bikiaris, D. N.; Karayannidis, G. P. Effect of Carboxylic End Groups on Thermooxidative Stability of PET and PBT. *Polymer Degradation and Stability* **1999**, *63* (2), 213–218. [https://doi.org/10.1016/S0141-3910\(98\)00094-9](https://doi.org/10.1016/S0141-3910(98)00094-9).
- (209) González, M. G.; Cabanelas, J. C.; Baselga, J.; González, M. G.; Cabanelas, J. C.; Baselga, J. Applications of FTIR on Epoxy Resins - Identification, Monitoring the Curing Process, Phase Separation and Water Uptake. In *Infrared Spectroscopy - Materials Science, Engineering and Technology*; IntechOpen, 2012. <https://doi.org/10.5772/36323>.
- (210) Irska, I.; Paszkiewicz, S.; Gorący, K.; Linares, A.; Ezquerro, T.; Jedrzejewski, R.; Roslaniec, Z.; Piesowicz, E. Poly(Butylene Terephthalate)/Polylactic Acid Based Copolyesters and Blends: Miscibility-Structure-Property Relationship. *eXPRESS Polymer Letters* **2020**, *14*, 26–47. <https://doi.org/10.3144/expresspolymlett.2020.4>.
- (211) Tsochatzis, E. D.; Alberto Lopes, J.; Holland, M. V.; Reniero, F.; Emons, H.; Guillou, C. Isolation, Characterization and Structural Elucidation of Polybutylene Terephthalate Cyclic Oligomers and Purity Assessment Using a ¹H QNMR Method. *Polymers* **2019**, *11* (3), 464. <https://doi.org/10.3390/polym11030464>.
- (212) Alessi, S.; Caponetti, E.; Güven, O.; Akbulut, M.; Spadaro, G.; Spinella, A. Study of the Curing Process of DGEBA Epoxy Resin Through Structural Investigation. *Macromolecular Chemistry and Physics* **2015**, *216*. <https://doi.org/10.1002/macp.201400510>.
- (213) Montaudo, G.; Puglisi, C.; Samperi, F. Primary Thermal Degradation Mechanisms of PET and PBT. *Polymer Degradation and Stability* **1993**, *42* (1), 13–28. [https://doi.org/10.1016/0141-3910\(93\)90021-A](https://doi.org/10.1016/0141-3910(93)90021-A).
- (214) Ohtani, H.; Kimura, T.; Tsuge, S. Analysis of Thermal Degradation of Terephthalate Polyesters by High-Resolution Pyrolysis-Gas Chromatography. *Analytical Sciences* **1986**, *2* (2), 179–182. <https://doi.org/10.2116/analsci.2.179>.
- (215) Sato, H.; Kondo, K.; Tsuge, S.; Ohtani, H.; Sato, N. Mechanisms of Thermal Degradation of a Polyester Flame-Retarded with Antimony Oxide/Brominated Polycarbonate Studied by Temperature-Programmed Analytical Pyrolysis. *Polymer Degradation and Stability* **1998**, *62* (1), 41–48. [https://doi.org/10.1016/S0141-3910\(97\)00259-0](https://doi.org/10.1016/S0141-3910(97)00259-0).
- (216) Gallo, E.; Braun, U.; Schartel, B.; Russo, P.; Acierno, D. Halogen-Free Flame Retarded Poly(Butylene Terephthalate) (PBT) Using Metal Oxides/PBT Nanocomposites in Combination with Aluminium Phosphinate. *Polymer Degradation and Stability* **2009**, *94* (8), 1245–1253. <https://doi.org/10.1016/j.polymdegradstab.2009.04.014>.
- (217) Duquesne, S.; Fontaine, G.; Cérin-Delaval, O.; Gardelle, B.; Tricot, G.; Bourbigot, S. Study of the Thermal Degradation of an Aluminium Phosphinate–Aluminium Trihydrate Combination. *Thermochimica Acta* **2013**, *551*, 175–183. <https://doi.org/10.1016/j.tca.2012.10.025>.
- (218) Samyn, F.; Bourbigot, S. Thermal Decomposition of Flame Retarded Formulations PA6/Aluminum Phosphinate/Melamine Polyphosphate/Organomodified Clay: Interactions between the Constituents? *Polymer Degradation and Stability* **2012**, *97* (11), 2217–2230. <https://doi.org/10.1016/j.polymdegradstab.2012.08.004>.
- (219) 刘治国; 汪静莉; 朱建华; 焦德荣; 谢滋东; 钟柳. Diethyl Phosphinate Fire Retardation Agent Preparation Method. CN103319524A, September 25, 2013. <https://patents.google.com/patent/CN103319524A/en> (accessed 2023-06-24).
- (220) Vannier, A. Procédés d'ignifugation du poly(éthylène terephthalate) pour une application textile : Synergie entre OMPOSS et retardateur de flamme phosphoré. These de doctorat, Lille 1, 2008. <https://www.theses.fr/2008LIL10039>.
- (221) Didane, N.; Giraud, S.; Devaux, E.; Lemort, G. A Comparative Study of POSS as Synergists with Zinc Phosphinates for PET Fire Retardancy. *Polymer Degradation and Stability* **2012**, *97* (3), 383–391. <https://doi.org/10.1016/j.polymdegradstab.2011.12.004>.
- (222) Thirtha, V.; Lehman, R.; Nosker, T. Glass Transition Effects in Immiscible Polymer Blends. *Annual Technical Conference - ANTEC, Conference Proceedings* **2005**, *6*.
- (223) Chiou, K.-C.; Chang, F.-C. Reactive Compatibilization of Polyamide-6 (PA 6)/Polybutylene Terephthalate (PBT) Blends by a Multifunctional Epoxy Resin. *Journal of Polymer Science Part B: Polymer Physics* **2000**, *38* (1), 23–33. [https://doi.org/10.1002/\(SICI\)1099-0488\(20000101\)38:1<23::AID-POLB3>3.0.CO;2-Y](https://doi.org/10.1002/(SICI)1099-0488(20000101)38:1<23::AID-POLB3>3.0.CO;2-Y).

- (224) Huang, C.-C.; Chang, F.-C. Reactive Compatibilization of Polymer Blends of Poly(Butylene Terephthalate) (PBT) and Polyamide-6,6 (PA66): 1. Rheological and Thermal Properties. *Polymer* **1997**, *38* (9), 2135–2141. [https://doi.org/10.1016/S0032-3861\(96\)00740-9](https://doi.org/10.1016/S0032-3861(96)00740-9).
- (225) Rouif, S. Radiation Cross-Linked Polymers: Recent Developments and New Applications. *Nuclear Instruments and Methods in Physics Research Section B: Beam Interactions with Materials and Atoms* **2005**, *236* (1–4), 68–72. <https://doi.org/10.1016/j.nimb.2005.03.252>.
- (226) Chen, Z.; Sun, Y.-C.; Wang, J.; Qi, H. J.; Wang, T.; Naguib, H. E. Flexible, Reconfigurable, and Self-Healing TPU/Vitrimer Polymer Blend with Copolymerization Triggered by Bond Exchange Reaction. *ACS Applied Materials and Interfaces* **2020**, *12* (7), 8740–8750. <https://doi.org/10.1021/acsami.9b21411>.
- (227) Jourdain, A.; Asbai, R.; Anaya, O.; Chehimi, M. M.; Drockenmuller, E.; Montarnal, D. Rheological Properties of Covalent Adaptable Networks with 1,2,3-Triazolium Cross-Links: The Missing Link between Vitrimers and Dissociative Networks. *Macromolecules* **2020**, *53* (6), 1884–1900. <https://doi.org/10.1021/acs.macromol.9b02204>.
- (228) Liu, Y.; Wang, L.; Xu, Q. Y.; Lin, P. J.; Guo, Z. H.; Wang, Y. P.; Wang, Y. M. Rheological Study on of PBT with High Melt Flow Index. *Advanced Materials Research* **2012**, *487*, 644–648. <https://doi.org/10.4028/www.scientific.net/AMR.487.644>.
- (229) Li, L.; Chen, X.; Jin, K.; Torkelson, J. M. Vitrimers Designed Both To Strongly Suppress Creep and To Recover Original Cross-Link Density after Reprocessing: Quantitative Theory and Experiments. *Macromolecules* **2018**, *51* (15), 5537–5546. <https://doi.org/10.1021/acs.macromol.8b00922>.
- (230) Meng, F.; Saed, M. O.; Terentjev, E. M. Elasticity and Relaxation in Full and Partial Vitrimer Networks. *Macromolecules* **2019**, *52* (19), 7423–7429. <https://doi.org/10.1021/acs.macromol.9b01123>.
- (231) El-Zaatari, B. M.; Ishibashi, J. S. A.; Kalow, J. A. Cross-Linker Control of Vitrimer Flow. *Polym. Chem.* **2020**, *11* (33), 5339–5345. <https://doi.org/10.1039/D0PY00233J>.
- (232) Saed, M. O.; Gablier, A.; Terentjev, E. M. Liquid Crystalline Vitrimers with Full or Partial Boronic-Ester Bond Exchange. *Advanced Functional Materials* **2020**, *30* (3), 1906458. <https://doi.org/10.1002/adfm.201906458>.
- (233) Anaya, O.; Jourdain, A.; Antoniuk, I.; Ben Romdhane, H.; Montarnal, D.; Drockenmuller, E. Tuning the Viscosity Profiles of High- T_g Poly(1,2,3-Triazolium) Covalent Adaptable Networks by the Chemical Structure of the N-Substituents. *Macromolecules* **2021**, *54* (7), 3281–3292. <https://doi.org/10.1021/acs.macromol.0c02221>.
- (234) Ricarte, R. G.; Shanbhag, S. Unentangled Vitrimer Melts: Interplay between Chain Relaxation and Cross-Link Exchange Controls Linear Rheology. *Macromolecules* **2021**, *54* (7), 3304–3320. <https://doi.org/10.1021/acs.macromol.0c02530>.
- (235) Song, Z.; Wang, Z.; Cai, S. Mechanics of Vitrimer with Hybrid Networks. *Mechanics of Materials* **2021**, *153*, 103687. <https://doi.org/10.1016/j.mechmat.2020.103687>.
- (236) Ferry, J. D. *Viscoelastic Properties of Polymers*; John Wiley & Sons, 1980.
- (237) Dhinojwala, A.; Hooker, J. C.; Torkelson, J. M. Retardation of Rotational Reorientation Dynamics in Polymers near the Glass Transition: A Novel Study over Eleven Decades in Time Using Second-Order Non-Linear Optics. *Journal of Non-Crystalline Solids* **1994**, *172–174*, 286–296. [https://doi.org/10.1016/0022-3093\(94\)90447-2](https://doi.org/10.1016/0022-3093(94)90447-2).
- (238) Hall, D. B.; Dhinojwala, A.; Torkelson, J. M. Translation-Rotation Paradox for Diffusion in Glass-Forming Polymers: The Role of the Temperature Dependence of the Relaxation Time Distribution. *Phys. Rev. Lett.* **1997**, *79* (1), 103–106. <https://doi.org/10.1103/PhysRevLett.79.103>.
- (239) Nichols, M. E.; Robertson, R. E. The Origin of Multiple Melting Endotherms in the Thermal Analysis of Polymers. *Journal of Polymer Science Part B: Polymer Physics* **1992**, *30* (3), 305–307. <https://doi.org/10.1002/polb.1992.090300311>.
- (240) Yeh, J. T.; Runt, J. Multiple Melting in Annealed Poly(Butylene Terephthalate). *Journal of Polymer Science Part B: Polymer Physics* **1989**, *27* (7), 1543–1550. <https://doi.org/10.1002/polb.1989.090270714>.

- (241) Greene, J. P. 3 - Microstructures of Polymers. In *Automotive Plastics and Composites*; Greene, J. P., Ed.; *Plastics Design Library*; William Andrew Publishing, 2021; pp 27–37. <https://doi.org/10.1016/B978-0-12-818008-2.00009-X>.
- (242) Park, C.-S.; Lee, K.-J.; Kim, S. W.; Lee, Y. K.; Nam, J.-D. Crystallinity Morphology and Dynamic Mechanical Characteristics of PBT Polymer and Glass Fiber-Reinforced Composites. *Journal of Applied Polymer Science* **2002**, *86* (2), 478–488. <https://doi.org/10.1002/app.11011>.
- (243) *Poly(Butylene Terephthalate) in Handbook of Thermoplastic Polyesters: Homopolymers, Copolymers, Blends, and Composites*; Fakirov, S., Ed.; Wiley-VCH: Weinheim, 2002.
- (244) van Krevelen, D. W. Some Basic Aspects of Flame Resistance of Polymeric Materials. *Polymer* **1975**, *16* (8), 615–620. [https://doi.org/10.1016/0032-3861\(75\)90157-3](https://doi.org/10.1016/0032-3861(75)90157-3).
- (245) Brehme, S.; Scharrel, B.; Goebels, J.; Fischer, O.; Pospiech, D.; Bykov, Y.; Döring, M. Phosphorus Polyester versus Aluminium Phosphinate in Poly(Butylene Terephthalate) (PBT): Flame Retardancy Performance and Mechanisms. *Polymer Degradation and Stability* **2011**, *96* (5), 875–884. <https://doi.org/10.1016/j.polymdegradstab.2011.01.035>.
- (246) Alongi, J. Investigation on Flame Retardancy of Poly(Ethylene Terephthalate) for Plastics and Textiles by Combination of an Organo-Modified Sepiolite and Zn Phosphinate. *Fibers Polym* **2011**, *12* (2), 166–173. <https://doi.org/10.1007/s12221-011-0166-5>.
- (247) Batistella, M.; Regazzi, A.; Pucci, M. F.; Lopez-Cuesta, J.-M.; Kadri, O.; Bordeaux, D.; Ayme, F. Selective Laser Sintering of Polyamide 12/Flame Retardant Compositions. *Polymer Degradation and Stability* **2020**, *181*, 109318. <https://doi.org/10.1016/j.polymdegradstab.2020.109318>.
- (248) Reuter, J.; Greiner, L.; Kukla, P.; Döring, M. Efficient Flame Retardant Interplay of Unsaturated Polyester Resin Formulations Based on Ammonium Polyphosphate. *Polymer Degradation and Stability* **2020**, *178*, 109134. <https://doi.org/10.1016/j.polymdegradstab.2020.109134>.
- (249) Vahabi, H.; Sonnier, R.; Ferry, L. Effects of Ageing on the Fire Behaviour of Flame-Retarded Polymers: A Review. *Polymer International* **2015**, *64* (3), 313–328. <https://doi.org/10.1002/pi.4841>.
- (250) Capelot, M. Chimie de Polycondensation, Polymères Supramoléculaires et Vitrimères. Thèse de doctorat, Université Pierre et Marie Curie - Paris VI, Paris, 2013.
- (251) *Cooling Time Calculation - Biesterfeld AG*. <https://www.biesterfeld.com/en/xx/service/cooling-time-calculation/?toResult=1&cHash=cd1c7f0a8e9460d39cc76f94f51b640a> (accessed 2022-10-02).
- (252) Mechanical Behavior of Polymers. In *Introduction to Physical Polymer Science*; John Wiley & Sons, Ltd, 2005; pp 557–612. <https://doi.org/10.1002/0471757128.ch11>.
- (253) Dupretz, R.; Fontaine, G.; Duquesne, S.; Bourbigot, S. Instrumentation of UL-94 Test: Understanding of Mechanisms Involved in Fire Retardancy of Polymers. *Polymers for Advanced Technologies* **2015**, *26* (7), 865–873. <https://doi.org/10.1002/pat.3507>.
- (254) Hu, C.; Fontaine, G.; Tranchard, P.; Delaunay, T.; Collinet, M.; Marcille, S.; Bourbigot, S. In-Situ Investigation of Temperature Evolution of Drippings via an Optimized UL-94 Instrumentation: Application to Flame Retarded Polybutylene Succinate. *Polymer Degradation and Stability* **2018**, *155*, 145–152. <https://doi.org/10.1016/j.polymdegradstab.2018.07.015>.
- (255) RESEARCH TEMPERATURES OF IGNITION AND SELF-IGNITION OF COTTON AND POLYESTER FABRICS. *Fire Safety* **2021**, *38*, 32–37. <https://doi.org/10.32447/20786662.38.2021.05>.
- (256) Louisy, J. Synthesis of Novel Phosphinate Salts and Development of Formulations for the Flame Retardancy of Glass Fiber Reinforced PolyButylene Terephthalate (PBT). These de doctorat, Lille 1, 2012. <http://www.theses.fr/2012LIL10162> (accessed 2022-05-31).
- (257) Inata, H.; Maki, I.; Ishikawa, T.; Takeda, K. Diffusion of Additives and Deterioration with Passage of Time in Polypropylene. *Journal of Applied Polymer Science* **2006**, *99* (5), 2152–2162. <https://doi.org/10.1002/app.22020>.
- (258) Jimenez, M.; Bellayer, S.; Revel, B.; Duquesne, S.; Bourbigot, S. Comprehensive Study of the Influence of Different Aging Scenarios on the Fire Protective Behavior of an Epoxy Based Intumescent Coating. *Ind. Eng. Chem. Res.* **2013**, *52* (2), 729–743. <https://doi.org/10.1021/ie302137g>.

- (259) Antić, V. V.; Pergal, M. V. Poly(Butylene Terephthalate) — Synthesis, Properties, Application. In *Handbook of Engineering and Speciality Thermoplastics*; John Wiley & Sons, Ltd, 2011; pp 127–180. <https://doi.org/10.1002/9781118104729.ch5>.
- (260) Manabe, N.; Yokota, Y. The Method for Analyzing Anhydride Formed in Poly(Butylene Terephthalate) (PBT) during Thermal and Photo-Degradation Processes and Applications for Evaluation of the Extent of Degradation. *Polymer Degradation and Stability* **2000**, *69* (2), 183–190. [https://doi.org/10.1016/S0141-3910\(00\)00059-8](https://doi.org/10.1016/S0141-3910(00)00059-8).
- (261) Samperi, F.; Puglisi, C.; Alicata, R.; Montaudo, G. Thermal Degradation of Poly(Butylene Terephthalate) at the Processing Temperature. *Polymer Degradation and Stability* **2004**, *83* (1), 11–17. [https://doi.org/10.1016/S0141-3910\(03\)00167-8](https://doi.org/10.1016/S0141-3910(03)00167-8).
- (262) Chiu, S.-J.; Wu, Y.-S. A Comparative Study on Thermal and Catalytic Degradation of Polybutylene Terephthalate. *Journal of Analytical and Applied Pyrolysis* **2009**, *86* (1), 22–27. <https://doi.org/10.1016/j.jaap.2009.03.003>.
- (263) Kelleher, P. G.; Wentz, R. P.; Falcone, D. R. Hydrolysis of Poly(Butylene Terephthalate). *Polymer Engineering & Science* **1982**, *22* (4), 260–264. <https://doi.org/10.1002/pen.760220408>.
- (264) Bastioli, C.; Guanella, I.; Romano, G. Effects of Water Sorption on the Physical Properties of PET, PBT, and Their Long Fibers Composites. *Polymer Composites* **1990**, *11* (1), 1–9. <https://doi.org/10.1002/pc.750110102>.
- (265) Goje, A. S. Auto-Catalyzed Hydrolytic Depolymerization of Poly(Butylene Terephthalate) Waste at High Temperature. *Polymer-Plastics Technology and Engineering* **2006**, *45* (2), 171–181. <https://doi.org/10.1080/03602550500374012>.
- (266) Loyer, C.; Régnier, G.; Duval, V.; Ould, Y.; Richaud, E. PBT Plasticity Loss Induced by Oxidative and Hydrolysis Ageing. *Polymer Degradation and Stability* **2020**, *181*, 109368. <https://doi.org/10.1016/j.polymdegradstab.2020.109368>.
- (267) Dewimille, B.; Bunsell, A. R. Accelerated Ageing of a Glass Fibre-Reinforced Epoxy Resin in Water. *Composites* **1983**, *14* (1), 35–40. [https://doi.org/10.1016/0010-4361\(83\)90141-6](https://doi.org/10.1016/0010-4361(83)90141-6).
- (268) Tual, N.; Carrere, N.; Davies, P.; Bonnemains, T.; Lolive, E. Characterization of Sea Water Ageing Effects on Mechanical Properties of Carbon/Epoxy Composites for Tidal Turbine Blades. *Composites Part A: Applied Science and Manufacturing* **2015**, *78*, 380–389. <https://doi.org/10.1016/j.compositesa.2015.08.035>.
- (269) Zhou, Y. High-Performance Poly (Butylene Terephthalate) Vitrimers. PhD Thesis, Ph. D. thesis, Technische Universiteit Eindhoven, The Netherlands, 2017.
- (270) Jin, F.-L.; Li, X.; Park, S.-J. Synthesis and Application of Epoxy Resins: A Review. *Journal of Industrial and Engineering Chemistry* **2015**, *29*, 1–11. <https://doi.org/10.1016/j.jiec.2015.03.026>.
- (271) Delobel, R.; Bras, M. L.; Ouassou, N.; Alistiqsa, F. Thermal Behaviours of Ammonium Polyphosphate-Pentaerythritol and Ammonium Pyrophosphate-Pentaerythritol Intumescent Additives in Polypropylene Formulations. *Journal of Fire Sciences* **1990**, *8* (2), 85–108. <https://doi.org/10.1177/073490419000800202>.
- (272) Sun, L.; Qu, Y.; Li, S. Co-Microencapsulate of Ammonium Polyphosphate and Pentaerythritol in Intumescent Flame-Retardant Coatings. *J Therm Anal Calorim* **2013**, *111* (2), 1099–1106. <https://doi.org/10.1007/s10973-012-2494-0>.
- (273) Guillaume, E.; Saragoza, L. Methane Calibration Burner and C-Factor Determination with Cone Calorimeter – Validation of the Standardized Calibration Protocol. *Fire and Materials* **2016**, *40* (3), 511–515. <https://doi.org/10.1002/fam.2292>.
- (274) Chabert, E. Multiple Welding of Long Fiber Epoxy Vitrimer Composites. *Soft Matter* **2016**, *8*.
- (275) Zhang, F.; Wang, W.; Cheng, Y. Influence of Magnesium Hydroxide on Thermal Decomposition of Intumescent Fire-Retardant Epoxy Coatings. *Journal of Thermoplastic Composite Materials* **2014**, *29*. <https://doi.org/10.1177/0892705714563115>.
- (276) Pan, G.; Du, Z.; Zhang, C.; Li, C.; Yang, X.; Li, H. Effect of Structure of Bridging Group on Curing and Properties of Bisphenol-A Based Novolac Epoxy Resins. *Polymer Journal* **2007**, *39*, 478–487. <https://doi.org/10.1295/polymj.PJ2006201>.

- (277) Feng, X.; Fan, J.; Li, A.; Li, G. Multireusable Thermoset with Anomalous Flame-Triggered Shape Memory Effect. *ACS Applied Materials and Interfaces* **2019**, *11* (17), 16075–16086. <https://doi.org/10.1021/acsami.9b03092>.
- (278) Chen, J.-H.; Liu, B.-W.; Lu, J.-H.; Lu, P.; Tang, Y.-L.; Chen, L.; Wang, Y.-Z. Catalyst-Free Dynamic Transesterification towards a High-Performance and Fire-Safe Epoxy Vitrimer and Its Carbon Fiber Composite. *Green Chem.* **2022**, *24* (18), 6980–6988. <https://doi.org/10.1039/D2GC01405J>.
- (279) Poutrel, Q.-A.; Blaker, J. J.; Soutis, C.; Tournilhac, F.; Gresil, M. Dicarboxylic Acid-Epoxy Vitrimers: Influence of the off-Stoichiometric Acid Content on Cure Reactions and Thermo-Mechanical Properties. *Polym. Chem.* **2020**, *11* (33), 5327–5338. <https://doi.org/10.1039/D0PY00342E>.
- (280) Tao, X.; Duan, H.; Dong, W.; Wang, X.; Yang, S. Synthesis of an Acrylate Constructed by Phosphaphenanthrene and Triazine-Trione and Its Application in Intrinsic Flame Retardant Vinyl Ester Resin. *Polymer Degradation and Stability* **2018**, *154*, 285–294. <https://doi.org/10.1016/j.polymdegradstab.2018.06.015>.
- (281) Zhang, J.; Silcock, G.; Shields, T. Study of the Combustion and Fire Retardancy of Polyacrylonitrile and Its Copolymers by Using Cone Calorimetry. *Journal of Fire Sciences - J FIRE SCI* **1995**, *13*, 141–161. <https://doi.org/10.1177/073490419501300204>.
- (282) Schartel, B.; Bartholmai, M.; Knoll, U. Some Comments on the Use of Cone Calorimeter Data. *Polymer Degradation and Stability* **2005**, *88* (3), 540–547. <https://doi.org/10.1016/j.polymdegradstab.2004.12.016>.
- (283) *Fact.MR – Polybutylene Terephthalate (PBT) Market By Type (Reinforced, Unreinforced), By Processing Method (Extrusion, Injection Molding), By End-use (Automotive, Packaging, Electrical & Electronics, Consumer Goods)- Global Market Insights 2021 to 2031*. <https://www.factmr.com/report/2406/pbt-market> (accessed 2022-05-31).
- (284) Cheng, S. Z. D.; Pan, R.; Wunderlich, B. Thermal Analysis of Poly(Butylene Terephthalate) for Heat Capacity, Rigid-Amorphous Content, and Transition Behavior. *Die Makromolekulare Chemie* **1988**, *189* (10), 2443–2458. <https://doi.org/10.1002/macp.1988.021891022>.
- (285) Gomez, M. A.; Cozine, M. H.; Tonelli, A. E. *High-resolution solid-state carbon-13 NMR study of the .alpha. and .beta. crystalline forms of poly(butylene terephthalate)*. ACS Publications. <https://doi.org/10.1021/ma00180a017>.
- (286) Tashiro, K.; Nakai, Y.; Kobayashi, M.; Tadokoro, H. Solid-State Transition of Poly(Butylene Terephthalate) Induced by Mechanical Deformation. *Macromolecules* **1980**, *13* (1), 137–145. <https://doi.org/10.1021/ma60073a026>.
- (287) Takahashi, Y.; Murakami, K.; Nishikawa, S. Mechanism for the Phase Transition of Poly(Butylene Terephthalate). *Journal of Polymer Science Part B: Polymer Physics* **2002**, *40* (9), 765–771. <https://doi.org/10.1002/polb.10136>.
- (288) Nisticò, R. Polyethylene Terephthalate (PET) in the Packaging Industry. *Polymer Testing* **2020**, *90*, 106707. <https://doi.org/10.1016/j.polymertesting.2020.106707>.
- (289) Das, S. K.; Eshkalak, S. K.; Chinnappan, A.; Ghosh, R.; Jayathilaka, W. A. D. M.; Baskar, C.; Ramakrishna, S. Plastic Recycling of Polyethylene Terephthalate (PET) and Polyhydroxybutyrate (PHB)—a Comprehensive Review. *Mater Circ Econ* **2021**, *3* (1), 9. <https://doi.org/10.1007/s42824-021-00025-3>.
- (290) Desbonnet, J.; Apchin, G. Polyesters thermoplastiques PET et PBT pour injection. *Plastiques et composites* **2001**. <https://doi.org/10.51257/a-v1-am3376>.
- (291) *PBT IMPACT RESISTANCE*. <https://www.poliblend.it/de/gamma-prodotti/politer/pbt-impact-resistance> (accessed 2022-06-01).
- (292) Hine, P. J.; Duckett, R. A. Fiber Orientation Structures and Mechanical Properties of Injection Molded Short Glass Fiber Reinforced Ribbed Plates. *Polymer Composites* **2004**, *25* (3), 237–254. <https://doi.org/10.1002/pc.20019>.
- (293) Bergeret, A.; Bozec, M. P.; Quantin, J.-C.; Crespy, A.; Gasca, J.-P.; Arpin, M. Study of Interphase in Glass Fiber-Reinforced Poly(Butylene Terephthalate) Composites. *Polymer Composites* **2004**, *25* (1), 12–25. <https://doi.org/10.1002/pc.20001>.

- (294) Park, C.-S.; Lee, K.-J.; Nam, J.-D.; Kim, S.-W. Crystallization Kinetics of Glass Fiber Reinforced PBT Composites. *Journal of Applied Polymer Science* **2000**, *78* (3), 576–585. [https://doi.org/10.1002/1097-4628\(20001017\)78:3<576::AID-APP120>3.0.CO;2-M](https://doi.org/10.1002/1097-4628(20001017)78:3<576::AID-APP120>3.0.CO;2-M).
- (295) Li, X.; Kang, T.; Cho, W.-J.; Lee, J.-K.; Ha, C.-S. Preparation and Characterization of Poly(Butyleneterephthalate)/Organoclay Nanocomposites. *Macromolecular Rapid Communications* **2001**, *22* (16), 1306–1312. [https://doi.org/10.1002/1521-3927\(20011101\)22:16<1306::AID-MARC1306>3.0.CO;2-I](https://doi.org/10.1002/1521-3927(20011101)22:16<1306::AID-MARC1306>3.0.CO;2-I).
- (296) Hajiraissi, R.; Parvinzadeh, M. Preparation of Polybutylene Terephthalate/Silica Nanocomposites by Melt Compounding: Evaluation of Surface Properties. *Applied Surface Science* **2011**, *257* (20), 8443–8450. <https://doi.org/10.1016/j.apsusc.2011.04.127>.
- (297) Che, J.; Luan, B.; Yang, X.; Lu, L.; Wang, X. Graft Polymerization onto Nano-Sized SiO₂ Surface and Its Application to the Modification of PBT. *Materials Letters* **2005**, *59* (13), 1603–1609. <https://doi.org/10.1016/j.matlet.2004.09.057>.
- (298) Broza, G.; Kwiatkowska, M.; Rosłaniec, Z.; Schulte, K. Processing and Assessment of Poly(Butylene Terephthalate) Nanocomposites Reinforced with Oxidized Single Wall Carbon Nanotubes. *Polymer* **2005**, *46* (16), 5860–5867. <https://doi.org/10.1016/j.polymer.2005.05.073>.
- (299) Yang, W.; Zhou, H.; Yang, B.; Lu, H.; Song, L.; Hu, Y. Facile Preparation of Modified Carbon Nanotube-Reinforced PBT Nanocomposites with Enhanced Thermal, Flame Retardancy, and Mechanical Properties. *Polymer Composites* **2016**, *37* (6), 1812–1820. <https://doi.org/10.1002/pc.23354>.

Appendix 1 : Generalities on PBT

Part of the larger family of polyesters like its cousin PET, poly (butylene terephthalate), or PBT, saw its first commercialization in the late 1960s. Its resistance to solvent, low shrinkage, strong mechanical performances and high melt temperature ($>200^{\circ}\text{C}$), enabled it to make its place in the polymers market. Classified as one of the most used commercialized engineering thermoplastics, PBT is commonly used for automobile, electric and electronic applications for which it represents 51% of the total engineering plastic products and materials²⁸³. Its global demand raised by 5.7% in 2021 despite the COVID crisis, with an annual growth rate of 4.2% from 2016 to 2020.

T_g and network entanglement

PBT usually exhibits a glass transition ranging from 30 to 50°C, depending on average chain length and crystallinity, as both impact the mobility of the polymer chains^{5,284}. With an average molecular weight ranging from 5,000 to 40,000 g/mol and an estimated mass between entanglements reported to be about 55.000 g/mol¹⁹⁷, PBT chains are hardly entangled. Thus, around melting temperature, PBT hardly keeps dimensional stability and rapidly flows under its own weight^{5,34}.

Crystallinity

As a semi-crystalline polymer, PBT exhibits a partial crystallization of molecular chains in its solid phase (35 to 40%). Crystallinity comes from the presence of lamellae, composing bigger structures named spherulites. Crystals inside a PBT matrix are composed of elementary triclinic structures, which may be present in two possible phases: an α -form and a β -form²⁸⁵⁻²⁸⁷. α -form is the most common configuration, as it occurs when PBT transitions from a melting phase to a solid phase. It converts to a β -form only by uniaxial stretching of the material, like fiber drawing. The conversion to β -form is considered reversible when a low strain (up to 12%) is applied to the material.

Mechanical behavior

Mechanically, PBT has overall poorer performances than PET, with a lower strength (50 vs 70 MPa), rigidity (2.3 vs 3.1 GPa), glass transition (30-60 vs 67-81°C); and melting temperature (220-230 vs 260°C), but higher impact resistance on notched samples (9.5 vs 4.4 kJ.m²)²⁸⁸⁻²⁹¹. However, PBT is easier to adapt to molding applications due to lower glass transition (40°C vs 70°C) and melting temperature (200-220°C vs 240°C) combined with faster crystallization rates than any other polyesters²⁵⁹, allowing for faster cooling processes while keeping a high crystallinity.

Besides, PBT has very good electrical and dielectrical properties, including excellent creep current and arc-tracking resistance²⁴³, while environmental moisture has a low impact on the electrical properties. Besides, water absorption of PBT is around 0.1% after 24h and about 0.5% in the saturated state²⁵⁹. This allows the conservation of good dimensional stability in a humid environment.

Robustness

PBT also exhibits an overall good resistance to most chemical agents, like organic solvents (esters, ethers, alcohols, aliphatic hydro-carbons or petroleum derivatives), or other fluids like diols, aromatic products, diluted acid, or basic solutions²⁴³. Above 60°C, its resistance to acid and bases decreases and it is sensible to chlorinated substances, aromatics, and ketones. Moreover, above its glass transition, long-term immersion in water is not recommended due to the relative sensibility of polyesters to hydrolysis²⁴³. Dissolving PBT implies the use of very aggressive solvents like hexafluoroisopropanol (HFIP), 1,1,2,2-tetrachloroethane (TCE), cresol, or phenol:TCE mixtures.

Additives

The most used filler in PBT is glass fiber, usually added to increase flexural modulus, tensile strength, and dimensional stability at the cost of drastically reducing its elongation at break^{242,292}. The amount of fiber, size and orientation have a direct impact on the mechanical properties of the material. 5% glass content is a minimum to see the overlap of some fiber and reinforcing properties, while over 35%, properties start to decline due to non-homogeneous fiber mixing. Besides, sizing treatments, like epoxy, can be applied to fibers to reinforce interfacial adhesion in the composite²⁹³. Glass fiber also acts as nucleating agent, which affects crystallization²⁹⁴. Besides glass fiber, nanoclays, formed of nanophase layered silicates, also gives improvement in tensile modulus and tensile strength at lower filling quantities compared with glass fibers, but the use of epoxide compounds is usually necessary due to incompatibilities with the PBT matrix²⁹⁵. Other nanofillers like silica nanoparticles^{296,297} and carbon nanotubes^{298,299} also see a growing interest in the industrial applications of PBT.

The addition of flame-retardants is mostly mandatory nowadays to cope with the different requirements of the industrial sectors where engineering polymers are commonly used. Especially, in the case of PBT, its extensive use in electrical and electrotechnical applications, where accidental fires may be common, impose significant restrictions and norms.

Other additives commonly used are not specific to PBT applications and do not significantly impact mechanical performances due to the low amount added, like antioxidants^{5,154}, UV stabilizers, pigments, processing aids (plasticizers), or mold-releasing agents.

Appendix 2 : Relaxation curves fitting data

Chapter 2:

Formulation	PE _Z					
Equation	$G_0 \cdot \exp(-(x/\tau)^\beta)$					
T (°C)	240	245	250	255	260	265
G ₀ (Pa)	24621	24367	21928	18732	13148	8694
tau* (s)	297	185	145	119	89	64
<Tau> (s)	515	321	252	207	155	111
beta*	0.54					
Reduced Chi-Square	0.00013					
R-Square	0.9982	0.9989	0.9994	0.9997	0.9996	0.9986

Formulation	PE _Z A ₂₀				
Equation	$G_0 \cdot \exp(-(x/\tau)^\beta)$				
T (°C)	235	240	245	250	255
G ₀ (Pa)	17583	21353	26489	24171	18986
tau* (s)	1.21	1.00	0.70	0.49	0.31
<Tau> (s)	7.62	5.58	3.39	2.61	1.96
beta*	0.34				
Reduced Chi-Square	0.0058				
R-Square	0.9917	0.9941	0.9948	0.9909	0.9702

Formulation	PE _Z Z ₂₄					
Equation	$G_0 \cdot \exp(-(x/\tau)^\beta)$					
T (°C)	245	250	255	260	265	270
G ₀ (Pa)	4556	4643	4670	4625	2900	1751
tau* (s)	97	70	51	32	23	16
<Tau> (s)	310	224	162	101	73	51
beta*	0.41					
Reduced Chi-Square	0.00039					
R-Square	0.9961	0.9987	0.9985	0.9981	0.9987	0.9980

Formulation	P5E _{5Z} H ₂₀					
Equation	$G_0 \cdot \exp(-(x/\tau)^\beta)$					
T (°C)	235	240	245	250	255	260
G ₀ (Pa)	7256	3198	1808	956	599	443
tau* (s)	56	41	37	36	30	29
<Tau> (s)	197	143	129	127	105	102
beta*	0.39					
Reduced Chi-Square	0.00086					
R-Square	0.9947	0.9994	0.9986	0.9958	0.9966	0.9972

Chapter 3:

Formulation	PEA ₂₀				
Equation	$G_0 \cdot \exp(-(x/\tau)^\beta)$				
T (°C)	235	240	245	250	255
G ₀ (Pa)	21947	27148	27438	23423	16760
tau* (s)	2.39	1.32	0.80	0.536	0.47
<Tau> (s)	16.3	9.3	6.0	4.1	3.3
beta*	0.32				
Reduced Chi-Square	0.00259				
R-Square	0.9967	0.9966	0.9983	0.9977	0.9987

Formulation	PEA _{0.26}					
Equation	$G_0 \cdot \exp(-(x/\tau)^\beta)$					
T (°C)	240	245	250	255	260	265
G ₀ (Pa)	36333	37664	37385	31058	22323	13442
tau* (s)	2.23	1.94	1.80	1.74	1.49	1.32
<Tau> (s)	12.39	10.82	9.99	9.65	8.28	7.30
beta*	0.34					
Reduced Chi-Square	0.00012					
R-Square	0.9999	0.9999	0.9999	0.9999	0.9999	0.9999

Study of complex formulations based on vitrimer matrices – Application to flame-retardants

The addition of flame-retardant additives into vitrimers represents a challenge that has to be considered to obtain marketable materials. Indeed, the dynamics of the exchange reactions in such systems is complex and such additives may affect it or even modify its kinetics. In this work, various flame-retardants were added into two different matrices: a PBT vitrimer and an epoxy vitrimer considering the exchange dynamics within the networks based on transesterification reactions. In the first part, the effect of incorporating flame-retardant during the synthesis of PBT vitrimer through reactive extrusion was studied. It was shown that the use of phosphinate salts significantly accelerates transesterification, while their flame-retardant action was maintained. As far as epoxy is concerned, two approaches were followed. The first formulation consisted of adding intumescent formulations to a vitrimer coating. The material exhibited good flame-retardancy behavior and recyclability. Secondly, a comparison was drawn between a specific flame-retardant added into an epoxy matrix through a reactive or additive pathway. In this case, the fast reactivity of the flame-retardant leads to side reactions, depleting the available epoxies and preventing the formation of a highly cross-linked network. This work, among the first one dealing with the effect of the addition of flame-retardant additives in vitrimer shows that it is not a trivial topic and in the case of transesterification, the dynamic of the exchange reaction may be affected even if it is maintained.

Keywords : Vitrimer, Flame-retardancy, Transesterification, Reactive extrusion, PBT, Epoxy

Etude de formulations complexes à matrice vitrimer – Application aux retardateurs de flamme

L'ajout de retardateurs de flammes dans les vitrimères par voie additive représente un défi à relever pour obtenir des matériaux commercialisables. En effet, la dynamique des réactions d'échange dans de tels systèmes est complexe, et ces additifs peuvent influencer sur cette dernière voire modifier sa cinétique. Durant ces travaux de thèse, différents ignifugeants ont été ajoutés à deux matrices différentes : un vitrimer PBT et un vitrimer époxy et l'influence de ces additifs sur la dynamique des échanges basée sur des réactions de transestérification a été étudiée. La première partie de ce travail de thèse s'est intéressée à l'effet de l'incorporation d'ignifugeants lors de la synthèse du vitrimer PBT par extrusion réactive. Il a été démontré que l'utilisation de sels de phosphinate peut significativement accélérer la transestérification tout en conservant leurs propriétés retardatrices de flamme. En ce qui concerne les résines époxy, deux approches ont été suivies. La première consistait à formuler un matériau intumescent via l'ajout de charges dans le but d'obtenir un revêtement protecteur. Le matériau obtenu présente de bonnes performances au feu et sa recyclabilité a été mise en évidence. Dans une seconde approche, une comparaison a été établie entre un retardateur de flamme spécifique ajouté à une matrice époxy par voie réactive ou additive. Dans ce dernier cas, il a été proposé que la réactivité de l'additif a entraîné des réactions secondaires, menant à la consommation des époxydes disponibles empêchant d'obtenir un réseau fortement réticulé. Ce travail, l'un des premiers à aborder l'effet de l'ajout de charges retardatrices de flamme dans les vitrimères, montre que les interactions matrice/charge peuvent avoir des effets significatifs, et que dans le cas de la transestérification, la dynamique des réactions d'échange peut être affectée même si elle est maintenue.

Mots-clefs : Vitrimer, Ignifugation, Transesterification, Extrusion réactive, PBT, Epoxy